Austrian Armed Forces

Austrian Society of Automotive Engineers

6th EUROPEAN ISTVS CONFERENCE

4. ÖVK Symposium
"Off Road Vehicles in Theory and Practice"

Vienna, Austria
September 28-30, 1994

PROCEEDINGS
VOLUME II

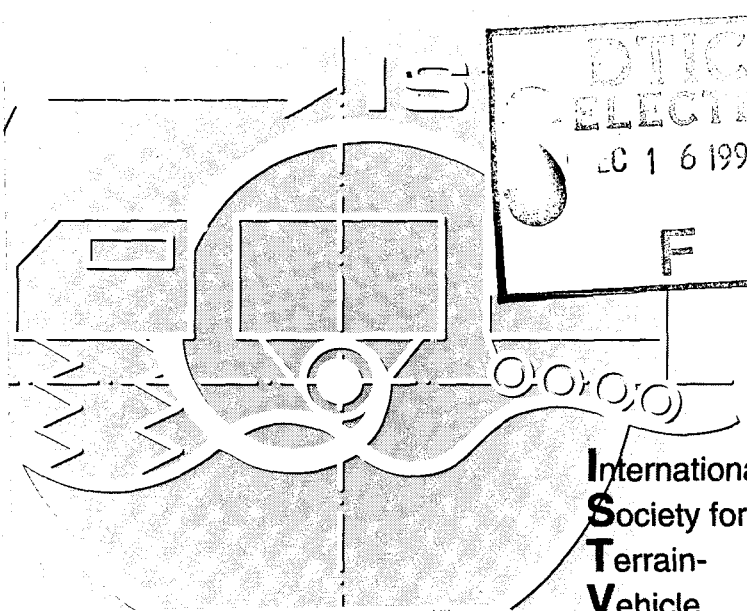

International Society for Terrain-Vehicle Systems

Austrian
Armed
Forces

Austrian Society
of Automotive
Engineers

6th EUROPEAN ISTVS CONFERENCE

4. ÖVK Symposium
"Off Road Vehicles in Theory and Practice"

Vienna, Austria
September 28-30, 1994

PROCEEDINGS
VOLUME II

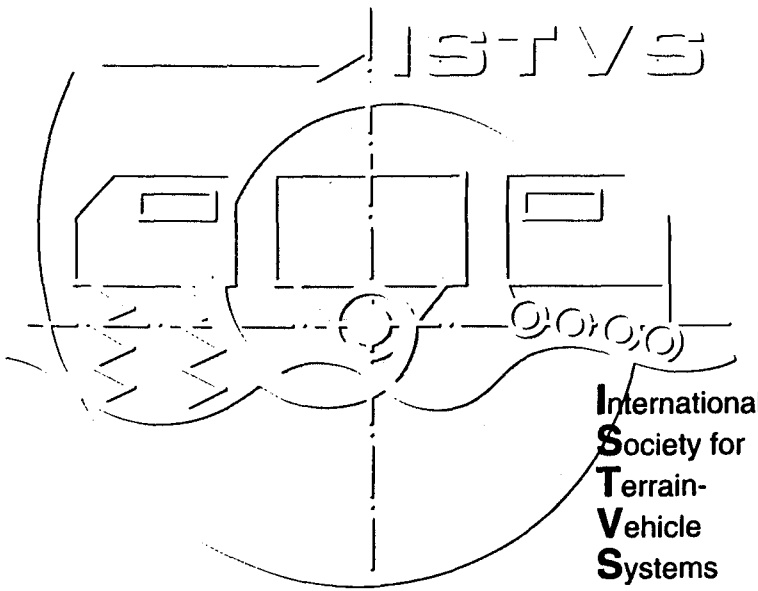

International
Society for
Terrain-
Vehicle
Systems

Table of Contents
Volume I
Plenary Lectures

Table of Contents
Volume II
Postersession

The list of the paper is arranged in a alphabetical order according to the first named author of the paper.
Die Liste der Beiträge wurden in alphabetischer Reihenfolge nach dem erstgenannten Autor gereiht.

Dornier
Deutsche Aerospace

ROBOT-MOTION IN UNSTRUCTURED ENVIRONMENT

Manfred B. Bartha, Dr. Max Eibert, Dr. Peter Lux, Dr. Christian H. Schaefer

DASA - Dornier, Verteidigung und Zivile Systeme
D-88039 Friedrichshafen

ABSTRACT

To operate an autonomous Vehicle in off-road terrain is one of the most difficult problems in Robotic. Since it is not possible to build a high resolution model of an unstructured terrain, in particular of a battlefield, a robot driving through this terrain has to be able to adapt its motion to the real world. In the German experimental program "Robotic for the Battlefield" therefore a key function is real time obstacle detection and avoidance. In conjunction with a gyro-system and an optical tracker this function ensures a cross-country driving on a pre-planned path by surveying the real world. Using an active (time-of-flight) laser-scanner a 3d-image, consisting of 128 x 64 Voxels, is generated once a second and real-time transformed into a 2d-obstacle-map. This map is used by the Navigation-computer to avoid obstacles while following the given path as close as possible.

A prototype of this system has been tested under real conditions in field-tests already.

1. EXPERIMENTAL PROGRAM "ROBOTIC FOR THE BATTLEFIELD"

The goal of the German Experimental Program "Robotic for the Battlefield" is to realize a set of functions ("Basic-Functions") which can be used as modules to build different Robot-systems, suited to different military missions.

The German MoD has set as a fundamental requirement that these Robots have to fulfil their missions without line-of-sight to a control center. Therefore, the techniques of teleoperation, needing a high capacity data link, cannot be used. This means, these Robot-systems and all of their functions (modules) have to operate autonomously, at least for a period of time.

2. AUTONOMOUS DRIVING IN OFF-ROAD-TERRAIN

One of the most important capabilities a battlefield-robot has to have is the capability to move in any given terrain.

Since autonomous road following has been shown already in various robot projects (e.g. ALV, GRS, NavLab, VaMoRs, ...) the efforts of the German experimental program on autonomous driving are concentrated on off-road-driving in unstructured terrain.

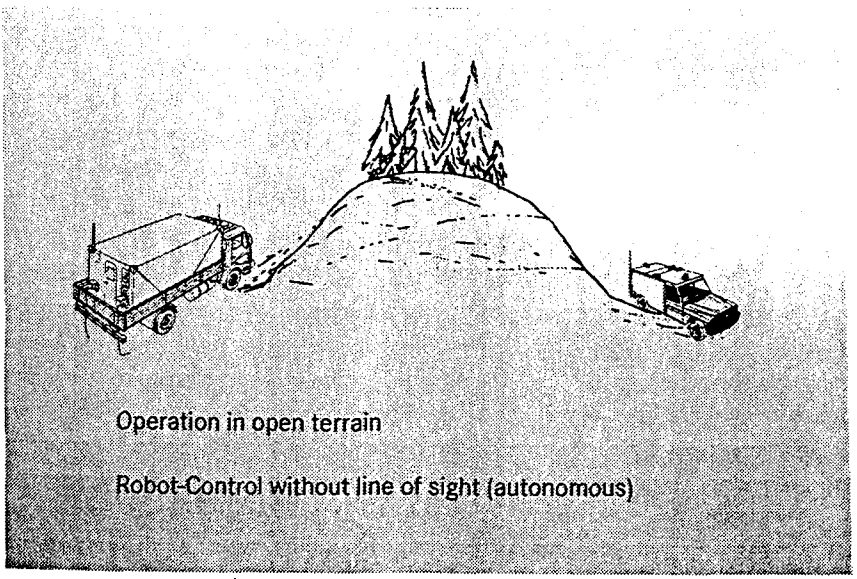

Fig. 1: General Scope of the German Experimental Program

2.1 Modes of Operation

For quick employment of the robot in the battlefield and in order to simplify the Man-Machine-Interface (MMI) in the control center, all moving capabilities will be controlled by only three types of commands (Modes of Operation).

These are:

- Path Following
- Track Mode
- Heading Mode

2.1.1 Path Following

Using a cursor on a digital map display, the path following command will be generated by marking the goal-point and, if there are any, way-points on the path which the robot has to meet on its travel.

After receiving this commando, the robot prepares itself autonomously for moving (e.g. starts the engine, looses the brake, ...) and starts driving to the goal-point - via all given way-points.

Controlled by a dead reckoning navigation system with an associated north seeking gyro, the robot drives on straight lines between way-points and changes its moving direction at way-points without stopping.

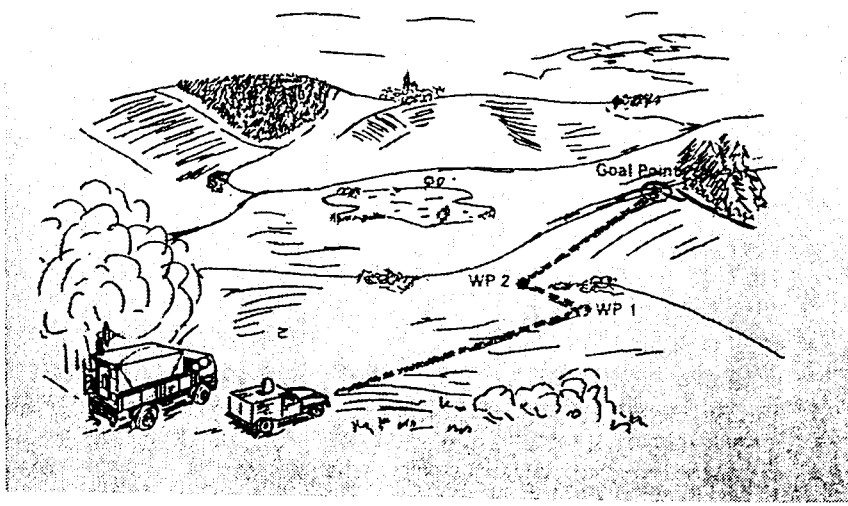

Fig. 2: Path Following Mode

2.1.2 Track Mode

In track mode operation the navigation is performed by an optical track system. On request of the operator, the robot transmits a single TV-image from its front camera (drive corridor camera) to the control center. By setting a cursor on any object in this picture (e.g. a tree, a bush, ...) the direction of driving is determined. After completion of the track command by the required driving distance, the robot moves, again on a straight line, for the given distance forwards the track goal.

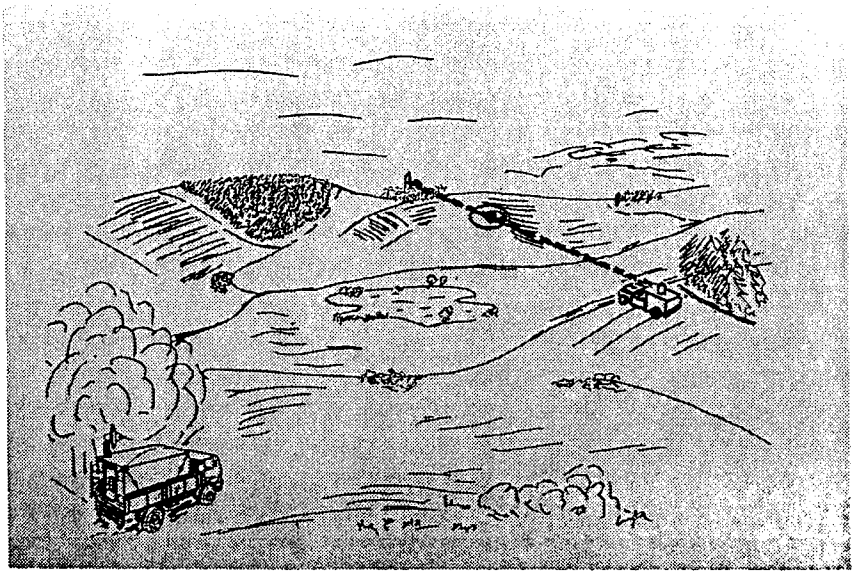

Fig. 3: Track Mode

2.1.3 Heading Mode

A heading command consists only of two information, the heading angle in respect to north and the distance to the goal-point in meters. The driving will be performed similar to path following on a straight line. This command is very helpful for alignment of the robot into a required direction. Therefore, it mainly will be used for short distances only (5 m to 10 m) as an "appendage" to a path following command to assure the required orientation of the robot.

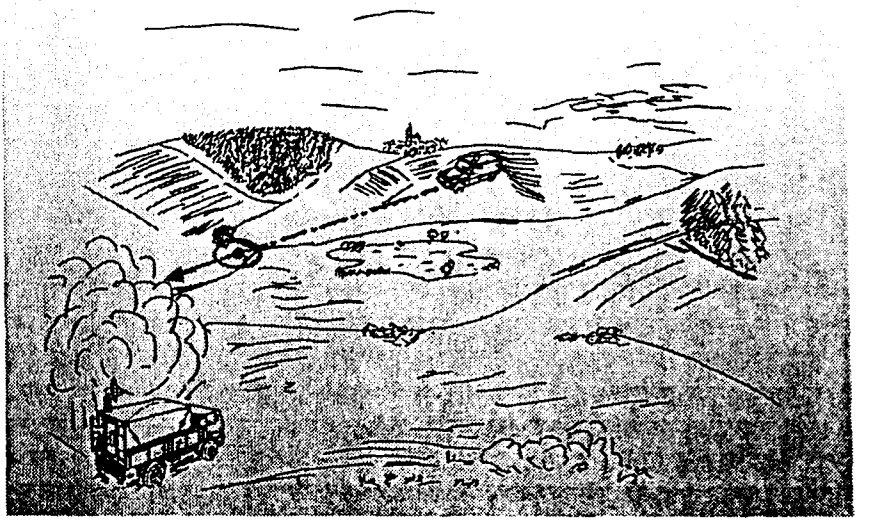

Fig. 4: Heading Mode

2.2 Need of Obstacle Avoidance

Since high resolution models or maps of unstructured terrain are not available, an obstacle free route cannot be preplanned. Taking this into account, all three operation modes are based on straight lines as route elements. In the real world, however, these straight lines will meet lots of obstacles in different sizes and shapes. Therefore, the most important function for off-road-driving is a reliable obstacle detection in order to perform a sufficient obstacle avoidance. This function will be used in parallel to each of the three operation modes for superposing bypass routes to the straight line route elements.

3. TECHNICAL APPROACH FOR OBSTACLE DETECTION

3.1 Range vs. Video Imaging

A 2-d scanning laser radar has been developed to serve as sensor in the vision system. A high resolution range image of 64 x 128 pixels is generated at a rate of 1 Hz and processed for the detection of obstacles.

Researchers have taken both, video images and range images as input to road following and obstacle-detection algorithms. Since video cameras are easily available, much effort has been devoted to the development of algorithms that process video images [e.g. 2, 3]. If proper model support is provided, video-based road following at speeds of nearly 100 km/s is feasible with little hardware. This has been demonstrated with VaMoRs [5]. An understanding of video images of off-road scenes, however, has proven extremely difficult and has led some researchers to support their vision systems with range sensors. On the ALV, for example, road following and obstacle avoidance are conducted at 20 km/h by fusing video- and range-date [7, 6]. In view of this situation and the fact that model support cannot be provided when unpredicted obstacles may occur, the choice of a laser scanner seems adequate in the present context.

In passing from video to range imaging, the task of image processing is substantially alleviated at the cost of introducing a more complex sensor. It is clear why range images are simpler to process for ground/obstacle detection than video images. Navigation of a land vehicle is basically a geometric issue: the auto pilot needs to know the distance and directions of obstacles, the extent of navigable terrain stretching out before the vehicle, the inclination of grades etc. Such numerical data is directly obtained from range images by purely geometrical algorithms, without requiring a symbolic understanding of the scene. From a range-image, an obstacle can be detected, located, and avoided without knowing what the obstacle is. This is not true for a video-image. Geometrical information about the scene is only available when a model has been properly matched with the image, i.e. when the image has been understood. Model support is obviously an elaborate affair; while it is desirable for range image interpretation at an advanced level, it is not required in the present context.

3.2 Description of Sensor

As opposed to the ERIM-sensor uses on ALV [1], the present laser scanner performs a time-of-flight range measurement. A GaAs laser diode of wavelength 0.9μ is used. The dual optics (for separate transmission and reception) are currently designed to provide a measurement range of 8 - 40 m. The typical range measurement accuracy is $\pm$ 0.5 %.

Eye-safety is warranted by supplying laser power only during active scan. The 2-d scan is currently mechanical in both directions (vertical and horizontal); however, electronic line scanners with 64 pixels have been in use at Dornier for some time, and this technology will be included in the future. The vertical scan is accomplished with a fast mechanical micro scanning system for both, laser source and detection channel. The horizontal scan is generated with a slowly oscillating mirror in front of the optics. Time-of-flight range measurement is carried out with light pulses on a single event for each pixel.

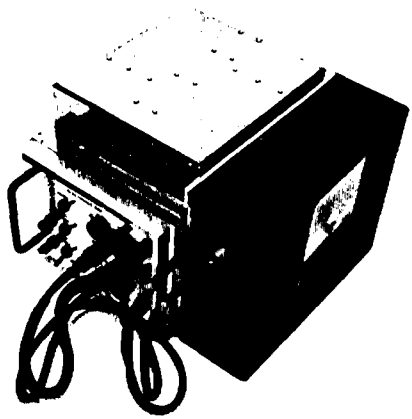

Fig. 5: Experimental 2-d laser scanner

Field-of-view is 30° x 60° (vertical x horizontal), giving rise to an angular resolution of the image of about 0.5°. At 40 m distance this yields 35 cm resolution. The experimental sensor is shown in figure 6; it is basically a cubical box of side-length 30 cm, and weighs 15 kg.

3.3 Description of Processor

The processing unit consists of a standard VME-rack equipped with two M68020-boards, a sensor interface, and an additional memory board. Image processing is performed in parallel on the two CPUs. For testing purposes, a third CPU-board plus video-board is added which runs graphical software. Operating software has been developed providing just the services required in this application. All application programs are written in ADA. To accommodate higher frame rates of a sensor, additional CPU-boards can be added. Correspondingly, obstacle-detection software has been designed for parallel execution on an arbitrary number of processors (within practical limits).

4. OBSTACLE DETECTION FROM RANGE IMAGES

This section presents an overview of the obstacle-detection algorithm implemented on the image processing unit of the vision system. Based on range images, this algorithm generates "maps of obstacles" (MO) that serve as input to the obstacle avoidance algorithm. Section 4.1 gives only a brief outline of this algorithm, as it has already been published in detail elsewhere [4]. Section 4.2 reports on how the algorithm has been tested and displays some results. An alternative approach to obstacle detection is found in [8].

4.1 Algorithm

Using a single range image and the associated vehicle state data as input, the algorithm generates a binary map of obstacles (Fig. 8). A MO constitutes a bird's eye view of the scene; the vehicle is represented as a red box at the lower center of the image. Each pixel of an MO assumes one of three colours: black, green, or red. A green pixel represents an area of terrain which is navigable, a red pixel is considered inaccessible (either because it is obstructed or because it is excessively inclined); a black pixel cannot be assessed with regard to its navigability. No reference map or reference model is employed. The MO displays clusters of red pixels, i.e. "obstacles"; at the current level, the algorithm has no means of identifying such obstacles.

We shall briefly outline the major steps leading from a range image to an MO. Due to the knowledge of the current vehicle position and orientation, the range value associated with each pixel of the image may be transformed into a 3-d positional vector in absolute space. In this way, from the range image a set of points in 3-space is obtained. Each point indicates the position in 3-space where the laser pulse emitted in the course of an individual range measurement was reflected.

In the following, this set of points will be called "3-d image". The MO is derived from the 3-d image without further reference to the original range image.

The 3-d image represents a silhouette of the scene scanned by the sensor. No attempt is made to fit surfaces to the 3-d image. Instead, a set of simple geometric rules [4] is applied to each data point which directly correlate this point with neighbouring points. The result of this correlation may lead to a colour label "green" or "red" being affixed to that point, indicating whether the point is considered associated with navigable terrain or with an obstacle. After all data points have been processed, the pixels of the MO inherit colour labels from geometrically associated data points. This completes the algorithm.

We summarize the properties of the algorithm:

- The algorithm is conceptually simple. It requires four essential parameters. They are easy to set, and algorithm-dependency is not sensitive.

- Non-linear filters have been added to the algorithm to eliminate incorrect measurements. After including these filters, the algorithm has shown to be robust with regard to measurement error.

- The algorithm is computationally efficient. It is parallel to a high degree.

4.2 Results

Since the development of the sensor and the algorithm proceeded in parallel, it was necessary to generate a number of range images for testing the algorithm before the sensor became available. Such images were obtained both in the in- and outdoors with the aid of a one-channel laser radar. The complete unit was scanned across a selected, static scene mechanically, producing a 64 x 128 range image. A large number of range images has been measured in the lab using a miniature landscape. They have been used to optimize and demonstrate sensor and algorithm performance for a vehicle moving slowly in both, an on- and off-road environment.

An example of an outdoor scene is given in figure 6. The vehicle is driving towards a parking military tuck, while crossing an air base access road.

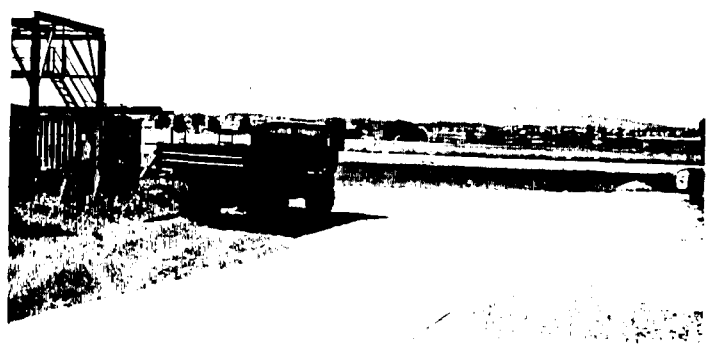

Fig. 6: Outdoor scene

Figure 7 shows a range image taken from this scene. A range interval of 0 - 40 m is mapped linearly on a gray-scale ranging from white to black. A limited number of measurement errors (drop-ins and drop-outs) are visible.

Fig. 7: Range Image (gray-scale)

Figure 8 shows how the algorithm has labelled data points in the 3-d image. The pixels in the range image have the same intensity as in the gray-scale presentation; however, a pixel giving rise to a green or red 3-d image point inherits this colour. The algorithm detects all obstacles.

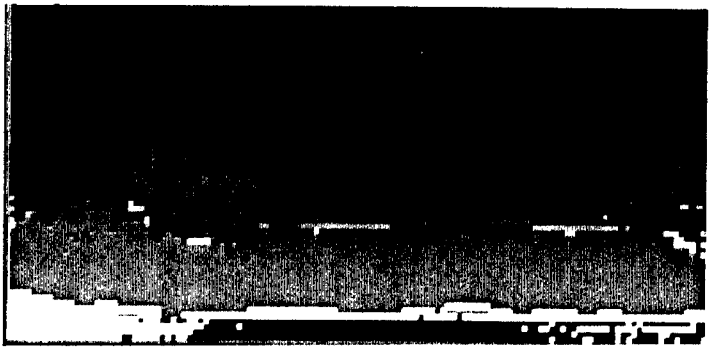

Fig. 8: Range Image (colour labelled)

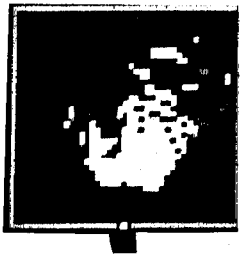

Figure 9 (left) displays the associated map of obstacles. The red box at the bottom represents the sensor-carrying vehicle.

Fig. 9: Map of Obstacles (MO)

5. OBSTACLE AVOIDANCE

5.1 Obstacle Detection Subsystem

Fig. 10 shows the two components of the obstacle detection subsystem, as described in section 4. The scanning laser radar generates a range image which is transformed into a map of obstacles (MO) by means of a VME-processor system.

This MO is used by the navigation processor as one of its two main information (data) sources. The second main information stream is originated by the dead reckoning navigation unit.

The navigation processor computes first, based on the co-ordinates delivered with the driving command, a straight line form the start-point to the goal-point (or next way-point). This line represents the center line of a "travel corridor" in which the robot may drive on its own decision without operator support.

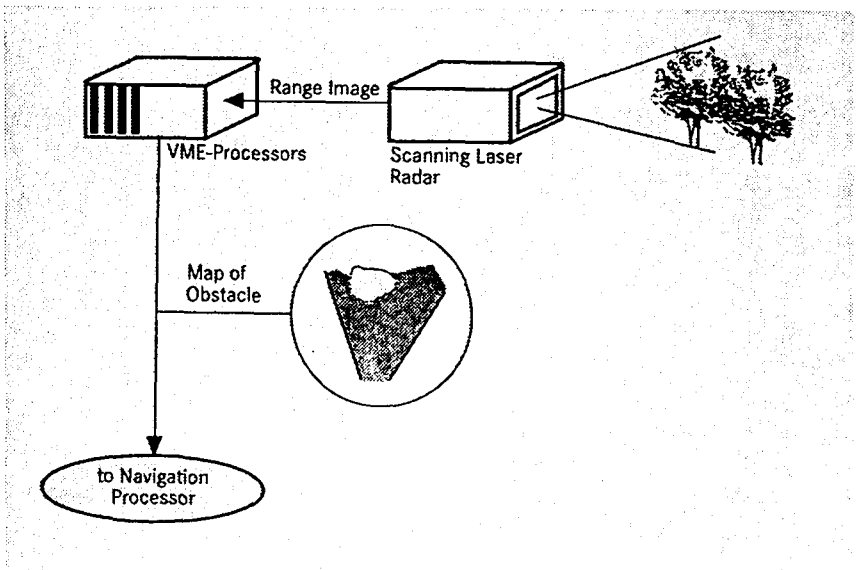

Fig. 10: Obstacle Detection Subsystem

5.2 Obstacle Avoidance Strategy

As maps of obstacles appears, one per second, they will be layed over the travel corridor and adjusted to the true co-ordinates. Even when the center line leads into an obstacle area the driving route will leave the center line, but stay close to the obstacle area in a "rubber hand" manner. This strategy ensures a driving route as close as possible to the commanded one.

If these "roundabout ways" cannot be placed inside the travel corridor, but have to cross the border of the corridor, the robot will stop autonomously and ask the operator in the control center for help, by transmitting him a single TV-image of the situation.

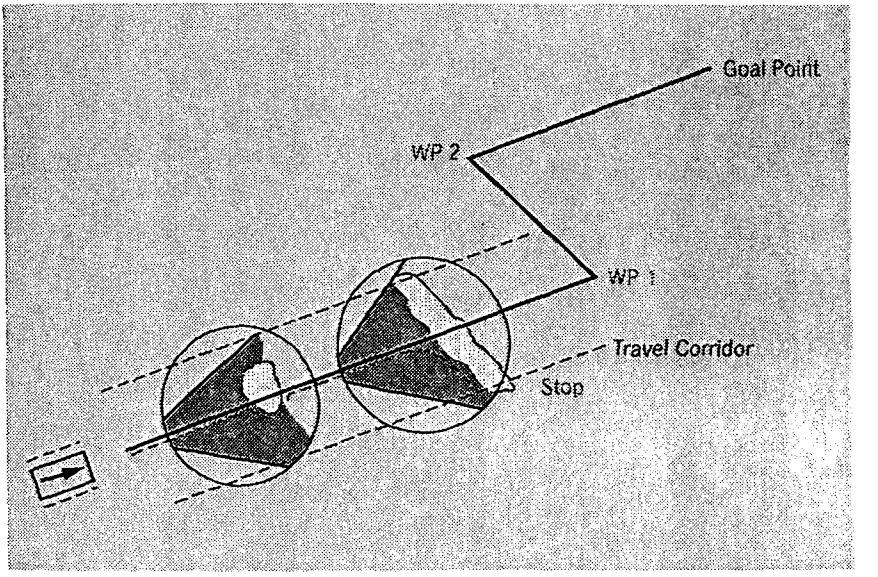

Fig. 11: Obstacle Avoidance Strategy

6. CONCLUSION

Among others, one goal of the German Experimental Program "Robotic for the Battlefield" is to realize autonomous functions for vehicle motion in unstructured off-road terrain. Since high resolution maps (including obstacles) are not available, autonomous real time obstacle detection and avoidance became a key challenge within the program.

A computer-vision system, consisting of a sensor and a processing unit will be used to provide the requested capability. The sensor is a 2-d scanning, high resolution laser scanner with range and frame rate currently designed for vehicle speeds of 15 km/h (for greater speeds, these sensor parameters will be increased by at least a factor 5). The sensor has recently been completed. Algorithms that perform obstacle detection and avoidance based on range images have been developed. The former algorithm is being implemented in parallel to run on two commercial microprocessors in real time. The capability of the integrated sensor/processor system to detect obstacles has been tested in the field under real conditions already. After integration into the designated unmanned vehicle, a demonstration of autonomous off-road-driving including obstacles avoidance was performed in july 1992 at the army training area near Pfullendorf (Germany).

Experimental Vehicle

REFERENCES

[1] Bair, M.E.; Sampson, R.; and Zuk, D.; **SPIE 726** (1986), 264 - 274

[2] Davis, L.S.; Le Moigne, J.; Waxmann, A.L.; **Visual navigation of roadways,** in: Hertzberger, L.O.; Groen, F.C.A. (eds.), **Intelligent Autonomous Systems** (North Holland, 1987), pp. 21 - 30.

[3] Dickmanns, E.D.; Zapp, E.; **SPIE 727 Mobile Robots** (1986), 161 - 168.

[4] Lux, P. W.; Schaefer, C.H.; **Signal Processing,** submitted.

[5] Mysliwitz, B. D.; Dickmanns, E. D.; **SPIE 852 Mobile Robots II** (1987), 72 - 79.

[6] Sharma, U. M.; Davis, L. S.; **SPIE 727 Mobile Robots** (1986), 169 - 179.

[7] Turk, M. A.; Morgenthaler D. G.; Gremban, K. D.; Marra, M; **Proc. 1987 IEEE Int. Conf. on Robotics and Automation**, 273 - 280.

[8] Veatch, P.A.; Davis, L.S.; **Range Imagery Algorithms for the Detection of Obstacles by Autonomous Vehicles** (Center for Automation Research, Univ. of Maryland, 1987).

APPLICATION OF INTELLIGENT SYSTEMS IN MODERN BUCKET LOADERS

Piotr Dudziński, Kazimierz Pieczonka, Zenon Wysłouch
Institute of Machine Design and Operations Research Technical
University of Wroclaw, Poland

ABSTRACT

The paper proposes the solutions concerning, the control of scooping the loader bucket with almost unmineable granular material and positioning of the operation systems in its duty cycle. It presents intelligent automatic systems of controlling these processes and their usability was confirmed by operation tests. It shows the concepts of the systems for automatic protection of the stability of the machine, first of all the articulated one, and the increase of efficiency of its driving and turning mechanisms.

1. INTRODUCTION

Mobile construction machines, including bucket loaders, after relatively rapid evolution, have assumed a stable form in the recent years as far as their fundamental concept and basic construction-operation indices are concerned.

Our analyses and world trends show that further development of these machines should be found in the use of modern achievements of technology especially of microelectronics [1-5].
The main needs which require the use of automation in new machine generations are facilitation of machine controlling, stability increase of capacity, decrease of energy-consumption and the increase of their work safety.

For some years the Institute of Machine Design and Operations Research of the Technical University of Wroclaw has been carrying out research into and tests on the automation of mobile construction machines. The following paper proposes exemplary solutions achieved in this Institute.

2. SCOOPING OF THE BUCKET

Scooping of the loader bucket with granular rocky material is achieved with two independent movements: rectilinear motion parallel to the base brought about by the driving mechanism of the loader and rotary motion in the plane which is perpendicular to the base, performed with the construction equipment (bucket with an extension arm).

The practice demonstrates that scooping of the bucket with granular material can be achieved in three different ways, the three typical ones being shown in Fig. 2 [7].

In case of the material which is hard to be mined, for instance material of high cohesion or high granulation, the distance to which the bucket is pushed into a dump, is restricted by external influence, that is, material resistance and the resistance increase gradually with the increase of the bucket penetration. If the value of resistance equals the maximum disposable value of the loader thrust force, there occurs stoppage of its dislocation, which can happen even at partial penetration of the bucket into the dump. The rotation closing the bucket leads to small scooping of the bucket with excavated material.

The test showed that the improvement of the performance can be obtained for instance by using appropriate motion procedures of the bucket consisting in its graduated partial rotations, that is elementary rotations, performed in the initial phase of the closing rotation (Fig. 2b) [8]. Due to the elementary rotation of the bucket thrust and bound in the dump of granular material, the state of inner equilibrium is disturbed , that is there occurs mutual displacement of material grains around its edge and walls, leading to the decrease of the resistance of the centre influencing the bucket.

Under the In influence of the thrust force, brought about by the loader, additional penetration of the bucket into the dump is obtained to the value restricted by the renewed resistance increment. The next elementary rotation of the bucket starts the next stage of the process of so called gradual scooping. After a number of stages there occurs the end of the scooping process by closing of the bucket. The bucket is scooped in a continuous way with the remaining disposable part of its rotation (Fig. 2a, Fig. 4) .

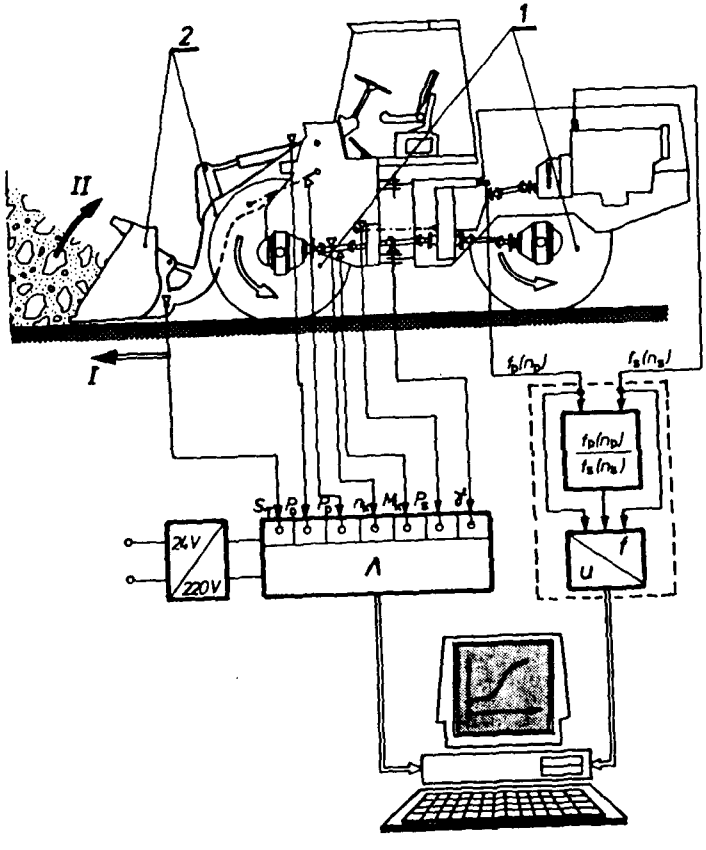

Fig. 1: Bucket scooping in a bucket loader; 1-driving system, 2- working unit, I, II -working movements (I- travel of machine, II- turn of bucket or boom)

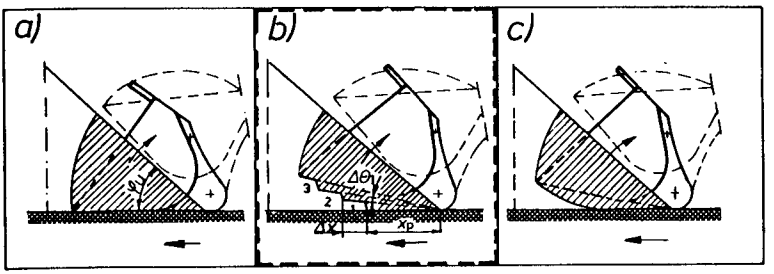

Fig. 2: Scooping the bucket with granular material; a) separated, b) gradual, c) combined

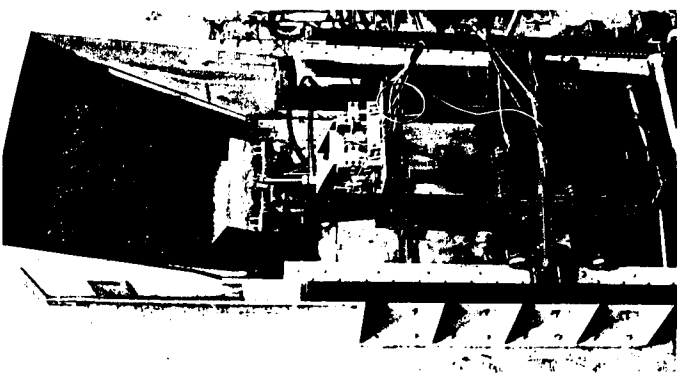

Fig. 3: The laboratory stand for testing the process of scooping the bucket on a bucket loader. The Institute of Machine Design and Operations Research, Technical University of Wroclaw

Fig. 4: Gradual scooping of the loader bucket in laboratory conditions. The Institute of Machine Design and Operations Research, Technical University of Wroclaw

This way of scooping the bucket with the granular material even that of high mining resistance makes it possible to thrust the bucket properly into the dump and to scoop the bucket with the excavated material after its closing.

In order to ensure the regularity and optimisation of such a process it is necessary to appropriately select the number and value of elementary angles of the bucket ratations. The tests conducted in this field show that the values of these magnitudes depend first of all on the type and condition of the mined material (Fig. 5, Fig. 6).

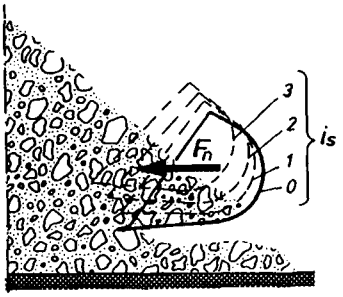

Fig. 5: Gradual scooping of bucket loader;
i_S - number of bucket's rotations;
F_n -maximum thrust force of a loader

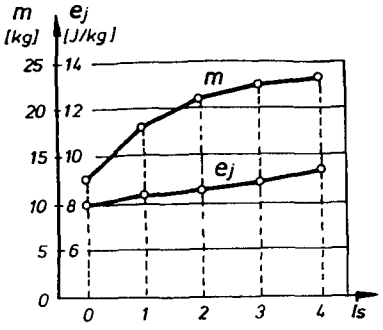

Fig. 6. Results of laboratory tests;
m - mass of scooped material;
e_j - unit energy of scooping the bucket with material.

Exemplary results of laboratory tests on the process of scooping a loader bucket have been shown in Fig. 7.

Detailed analyses and examinations of individual motions of the loader bucket in the scooping process show that the rectilinear motion pushing the bucket into the material dump is achieved by the driving mechanism of the machine in the continuous way without special intervention of the machine operator. On the other hand the bucket rotation during its closing at the bucket scooping especially at multi-stage scooping, is achieved by successive switching on and off of its drive. Thus, controlling requires some practice, attention and additional effort of the loader operator. The automation of the process was suggested in order to ease the operator physically and psychically as well as to integrate and optimise the process [9],[10]. Laboratory and field analyses and studies conducted for many years on bucket scooping with granular material, made it possible to put forward a simple system which automates this process with the use of a board computer (Fig. 8).

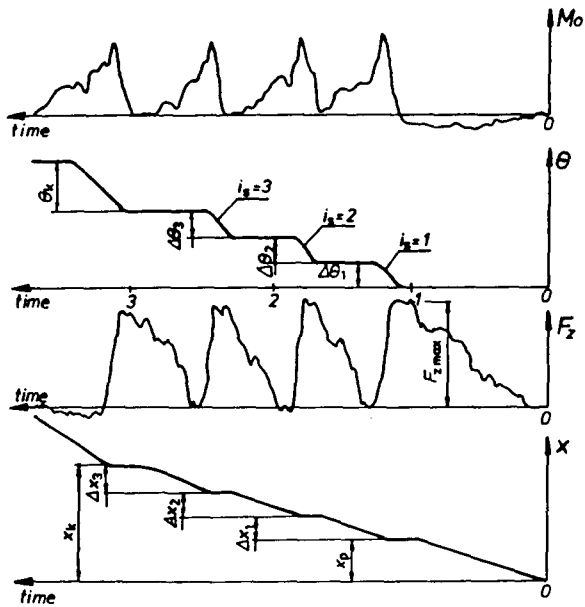

Fig. 7: Exemplary measurement records for:resistance torque of bucket's rotation M_o, rotation angle Θ, thrust force F_z, displacement of a bucket while scooping the bucket with breakstone material in a three-step mode

The suggested solution of the system gives the possibility of regulating wide range of the number of the process degrees, values of the elementary angles of the bucket rotation and the duration of breaks between them, that is the times of bucket penetration into the dump in successive degrees. Thus during the loader operation there are possibilities of the proper selection of these magnitudes according to the type and condition of the loaded material.

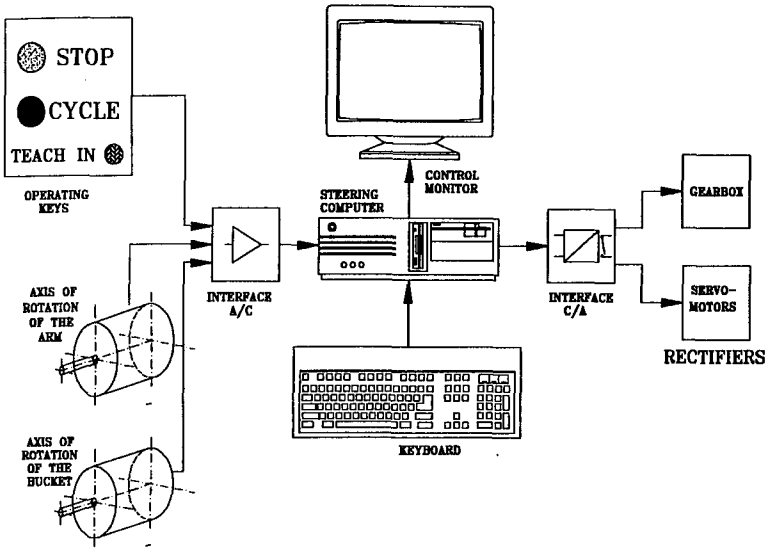

Fig. 8: Integrated system of automated working unit on a bucket loader [11]

The automated system in question having been tested in the laboratory conditions, was used in the Ł 220 loader manufactured by the Factory of the Construction Machines „FADROMA" Wroclaw, Poland. The results of in situ tests on the system show that it is correct and applicable in practice. High scooping of the bucket with the excavated material and thus high loader efficiency was obtained after the proper selection of parameters of the multi-stage steering. Comparison of the obtained capacity results of the loader with automatic and manual steering shows that they are similar only when the loader is manually operated by highly skilled and experienced the operator who is involved to a great extent both physically and psychically in these operations. Other cases prove the superiority of automatic programmer. In the presented automating system the first impulse to the bucket rotation after its initial thrust into the material dump is performed manually by the operator. According to the studies the moment of starting the rotation is significant in the performed process. Delay in its starting leads to the machine standstill and too long full slip of road wheels of the loader or hydrokinetic torque converter and at the same time to their high wear and heating. If the rotation is started

too early it can lead to incomplete scooping of the bucket with the excavated material.

In order to relieve the operator from the intensive attention while switching on the bucket rotation, the search was conducted for the signal of feedback for autogenous initiation [12] [13]. The obtained results turned out a solution which, if tested successfully, will be used in next generation of the system automating the scooping process on a bucket loader.

3. POSITIONING OF THE OPERATION SYSTEM

Following the improvement and in-situ tests of the system which automates the process of scooping the bucket, the research was undertaken to check automation of the remaining operation movements of the loader. The use of automation was to bring improved efficiency and quality of the loader operation irrespective of the skills, ability and the condition of the operator, if the automation of this type was employed.
The solution of the task was based on the methodical approach to loader automation, which can also be used in other machines working in cycles [14].

At the beginning the following assumptions were made:
- rationalisation of the loader should result from the automation of its steering,
- automated loader will also be steered manually by the operator,
- the operations of steering by the operator should be absorbing to such a degree as to keep his attention on the level of constant interest in the machine that is should not be dull or tiring.

Methodical solution of the set question consisted in a detailed analysis of the operation functions of the loader assigning them appropriate steering operations and classifying them, using appropriate evaluation criteria, to the group of automatically and manually steered ones. The tendency behind the classification was to obtain logical sequence of a few possibly simple operations for manual steering corresponding to natural habits of the operator, however absorbing his attention in order to make his work not monotonous and relatively interesting. In accordance with the aforementioned principles a detailed analysis of the operational activities of the loader working on the storage yard was conducted (Fig. 9, Fig. 10).

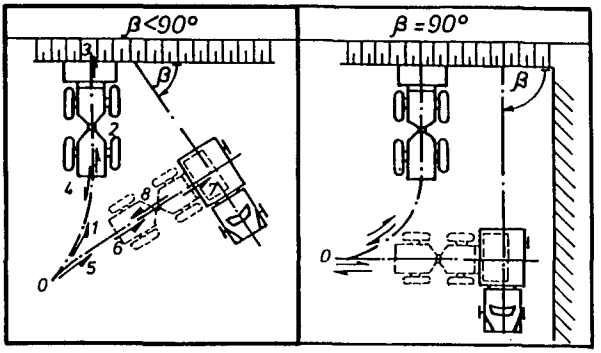

Fig. 9: Phases of the typical cycle of bucket loader in operation-machine's positions

On this basis its basic operation cycle was determined which was divided into successive phases and they were attributed appropriate functions of individual mechanisms and respective steering operations.

Steering operations, in turn, were divided into two groups:

- manual steering, simpler (e.g. keeping the driving track, change of engine rotations) and especially important in the operation (e.g. steering the brakes in case of safety requirements).
- automatic steering in the system coupled in such a way that one operator's motion initiating the main operation starts programmed sequences of steering operations (e.g. the change of driving direction, positioning of the extension arm and the bucket, the change of gears).

On this basis the system was designed which carried out the above operations. The system was integrated with the system of automatic scooping of the bucket (Fig. 8).

Thus designed the system of automated steering of a working unit and a gear box was tested on Ł 220 loader manufactured by FMB FADROMA. The results of test were satisfactory which will be shown in a video film including the system for automatic scooping of a bucket on a bucket loader.

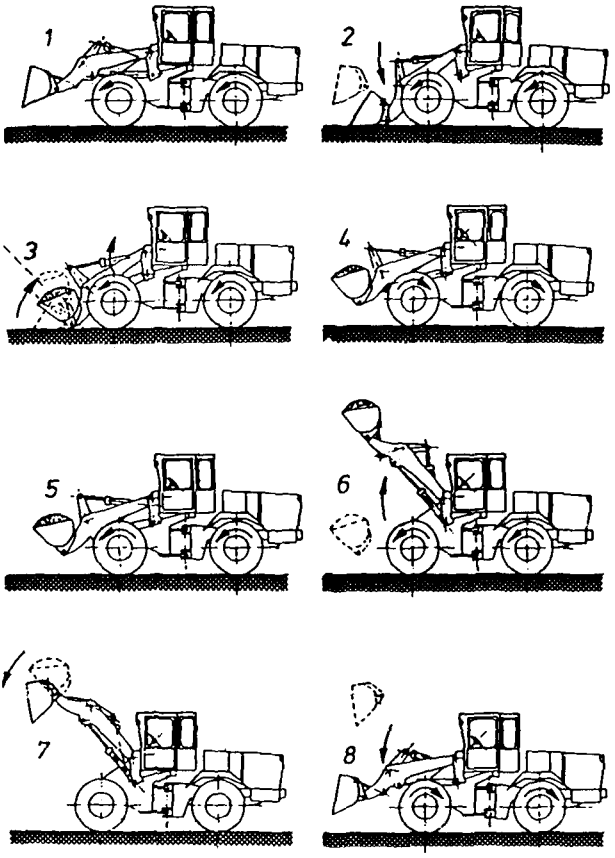

Fig. 10: Phases of the typical cycle of bucket loader in operation-working units position: 1- access to the scooping place, 2- position to scoop, 3- scooping, 4- withdrawal after scooping, 5- access to the emptying area, 6- position to empty the bucket, 7- emptying, 8- withdrawal after emptying.

4. MACHINE STABILITY IN OPERATIONS

The problem of stability and operation safety of a construction machine is one of the most significant performance indicators. A construction machine is regarded as stable when, in most inconvenient conditions, all its four wheels do not lose contact with ground, that is when ground's all normal loads acting on wheel, are greater than zero [15] [16]. The criterion of stability loss of a construction machine has been assumed to be such a dynamic state of a machine in which one of the normal loads of wheels is close to zero, or in extreme case is equal to zero (for a machine at a standstill). The stability of a wheeled machine depends on a number of factors. The main ones are: geometry and design of steering system (for example an articulated frame steering vehicles, or machine with steered wheels), the angle of grounds slope and the angle of machine's position on ground, the angle of machine's steering, the location of the centres of gravity of machine's units, the location of an articulation joint and pendulum joint, and finally, primary and secondary loads (Fig. 11).

Instationary movement of machine's working part, starting, braking and running at low speed over rough ground bring about additional dynamic loads which also affect stability.

Operating construction machines under hard conditions such as slopes, for example, may as it has been noted in practice lead to the overturn situation frequently followed by rolling over (Fig. 12).

Standard cabins on construction machines, which are, basically, to protect an operator against weather conditions, dust or noise are usually crushed when a machine overturns. In effect, overturn accidents involve heavy injuries or even death of an operator, considerable damages to equipment and cause danger to the people working nearby.

To increase operating safety of construction machines, the manufactures of these machines are to observe the regulations and norms specifying the concrete demands with regard to the structures protecting an operator. As an example, the international norm ISO 3471-1980 and, also, the Polish Norm PN-84/M-47024/02 require the reinfored cabin of ROPS (roll over protective structures) to be incorporated in construction works equipment, which significantly reduces the danger to an operator in an overturn accident [17].

In some countries, for example in West Germany, as additional protective measures special seats with a safety belt mounted on two points are introduced. Such systems, give only a partial protection to an operator in

an overturn accident, do not actually prevent the machine from losing its stability [18].

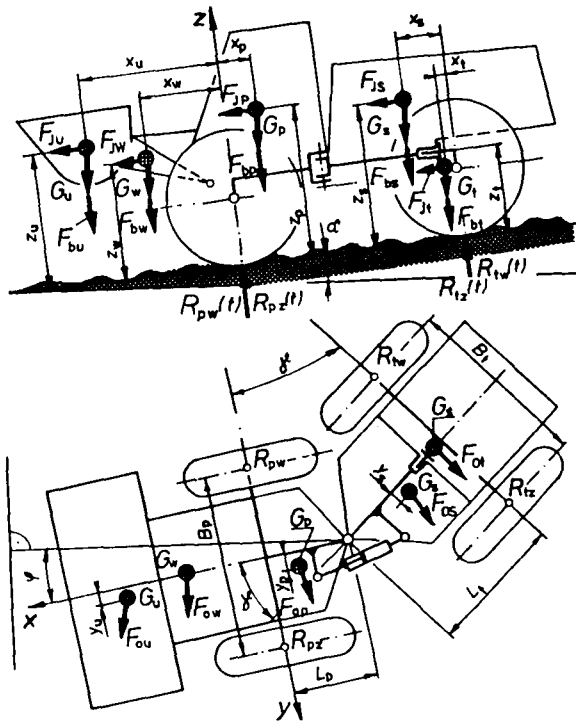

Fig. 11: The design and loads schematic for an articulated frame steering vehicle on slope ground

Unlike the so called passive safety system for construction machines presented earlier, the protection system designed at the Institute of Machine Design and Operations Research, Technical University of Wroclaw provides active protection [19] [20] (Fig. 13).

The system involves permanent automatic control over the loads normal to all the wheels.

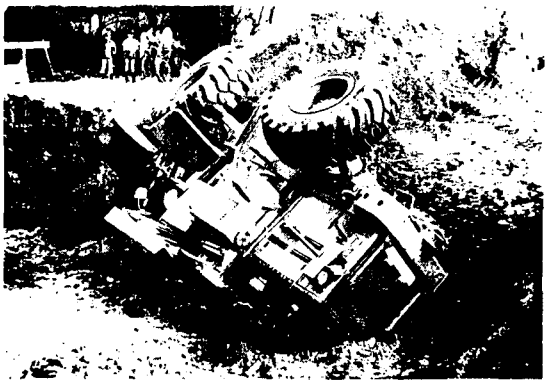

Fig. 12: The example of a complete stability loss in a loader during operation

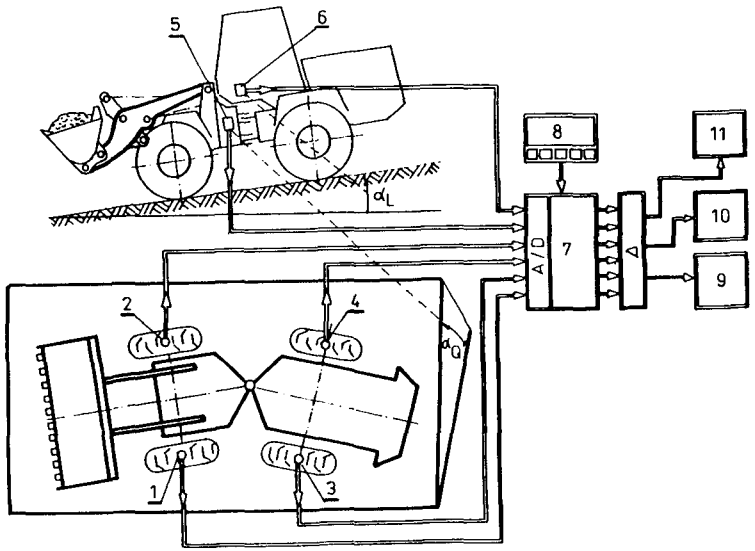

Fig. 13: Automatic control system of stability, capacity and automatic determination of real efficiency of wheeled bucket loaders: 1,2,3,4- the sensors of normal loads on a machine's wheels, 5,6- base inclination converters, 7- microprocessor, 8- set of switches e.g. nominal capacity, 9- warning signalliser, 10- numerical indicator, 11- printer

Force sensors 1,2,3,4 react to the value of normal load on the wheels of construction equipment. When one of the machine's wheels has a normal load close to zero, the warning signalliser is automatically switched on. This informs the machine's operator well in advance of the danger of the machine losing its stability, so a driver has time to prevent the accident. The system also makes it possible to estimate the current efficiency of a machine. Permanent control of machine's stability allows increasing its carrying capacity which, in effect, means increasing its real efficiency.

5. EFFICIENCY OF THE CHASSIS MECHANISMS

Kinematic discrepancy often occurs in the driving mechanisms of mobile 4WD machines (which the drive achieved by driven shafts).

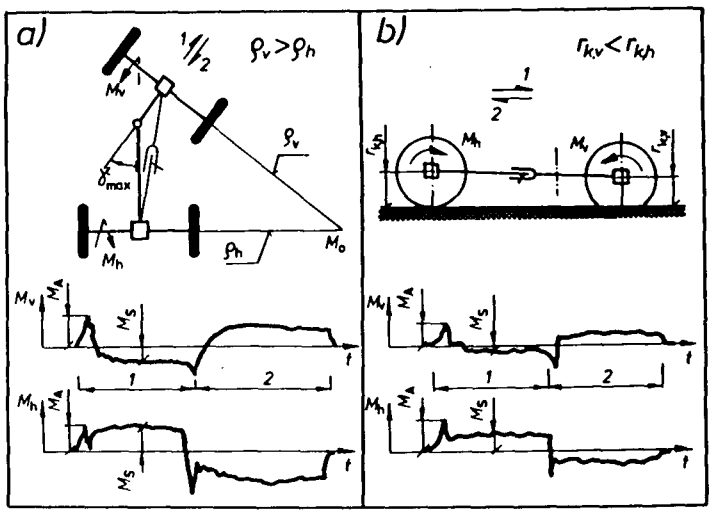

Fig. 14: The moments on the halfaxles of an articulated body steer construction machine running on dry concrete [23]:
a) with maximum articulation angle (γ=0.7 rad),
b) straight running (γ=0), the difference in front and rear wheels radii Δr=0.03m, 1- travelling forwards, 2- travelling backwards, M_S- starting moments, M_U- moment in fixed motion.

It results from the difference of tyre deflection, difference of the covered distances, axles, and while turning at standstill of the articulated machine, from the difference of rolling direction, of the wheels of both axles. Kinematic discrepancy brings about additional wheel slips and negative effects in driving mechanisms leading to the increase of resistances and energy loss as well as wear of driving elements and tyres [21] [22] (Fig. 14, Fig. 15).

These discrepancies can be eliminated by uncoupling of the machine drive axle in good time, which in the hitherto existing practice has not been conducted in time at manual operation [23] [24] [25].

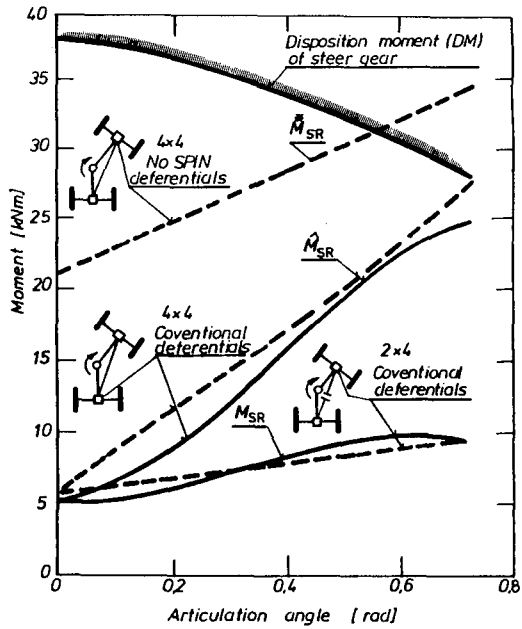

Fig 15. Disposition moment (DM) and steering resistance moments (M_{SR}) on concrete for articulated frame steer loader (total weight of machine 102.5 kN, tyres 17.5-25) vs articulation angle for various of differential gears and axles coupling with driving shaft, ——— calculation, ---------- in situ measurements [22]

Therefore the authors suggest the elimination of these phenomena by automatic uncoupling of the machine drive axles in the moment when kinematic discrepancy appears. For this purpose it is necessary to conduct a permanent measurement of displacement values and directions of the both drive axles (Fig.16).

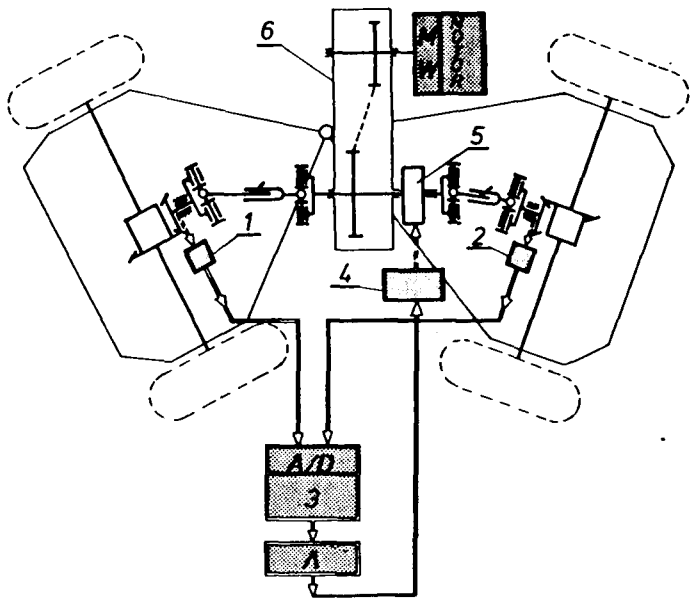

Fig. 16: The system for automatic uncoupling of the drive axles in mobile construction machine 1,2- displacement sensors, 3- microprocessor, 4- electrical control valve, 5- cluth, 6-driving gear

The displacement differencies, which occur in the moment of the kinematic discrepancy in driving system give a signal to the electro-mechanical system which is switched on in order to uncouple or couple the axles. In case of the turning at the standstill of the articulated machines the moment of switching of the driving mechanism is the signal for the automatic uncoupling of the axle.

REFERENCES

1. G.Kühn, Automatisierung der mobilen Baumaschinen eine Zukunftsperspektive, BMT, No. 8, 1984.
2. P.Dudziński, Einsatzoptimierung der mobilen Baumaschinen durch die Anwendung der Mikroelektronik (not published), Institut für Maschinenwesen im Baubetrieb, Universität Fridericana Karlsruhe, Juli 1985 .
3. Z.Wysłouch, Tendencies and Prospects for Development of a Loader in Poland (in Polish), Przegląd Mechaniczny, No. 20, 1985.
4. Baumaschinentechnik, Fortschritte durch Mikroelektronik und Automatisierung. Tagung Baden-Baden, 21 und 22 März, 1990.
5. W.Poppy. Automation and Robotics in Construction, 8th International Symposium on Automation and Robotics in Construction. 3-5 June 1991, Fraunhofer - Institute IPA/IAO, Stuttgart.
6. P.Dudziński, K. Pieczonka, Basic Problems of Designing New Generations of Mobile Construction Machines (in Polish), Raport No. 23/91, IKiEM, Technical University of Wroclaw.
7. K.Pieczonka, P. Dudziński, The Problems of Scooping the Bucket Loader (in Polish), Górnictwo Odkrywkowe, No. 4, 1994.
8. A.Lasmanowicz, K.Pieczonka, Studies on the Process of Scooping the Bucket with Rock Material (in Polish), 5th Conference: "Problems of Mining and Processing Rocks", AGH, SMGKG, PAN, STTG, Kielce 1988
9. K.Pieczonka, Z. Wysłouch, Probleme der Automatisierung des Schaufelfüllvorganges am Radlader, XIII. Internationale Konferenz „Mechanisierung im Erdbau", Dresden 1988.
10. P.Dudziński, K.Pieczonka, Z.Wysłouch, Automation of Bucket Loaders (in Polish), Mechanizacja i Automatyzacja Górnictwa, No.1, 1992.
11. P.Dudziński, K.Pieczonka, Z.Wysłouch, Automation of Working Unit on a Bucket Loader, The Eleventh International Symposium on Automation and Robotics in Construction. ISARC'94, Brighton, U.K. 24 May, 1994.
12. P.Dudziński, K. Pieczonka, J. Włodarczyk, Studies on the Signal Initiating the Scooping Process of a Bucket on a Loader, (in Polish), Report No. S-057, IKiEM, Technical University of Wrocław.
13. P.Dudziński, K.Pieczonka, Z.Wysłouch, Problems of Automation in Scooping the Bucket on a Bucket Loader (in Polish), Research Papers of IKiEM of Technical University of Wrocław, Conference Series, 1991.

14. Z.Wysłouch, How to Automate Earth Moving Machines (in Polish), Papers of the Institute of Machine Performance in Civil Engineeing and Rock Mining, No.3, Warszawa 1988.
15. K.Pieczonka, Analytical Methods for Determining the Design and Operating Parameters for Self-propelled Machines with Articulated Frame Steering (in Polish). Prace Naukowe Instytutu Konstrukcji I Eksploatacji Maszyn Politechniki Wrocławskiej, No. 31, 1976.
16. P. Dudziński, K. Pieczonka, The problems of In-service Stability of Wheel Bucket Loaders with Respect to Providing Active Safety of Operations (in Polish). The 2nd Conference "The Problems of Construction Equipment Design". OBRMZiT HSW Stalowa Wola, September 1988.
17. Polish Norm PN-84/M-47024/02; Earth-moving machinery, roll-over protective structures, requirements and laboratory tests.
18. J.Speck, Überrolschutzaufbauten und Schutzdächer für Erdbaumaschinen. BMT, Juli 1979.
19. P.Dudziński, K.Pieczonka, The Method and System of Preventing a Wheeled Vehicle from Overturning. Patent.
20. P.Dudziński, K.Pieczonka, Automatic System of Warning and Preventing a Machine from Losing its Stability in Wheeled Construction Machines. International Symposium and Construction Machines, May 1989, Magdeburg/Berlin.
21. P.Dudziński, Design Characteristics of Steering Systems for Mobile Wheeled Earthmoving Equipment. Journal of Terramechanics, Vol.26, No. 1. pp 25-82.
22. P.Dudziński, Vergleich verschiedenen Lenksysteme bei geländegängigen Maschinen mit Radfahrwerken und verschiedenen Antriebsarten. Manuskript der Habilitation, TU Dresden, 1990.
23. P.Dudziński, K.Pieczonka, Automated Devices to Eliminate Undesirable Performance in Mobile 4 WD Construction Machines. 8 th International Symposium on Automation and Robotics in Construction. 3-5 June 1991. Fraunhofer - Institute IPA/IAO, Stuttgart.
24. P.Dudziński, K.Pieczonka, and J.Zięba, Selbsttätige Anlage zur Enkupplung der Antriebsachsen. Patent.
25. P.Dudziński, Anlage für die Reifenschlupfbeschränkung im Lenkvorgang eines Fahrzeugs mit Knicklenkung. Patent

Parallel Tests with a 6 and 7 Roadwheel Tracked Vehicle

Colonel Dipl.Ing. Andrä ENGELER

Military Technology Agency, Vienna, Austria

Abstract:

In the course of the developement of the infantery fighting vehicle "ASCOD", the Military Technology Agency carried out mobility tests in autumn 1993. The test objects were the infantery fighting vehicle prototypes ASCOD PT3 with a set of 7 roadwheels (each side)and ASCOD PT2 with a set of 6. The purpose of the test was to assess the advantages and disadvantages of a 7th set of roadwheels.

Test programme:

- Configuration
- Dimensions
- Load and Pressure
- Cross Country Capability
- Speed and Braking Capability
- Steering
- Traction
- Rolling Resistance
- Noise
- Prestabilisation Ability.

1. General

Special conditions:

There was only one turret available. The checks of pressure, dimensions and load were carried out with turret on both vehicles, the other tests were carried out with a dummy instead of turret on PT2. The vehicles were ballasted to combat weight.

Test locations:

Steyr Spezialfahrzeugfabrik	Vienna
Liechtensteinkaserne	Allentsteig
Army training aerea	Allentsteig
Empty water reservoir	Allentsteig

2. Configurations

PT3:

7 sets of roadwheels,
3 double support rollers,
hydrodynamic buffers at the roadwheel sets number 1,2 and 7,
friction dampers at the roadwheel sets number 1,2 and 6,
ground contact length 3,990 mm
combat weight 27,650 kg
engine power 444 kW

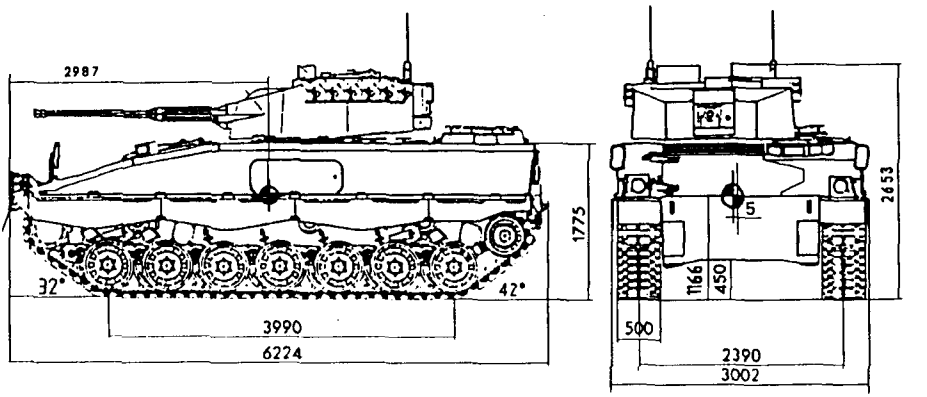

PT2:

6 sets of roadwheels,
4 single support rollers,
friction dampers and hydrodynamic buffers
at the roadwheel sets number 1,2 and 6,
ground contact length 3,697 mm
combat weight 27,340 kg
engine power 441,000 W

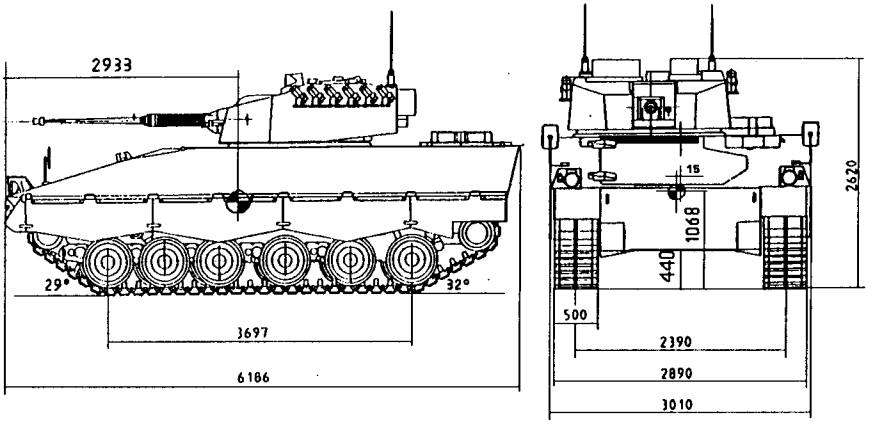

The weight of all crew members and the equipment was simulated with sandbags, so the center of gravity under combat conditions may be slightly different.

3. Roadwheel Load and Force Distribution

This figure shows the load on the different roadwheels. The load of the 7th roadwheel (left side) of PT3 was only 600 daN, due to a missaligned torsion–bar.

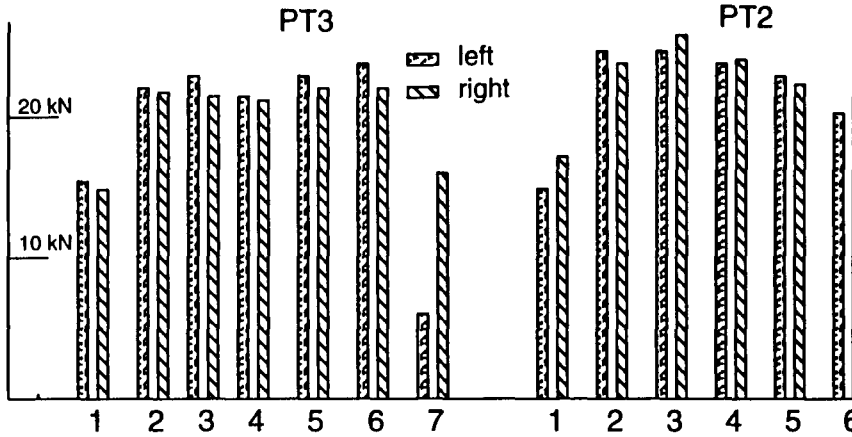

Fig. 3.1 Roadwheel load distribution

This figure shows the vertical force (daN) under each track pad.

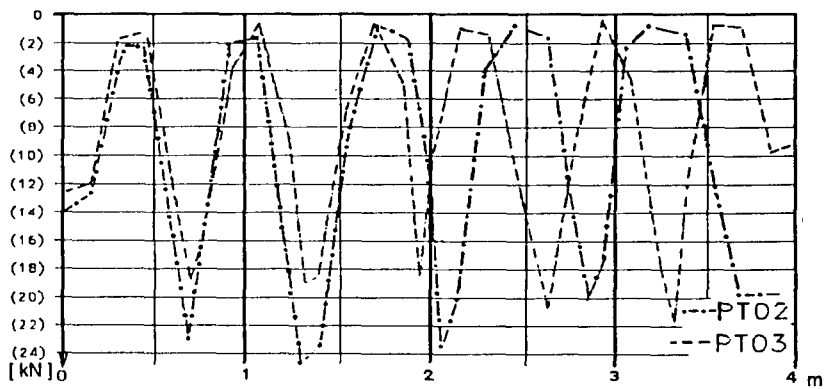

Fig 3.2 Force distribution vs contact length

4. Mean Maximum Pressure

To calculate the mean maximum pressure, Rowland proposed the following equation:

$$MMP = \frac{1{,}26\ W}{2n\ A\ b\ \sqrt{t\ D}}\ kPa$$

W = vehicle weight (kN)
n = number of wheels of one track
A = rigid aerea of link (proportional)
b = track width (m)
t = track pitch (m)
D = diameter of roadwheel (m)

PT3:

$$MMP = \frac{1{,}26 * 9{,}81 * 27{,}65}{2 * 7 * 0{,}5\ \sqrt{0{,}154 * 0{,}58}} = 163\ kPa$$

PT2:

$$MMP = \frac{1{,}26 * 9{,}81 * 27{,}34}{2 * 6 * 0{,}45\ \sqrt{0{,}154 * 0{,}58}} = 209\ kPa$$

5. Cross Country Capability

On hard ground and artifical obstacles, the following values were mesasured

trench crossing: **2.5 m**

vertical step: **0.8 m**

On an off–road training field the following values were measured:

gradient climbing: **68%**

side slope performance: **40%**

This obstacles were negotiated with both vehicles and there was no significant difference between PT3 and PT2.

6. Offroad Mobility (subjective observation)

This check was carried out on a real offroad course with different slopes, curves and a muddy ditch. There were no significant differences in speed and manouverability, but we found, that the PT3 had the better tuned suspension.

7. Speed and Acceleration

Acceleration (on concrete)
On concrete surface there was no significant difference between prototype 3 and prototype 2.

500 m Acceleration

PT3 in 39.6 seconds from zero

PT2 in 39.9 seconds from zero

We assume that the difference in the results is not due to the different number of roadwheels.

Acceleration (soft terrain)

Location: . Kühbach
On soft terrain a 500 m distance was not available, therefore the distances were reduced according to the local situation.
Conditions: ploughed dry field, two laps in opposite directions

time in seconds

	PT3	PT2
50m	11.9	12.0
	13.9	13.6
150m	22.1	23.6
	35.9	34.2

Location: . Mannshalm
Conditions: mowed dry field, gradient 6%

time in seconds

	PT3	PT2
50m	9.4	9.6
100m	16.7	17.0

8. Braking

After having observed incorrect speedometer readings, a deceleration check was carried out with stopwatch .

Speed	Mean Values		
	Distance	**Time**	**Deceleration**
PT3			
36 kph	**8.68 m**	**1.8 sec**	**5.64 msec^{-2}**
49 kph	**18.95 m**	**2.8 sec**	**4.88 msec^{-2}**
PT2			
32 kph	**6.90 m**	**1.5 sec**	**6.12 msec^{-2}**
49 kph	**17.42 m**	**2.8 sec**	**4.49 msec^{-2}**

9. Steering Circles

(first gear)

Steering circles on hard ground:

12m to 13 m
at 2400 rpm

12m to 13 m
at 1500 rpm .

Steering circles on gravel (sandy):

14 m at 2400 rpm

14 m at 1500 rpm

Note: Both vehicles gave nearly the same results. On hard ground the pressure in the hydraulic system was 260 to 300 bar, on gravel 240 to 260 bar.

10. Pivoting

Both vehicles have very good pivoting ability,
there is no horizontal offset while pivoting.

Pivoting checks were performed

at 2,400 rpm engine speed,
on concrete and gravel,
clockwise and counterclockwise.

pivoting circle diameter:	**7 to 8.5 m**
time for full turn:	**8 to 10 sec**
pressure in the hydraulic:	**330 bar**

11. Traction

Measured as drawbar force with dynamometer.

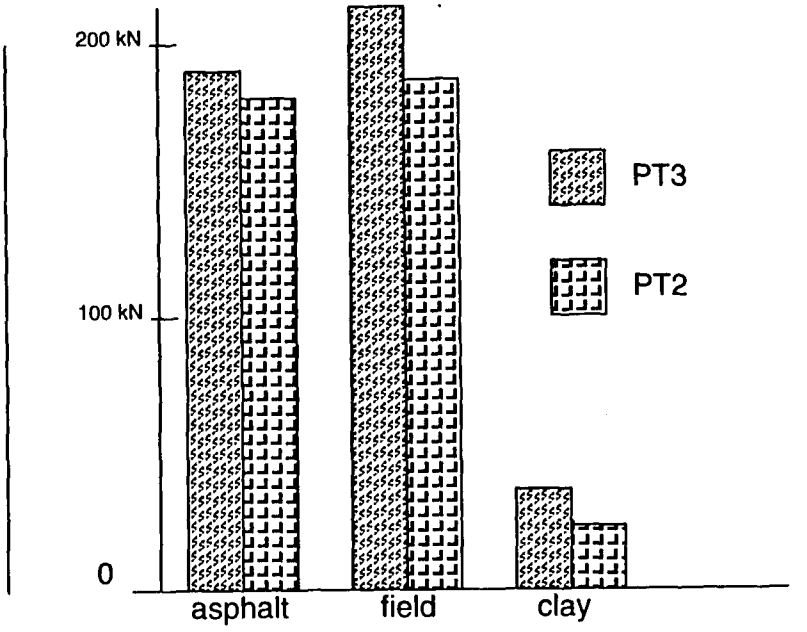

12. Sinkage on Soft Ground

PT3

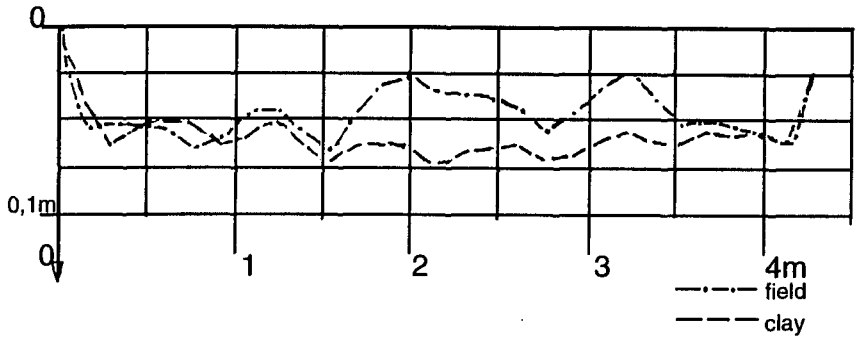

PT2

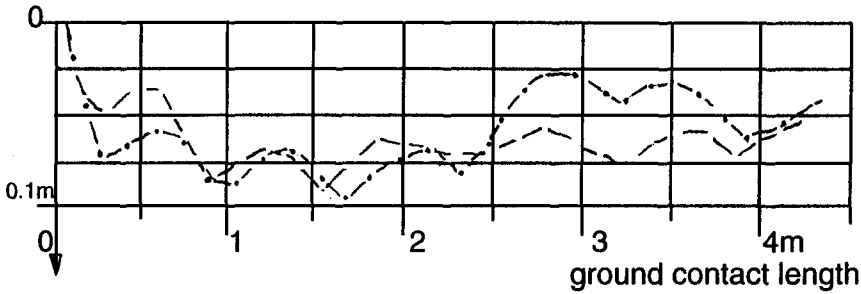

On soft ground the most important element of the rolling resistance is the deformation of the soil.
It is influenced by:

- soil condition
- ground pressure
- number of roadwheels
- roadwheel distance.

Both vehicles differ in:

- ground pressure
- roadwheel number and
- roadwheel distance.

13. Rolling Resistance

On soft clay we found a great difference between PT3 and PT2. The advantages of the increase of ground contact length and the better force distribution are decisive in soft ground conditions.

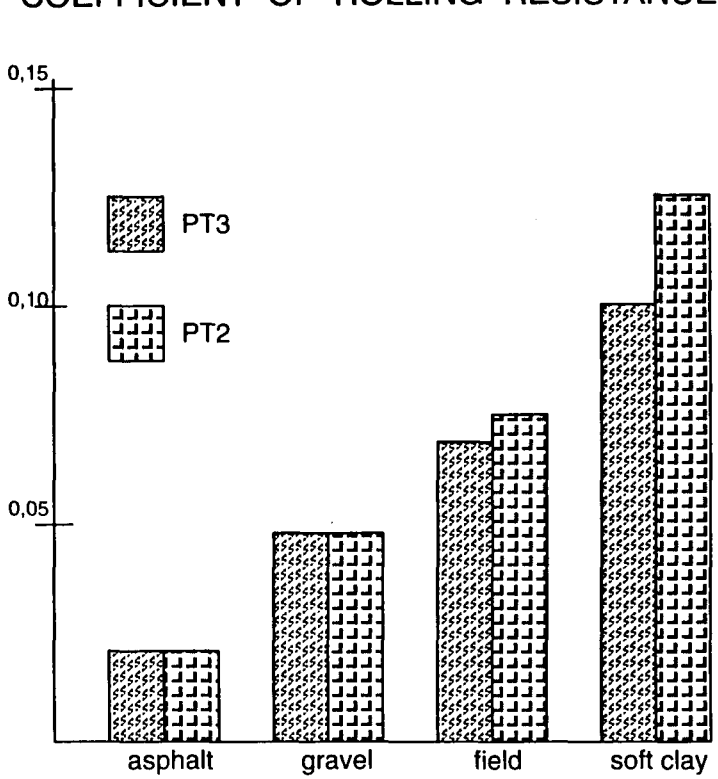

There is a "multi–pass situation", and the sum of the rolling resistances of all road–wheels is the whole rolling resistance. The deformation caused by the first wheel might be nearly the same in both vehicles. The additional deformation you can see is proportional to the displaced volume between track and horizontal ground aerea. If we assume a nearly parabolic shape of the track deflection, the volume is approximately :

$$V = 2/3 * l * b * h * (n - 1)$$

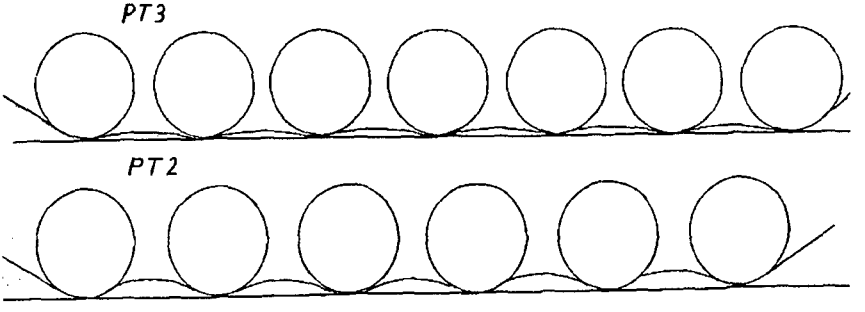

	PT3	PT2
V = displaced volume	**0.013**	**0.020**
l = wheel distance (mean)	0.660	0.740
b = track width	0.450	0.450
h = deflection	0.011	0.018
n = number of wheels	7	6

(dimensions in meters and cubic meters)

Note:
In this comparison, the rolling resistance is proportional to the displaced volume

14. Prestabilisation Ability

After tuning of the damping and suspension system (the position of the friction damper was changed from the 7th to the 6th set of roadwheels) at the APG–course, the pitch angle was reduced at all speeds.

pitch angle (mrad) versus time (seconds)

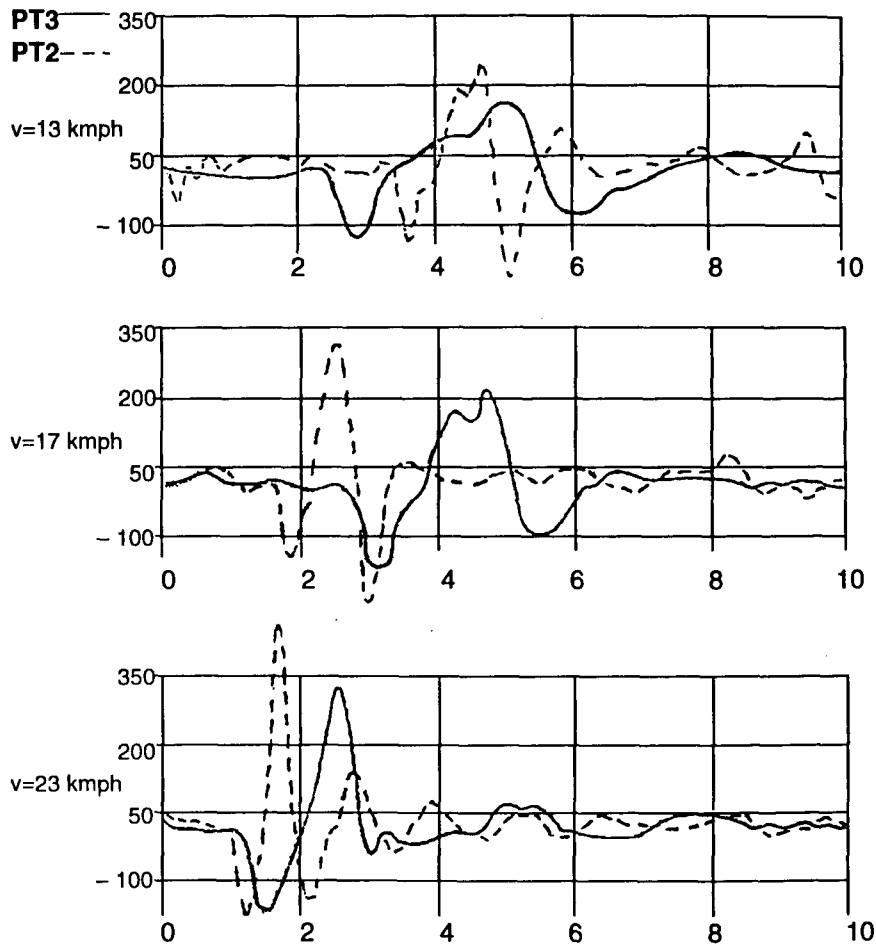

Summary

The parallel test of the prototypes 2 and 3 of the ASCOD showed the advantages of the 7th roadwheel set, especially on soft ground like clay. In another test in Norway the same effects were observved on snow. The modification was not simply the addition of a 7th set of roadwheels; the suspension was tuned, too. Besides the cost of the additional elements a small problem was found. The close spacing of the wheels made it nececcary to mount the wheel arms in such a way that they turn in the same direction, so the vehicle sometimes had pitch problemes. The ground clearance of the vehicle front and rear was not always the same. In conclusion we can say that the modification from PT2 to PT3 was sucessful and resulted in a remarkable increase of off–road mobility.

FE-Simulation of Tyre-Profile-Effects on Terrain Mobility of Vehicles

C. Wolfgang Fervers
Institute of Automotive Engineering (IKK)
- Prof. Dr.-Ing. I. C. Schmid -
University of the Federal Armed Forces Hamburg, Germany

ABSTRACT

Many simulation-models have been established to predict the terrain-mobility of vehicles. Among the models describing the tyre-soil interaction the tyre profile effects are rarely considered. At the IKK a new FEM based simulation model which includes the tyre profile effects has been developed. In this article the new model is introduced. First simulation results are presented an discussed. It can be seen that the simulation results concerning soil deformation, traction forces and slip-sinkage correspond well with natural observations. The new model is able to simulate effects of wheel-soil interaction which are not considered in any other model.

1 INTRODUCTION

Terrain vehicle mobility on soft soil is not only a military aspect but as well important for earthmoving and farming processes. For the prediction of terrain vehicle mobility it is necessary to know something about the effects of land locomotion. Those effects are often investigated by experiments. As a disadvantage experimental testing means high costs and time expenditure, or sometimes is not even possible. Therefore models have been elaborated which simulate the effects of land locomotion and allow a prediction of terrain vehicle mobility. Among others the models describing the interaction between the wheel and the soft soil are of great importance.

Although these models have been improved over the years, there is still a demand for higher performanced models. The influence of the tyre profile on traction has not been investigated by simulation so far. In recent time with the increase of computer capacity the Finite-Element-Method has turned out to be a capable mean for the simulation of wheel-soil interaction. In this a great potential can be seen for extending the simulation facilities by tyre profile effects.

2 STATE OF THE ART

Regarding the existing models the tyre profile effect is rarely considered. In the well known BEKKER-model [1] in connection with the JANOSI-model [2] the tyre profile is neglected and the circumferential forces are purely calculated from the shear stresses in the soil. Up to now in analytical models the tyre profile has only been taken into account for the calculation of the slip-dependent sinkage [3]. In contrast to that, tests by HOLM [4] and SCHWANGHART et al. [5] have shown a considerable influence of the tyre profile on traction.

First FEM based simulations of tyre profile effects were made by REGLI et al [6]. Hereby the tyre is not modelled entirely but replaced by stepwise displacements of loads, fig. 1. For that reason the interaction has no real rolling contact and as a matter of fact cannot represent a free rolling wheel with a wheel load. The loads and displacements in that simulation were calculated from experimental tests and estimated before the simulation. The interaction is only shown for small displacements within the track, fig. 2.

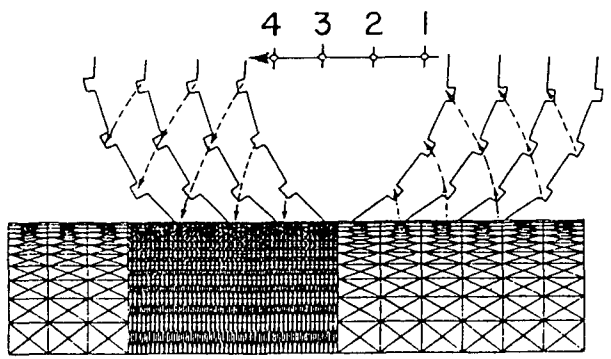

Fig. 1: Incremental load for 10% slip [6]

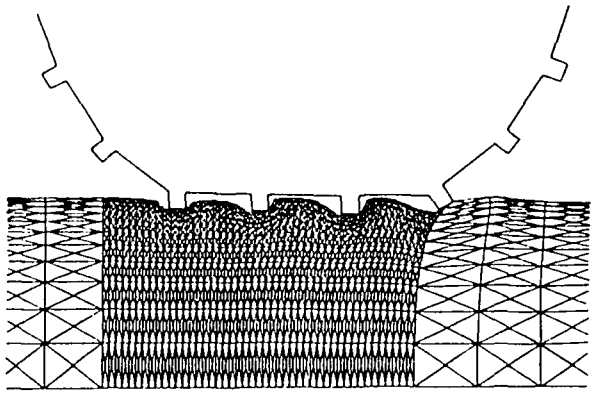

Fig. 2: Soil deformation after 4th load step with 10% slip [6]

The FEM simulation model VENUS developed at the IKK by AUBEL [7] is the first model showing a real rolling contact and the movements of a free rolling wheel, fig. 3.

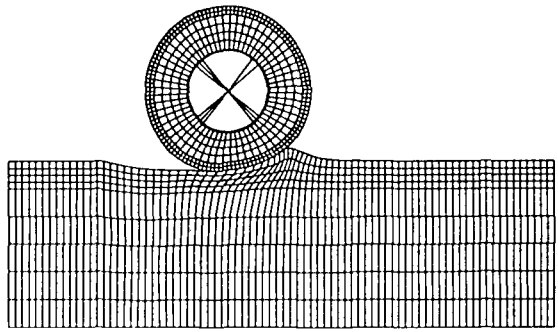

Fig. 3: Simulation model VENUS [7]

In this model the interaction is not governed by values gained from tests and observations as in the case of other FEM-models. The calculation is only based on tyre and soil parameters and the given loads. Therefore VENUS proved to be the most useful model for further investigations. The tyre profile is not yet considered.

3 THE NEW MODEL

Based on the results of VENUS a new simulation model is being worked out for the investigation of tyre profile effects on traction.

3.1 The wheel model

To minimise computer capacity for the first steps, the wheel is built up of a rigid disc which has a regular profile, fig. 4. The actual wheel load is placed as a force "F_Z" at the axle of the wheel. The wheel is free movable in plane. A horizontal velocity "v" as well as a rotational velocity "ω" can be constrained to the wheel without affecting the vertical displacement "z".

The tyre profile simulated here has a symmetrical geometry with 40 lugs. The ratio positive/negative-profile is 1. The orientation backward/forward is equal. The tyre has a diameter of 1200 mm. Different profile shapes are generated by changing the height of the lugs. A height of 10 mm is doubled to 20 mm and halved to 5 mm. A height of 0 mm is generated to represent a tyre with no profile.

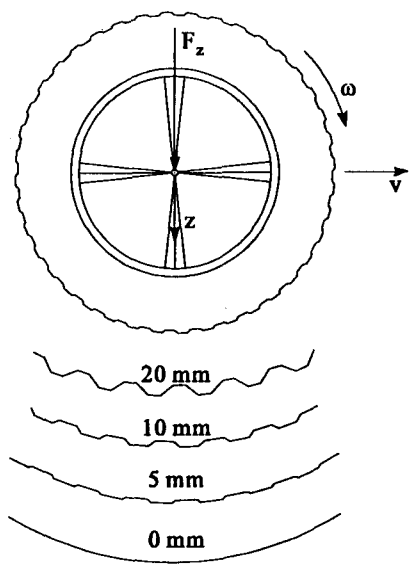

Fig. 4: Wheel model

3.2 The soil model

The soil is generated by a FEM mesh which is refined in the contact zone of wheel-soil interaction. The soil behavior is represented by an elastoplastic behavior [8]. The plastic material law is based on the constitutive model of Drucker-Prager modified by the dilatation behavior. By this modification a consolidated loam can be described with a dilatation angle of 0° [7].

A soil bin with a length of 8000 mm and a depth of 1200 mm is represented here, fig. 5. The wheel-soil interaction is possible for a distance of up to 5000 mm.

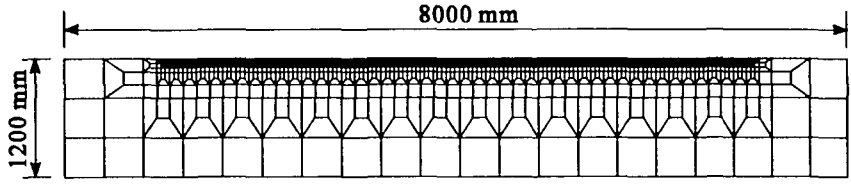

Fig. 5: Soil model

Two different loams with the following data were used

	loam 1	loam 2
E modulus:	8 N/mm²	8 N/mm²
Poisons ratio:	0.3	0.3
friction angle (Mohr-Coulomb):	27.5°	15°
cohesion (Mohr-Coulomb):	0.02 N/mm²	0.02 N/mm²
density:	1.9 kg/dm³	2.5 kg/dm³

3.3 The interaction model

In this model the interaction between the tyre and the soil is made up of a mathematical restriction. The surface nodes of the soil mesh are not allowed to pass through the surface lines of the tyre mesh, fig. 6.

Hereby the factor of surface friction "μ" between soil nodes and tyre surface lines is considered to be $\mu = 0.1$

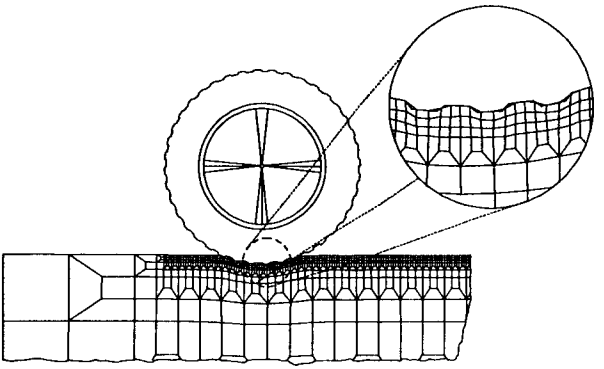

Fig. 6: Interaction model

As the tyre profile is periodically convex and concave, some lines of the soil mesh may overlap the tyre surface. Geometrically this seems to be not absolutely accurate. But as the simulation only considers the nodes of the soil mesh for the contact calculation the solution is still correct within the accuracy of element length.

Like it is in VENUS this model provides the soil deformation, the pressure distribution and the reaction forces and moments as a result of the simulation. As input data only the soil and tyre parameters and the wheel loads must be given.

3.4 The simulation proceeding

The effects of tyre profile are strongly influenced by the slip. For that reason the simulation was carried out with a slip controlled driving. In every simulation run the tyre was driven with constant slip over a distance of 5000 mm. For every profile the simulation was executed with -20%, -10%, 0%, 10% and 20% slip.

The slip "s" is defined as:

$$s = -\frac{v - u}{v} \quad \text{with} \quad v > u \qquad \text{and}$$

$$s = \frac{u - v}{u} \quad \text{with} \quad u \geq v$$

with s = slip
v = horizontal velocity
$u = \omega r$
ω = rotational velocity
r = radius of the wheel

v and ω are measured in relation to a fixed co-ordinate system.

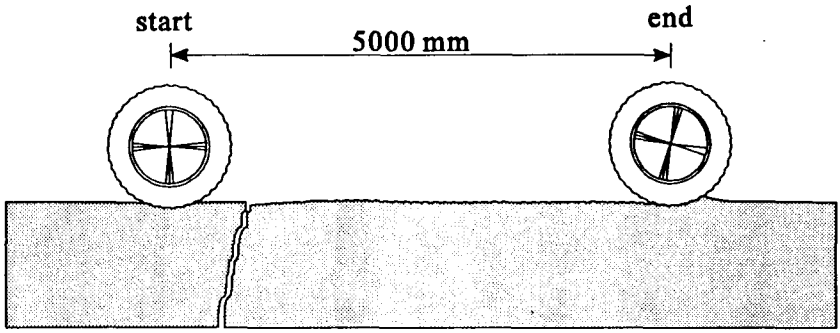

Fig. 7: Start and end of simulation run

4 SIMULATION RESULTS

With the above described new model some simulation runs have already been made. The results will be presented and discussed in the following with regard to the soil deformation, the traction forces and the sinkage.

4.1 The soil deformations

A profiled wheel rolling over a soft ground normally leaves a rut in the soil. The simulation model represents this behavior in good quality. With a slip of 0%, fig. 8, the trace is nearly an exact print of the tyre profile. The distance between the gaps in the soil "Δt_S" is the same as the distance of the lugs "Δt_P". For higher slip the distance between the gaps in the soil becomes smaller. This is caused by the relative displacement between tyre and soil in the contact zone. The same effect could be observed in tests made by HOLM [4]. As it is expected the gap distance becomes larger with negative slip.

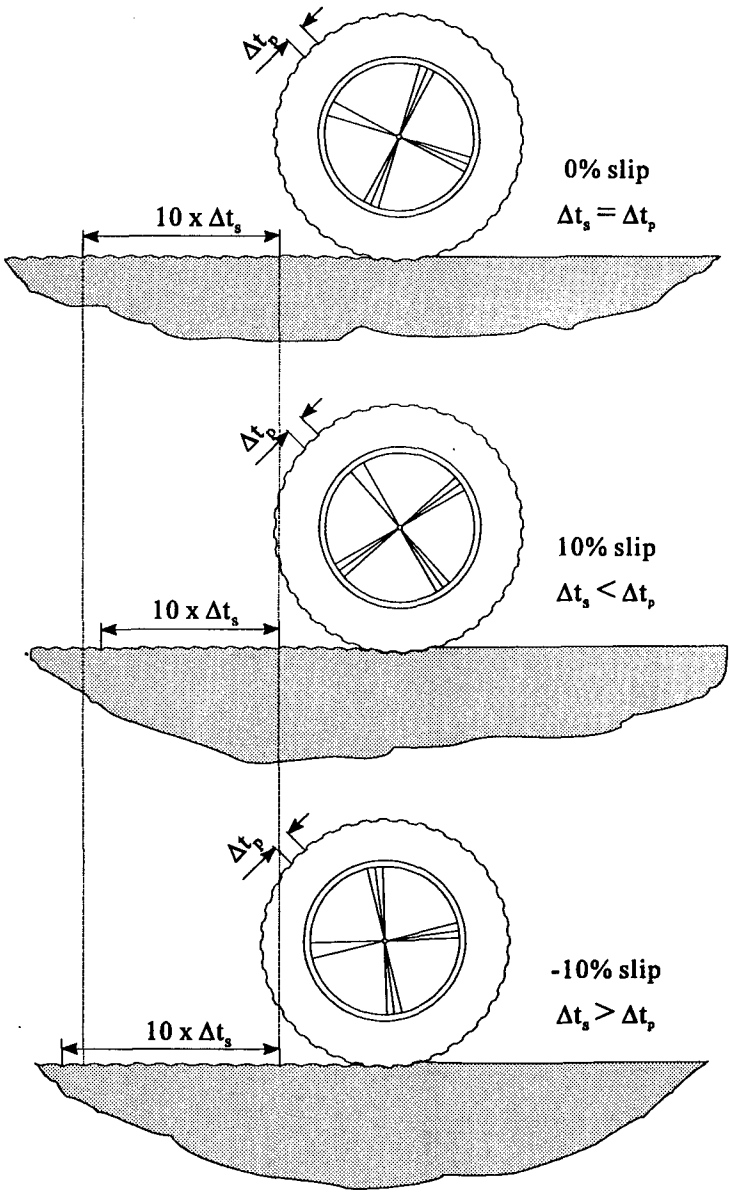

Fig. 8: loam 1, wheel load 20 kN, profile 10 mm

The gap distance in relation to the lug distance can be described with the slip equation like

$$s = -\frac{v-u}{v} = -\frac{\Delta t_s - \Delta t_p}{\Delta t_s} \text{ for } s < 0 \quad \text{and}$$

$$s = \frac{u-v}{u} = \frac{\Delta t_p - \Delta t_s}{\Delta t_p} \text{ for } s \geq 0$$

In general this behavior can be observed for all profiles and both soils. In special on softer soil and with higher slip the gaps become more unidentifiable, fig. 9.

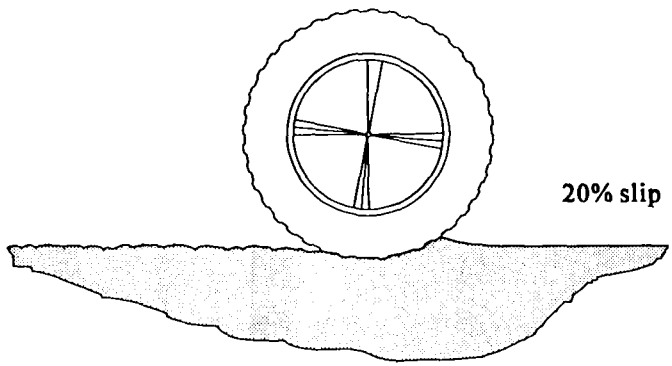

Fig. 9: loam 2, wheel load 23 kN, profile 10 mm

The contact zone of wheel-soil interaction is usually represented by the run-in angle "θ_1" and the run-out angle "θ_2". Fig. 10 shows these angles for different slip values on loam 2.

It is to be seen that the angle θ_1 is hardly dependent on the slip. This is explicable by the contrary influence of the sinkage and the bulldozing effect. A higher slip increases the sinkage and therefore the angle θ_1. In contrast to that, due to higher slip, more material is moved from in front of the wheel to the back, which makes the bulldozing effect and therefore the angle θ_1 decreasing. On the angle θ_2 both effects have common influence. The angle θ_2 increases with a higher sinkage as well as with a higher amount of material being moved from the front to the back.

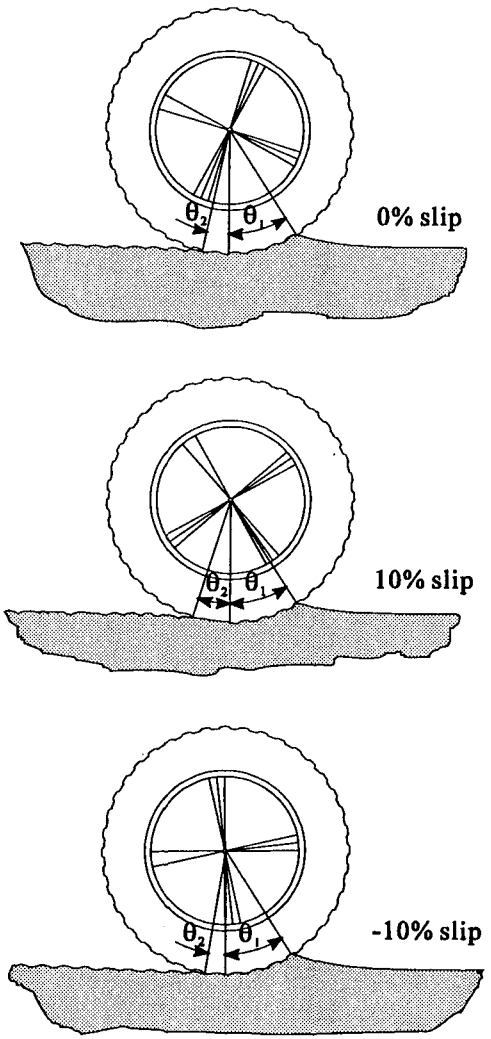

Fig. 10: loam 2, wheel load 23 kN, profile 10 mm

These effects are strongly dependent on the soil parameters and the wheel load. They may have a different quantity on other soils or with other wheel loads.

4.2 Traction forces

Characteristic parameters for terrain mobility are the drawbar pull "T", the circumferential force "U" and the rolling resistance "R", fig. 11. The simulation model provides values for the reaction force "F" which is the counter force to T and the reaction Moment "M". With the wheel diameter "D", "U" and "R" can be calculated.

$$U = \frac{M}{D/2}$$

$$R = U - T$$

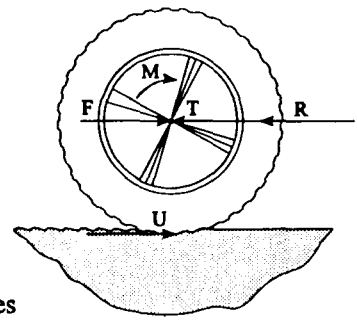

Fig. 11: Reaction forces

In the figures 12 to 14 the forces T, U and R are shown in relation to the slip for the different profile shapes on loam 1. As usual T, U and R are presented in relation to the wheel load.

With positive slip the circumferential force, fig. 12, for the tyre with no profile (0 mm) shows a maximum of 0.1 which is exactly the value of the considered surface friction between tyre and soil. As is expected the profiled tyres can transmit a much higher circumferential force. The difference in circumferential force between profiled and unprofiled tyres is larger than between the various profile shapes. This is strongly dependent on the factor of surface friction. In this simulation the surface friction coefficient between tyre and soil was assumed to be 0,1, which is low. In reality it might be higher. At negative slip the curves for the circumferential force are much closer together. The unprofiled tyre does not reach a minimum circumferential force up to the limit of -20% slip.

The drawbar pull shows the same tendency, fig. 13. The 0 mm profile can provide only a very small or even no positive drawbar pull. The gradient of the curves increases with the increase of profile height, which proves the influence of the profile on traction. According to the circumferential force the curves for the drawbar pull at negative slip are closer together.

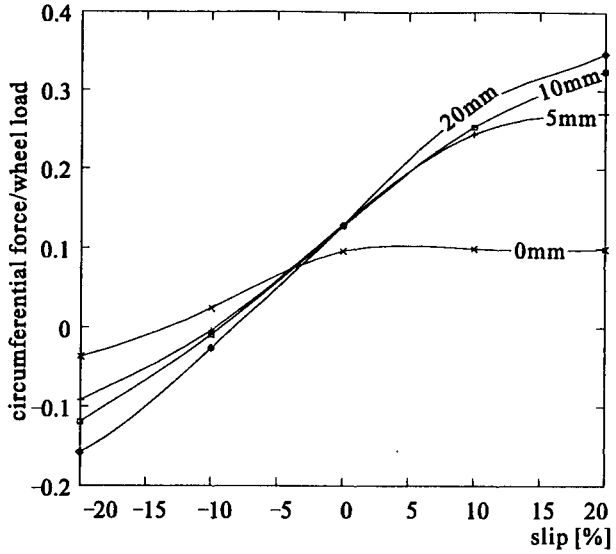

Fig. 12: Circumferential force over slip, loam 1, wheel load 20 kN

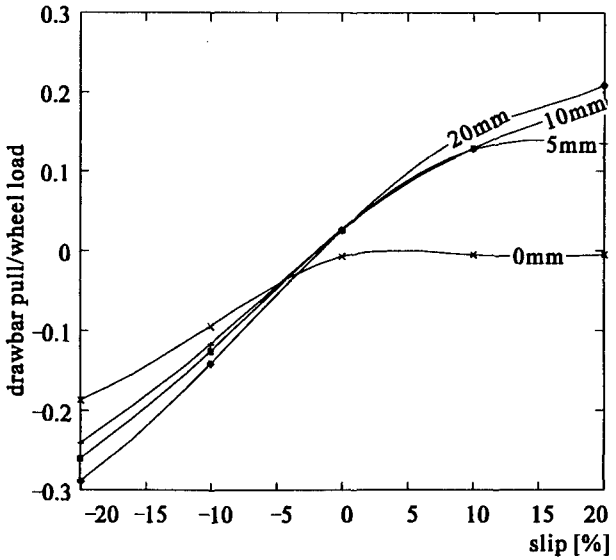

Fig. 13: Drawbar pull over slip, loam 1, wheel load 20 kN,

In fig. 14 the rolling resistance on loam 1 is shown. It can be seen that there is a minimum around 0% slip for all profile shapes. Up to positive slip rates the higher profile shows a larger rolling resistance, which is caused by the higher sinkage (see fig. 16). For negative slip the bulldozing effect becomes dominant. Therefore the 0 mm profile has the highest rolling resistance, because it is not able to reduce the bulldozing wave by moving material to the back.

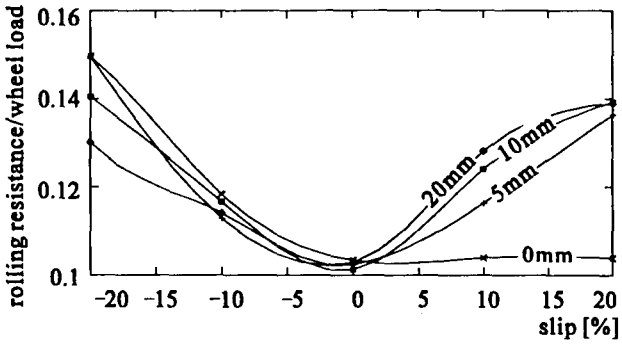

Fig. 14: Rolling resistance over slip, loam 1, wheel load 20 kN

The influence of the bulldozing effect can be underlined by the rolling resistance on loam 2, fig. 15. Here the bulldozing effect even occurs with positive slip (see fig. 9). Therefore the 10 mm profile compared to the 20 mm profile has a higher rolling resistance not only with negative but as well with positive slip. The 0 mm and 5 mm profile were not simulated on loam 2 because the extreme bulldozing wave caused problems with the deformation of the FE-mesh.

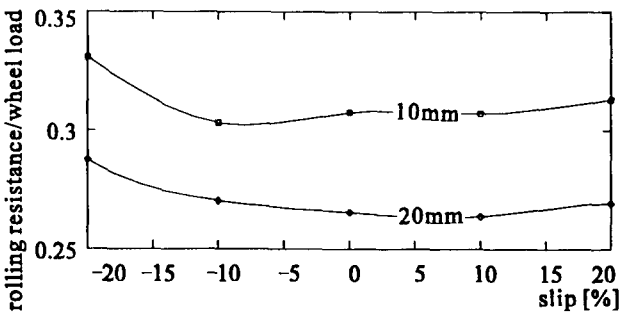

Fig. 15: Rolling resistance over slip, loam 2, wheel load 23 kN

4.3 The sinkage

The sinkage has the most important effect on the rolling resistance. In almost every analytical model the sinkage is calculated in relation to the wheel load. Apart from the load dependent sinkage a slip-dependent sinkage can be observed.

In fig. 16 the total sinkage of the various tyres on loam 1 are shown. The sinkage is measured from the outer diameter of the lugs, so that the different profiles have not the same sinkage at 0% slip. The higher profiled tyres sink deeper, because the negative profile has to be filled with soil to establish the whole contact length. As a result of the pressure peaks at the lugs the difference in sinkage is less than the difference in profile height.

The slip dependent variation of the sinkage is close to a linear curve when regarding positive slip. This is also assumed in most of the analytical models. As expected the additional sinkage is greater for higher profile. At negative slip the curves become more parallel. This indicates that there might be a minimum of sinkage for negative slip, which does not depend on the profile shape.

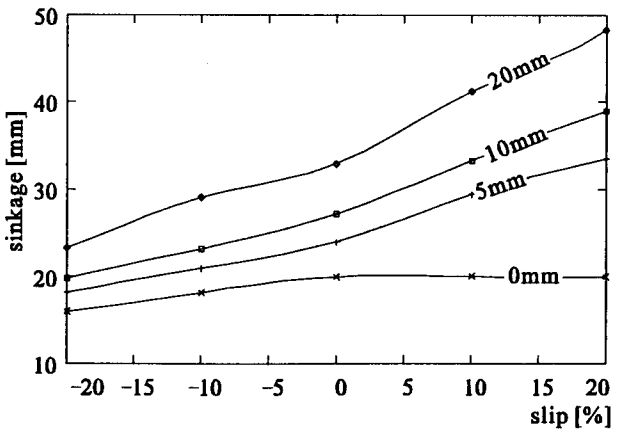

Fig. 16: sinkage over slip, loam 1, wheel load 20 kN

The sinkage curves for loam 2, fig. 17, underline this assumption. For positive slip they show as well a linear relation but with decreasing slip they come closer together and seem to reach a certain minimum limit.

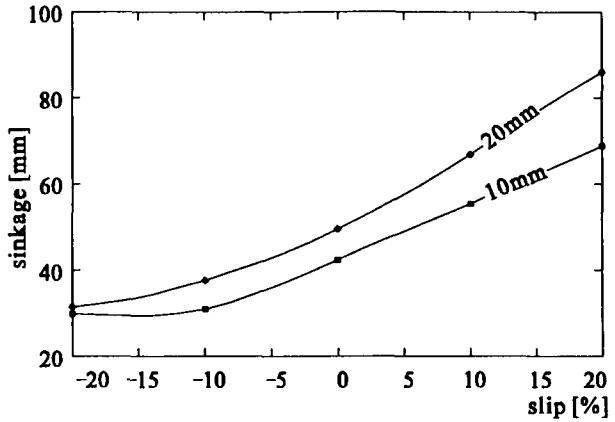

Fig. 17: sinkage over slip, loam 2, wheel load 23 kN

5 CONCLUSIONS

The results presented here are in good accordance to natural observations. This proves that the new model is working well. It is able to simulate the influence of tyre profile on effects like rolling resistance, sinkage and bulldozing effect, which could not be calculated entirely up to now. For example the bulldozing effect in relation to the profile shape is not represented in any other model.

With this model effects of tyre profile on terrain mobility can be as well studied as the consequences of land locomotion on farming processes. Furthermore the model will be a suitable tool to optimise the tyre profile regarding different soils.

Further investigations should be done with attention to other profile shapes and soil parameters. Moreover higher slip rates should be considered. A validation has not taken place so far and should be done in connection with experimental data. With the steady increase of computer capacity the model could be extended by a deformable tyre and 3D-effects for the future.

REFERENCES

[1] BEKKER, M. G.: Theory of Land Locomotion : The Mechanics of Vehicle Mobility. Ann Arbor: The University of Michigan Press, 1956

[2] JANOSI, Z.; HANAMOTO, B.: Analytical Determination of Drawbar Pull as a Function of Slip for Tracked Vehicles in Deformable Soils. In: Proceedings of the 1st International Conference on Terrain-Vehicle Systems. Turin, 1961

[3] LUDEWIG, J.: Triebkraft-Rechenprogramm für ein elastisches Rad mit Schlupfeinsinkung. Hamburg, Universität der Bundeswehr, Institut für Kraftfahrwesen und Kolbenmaschinen. Forschungsbericht. IKK-Nr. 91-05, 1991

[4] HOLM, C.: Das Verhalten von Reifen beim mehrmaligen Überfahren einer Spur auf nachgiebigem Boden und der Einfluß auf die Konzeption mehrachsiger Fahrzeuge. VDI-Fortschrittsberichte Reihe 14 Nr. 17, VDI-Verlag, Düsseldorf, 1972

[5] SCHWANGHART, H.; ZWEIER, A.: Einfluß des Profils auf das Triebkraft-Verhalten von Geländewagenreifen im lockeren Boden. In Symp. für Geländefahrzeuge in Theorie und Praxis, S. 216 - 224. TU Wien, Laxenburg / Wien, Sept. 1989

[6] REGLI, G. et al.: Material laws as a basis for simulation models for the calculation of wheel-soil interaction examination using the Finite element method. Journal of Terra mechanics, Vol. 30, No. 3, pp. 165-179, 1993

[7] AUBEL, Th.: Simulationsverfahren zur Untersuchung der Wechselwirkung zwischen Reifen und nachgiebiger Fahrbahn auf der Basis der Finite Elemente Methode. Dissertation UniBwH, Hamburg, 1994

[8] HIBITT, KARLSSON & SORENSEN, INC.: Manuals for the program "ABAQUS" Vers. 5.2 , Pawtucket, 1992

SMART ELECTROMECHANICAL AWD × AWB × AWA INTELLIGENT MAIN BATTLE TANK

Bogdan T. Fijalkowski
Cracow University of Technology, Cracow, Poland
Institute for Automotive Vehicles & Combustion Engines
Automotive Mechatronics Institution
pmfijalk@cyf-kr.edu.pl

To the Living Memory of Prof. Dr. M. Gregory Bekker

ABSTRACT

The present status and future trends of electromechanical All-Wheel-Driven (AWD) propulsion, All-Wheel-Braked (AWB) dispulsion and All-Wheel-Activated (AWA) suspension for caterpillar tracks of Intelligent Main Battle Tanks (IMBT) is presented in the paper. The use of these new concept AWD propulsion, AWB dispulsion and AWA suspension spheres for caterpillar tracks opens up wide possibilities for improving fossil and non-fossil fuel economy, cutting initial and whole-life caterpillar-track costs, protecting the environment and bettering distribution of terrain thrust (gross tractive effort) as well as keeping both the net motion resistances of the caterpillar track and track sinkages (rut depth) low not only by increasing the speed of travel but also decreasing the rolling resistances of all the electromechanical motorized sprocket-, road- and tensioner-wheels etc.

1. INTRODUCTION

In October 1979, one of the greatest scientists in the history of *'terra-mechanics'*, the never-enough-to-be-regretted Pole Professor Dr M G ('Greg') Bekker [1] *'Father of Terrain-Vehicle Systems'*, best known for the invention of a steel transparent-type caterpillar track for tracked all-terrain vehicles and pioneering construction of a wire-mesh tyre and

other members for Lunar Roving Vehicle (LRV) for the *National Aeronautics and Space Administration (NASA)*, asked the author to develop an all-automatic Continuously Variable Transmission (CVT) for civilian and military tracked all-terrain vehicles suitable for mass use (inexpensive and easily manufactured) that would improve Internal Combustion Engine (ICE) or External Combustion Engine (ECE) performance and vehicle drivability when operated by any (even unskilled) Human Driver (HD).

Tracked all-terrain vehicles generally have distinct advantages over wheeled all-terrain vehicles on cross-country terrain, primarily because the caterpillar track results in a lower ground pressure, leading to reduced sinkage and a better distribution of tractive effort. Against this the steering-conversion sphere, which is usually integrated with the propulsion, dispulsion and suspension spheres, is more complex.

When the road wheels are connected by a caterpillar track, their motion is not independent, and this, together with the motion of the caterpillar track itself, makes prediction much more difficult. Bearing in mind the sophistication and high cost of such tracked all-terrain vehicles, this difficulty is a serious handicap for the automotive scientists and engineers. This is particularly true of fighting vehicles which additionally usually have quite complex active suspension spheres.

By contrast the motion of the caterpillar track or *'chain'* of modern unconventional electrically-powered and mechatronically-controlled tracked all-terrain vehicle is very different and much more sophisticated because:

- sprocket torque is applied through an electromechanical motorized sprocket wheel as in conventional tracked all-terrain vehicles, but additionally auxiliary road-wheel torques are applied through electromechanical motorized road wheels, and auxiliary tensioner-wheel torque is applied through an electromechanical motorized tensioner-wheels which all moves with the vehicle;
- the load is distributed in an indeterminate manner along a finite length of essentially stationary caterpillar track in contact with the ground;
- the caterpillar-track inertia is a significant function of the hypersphere inertia, and its motion is very non-linear;
- there is significant coulomb friction between adjacent caterpillar-track links.

The author started his Very Advanced Technology (VAT) Programme for original Research and Development (R&D) work on mono- and/or poly-drive propulsion spheres in the early 1980s [2-5]. His developments were directed toward the automotive industry but his electromechanical mono- and/or poly-drive propulsion spheres also had some industrial applications.

The author boast of yourself as a pioneer in the application of electromechanical mono- and/or poly-drive propulsion spheres in particular AWD propulsion to civilian and military, wheeled and tracked, on- and/or off-road vehicles. As early as 1982, the author introduced electromechanical AWD propulsion spheres to wheeled road vehicles [2,3,5], and as early as 1984 - to wheeled and tracked all-terrain vehicles [4,8,10,12-15]. Only as early as 1987 the other authors published papers [19,20,22,27-30] on electromechanical AWD propulsion of civilian and military, wheeled and tracked all-terrain vehicles.

Recently developed high-efficiency electrical dynamotors (generators/motors) to be mounted inside the wheel hub promise advantage for smart electromechanical All-Wheel-Drive (AWD) x All-Wheel-Brake (AWB) x All-Wheel-Activate (AWA) wheeled and tracked all-terrain vehicles. Then, for wheeled all-terrain vehicles too, skid steering could easily be realized, where, instead of a steering angle of the wheels, controversially sensed circumferential forces on the two sides of the vehicle produce the cornering motion such as for tracked all-terrain vehicles.

According to the author's hierarchical *systems approach* (systems thinking) [9,12-15] on automotive vehicle dynamics, for instance, the term *'propulsion sphere'* is defined to include all the hierarchical dynamical hypospheres, hypersystems, systems, hyposystems and elements which are arranged in a dynamical sphere (from the human- or telerobotic-driver input to all the vehicle tracks' motorized sprocket-, road- and tensioner-wheels) that are required to store electrical energy on board the vehicle and, using that energy, to provide motive power to all the vehicle-tracks' motorized sprocket-, road- and tensioner-wheels. Just for that reason, tracked all-terrain vehicles are also determined as *'dynamical heterogeneous hyperspheres'*, including various energetic assemblies as *'automotive functional dynamical spheres'*, eg propulsion, dispulsion, suspension and conversion, as well as cooling, heating, lubrication and other trade-off spheres.

Civilian and military tracked all-terrain vehicles are characterized by a variety of solutions and form a sophisticated dynamical hypersphere with many degrees of freedom, the vehicle hypersphere affected by various ground input forces, mostly of probabilistic character.

Contemporary computer techniques make it possible to solve sophisticated dynamical hyperspheres, the problem, though, is in adopting a proper physical model and next in creating a correct mathematical model of the interaction of tracks with terrain [1,14,23,31]. The difficulty results from a wide variety of terrain conditions in which a tracked all-terrain vehicle must travel and from the lack of the sphere hypermatrix equation of state being the formal evaluation of actual terrain medium.

The experimental proof-of-concept series hybrid thermo-mechano-electromechanical and/or electromechanical All-Wheel-Driven (AWD) propulsion, All-Wheel-Braked (AWB) dispulsion and All-Wheel-Activated suspension spheres will have an operating efficiency of 80 % and it enabled the tracked all-terrain vehicle to exhibit a 25 % improvement in fuel consumption and a 50 % reduction in both the net motion resistance of the AWD & AWB & AWA caterpillar tracks and track sinkage compared to the existing conventional thermomechanical Sprocket-Wheel-Drive (SWD) propulsion sphere as well as advanced thermo-mechano-electromechanical and thermo-mechano-fluido-mechanical SWD propulsion sphere, the latters two became available in the late 1910s and 1930s, respectively.

The author envisages a time when fully-automatic motion control of fighting vehicles will be standard equipment on all Main Battle Tanks (MBT). In the nearest future, the Intelligent Main Battle Tank (IMBT) is expected to make a big contribution to the society composed largely of unskilled human drivers. It will be of great help to the unskilled soldiers, vastly improving their quality of fighting. Moreover, it also will be useful for human drivers who are not used to MBTs. For this reason, the author is pursuing R&D work in this field.

Motion control, ie propulsion x dispulsion x suspension x conversion control is one of the most important driver-vehicle and terrain-vehicle real-time expert hypersphere for fighting vehicles. Previous methods were primitive. For example, the primary area of interest has been in autonomy due to problems of communication on the battle field, though some interaction with the HD will obviously still be required and

the author is working on driver-vehicle and terrain-vehicle real-time expert hyperspheres allowing local and remote motion control.

The primary interest has been directed towards cross-country operation; the fighting vehicles the author is conceiving and designing being specially electromechanical AWD & AWB & AWA caterpillar tracks [4,8,10,12-14] propelled (driven) and converted (steerable) to make off-road driving as easy as possible by avoiding many of the normal failure modes. This reduces the number of hazards and makes them simple to classify. Safe operation of the MBT will be assisted by local sensors such as tilt and proximity detectors. The behaviours will be varied from timid to extremely bold as warranted by the circumstances.

On the other hand, in the case of MBT moving on the battlefield, the motion control must be smoother. It must feel as if a well-skilled human being were driving. It may seem that by improving the MBT's sensors and the algorithms that interpret the sensors' data the smoothness of ride can be improved. This is not, however, necessarily so. Higher precision sensing can result in a rougher ride because of its noisy signal. In this case, the soldiers may feel not only discomfort but also extra fear. For this reason, the author selected fuzzy-logic motion control algorithms for the motion control of the BMT. Fuzzy logic [32] was chosen because of the following characteristics. It is easier to implement Human- and/or Telerobotic-Driver (H&TD) skills using fuzzy-logic motion control than using conventional motion control algorithms. It filters even the uncertainty of the precision of the sensor. Therefore, the IMBT may move as smoothly as a well-skilled human being drives.

Modern unconventional IMBTs such as other tracked all-terrain vehicles are characterized by extremely high mobility (even in rough terrain), slope and acceleration capabilities. The turning behaviour is also very important [28].

The impact of the turning resistance onto the AWD propulsion, AWB dispulsion and AWA suspension spheres is of primary interest. For instance, during cornering the torques on the electromechanical motorized sprocket wheels (sprockets) can be circa 20 times higher than in straight ahead motion [28]. The cornering capability of an IMBT must therefore be considered in the design stage. For instance, when an IMBT is driving in a curve the turning resistance is added to the motion resistances of straight ahead motion.

The turning resistance is caused by lateral forces at the AWD & AWB & AWA caterpillar tracks. These horizontal (longitudinal and lateral) forces are always combined with horizontal displacement between the AWD & AWB & AWA caterpillar tracks and the ground surface.

2. VAT PROGRAMME

Dealing with the intelligent fighting vehicle problems requires a systems approach (systems thinking). This requires equipment and systems that are reliable, compact, and affordable. Realistic goals and objectives must be established for VAT availability, performance and cost, that is the VAT must be *'rational'* for the operation and the operational environment. This will also emphasize concepts such as model-based object recognition, knowledge-based methods, artificial neural networks, multi-sensor and information fusion and management, as well as advanced signal and data acquisition, coding, processing, and display visual information concepts for such applications as detection, tracking, and identification recognition new methodologies for sonar-, laser-, radar-, IR-, as well as visible and UV-sensor-based systems.

Areas of particular concern include Automatic Target Recognition (ATR) and tracking mechatronics systems, reconnaissance, diagnostics and specialized sensors (e.g. guidance and navigation quality sensors for laser gyros, accelerometers, etc.) as well as passive and active space-based remote sensing. Laser, fiber optic, and scanning VAT can provide improved IMBT motion (propulsion, dispulsion, suspension and conversion) in many phases of mission scenario, including the garage phases of the drive, prevention of ramp incursion, and refueling operations.

The need to improve the margin of safety and precision of IMBT operations has driven the search for additional methods to solve these and related problems. These systems range from Command Control Communication and Intelligent (C^3I) systems to Air Defence (AD) systems, and recently Air Traffic Control (ATC) systems. All of these systems share a number of common elements with the IMBT Motion Control (MC) systems. Motion control for an IMBT requires many of the same elements that the existing military C^3I systems use. These elements fall into four categories: sensors, communications, command centres (processors and display), and software (strategies and tactics). In human- and/or telerobotic-driver terms, the sensors are used to determine the current situation in the geographic area of responsibility,

the *'eyes and ears'* of the MC system. The communications are used to bring the information back to the centre for processing, the *'nerve system'* element. The command centre and its software make the decisions necessary to control the situation or respond to unexpected events, the *'brain'* of the MC system [25].

In the military, C^3I is a vital part of any defense system as was demonstrated in the *Gulf War* by the *Coalition Forces*. The first activity of the *Coalition Forces* was to disable the opponents C^3I system. In doing so, they were able to *'blind'* the opponent and break the communication to the command centre. Once this was accomplished, Iraq had no knowledge of the *Coalition Forces'* situation. Thus the *Coalition Forces* gained air supremacy. Fifty-five different *Hughes Aircraft Co* advanced technologies were used in the *Gulf War* including radar, satellite and spread spectrum communications, IR image processing, and a C^3I system [25].

The same advanced technologies may be transferable directly to motion control for the IMBT using macroelectronic Application Specific Integrated Matrixer (ASIM) macroconverter-based commutators (ASIM macrocommutators and Artificial Intelligence (AI) Fuzzy-Logic and Neural-Network (FN) microelectronic Application Specific Integrated Circuit (ASIC) microcomputer-based controllers (AI FN ASIC microcontrollers).

The author's VAT Programme R&D effort is concentrated on technologies that will adapt the AWD propulsion, AWB dispulsion and AWA suspension spheres' concept to an IMBT. Major technological advances that have been accomplished in this R&D programme include: novel DC macrocommutator reluctance & magnetoelectric [unwound Magnetized-Soft-Iron (MSI) outer rotor and wound & Interior Permanent Magnet (IPM) inner stator] electromechanical single- or twin-wheel-hub motors for track assembly, which are integrated into AWD propulsion sphere mechanism of the IMBT contained within the envelopes of the AWD & AWB & AWA caterpillar tracks; development of the control algorithms required for torque and/or speed control of the electromechanical sprocket-, road- and tensioner-wheel-hub motors; further development of the unique macroelectronic modules, that are AC-to-DC and/or DC-to-AC ASIM macrocommutators [7,9,11]; improvements to the AC-to-DC and/or DC-to-AC ASIM macrocommutators to bring them closer to manufacture; and integration of the AI FN ASIC microcontrollers that are in command of the entire AWD propulsion, AWB dispulsion and AWA suspension spheres to provide an on-board AI FN

ASIC microcomputer-based fuzzy-logic programmable and neural-network learning (P&L) controller (commander). In addition, specifications and integrations of the Automotive Gas Turbo-Generator (AGTG) that is based on the Fijalkowski Turbine Boosting (FTB) system or the Fijalkowski engine (FE) with constant output [5,6,8,10,12], co-operating with the on-board Chemical Energy Store (CH-ES), that is the advanced nickel- or silver-metal hydride DC chemoelectrical Storage Battery (SB) and the Mechanical Energy Store (M-ES), that is the mechanical energy-storing Dynamotorized Flywheel (DF) with the brushless DC macrocommutator flywheel-hub dynamotor were included in the VAT Programme to assure that these important components of the new concept AWD propulsion, AWB dispulsion and AWA suspension spheres were included in all of the IMBT hypersphere's design trade-offs.

The integrations of two AGTGs that are based on the FTB system, or two FE with constant output, co-operating with the on-board CH-ES, consisted of the DC chemoelectrical SB and M-ESs, consisted of the mechanical energy-storing DFs with the brushless DC macrocommutator flywheel-hub dynamotors as well as power trains, that are all the MBT caterpillar-tracks' motorized sprocket-, road- and tensioner-wheels form a complete proof-of-concept series hybrid thermo-mechano-electromechanical and/or electromechanical AWD propulsion, AWB dispulsion and AWA suspension spheres.

R&D work will also continue on mobility and steerability, including attempts to boost ICE or ECE power and speed of travel. To ensure the success of these efforts R&D work is also going forward on experimental proof-of-concept electromechanical AWA suspension spheres and riding control; as well as skid-steering conversion spheres and both stability and handling at high speed of travel, lower mass and higher durability for caterpillar-track pad and shoes, higher efficiency in electro-mechanical motorized sprocket-, road- and tensioner-wheels as well as pad and shoe systems, and improved track shoe traction.

Many demands are also made on power boosting during fast-acceleration, hill climbing and high-speed travelling as well power recuperation during coasting and braking of the vehicle, and both new concept electromechanical AWA supension spheres and skid-steering conversion spheres used as integral spheres together with future new concept hybrid thermo-mechano-electromechanical and/or electromechanical AWD propulsion, AWB dispulsion and AWA suspension spheres for civilian and military tracked all-terrain vehicles.

Operational economy has become increasingly important with the growing costs of fuels. It is now profitable to invest in newly designed energy-saving thermo-mechano-electromechanical and/or electromechanical AWD propulsion, AWB dispulsion and AWA suspension spheres as an alternative to, or replacement of, existing conventional thermo-mechanical SWD propulsion spheres as well as advanced thermo-mechano-electromechanical or thermo-mechano-fluido-mechanical propulsion spheres for civil and military tracked all-terrain vehicles.

The contemporary BMT must be an intelligent fighting vehicle with extremely high mobility and steerability on a wide range of environments and soils. In recent years, IMBTs have become increasingly sophisticated, incorporating novel mobility enhancing concepts such as electromechanical AWD & AWB & AWA caterpillar tracks, track tension regulating devices and adaptive suspensions, the use of which permits the Human Driver (HD) to *'tune'* his MBT to optimize its performance in a particular type of terrain or mission scenario. As the design of IMBTs becomes more sophisticated so too the Intelligent Computer Aided Design (ICAD) analytical methods used are more complex. While to the author's systems approach [9,12,14] to studying driver-vehicle and terrain-vehicle interactions first formalized by Prof. Bekker [1] is still useful up to now, with the ICAD as well as physical and mathematical models [14,23,31], the study has become an increasingly specialized one.

3. EXPERIMENTAL PROOF-OF-CONCEPT AWD PROPULSION, AWB DISPULSION AND DISPULSION SPHERES

The experimental proof-of-concept AWD propulsion, AWB dispulsion and AWA suspension spheres used on high-speed, terrestrial and water IMBTs satisfy nearly all the same essential requirements as for the running gear systems used on high-speed military tracked all-terrain vehicles [26], namely:

(i) to apply an all-electric-wheel *'single-shaft'* AWD propulsion sphere to a large number of electromechanical motorized road wheels;
(ii) to apply an all-electric-wheel *'single-shaft'* AWB dispulsion sphere to a large number of electromechanical motorized road wheels;
(iii) to allow a large AWA suspension displacement to allow high-speed motion over cross-country difficult terrain;
(iv) to allow at the outer side of the curve a positive propelling (driving) torque and at the inner side - a negative dispelling (braking) torque, achieving their maximum value for pivot skid steering;

(v) to occupy the minimum volume within the space envelope of the IMBT;
(vi) to distribute the mass of the IMBT over a relatively large ground surface or soil area.

The requirements (i) and (ii) will contribute to the very good soft soil performance of IMBTs. The feature (v) will tend to conflict with requirements (i) and (ii).

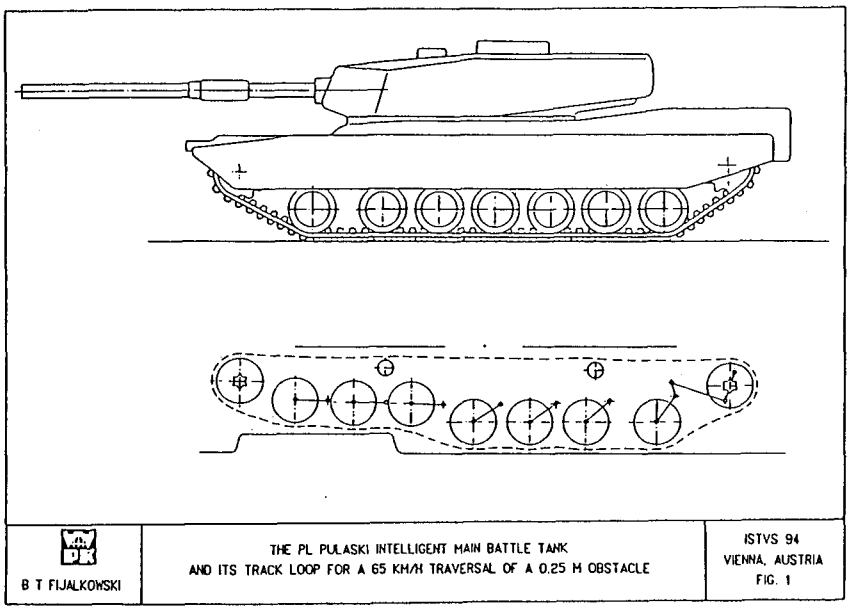

B T FIJALKOWSKI	THE PL PULASKI INTELLIGENT MAIN BATTLE TANK AND ITS TRACK LOOP FOR A 65 KM/H TRAVERSAL OF A 0.25 M OBSTACLE	ISTVS 94 VIENNA, AUSTRIA FIG. 1

The AWD propulsion, AWB dispulsion and AWA suspension spheres must be of minimum mass, reliable and durable as well as easy to maintain and, compared to some other MBT components, reasonably inexpensive to manufacture.

In the fighting-vehicle field an example of study is represented by an experimental proof-of-concept series hybrid thermo-mechano-electro-mechanical and/or electromechanical AWD propulsion, AWB dispulsion and AWA suspension spheres for an electrically-powered and mecha-tronically-controlled AWD x AWB x AWA IMBT with extremely high mobility and steerability,which is conceived and designed by the author at *Cracow University of Technology*, Cracow, Poland [14].

The experimental proof-of-concept series hybrid thermo-mechano-electromechanical and/or electromechanical AWD propulsion, AWB dispulsion and AWA suspension spheres are designed for installation in the high-speed, terrestrial and water, PL Pulaski IMBT armed with a light anti-tank gun and/or uranium arrow missile with loading automat. It will have a turret that is a strong and hard thick active heavily armoured metal-powder structure protecting a gunner or crew (two men only), made so as to revolve with the gun and/or rocket. It will also have very small windows that withstand sledgehammer blows, a hull and road-wheel tyres that endure multiple shots from a firearm, and a rampart that sprays tear gas.

Figure 1 shows an overall view of the PL Pulaski IMBT and its caterpillar-track loop for a 65 km/h traversal of a 0.25 m high obstacle. The barycentre is located at the centre of the hull. The seven electromechanical motorized road wheels on each side of the hull have independent rotary-damper AWA suspensions. The front electromechanical motorized sprocket wheel (sprocket) and fourteen (seven on each side) electromechanical motorized road wheels as well as the rear electromechanical motorized tensioner wheel are driven individually by the DC macrocommutator sprocket-wheel-hub motor and fourteen DC macrocommutator road-wheel-hub motors as well as DC macrocommutator tensioner-wheel-hub motor, respectively, and the rotating speed of each AWD & AWB & AWA caterpillar track and each motorized sprocket-, road- and tensioner-wheels can be arbi-trarily controlled by driver-vehicle and terrain-vehicle real-time expert hypersphere, incorporating model following fuzzy-logic programmable and neural-network learning motion control of an IMBT. For changing the adhesion coefficient two kinds of the caterpillar track may be used, namely wide moulded-rubber belt- or narrow uranium-powder transparent-type caterpillar tracks. The accelerometers were attached at the geometric centre of the IMBT.

The required skid-steering power of each AWD & AWB & AWA caterpillar track can be measured by the sprocket-, road- and tensioner-wheel torque gauges which are specially designed to eliminate the bending effects of caterpillar-track tension on sprocket-, road- and tensioner-wheel shafts.

The IMBT shown in Figure 1 is intended only to be the Test and Evaluation (T&E) fighting vehicle of this proof-of-concept series hybrid thermo-mechano-electromechanical and/or electromechanical AWD propulsion, AWB dispulsion and AWA suspension spheres, rather than

an engineering prototype. Therefore no modification of the base MBT characteristics or structure are planned except these required for AWD propulsion, AWB dispulsion and AWA suspension spheres mounting. For example, the piston-type ICE or conventional AGT is replaced by two AGTGs that are based on the Fijalkowski turbine boosting (FTB) system [5,6,8], or two Fijalkowski engines [8] with constant output, and the thermo-mechano-fluidomechanical rear SWD propulsion sphere is replaced by the experimental proof-of-concept series hybrid thermo-mechano-electromechanical and/or electromechanical AWD propulsion, AWB dispulsion and AWA suspension spheres [4,8,10,12-14].

The IMBT will have extremely high mobility and steerability is driven by the same two wide moulded-rubber belt- or narrow uranium-powder transparent-type caterpillar tracks. All two caterpillar tracks are consequently AWD & AWB & AWA ones.

The core of the experimental proof-of-concept series hybrid thermo-mechano-electromechanical and/or electromechanical AWD propulsion, AWB dispulsion and AWA suspension spheres are not only two AGTGs that are based on the FTB system [5,6,8], or two FEs [8,10], that are rectilinear reciprocating ICEs with eight (Square-Four Engine) or sixteen (Octagon-Eight Engine) pistons moving the mover of the linear DC macrocommutator (unwound IPM inner mover and wire-wound outer stator) generators which directly convert into electrical energy the mechanical energy supplied to the pistons by the combustion of usual hydrocarbons, as well as on-board advanced nickel- or silver-metal hydride DC chemoelectrical SB and mechanical energy-storing DF with the brushless DC macrocommutator flywheel-hub or twin-flywheel-disc dynamotor (generator/motor) but also DC macrocommutator (MSI and IPM) electromechanical wheel-hub motors for each of the individual motorized sprocket-, road- and tensioner-wheels.

The high power factor mechanoelectrical disc-shaped rotor generator and electromechanical wheel-hub motors use *Sm-Fe-Ti-B*, *Sm-Fe-Mo* or *Nd-Fe-B* magnets to supply inductor (mover/rotor) magnetic fluxes, which almost eliminate mover/rotor or stator losses and result in highly compact efficient designs. These components are interconnected through AWD propulsion, AWB dispulsion and AWA suspension spheres, and the propelling or dispelling power flow is controlled by an on-board AI FN ASIM microcontroller which receives commands from the H&TD.

The PL Pulaski IMBT (Fig. 1) has both unique types of AWD propulsion, AWB dispulsion and AWA suspension spheres and an unique type of very advanced skid-steering conversion sphere which incorporate adjustable torque and/or speed AWD & AWB & AWA caterpillar tracks. When the steering joystick is turned the AWD & AWB & AWA caterpillar tracks are activated and push/pull the IMBT until desired turn is made. This steering-conversion sphere has proven to be a relatively effective mobility feature because there is no power loss in dispelling (braking) the AWD & AWB & AWA caterpillar tracks for steering as on a conventional only SWD caterpillar track's fighting vehicle, for instance, the US Abrams MBTs. When steering the PL Pulaski IMBT both caterpillar tracks are still powered, providing smooth and continual power to them which allows it to achieve maximum tractive effort.

Cracow University of Technology's Mechatronics R&D Team instead choose to perform a prestudy on two AGTGs for the PL Pulaski IMBT as substitute for the Diesel engine or AGT. This is because the two prime-mover design offers a series of advantages in addition to enabling Catalytic Exhaust Gas Cleaning (CEGC). Among these advantages is low price through long series manufacture, proven high technology (high-tech) and inexpensive parts, known service routines, light mass and the AGTGs' ability for independent power output.

Moreover, the PL Pulaski IMBT can operate using one prime mover only, in case the other breaks down. Obviously, there are also some disadvantages, such as complexity compared with a single prime mover, the duplication of certain auxiliary equipment and special work for mounting two electromechanical motorized sprocket wheels and fourteen electromechanical motorized road wheels as well as two electromechanical motorized tensioner wheels for 18 x (2S + 14R + 2T) wheel arrangement (See Figure 1). In addition, this didn't also require an automatic mechanical transmission and gear unit which transfers the torque through the propeller shaft to each prime mover.

Figure 1 also shows the AWD propulsion, AWB dispulsion and AWA suspension spheres of the PL Pulaski IMBT and is typical of modern unconventional Drive-By-Wire (DBW) practice. Trailing adaptive & predictive AWA suspension arms carry rubber-tyred electromechanical motorized road wheels and operate transverse (lateral) torsion bars running across the floor of the PL Pulaski IMBT's hull. Rotary vane electromechanical activators with the Electro-Rheological-Fluid (ERF) shock absorbers (dampers) are incorporated into the pivots of the AWA suspension arms on the front, second and rear road-wheel stations.

Linked AWD & AWB & AWA caterpillar track will run under the electromechanical motorized road wheels and around hull-mounted electromechanical motorized sprocket wheel (drive sprocket) and return electromechanical motorized tensioner wheel. Caterpillar-track pretension will be adjusted by ERF filled electromechanical rams reacting against the electromechanical motorized tensioner wheels.

Electromechanical motorized sprocket wheels could be at the front of the PL Pulaski IMBT, because are not depending on the position of the prime-movers' pack. Two small diameter rollers support the top run of the AWD & AWB & AWA caterpillar track. Caterpillar-track return electromechanical motorized tensioner wheel will be mounted to the hull through short swing links to allow the caterpillar track to be pretensioned. Electromechanical rams have replaced screw devices as the tensioning mechanism. Not only is tensioning easily effected with an electromechanical ram, but the pretension can be accurately set by using an Electro-Rheological (ER) fluidical valve.

On the PL Pulaski IMBT electromechanical tensioners will be used in conjunction with an internally mounted ER fluidical valve. This will enable the caterpillar track to be pretensioned by the human driver from inside the IMBT. On the Pulaski IMBT the tensioners will be interconnected to the rear AWA suspension arms to give a so-called compensating electromechanical motorized tensioner wheel. This arrangement will give a measure of brake anti-dive and will also take up caterpillar-track *'slack'* as the front electromechanical motorized road wheel will move in the bump sense of motion direction.

With the use of an AWA suspension sphere, high strength aluminium alloys and better design and manufacturing techniques the proportion of the PL Pulaski IMBT's mass taken up by the AWD propulsion and AWB dispulsion spheres has fallen.

The calculations performed in the prestudy assume the PL Pulaski IMBT with two smaller FTB system AGTGs of 2 x 500 kW, as compared with the US Abrams MBT with the large AGT output of 1,200 kW. Acceleration performance and hill climbing ability will be approximately the same.

An initial analysis of various control strategies has shown that the lowest SFC will be obtained if one AGTG worked as the base load prime mover and the other as the peak load prime mover for high power requirements. The peak load would be shut OFF during idle run

and low to medium power requirements. The results of calculation show, among others, that the emissions of health-hazardous particles from the two-AGTG-powered PL Pulaski IMBT would be almost negligible, and NO_x emissions very low, compared with those from the AGT-powered US Abrams MBT.

The possibility of installing an advanced mechanical energy-storing DFs in the two-AGTG-powered PL Pulaski IMBT has also been investigated. All of the reduction gained in AGTG mass will thereby be used to provide mechanical energy-storing DFs. In this FTB system a mechanical energy-storing DF accumulates mechanical energy into a flywheel-hub or twin-flywheel-discs while the IMBT is braking. When the IMBT is start again, the mechanical energy-storing DF will accelerate the IMBT using stored mechanical energy.

The prestudy on the two-AGTG-powered PL Pulaski IMBT, which also describes the author's project to replace the large AGT with two smaller AGTGs in a standard MBT, will also provide the basis for a possible decision to proceed with a prototype.

4. MAJOR COMPONENTS OF AWD PROPULSION, AWB DISPULSION AND AWA SUSPENSION SPHERES

Major components that determine the tractive performance of the experimental proof-of-concept series hybrid thermo-mechano-electro-mechanical and/or electromechanical AWD propulsion, AWB dispulsion and AWA suspension spheres for the IMBT are: two AGTGs that are based on the FTB system, or two Fijalkowski engine (FE) with constant output, co-operating with the on-board CH-ES, that is the advanced nickel- or silver-metal hydride DC chemoelectrical SB and the mechanical energy-storing DF with the DC macrocommutator flywheel-disc dynamotor; two AWD & AWB & AWA caterpillar tracks with the two front motorized sprocket wheels and two rear motorized tensioner wheels as well as fourteen motorized road wheels, including eighteen brushless DC macrocommutator (MSI and IPM) wheel-hub motors each; and the on-board AI FN ASIC microcomputer-based fuzzy-logic programmable and neural-network learning (P&L) controller (AI FN ASIC microcontroller).

4.1 Automotive Gas Turbo-Generator that is based on the FTB system

Based on a previous R&D work of the author at *Cracow University of Technology* in Poland, a systems approach has been taken to the Automotive Gas Turbo-Generator (AGTG) or the Fijalkowski Engine (FE) powered AWD propulsion as a sphere [5,6,8,10].

A whole new family of integrated AWD propulsion spheres has been conceived by the author. As a result of this work, novel integrated mechanically power boosted AGTs with integral Mechanical Power Boosters (M-PB) and ASIC microcontrolers, and Energy Stores (ES), for example, Chemical Energy Stores (CH-ES) and/or Mechanical Energy Stores (M-ES) have been conceived by the author in a paper presented at the *International Forum on New Automotive Technologies* held in Monte Carlo, Monaco on January 21-25, 1985 [6] - in turbine world this configuration is called the *'Fijalkowski Turbine Boosting (FTB) system'*. Another method of AGTs' power boosting with low Specific Fuel Consumption (SFC) and low Pollutant Emission Capability (PEC) was previously conceived by the author in a paper presented at the *International Symposium on Automotive Technology and Automation* held in Milan, Italy on September 24-28, 1984 [5].

A mechanically power boosted Automotive Gas Turbo-Generator (AGTG) that is based on the FTB system is one in which at least one of ESs can deliver electrical energy. Practically, this AGTG is being done with only two ESs and therefore in this paper the author considers only these versions that are based on the FTB system in which there are fossil or non-fossil fuel for the AGTG, and the M-ES, that is the secondary near-frictionless bearing, mechanical energy-storing Dynamotorized Flywheel (DF) with the brushless DC macro-commutator flywheel-hub dynamotor for the M-PB.

The M-PB, that is a mechanical energy-storing DF with the brushless DC macrocommutator flywheel-hub dynamotor having the highest possible speed for a given application is preferable, since it is smaller in size and lighter in mass, and has a high efficiency and power factor.

The M-ES, that is also a near-frictionless bearing, mechanical energy-storing DF with the brushless DC macrocommutator flywheel-hub dynamotor is maintained sufficiently charged to boost the AGTG's power for fast-acceleration starting, hill climbing as well as high-speed travelling and cruising.

Thus, the power boosted AGTG design philosophy is based in using electricity (electrical energy) as the predominant *'fuel'* with fossil or non-fossil fuel consumed only to meet the requirements which the M-PB cannot meet.

Hence, the initial preferred strategy is M-PB only operation up certain power, then the AGTG is turned ON to complete the operation (with the M-PB propulsion used, if required, for power boosting). The strategy is expected to result in substantial fossil or non-fossil fuel savings over a comparable conventional AGTG because a substantial portion of the Annual Engine Hours Operation (AEHO) and the percentage of normal daily works can be satisfied with a power boosting or with Drive-By-Wire (DBW) all-electric operation.

Based opon this philosophy, the author has designed novel AWD propulsion and AWB dispulsion spheres which are presented in this paper. The potential fossil or non-fossil fuel savings of these automotive functional spheres can be realized if there ia appropriatecontrol strategy to govern the function of each component arrangement of the FTB system. After extensive R&D work of various turbine transmission and component arrangement as mentioned above, the FTB system with a component arrangement as shown in Figure 2 was chosen for the experimantal mechanically power boosted AGTGs.

The arrangement of the mechanical components for the KTT system AGT used in the FTB system AGTG were briefly described in Prof. Kronogård's paper [24]. The environmental and economic factors, which have lead to R&D work of novel mechatronically power boosted AGTGs that are based on the FTB system for energy-saving IMBTs in the world (oil crises, atmospheric pollution, noise) have become increasingly pressing. The mechanical power boosting of AGTGs offers a very useful solution for applications in demanding environments. High reliability combined with the minimum of maintenance, low mass, small dimensions are some of avantages that are particularly valued. The M-PBs have been specially designed to solve the mechanical power boosting problems net with the mechanically power boosted AGTG field. The simplest design involves a direct substitution of M-PBs with M-ES for conventional or the KTT system AGTs resulting in a fuel saving improvement attributable to more efficient operation of the AGTGs.

The heart of the FTB system is a M-PB, that is a primary-power-source, mechanical energy-storing DF with the brushless DC macrocommutator

flywheel-disc dynamotor (generator/motor) electrically connected to the M-ES, that is the secondary-power-source, near-frictionless bearing, mechanical energy-storing DF with the brushless DC macrocommutator flywheel-hub dynamotor, which will be arranged in the AWD propulsion and AWB dispulsion spheres in a unique way. The arrangement is very simple as shown in Figure 2.

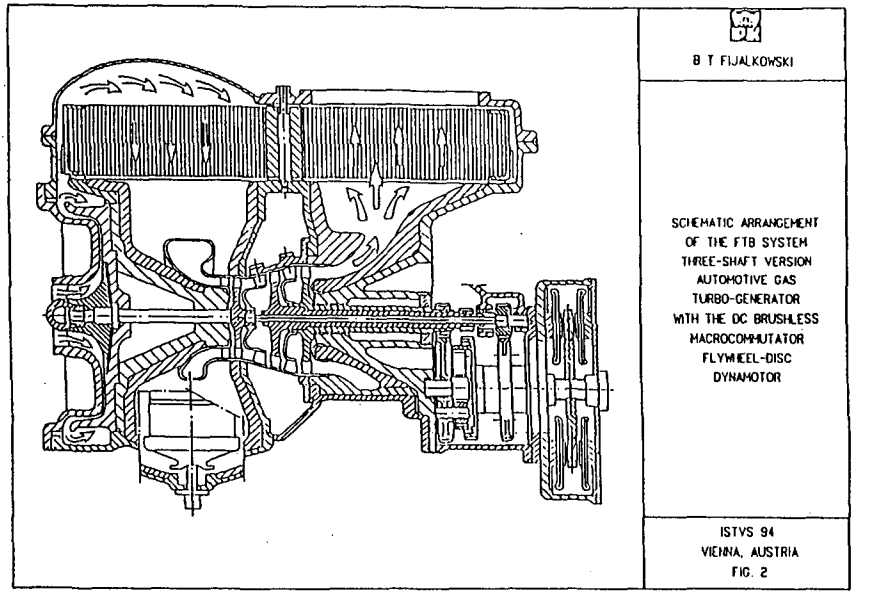

The axial-gap, Interior (Rare-Earth) Permanent Magnet (IPM) unwound disc rotor, wire-wound slotted core stator, high-power density (circa 0.1 kg/kW), primary-power-source, mechanical energy-storing DF with the brushless DC macrocommutator flywheel-disc dynamotor has been applied where high-speed, low-inertia AWD propulsion and AWB dispulsion spheres' control is important, or where reduced flywheel-disc dynamotor length is required. The basic concept is also shown in Figure 2.

A flywheel-disc dynamotor, consisting of one rotor containing IPMs centre between two stators, will be developed and installed for a mechanical energy storage and retrieval PB. This flywheel-disc dynamotor will eliminate the rotor magnetic-flux return ring (back iron), will reduce overall electrical machine volume and rotor inertia, and will eliminate the thrust bearing required to account for attractions between the rotor

and stators. Here, the back iron is removed, and the magnetic-flux return path are through the two stator yokes. A grease-lubricated ball bearing is mounted on a titanium shaft. This flywheel-disc dynamotor will be driven by a 416.6 rps (25,000 rpm) prime mover.

4.2 Mechanical Energy-Storing Dynamotorized Flywheel

The FTB system concept (See Figure 2) is one which, if any, may require an auxiliary M-ES, that is the secondary-energy-source, mechanical energy-storing DF with the brushless DC macrocommutator flywheel-hub dynamotor (generator/motor). The latter is an unconventional mechanical energy-storing DF, ie M-ES with an integrated electrical machine which can operate as a mechanoelectrical flywheel-disc generator (discharging the M-ES) or as an electromechanical flywheel-disc motor (charging M-ES) as required.

The kinetic mechanical energy carrier in the M-ES will be a hollow, cylindrical fiber-glass outer rotor. Air friction losses will be almost eliminated by encasement of the cylindrical outer rotor in a vacuum shell. The hollow interior of the mechanical energy-storing DF will house the DC macrocommutator flywheel-hub dynamotor which will absorb and deliver electrical energy.

Topmost compact AC-to-DC and/or DC-to-AC ASIM macrocommutator with the AI ASIC microcontroller will control the M-ES and will absorb or deliver the desired electrical energy according to the software programme selected.

Thus, the kinetic mechanical energy carrier of the M-ES, ie the energy-storage DF will be a hollow cylindrical outer rotor made of fiber glass. The rotational axis will be horizontal. The DC macrocommutator flywheel-hub dyna-motor will be contained within the hollow interior of the fiber-glass outer rotor. Electrical energy will be absorbed and/or emitted through this flywheel-hub dynamotor. The whole, most compact mechanical energy-storing DF will be encased in a vacuum shell.

Besides, automotive researchers are devising innovative ways of using high-temperature (hT_c) superconductors even while they struggle to perfect the properties of new materials.

Cracow University of Technology's Mechatronics Team has reported progress on a mechanical energy-storing DF that exploits the unusual magnetic repulsion in superconductors. According to the author, when

non-superconducting elements will be dispersed in superconducting material, to *'pin'* the magnetic fluxes of the levitation-magnet and/or suspension magnet, respectively. This means that a levitation-magnet disc-shaped rotor and suspension-magnet disc-shaped rotor can be levitated above and suspended under the superconductor disc-shaped stator, respectively. And because there will be a slice of air between the two, the levitation-magnet disc-shaped rotor and the suspension-magnet disc-shaped rotor can rotate freely in opposite senses of rotation. These properties could it possible to construct mechanical energy-storing DFs with near-frictionless magnetic bearings.

The prototype will consist of two disc-shaped rotors, made of *Sm-Fe-Ti-B*, *Sm-Fe-Mo* or *Nd-Fe-B* levitation-magnet and/or suspension-magnet rings embedded in aluminium, that will float 10mm above and/or under a stationary superconducting disc-shaped stator. The latter will contain plenty of yttrium-based bulk superconductors, cooled by liquid nitrogen. Both discs will be about a 0.3 m in diameter.

On a larger scale, such a mechanical energy-storing DF can help the topmost compact series hybrid prime movers: AGTGs balance their power requirements. The mechanical energy-storing DF would store kinetic mechanical energy during periods of the IMBT's low-speed cruising and regenerative normal coasting (low energy usage) and/or regenerative normal braking and then generate electrical energy (electricity) to meet the peak power demands during periods of fast-acceleration starting, hill climbing as well as high-speed travelling and cruising, and regenerative braking and/or pivot skid-steering.

4.3 Electromechanical Motorized Sprocket-, Road- and Tensioner-Wheels

The electromechanical sprocket-,road- and tensioner-wheel-hub motors are brushless type DC macrocommutator (unwound MSI outer rotor and wire-wound IPM inner stator) electromechanical wheel-hub motors. The rotating housing is made in the form of sprocket-, road- and temsioner-wheel hubs, designed to fit standard rim sizes on the market.

The electromechanical wheel-hub motor CVT offers complete freedom in the design of the new concept experimental proof-of-concept hybrid thermo-mechano-electromechanical and/or electromechanical AWD propulsion, AWB dispulsion and AWA suspension spheres for civilian and military tracked all-terrain vehicles. Whereas with existing thermo-mechano-electromechanical SWD propulsion spheres, including mech-

anical axles and drive shafts the ICE (eg, the Diesel engine or the Fijalkowski engine) or ECE (eg, the AGT that is based on the FTB system) must be located *'in line'* the newly designed hybrid thermo-mechano-electromechanical and/or electromechanical AWD propulsion and AWB dispulsion spheres with the front sprocket- and rear tensioner- as well as road-wheel-hub motor concept makes it possible to install the ICE (eg, the Diesel engine or the Fijalkowski engine) or the ECE (eg, the AGT that is based on the FTB system) at any suitable location on the civil and/or military tracked vehicles.

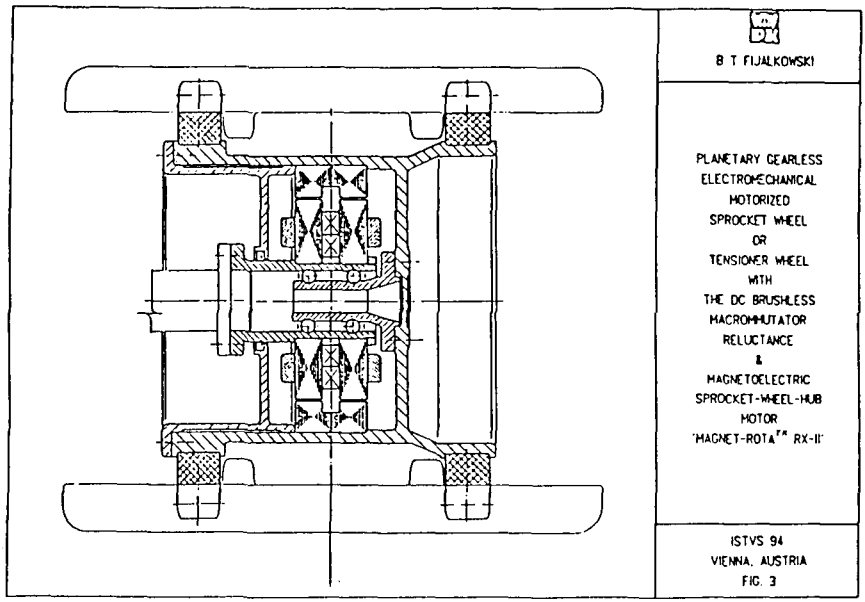

The electromechanical sprocket-, road- or tensioner-wheel-hub motor requires a minimum of space and can be mounted directly into the rim of the driven sprocket-, road- or tensioner-wheel due to its compact design. The result is substantially increased ground clearance and the space between the AWD & AWB & AWA caterpillar tracks can be used to locate a crew and payload (implements, armour protection, weapon and communications systems, ammunition, fuel, etc).

As a result of the ASIM macrocommutator design principle [3-5,7,9,11] of the electromechanical single- or twin-wheel-hub motors, the following important features are obtained: full starting torque directly in the motorized sprocket-, road- or tensioner-wheel without the loss of

efficiency caused by intermediate gearing; superior smoothness in speed control through outstanding low speed tractive performance; no mechanical axles - complete freedom in the design of the new concept AWD propulsion, AWB dispulsion and AWA suspension spheres; high external loads; constant torque throughout the full rotation; mechano-electrical regenerative coasting and braking; reversibility; free-wheeling; and extremely low noise level (especially valid during the DBW all-electric operation on the battle fields).

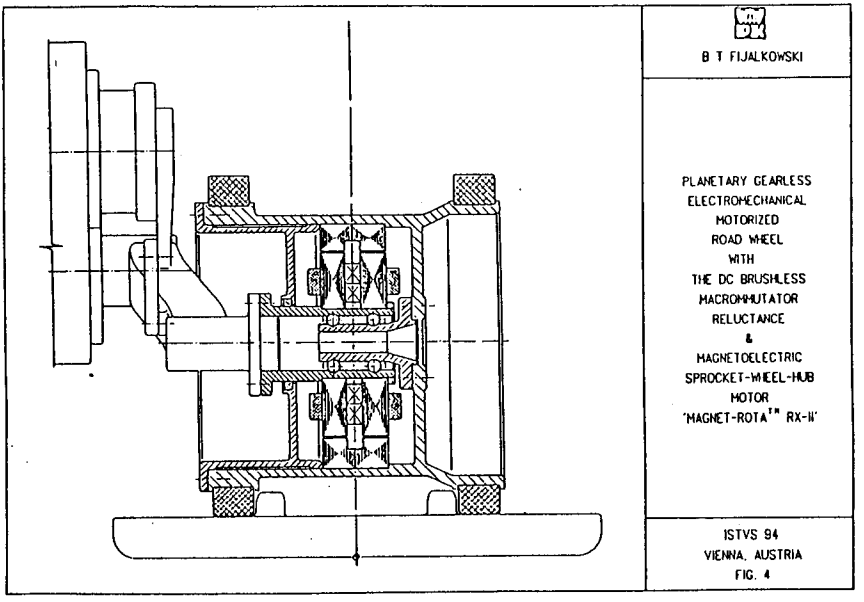

Figure 3 shows the principle layout of a planetary-gearless electro-mechanical sprocket- or tensioner-wheel with the brushless DC macrocommutator reluctance & magnetoelectric (unwound MSI outer rotor and wound & IPM inner stator) wheel-hub motor *MAGNET-ROTA™ RX-II* and Figure 4 - the principle layout of a planetary-gearless electromechanical road wheel with the same brushless DC macro-commutator reluctance & magnetoelectric wheel-hub motor *MAGNET-ROTA™ RX-II* conceived and newly designed by the author.

The electromechanical motorized sprocket-, road- or tensioner-wheel hub can be designed as to realize high radial stiffness and slim construction with less materials by using finite-element modal (resonant frequency) analysis methods and, together with the use of

special-sealed double-row angular-contact ball bearing, lubricated-for-life, and having preadjusted internal clearance, the excellent specific torque, that is torque/mass ratio (Nm/kg) can be realized.

The planetary-gearless electromechanical motorized sprocket-, road- and tensioner-wheels with the brushless DC macrocommutator reluctance & magnetoelectric wheel-hub motors thoroughly eliminate backlashes or hysteresis which are inevitable in using any speed reducers.

5. DRIVER-VEHICLE & TERRAIN-VEHICLE REAL-TIME EXPERT HYPERSPHERE

Figure 5 shows the driver-vehicle and terrain-vehicle real-time expert hypersphere incorporating model following fuzzy-logic programmable and neural-network learning motion control of the PL Pulaski IMBT. Very advanced control algorithms are required to motion control the PL Pulaski IMBT under highest order dynamics. They can be derived from a physical model and mathematical model of the PL Pulaski IMBT. These physical and mathematical models [14,23,31] ought to take coupling effects between horizontal (longitudinal and lateral) as well as vertical IMBTmotion dynamics into consideration and to include fast lateral accelerations. All states variables of the mathematical model, for instance, yaw angle and yaw speed, sideslip angle etc, can be evaluated by an state observer or measured directly by sensors [16-19].

According to the dynamical states and the target course (desired trajectory) of the PL Pulaski IMBT the control signals for hull AWA suspension, AWB dispulsion, AWD propulsion and skid-steering conversion can be calculated [28,29].

The driver-vehicle and terrain vehicle real-time expert hypersphere incorporating model following fuzzy-logic programmable and neural-network learning motion control of the PL Pulaski IMBT configurated as described above is hierarchical structured and a systems approach to study has adopted [9,14].

As shown in Figure 5, the structure is created with a seven-level hierarchy. On the first level named 'Human- and/or Telerobotic Driver' (H&TD) the target course (the desired trajectory), that is the desired for- and/or backward motion (manner of moving) in terrain and time of the full-time IMBT is evaluated according to H&TD-level multi-input (MI) signals and dashboard colour multi-function Head Down Display (HDD)

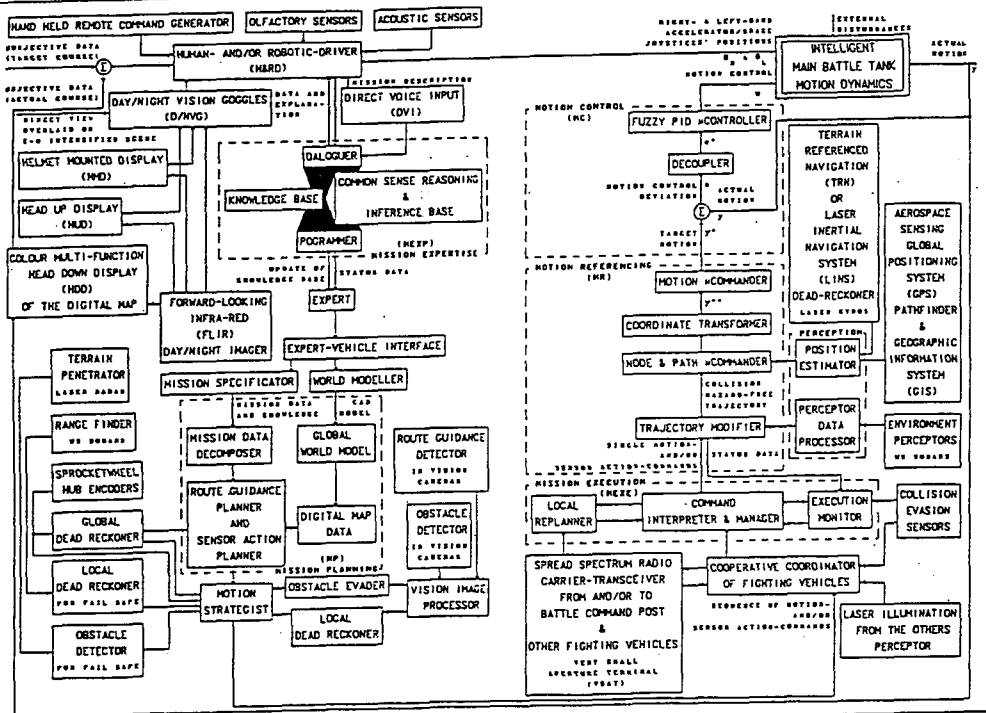

B T FIJALKOWSKI

DRIVER-VEHICLE & TERRAIN-VEHICLE REAL-TIME EXPERT HYPERSPHERE INCORPORATING MODEL FOLLOWING FUZZY-LOGIC MOTION CONTROL OF THE PL PULASKI INTELLIGENT MAIN BATTLE TANK

ISTVS 94
VIENNA, AUSTRIA
FIG. 5

of the Digital Map (DM) with the Horizontal Situation Indicator (HSI) overlay which displays heading track, tactical and other data to the H&TD, as well as Head Up Display (HUD) and Helmet Mounted Display (HMD) acting like feedback multi-output (MO) signals.

The dashboard HDD and/or HUD and/or HMD perform the main interface between the 'Human Driver' HD and the Internal On-Board Sensors (IOBS) as well as the External Anti-Collision Sensors (EACS) for terrain detection. The data displayed on the dashboard HDD, HUD and HMD are: motion data (for instance, driving data), diagnostic data, data requested by the HD and activated loads, as well as the DM with the HSI format. The H&TD-level of the hierarchical structure also receives the feedback IVS's MO signals which are displayed and the HMD and/or HUD and/or HDD for the DM with the HSI for driver-vehicle communication. The HD can also access all the additional data available by means a Mobile Keyboard (MK).

The integral steering-joystick position Θ_S or the right- and/or left hand accelerator/brake-joysticks' positions: Θ_R and Θ_L, respectively as H&TD-level's command MO signals are transferred not only to the on-board skid-steering and accelerator/brake actuators but also to the second level named 'Mission Expertise' (MEXP) or 'Reference Model Determiner' (RMD) as its determination MI signals. The right- and/or left-hand accelerator/brake joysticks are control levers in the PL Pulaski IMBT which the H&TD-level uses to order or control the sense of skid-steering direction, AWD propulsion, AWB dispulsion and AWA suspension motion directions. The mission description MI signals can be also transfered with the aid of a Direct Voice Input (DVI) with the Voice Synthesizer (VS). Development of DVI has taken place allows the HD to carry out switching actions such as mission description MI signals' change-of-mode or HDD format by spoken command. DVI offers a powerful means of control without HD having to remove his hands from the accelerator/brake joysticks. DVI is an attractive system and will undoubtedly be fitted to some, if not all, future fighting vehicles. However, on the ground of redundancy to cater for fail safe, the controls replaced by the DVI will not be removed from the PL Pulaski IMBT.

On the MEXP-level is provided necessary expertise for different missions in a problem oriented description. This basic elements of it are a dialoguer and programmer with the main components: knowledge base as well as common sense reasoning and inference base. Within the knowledge base the expertise is mainly stored in the form of logical

rules, semantic network, mission processing rules or frames. The common sense reasoning and inference base comprise strategies and rules for the search and the processing of the expertise in the knowledge base. The mission data requested by a H&TD-level are first decomposed into locomotion and combat missions. Then, a detailed route guidance planning, including the sensor action planning is done on the third level named 'Mission Planning' (MP) resulting in a sequence of motion- and/or sensor-action-commands' MO signals. The formation of the Global World Model (GWM) will be done completely menu-driven on the PL Pulaski IMBT's on-board Intelligent Computer Aided Design (ICAD) work station. The results may be stored as DM data and can be seen on a colour multi-function HDD.

The sequence of motion-commands' MO signals can possibly lead to collision hazards are transferred to the fourth level named 'Mission Execution' (MEXE) or 'Anti-Collision Predictor' (ACP) as its prediction MI signals. They are compared to the actual courses of obstacles which can be sensed and observed by External Anti-Collision Sensors (EACS). If collision hazards will be recognized the prediction MI signals will be converted to Collision-Hazard-Free (CHF) predicted MO signals and will be transmitted to the fifth level named 'Motion Referencing and Perception' (MR&P). Status data from MR&P and warnings from the EACSs are supervised by the Execution Monitor (EM). When an error occurs, especially when resulting from an unsuspected or unknown obstacle, a Local Replanner (LR) is performed by the error recovery procedure, thereby starting a sensor-based route guidance strategy.

On the MR&P-level can be used a very powerful motion referencing with an accurate guidance on continuous routes. Trajectory interpolation, feedforward and/or feedback commanding and coordinate transformation from global- and/or local-coordinates to target motion (propulsion, dispulsion, suspension and conversion) MI signals that are propulsion, dispulsion, suspension and conversion actuators' position MI signals are included. If there is no collision-hazard recognition the MR&P-level refrence-model determined MO signals can be directly transmitted to the inputs of the sixth level named 'Motion Control' (MC) or 'Decoupler' (D) that means the MR&P or ACP reference-model determined MO signals will be identical with the CHF predicted MO signals.

In the MC-level or D-level, the control MO signals will be decoupled that means separation of the individual Input/Output (I/O) channels depends on the new target motion MI signals of the IMBT's driver-

vehicle and terrain vehicle real-time expert hypersphere provided by the Motion μCommander (MμC) and on the horizontal (longitudinal and lateral) as well as vertical motion dynamics of the IMBT, that is the actual (measured) motion MO signals of the IMBT to stabilize it on the target motion in terrain and time. On the MC-level the control MO signals will be transferred to the seventh level of the hierarchical structure named 'Battle Tank Motion Dynamics' (BTMD) that represents the horizontal (longitudinal and lateral) as well as vertical dynamics of the PL Pulaski IMBT. The actual motion MO signals, that is the dynamical state variables can be measured directly by IVSs or can be estimated by a state observer. The six level of the hierarchical structure also includes the EACSs for obstacles detection and the dashboard display for driver-vehicle communication.

Thus, the full-time AWD x AWB x AWA PL Pulaski IMBT will have an MEXE-level or ACP-level that will be equipped with the EACSs for recognizing its position and also the positions of obstacles in front of it. In the case of collision hazards the MEXE-level or ACP-level will make changes in the target course of the IMBT. The vehicle-driver and terrain-vehicle real-time expert hypersphere incorporating model following fuzzy logic motion control generates the MIMO motion control signals for AWD propulsion, AWB dispulsion, AWA suspension and skid-steering conversion spheres of the IMBT's hypersphere. These MIMO motion control signals are transferred to the electromechanical ac-celerator/brake-joysticks actuators and electromechanical motorized sprocket, road- and tensioner-wheels of the AWD propulsion sphere, electromechanical brake-calliper actuators of the AWB dispulsion sphere, electromechanical activators' ER fluidical valves of the AWA suspension sphere as well as electromechanical accelerator/brake-joysticks actuators and electromechanical sprocket- road- and tensioner-wheels of the skid-steering conversion sphere of the IMBT's hypersphere. Hence the horizontal (longitudinal and lateral) IMBT motion dynamics is acted to stabilize MBT on the CHF path calculated by the Trajectory Modifier (TM) of the MEX-level or ACP-level.

6. SUMMARY, CONCLUSIONS AND SPECULATIONS

The R&D work, accomplished on the author's VAT Programme, has resulted in an experimental proof-of-concept series hybrid thermo-mechano-electromechanical and/or electromechanical AWD propulsion, AWB dispulsion and AWA suspension spheres, suitable for civilian and/or military tracked vehicles. Further it has been developed to a

state such that decisions on putting to practical use will be possible by the industrial community. Some of the specific advances include: novel single- or twin-wheel-hub motors mounted and integral with the new concept hybrid thermo-mechano-electromechanical and/or electro-mechanical AWD propulsion, AWB dispulsion and AWA suspension spheres of the tracked all-terrain vehicle; improved high-power ASIM macro-converter-based commutators in AC-to-DC and/or DC-to-AC ASIM macrocommutators of unique design and an on-board AI fuzzy-logic programmable and neural-network learning (P&L) low-power ASIC microcontroller (μC) in command of all of the sophisticated functions of the tracked all-terrain vehicle.

With the given hypothetical PL Pulaski IMBT, the ability to provide adequate mobility and steerability at high speed of travel will in conclusion depend upon interaction established between the AWD & AWB & AWA caterpillar tracks and the supporting-terrain different inorganic ground materials or snows. For this particular examination, AWD & AWB & AWA caterpillar tracks are considered as tractive implements creating the transfer of mechanical energy between the PL Pulaski IMBT and the terrain surface. If consideration of the proper utility of input mechanical energy is to be made in regard to efficient tractive performance of AWD & AWB & AWA caterpillar tracks under bearing loads relative to the nature of the supporting terrain, losses in energy arising from energy-dissipating characteristics of the AWD & AWB & AWA caterpillar tracks must be minimized. The efficiency of mechanical energy transfer from the AWD & AWB & AWA caterpillar tracks to the terrain surface will then be maximized. The terrain-track contact patches established between the AWD & AWB & AWA caterpillar tracks and the terrain surface and the manner in which the sets of forces are distributed and transferred across these contact patches are the controlling parameters which will establish the efficiency and creativity of the AWD & AWB & AWA caterpillar tracks in mobility/tractive performance.

Recently, VAT for civilian and/or military tracked all-terrain vehicles has received greater attention throughout *terramechanics* as part of measures for reducing a total motion resistance not only by increasing the speed of travel but also by decreasing the rolling resistances of all the motorized sprocket-, road- and tensioner-wheels; improving the mobility and steerability (especially for IMBTs, that are special-purpose unmanned battle field tracked all-terrain vehicles driven by Telerobotic-Drivers (TD) in eventuality of nuclear or neutron war); preserving the environment and saving energy.

Included as an integral part of this R&D work are specifications of the AGTG that is based on the FTB system, or the Fijalkowski engine with constant output, co-operating with the CH-ES, consisted of the advanced nickel- or silver-metal hydride DC chemoelectrical SB and the M-ES, consisted of the mechanical energy-storing DF with the brushless DC macrocommutator flywheel-disc dynamotor (generator/ motor) that are projected to have long life, high efficiency and are able to power the IMBT for over 500 km (300 miles).

The FTB system consisted of a M-PB, that is a primary M-ES, ie a mechanical energy-storing DF with the brushless DC macrocommutator (unwound IPM disc-shaped rotor) flywheel-disc dynamotor mounted on the output shaft of the AGTG. The use of new IPMs, for instance, *Sm-Fe-Ti-B*, *Sm-Fe-Mo* or *Nd-Fe-B* alloys' ones, in the primary M-ES, ie the mechanical energy-storing DF with the brushless DC macrocommutator flywheel-disc dynamotor and the secondary M-ES, ie the mechanical energy-storing DF with the brushless DC macrocommutator flywheel-hub or twin-flywheel-disc dynamotor offer benefits in terms of their specific power [kW/kg] and specific torque [kNm/kg] as well as efficiency.

This AGTG that is based on the FTB system allowed experimental investigation of what is referred to as *'no-wall-plug'* types of its use, where the M-ES starts and ends the propulsion mission at essentially the same state of charge and fossil or non-fossil fuel is only net supply energy. Lower SFC is achieved by mechanoelectrical regeneration of braking kinetic mechanical energy and by operating the AGTG in more efficient regions of the torque/speed domain. The FTB system has the advantage of relatively low mass, since very little mechanical energy is required to provide the AGTG's power boosting function.

The author's experience with this AGTG that is based on the FTB system verified that up to 50 % improvement in fossil or non-fossil fuel saving may be achievable with a one of this type. The experience gained with the experimental mechanically power boosted AGTG has shown that FTB configuration will be accorded increasing importance. If the FTB system is designed so that it is also feasible for energy-saving IMBTs in lower middle range, a wide application potential will be created. In principle this may result in large series manufacture runs, in turn meaning lower purchase prices which also means more favourable operating costs.

Recent author's studies of the AGTG that is based on the FTB system have suggested that AGTG need not be capable of supplying the peak power demands as the M-PB, that is the mechanical energy-storing DF with the brushless DC macrocommutator flywheel-disc dynamotor can meet part of the load. It is argued that reducing AGTG size contributes to the overall reduction in SFC of this AGTG compared to conventional AGTGs. As the AGTG that is based on the FTB system utilizes small turbine wheels in its most efficient modes, emissions can be greatly reduced.

In environmentally sensitive areas the PL Pulaski IMBT can also be powered by the CH-ES and/or M-ESs alone for short distances at medium speed. Some IMBTs' users are also concerned about noise, particularly when they are making noiseless day- and/or night-time special- and/or landing-operations in battle fields. The smaller, quieter turbine wheels of the AGTG that is based on the FTB system can if necessary be turned OFF when making noiseless special and/or landing operations in battle fields. The M-PB, that is the primary M-ES, consisted of mechanical energy-storing DF with the brushless DC macrocommutator flywheel-disc dynamotor then is acting as the DC macrocommutator flywheel-disc generator co-operating with the CH-ES and/or secondary M-ES and powering two front electromechanical motorized sprocket wheels (sprockets) and two rear electromechanical motorized tensioner wheels and fourteen electromechanical motorized road wheels in 18 x (2S + 14R + 2T) wheel arrangement. Fossil or non-fossil fuel saving obtained in the FTB system is enough to pay extra costs of the AGTG with an integral M-PB, that is a primary M-ES and an ASIC microcontroller as well as a CH-ES and a secondary M-ES.

Another advantage of the AGTG that is based on the FTB system is that lower grade fuels, such as lead-free petrol, diesel oil, kerosene, ethanol, methanol, liquefied petroleum gas or coal as well as compressed natural gas, vegetable oil, hydrogen etc. can be utilized without loss of performance, as the AGTG's thermo-mechanoelectrical power will provide only the average mechanical energy and the AGTG's thermo-mechanoelectrical power will give the short burst of mechanical energy needed when the IMBT is fast accelerating, hill climbing and high-speed travelling or cruising.

The use of two AGTGs offers a number of additional advantages:
- in contrast to the one AGTG, the two AGTGs can be controlled individually in a way that can effect a certain fossil or non-fossil fuel savings;

- in case of a breakdown, the IMBT can be powered by one AGTG only;
- the AGTG has a low total mass compared with the Diesel engine;
- low price through mass manufacture;
- inexpensive and proven parts and accessories;
- available parts and well-known service routines;
- use is made of the intensive R&D under way in AGTG design.

A basic feature of the AGTG that is based on the FTB system is that the AGTG and the M-PB as well as the ASIM macrocommutator and the ASIC microcontroller form an integral unit. Thus, the AGTG that is based on the FTB system is very light and compact.

The electromechanical motorized sprocket wheels (sprockets) and motorized road wheels as well as motorized tensioner wheels are driven individually by brushless DC macrocommutator (unwound MSI outer rotor & wound IPM inner stator) wheel-hub motors, and the rotation speed of each wheel-hub motor as well as speed of each AWD & AWB & AWA caterpillar track can be controlled arbitrarily by an on-board AI fuzzy-logic programmable and neural-network learning (P&L) ASIC microcontroller (ASIC microcommander). It was testified that the rolling resistances of driving motorized road wheels are lower than in the case of the free rolling road wheels.

Skid-steering conversion is achieved by varying the speeds and senses of rotation of the AWD & AWB & AWA caterpillar tracks which are powered from the AGTG that is based on the FTB system, or the Fijalkowski engine with constant output by an independent variable ratio proof-of-concept series hybrid thermo-mechano-electro-mechanical and/or electromechanical AWD propulsion sphere. The IMBT is highly mobile.

The AWD propulsion, AWB dispulsion and AWA suspension spheres' mechanisms are contained within the envelopes of the AWD & AWB & AWA caterpillar tracks (very little ground clearance being needed) giving a very low barycentre.

Besides, it has concluded that AWD & AWB & AWA caterpillar track's IMBT in comparison with only rear or front SWD caterpillar track's MBTs will show far better mobility and steerability on soft terrain or deep snow which is influenced first of all, by lower track sinkage during turning and steering response when changing the sense of the turning direction by a vehicle operated at high speed of travel.

New concept hybrid thermo-mechano-electromechanical and/or electro-mechanical AWD propulsion, AWB dispulsion and AWA suspension skid-steering conversion spheres usually have quite distinct advantages over existing thermo-mechanical SWD propulsion spheres as well thermo-mechano-electro-mechanical and thermo-mechano-fluido-mechanical SWD propulsion spheres for civilian and military tracked vehicles on cross-country difficult terrain, especially because the AWD & AWB & AWA caterpillar tracks result not only in a best distribution of terrain thrust (gross tractive effort) but also lowest net motion resistances and sinkages. The latters caused not only by an increase in the speed of travel but also a decrease in the rolling resistances of both the electromechanical motorized sprocket-, road- and tensioner-wheels.

Moreover, the new concept electromechanical skid-steering conversion sphere, which is recently integrated with new concept AWD propulsion and AWB dispulsion spheres, is straight-forward and recovered natural simplicity.

Tracked all-terrain vehicles with the new concept electromechanical AWD propulsion, AWB dispulsion, AWA suspension and skid-steering conversion spheres, thanks to their tractive performance advantages such as extremely high mobility and steerability, small slip and low track sinkage in turning on soft terrain and deep snow, as well as good steerability process at high speed of travel, will be increasingly employed in the civilian and/or military sectors.

Thus, the use of these new concept automotive functional spheres for AWD & AWB & AWA caterpillar tracks, conceived and designed by the author, opens up wide possibilities for improving fossil and non-fossil fuel economy, cutting initial and whole-life caterpillar-track costs, protecting the environment and bettering distribution of terrain thrust (gross tractive effort) as well as keeping both the net motion resistances of the AWD & AWB & AWA caterpillar track and track sinkages (rut depth) low not only by increasing the speed of travel but also decreasing the rolling resistances of all the electromechanical sprocket-, road- and tensioner-wheels, as well as significant reducing the peak track tensions, thereby opening the way for greater use of non-metallic materials on caterpillar tracks, for example, moulded rubber belt-type caterpillar tracks.

Such development could greatly reduce caterpillar-track mass and logistic burden associated with metallic materials for caterpillar tracks, for example, narrow uranium-powder transparent- type tracks. In simple

terms, the state of a given automotive heterogenous discrete dynamical hypersphere, that is an IMBT motion dynamics may be considered to be the smallest amount of data necessary to characterize completely any possible future behaviour of the hypersphere.

A driver-vehicle and terrain-vehicle real-time expert hypersphere incorporating model following fuzzy-logic and neural-network motion control of an IMBT provides necessary expertise for different tasks in a problem oriented description. The basic elements of it are a programming level and dialogue level with the main components: knowledge base and inference mechanism. Within the knowledge base the expertise is mainly stored. A human-driver perceives terrain conditions by visual sensation and senses, for instance, motorized road-wheel slippage by bodily sensation. By comparison with past experience, the human-driver decides on a given amount of command MI signals to be applied (Fig. 5), that is the skid-steering-joystick position Θ_S or the right- and/or left-hand accelerator/brake-joysticks' positions: Θ_R and Θ_L. While fuzzy logic [32] is considered to be applicable to qualitative approaches, it can replace perception and sense. Thus, the driver-vehicle and terrain-vehicle real-time expert hypersystem incor-porating ASIM microcontroller proves to be a highly applicable means of fuzzy-logic and neural-network motion control.

Driver-vehicle and terrain-vehicle real-time expert hyperspheres are much more practical and likely to be manufactured in the nearest future. Human-driver involvement may not only be at high hierarchical levels of abstraction - some low hierarchical level tasks are very difficult for AI. Automotive engineers and scientists are very good at image interpretation though route (node and path) planning (deciding which way to drive) is relatively easy to computerise. It is possible to comtemplate the capabilities of the human being utilized by the AI.

The PL Pulaski IMBT represents the Intelligent Vehicle Concept (IVC) of the future. A combination of medium profile hull with two front electromechanical motorized sprocket wheels (sprockets) and two rear electromechanical motorized tensioner wheels as well as fourteen (seven on each side) electromechanical motorized road wheels with the brushless DC macrocommutator sprocket-, road- or tensioner-wheel-hub motors will form the ideal 'green fighting vehicle' concept a reality.

The PL Pulaski IMBT will use the VAT (high-tech) for energy-storage DFs in particular the brushless DC macrocommutator twin-flywheel-disc dynamotors (generators/motors).

The sprung electromechanical motorized sprocket- and tensioner-wheels and unsprung electromechanical motorized road wheels are the hearts of the AWD propulsion and AWB dispulsion as well as AWA suspension spheres' concept, and they are uniquely packaged as integral parts of the latter automotive functional spheres of the PL Pulaski IMBT, thus improving efficiency and obviating the need for costly and complex axles and drive shafts.

The mobility and steerability as well as manoeuvrability of the PL Pulaski IMBT on all types of terrain surfaces, being in block terrain, swamps or on snow, will be without comparison better than other MBTs. It will also possible to considerably increase the rate of speed in cross-country difficult terrain.

Major performance parameters affected by the AWD propulsion, AWB dispulsion and AWA suspension spheres of the IMBT are nearly the same as for the running gear of conventional MBTs [26], viz.:

- good suspension/ride performance that is essential for high-speed cross-country movement on rough terrains;
- soft-soil performance (rolling resistance, traction, trafficability);
- hard surface rolling resistance that is caused in particular by rubber hysteresis losses in AWD & AWB & AWA caterpillar tracks and electromechanical motorized road wheels and also by frictional losses in AWD & AWB & AWA caterpillar tracks (dry pin), guide horns, sprocket/track interaction, bearings etc;
- noise and vibration caused by link back is a significant drawback;
- step climbing and gap crossing, closely related to the overall dimensions of the IMBT;
- swimming/water exiting and entry which often will present limiting soft-soil traction conditions.

The PL Pulaski IMBT incorporating the all-electric-wheel *'single-shaft'* AWD propulsion, AWB dispulsion and AWA suspension spheres and the flexible caterpillar tracks will have significantly reduced noise and vibration levels. Being traction (friction drive) a high level of caterpillar track pretension will be necessary and this would demand considerable changes to the AWD propulsion, AWB dispulsion and AWA suspension spheres of the PL Pulaski IMBT. PL Pulaski IMBT's AWD propulsion, AWB dispulsion and AWA suspension spheres have seen considerable progress in particular in areas of AWA suspension, ride performance, mass reduction and major electromechanical component durability.

The conventional SWD propulsion sphere for MBTs employs a single driven sprocket wheel (drive sprocket) for each SWD caterpillar track, that simultaneously performs two major functions [21], namely:

(i) to translate torque at the driven sprocket wheel into a backward shear force, thus providing traction;
(ii) to provide a caterpillar trackway surface to spread the road-wheel loads, thus reducing rolling resistance and sinkage.

VAT opens the way for new concept smart electromechanical AWD x AWB x AWA IMBT design and permits a radical new concept of MBTs. The preliminary results of the author's *Automotive Mechatronics R&D Team* work are as follows:

(i) compact AGTGs that are based on the FTB system with the brushless DC macrocommutator flywheel-disc dynamotor (generator/motor) for on-board centralisation of electrical energy generation by series conversion of chemical energy firstly to thermal energy (combustion of fossil or non-fossil fuel) and secondly to mechanical energy and thirdly to electrical energy for ease and effective power distribution to all the wheel drive stations and trade-offs according to requirement (supplying electrical energy where it is necessary);
(ii) compact M-ES that is the brushless DC macrocommutator flywheel-hub or twin-flywheel-disc dynamotor for short-term on-board mechanical energy storage to facilitate regenerative braking and/or skid steering and the potential for DBW all-electric movement with stealth;
(iii) compact electromechanical motorized sprocket-, road- and tensioner-wheels with the brushless DC macrocommutator sprocket-, road- or tensioner-wheel-hub motors converting electrical energy to mechanical energy, thus providing all-electric-wheel *'single-shaft'* AWD propulsion sphere, and offering the following features: ability to remain mobile after loss of a single- or both the caterpillars tracks and several electromechanical motorized road wheels; improved draw-bar pull characteristics; improved obstacle crossing; improved efficiency; greatly enhanced specific power per unit mass (kW/kg) and specific power per unit volume (kW/dm^3), that is reduction in mass and volume of the electromechanical AWD propulsion sphere; reduction in caterpillar-track tension; reduction in caterpillar-track mass through adoption of new materials; elimination of gear boxes and clutches; and greater flexibility in design of IMBT layout;
(iv) compact high-power ASIM macrocommutators, capable of switching and controlling very large electrical currents;

(v) compact AI FN low-power ASIM microcontrolers, capable of controlling and monitoring power and loads within the AWD propulsion, AWB dispulsion, AWA suspension and skid-steering conversion spheres to provide effective power delivery and propulsion, dispulsion, suspension and skid-steering control.

These preliminary results of the author's *Automotive Mechatronics R&D Team* work have offered significant advantages of the PL Pulaski IMBT over conventional MBTs, but there are many problems to be overcome which will be reported in a future paper.

The most advantageous use of the PL Pulaski IMBT will be as a normal MBT or noiseless special- and/or landing-operation within battle fields for transportation soldiers to and from battle command posts. At battle fields this IMBT will be an excellent means of transporting crews or VIP and wounded soldiers battle side in a quiet, non-polluting, efficient style. An ability of the PL Pulaski IMBT to retain an enough level of mobility will exist even when it has sustained the loss of single or both caterpillar tracks, or even it has lost single or more electromechanical motorized sprocket-, road- or tensioner-wheels.

The PL Pulaski IMBT will incorporate the author's latest design features for improved tractive performance as well as mobility and steerability in varying cross-country difficult terrain conditions. This medium mass, strong and hard thick active heavily armoured metal-powder PL Pulaski IMBT will be especially useful for sand, mud, snow or ice. Its low profile and heavy-duty construction will make it ideal for use as an manned and/ or unmanned tracked fighting vehicle.

7. REFERENCES

[1] BEKKER M G: *Off-the-road locomotion*. Ann Arbor: The University of Michigan Press 1960.

[2] FIJALKOWSKI B T, and S STARUCH: Thyristor control for ***melex*** electric cars. *Proc. DRIVE ELECTRIC International Conference and Exhibition*, Wembley, England UK, 14-17 October 1980.

[3] FIJALKOWSKI B T: Trigistor frequency changer-controlled toothed gearless propulsion systems for electric and hybrid vehicle. *Proc. Europe's International Conference on Electric Road Vehicle Systems DRIVE ELECTRIC Amsterdam '82*, Amsterdam, The Netherlands, 25-28 October 1982.

[4] FIJALKOWSKI B T: Electronic-commutator AC/DC motor-driven tracked all-terrain vehicles with extremely high mobility. *Proc. 8th International Conference of the ISTVS, The performance of off-road vehicles and machines*. Vol. III, Cambridge, England UK, August 6-10, 1984, 1045-1063.

[5] FIJALKOWSKI B T: Power electronics propulsion systems for energy-saving automotive vehicles. *Proc. ISATA 84: International Symposium on Automotive Technology and Automation*. Vol. 1. Milan, Italy, 24-28 September 1984.

[6] FIJALKOWSKI B T: Very advanced propulsion automotive gas turbines' power boosting with low specific fuel consumption and low pollutant emission capability. *Proc. Autotechnologies '85: International Forum on New Automotive Technologies*, Monte Carlo, Monaco, 23 January - 2 February 1985.

[7] FIJALKOWSKI B T: On the new concept MMD electrical machines with integral macroelectronic commutators - Development for the future. *Proc First European Conference on Power Electronics and Applications*, Brussels, Belgium, 16-18 October, 1985, 3.377-3.384.

[8] FIJALKOWSKI B T: Future hybrid electromechanical very advanced propulsion systems for civilian wheeled and tracked all-terrain vehicleswith extremely high mobility. *Proc EVS 8: The 8th International Electric Vehicle Symposium*, Washington, DC, USA, 20-23 October 1986.

[9] FIJALKOWSKI B T: *Mathematical models of selected aviation and automotive mechano-electro-thermal discrete dynamical hypersystems (Modele matematyczne wybranych lotniczych i motoryzacyjnych mechano- elektro-termicznych dyskretnych nadsystemow dynamicznych)*. Monografia 53, Krakow, Politechnika Krakowska imienia Tadeusza Kosciuszki, 1987 (In Polish; Summary: In English, German and Russian).

[10] FIJALKOWSKI B T: Choice of hybrid propulsion systems: - wheeled city and urban vehicle; - tracked all-terrain vehicle. Parts I and II, *Electric Vehicle Developments - An International Publication*, October 1987, Vol. 6, No. 4, 113-117,142; and January 1988, Vol. 7, No. 1, 31-34; respectively.

[11] FIJALKOWSKI B T: Single-chip macrocommutator - An indispensable module of new concept AC and/or DC dynamotors for automotive very advanced propulsion systems. *Proc EVS 9: The 9th International Electric Vehicle Symposium*, Toronto, Ontario, Canada, November 13-16, 1988, EVS88-031, 1-6.

[12] FIJALKOWSKI B T: Very advanced propulsion spheres for high speed tracked vehicles. *Proceedings of the 10th International Conference of the ISTVS* , Vol. III, Kobe, Japan, August 20-24, 1990, 783-797.

[13] FIJALKOWSKI B, and J KROSNICKI: All-wheel driven track - A key component of future tracked electric/hybrid vehicles. *Proc 24th ISATA: Dedicated International Conference on ELECTRIC/HYBRID VEHICLES in conjunction with the 25th International Symposium on Automotive Technology and Automation*, Florence, Italy 20-24 May 1991, Paper No. 910630, 87-94.

[14] FIJALKOWSKI B T: Mechatronically controlled intelligent mobile battle tank. *Proc 25th ISATA: Dedicated International Conference on MECHATRONICS in conjunction with the 25th International Symposium on Automotive Technology and Automation*, Florence, Italy 1-5 June 1992, Paper No. 920816.

[15] FIJALKOWSKI B T, and K I TROVATO: A concept for mechatronically controlled full-time 4WD x 4WB x 4WA x 4WS intelligent vehicle for drivers with special needs. *Proc. 27th ISATA: Dedicated International Conference on MECHATRONICS in conjunction with he 27th International Symposium on Advanced Transportation Applications*, Aachen, Germany, 31 October - 4 November 1994, Paper No. 94ME060.

[16] FREUND E, and B LAMMEN: Collision avoidance in vehicular traffic. *Proc 20th ISATA: The 20th International Symposium on Automotive Technology and Automation*, Florence, Italy, 29th May - 2nd June 1989, Vol. I, 131-145.

[17] FREUND E, and R MAYR: A control system for automatically guided vehicles. *Proc 20th ISATA: The 20th International Symposium on Automotive Technology and Automation*, Florence, Italy, 29th May - 2nd June 1989, Vol I, 147-158.

[18] FREUND E, Ch BUCHLER, U JUDASCHKE, B LAMMEN, and R MAYR: A hierarchically structured system for automated vehicle guidance. *Proc 22nd ISATA: The 22nd International Symposium on Automotive Technology and Automation*, Florence, Italy, 14-18 May 1990, 351- 359.

[19] GIBSON P: Control and navigation for unmanned battlefield vehicles. *Proc 16th ISATA: The 16th International Symposium on Automotive Technology and Automation*, Florence, Italy, 11-15 May 1987, Paper No. 87046

[20] GREEN M: Electric drive could mean smaller, light tanks. *Armed Forces J. Int.*, October 1989

[21] HETHERINGTON J G: Electric, all-wheel-drive, tracked vehicles. *Journal of Terramechanics*, 1991, Vol. 28, No. 1, 79-85.

[22] JACKSON D M: *Construction and testing of an electric multiwheel drive tracked vehicle model.* MSc. Project Report, November 1989.

[23] KARAFIATH L L: Finite element analysis of ground deformation beneath moving track loads. *Proc 8th International Conference of the ISTVS , The performance of off-road vehicles and machines*, Vol. I, Cambridge, England UK, August 6-10, 1984, 277-290.

[24] KRONOGARD S-V, AND L MALMRUP: Advanced automotive turbine transmission system - Diesel competitive fuel economy with low emissions. *Proc. First International Automotive Fuel Economy Research Conference*, Arlington, Virginia USA, October 30 - November 1,1979.

[25] KRUEGER M E: The application of military and commercial technology to advanced traffic management systems. *Proc. 24th ISATA: Dedicated International Conference on RTI/IVHS in conjunction with the 27th International Symposium on Automotive Technology and Automation*, Florence, Italy, 20-24 May 1991, 1-3.

[26] MACLAURIN E B: Running gear design for speed tracked vehicles. *ISTVS/ FISITA 92 Seminar on Off-Road Vehicles, IMechE*, London, England UK, June 1992.

[27] OGORKIEWICZ R M: Electric transmission progress in Germany. *International Defence Review*, February 1992.

[28] POTT S: Improved calculation of the turning resistance of tracked vehicles. *ISTVS/FISITA 92 Seminar on Off-Road Vehicles, IMechE*, London, England UK, June 1992.

[29] SCHMID I C, and W TOMASKE: Power and torque requirements for skid steering vehicles. *ISTVS/FISITA 92 Seminar on Off-Road Vehicles, IMechE*, London, England UK, June 1992.

[30] THOMASON J: *The construction and testing of a model to investigate the concept of an electric multiwheel driven tracked vehicle*. MSc. Project Report, November 1987.

[31] WONG J Y, and J PRESTON-THOMAS: Investigation into the effects of suspension characteristics and design parameters on the tracked vehicles using an advanced computer simulation model. *Proc IMechE*, 1988, Vol. 202, No. D3,143-161.

[32] ZADEH L A: Fuzzy sets. *Information and Control*, 1965,No. 8, 338-353.

Ceramic Components in Tracks for Construction Equipment

Karl-Friedrich Fischer *, Michael Ketting°, Mathias Woydt^

Abstract

The total wear, especially of lubricated tracks, on construction equipment, is determined by the wear between the track bushing and the tooth of the sprocket.
To achieve an equal wear life for bushing and link, investigations have started to substitute the steel bushing with ceramic material. The newest material qualities of silicon nitride (Si_3N_4) were wear tested using simulated service conditions. Wear intensity was tested for different steel-ceramic pairs as well as the critical compressive rupture load of the bushing.
Because of the different coefficients of elasticity for steel and ceramic, it is necessary to

- establish a reliable method for pressing of the assemblies
- guarantee functionally correct dimensioned press fit between the bushing and the link
- prevent additional stresses in the ceramic components

by using FEM-Modelling for the press fit optimisation. The first test and calculation results are discussed.

1 INTRODUCTION

Wear of tracked running gears and transport chains represents a permanent problem [1 to 7].
The propulsion of tracked construction equipment occurs due to gearing of the sprocket with the track (fig. 1). By this, considerable wear occurs between the two elements. Generally it can be assumed that the bushing wear, dependent upon the service application and the abrasive medium, is two to three times higher than the wear of the link for dozers and loaders. That is the reason for the common practice of bushing turns and

* Prof.Dr.-Ing.habil.; Head, Institute for Strength and Machine Dynamics, IAMT-Ingenieurgesellschaft für allgemeine Maschinentechnik mbH, Plauen, Germany
° Dr.phil. Dipl.-Ing. (TU); General Manager, Product Engineering and Development, Intertractor AG, Gevelsberg, Germany
^ Dr.-Ing.; Head, Laboratory Advanced Materials and Components Tribology, Federal Institute for Materials Research and Testing (BAM), Berlin, Germany

bushing replacements, that is the bushing receives a multi-usage within the same track and the links are reused to assemble reworked track. With this, evidently the wear between sprocket and bushing determines essentially the total wear on the overall track.

2 KINEMATICS AND WEAR BETWEEN SPROCKET AND BUSHING

To understand the significance of the wear between sprocket and bushing, it is necessary to examine the kinematic motion of the pairing as well as the abrasion mechanism. The evaluation must differentiate between wear on the sprocket tooth and the bushing.

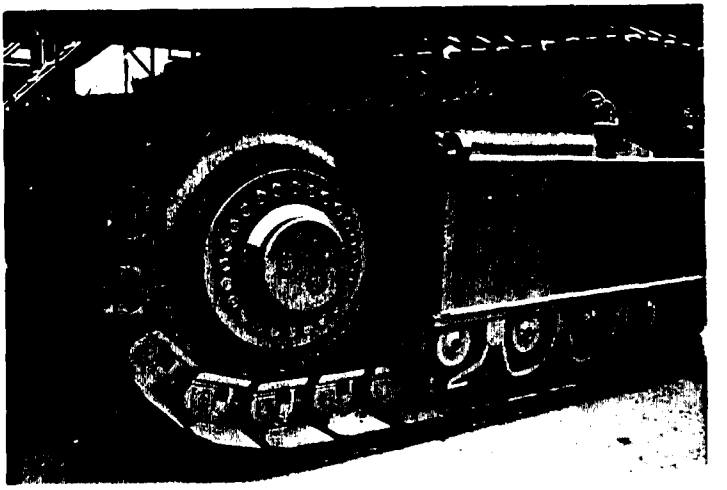

Fig. 1 Meshing of Sprocket and Track (Photo: Intertractor AG)

For the sprocket, the wear on the tooth flanks and root must be studied separately. Also, it is logical to differentiate between forward and reverse driving, as the force transmission occurs on opposite tooth flanks (fig. 2). Similar conditions are also found for the bushing. Therefore, it be can assumed that the wear between sprocket tooth and bushing will correspond to the ratio of forward and reverse travel of the equipment as well as to the different kinematics of the tooth to bushing meshing during this travel (fig. 3).
Figure 2b shows that the abrasion on the tooth flanks and the contact surface of the bushing during forwards travel are mostly due to the sliding of the bushing towards the tooth root. The sliding in the tooth root happens as the tracks wraps around the sprocket. The amount of sliding

motion that occurs is also dependent upon the track pitch, which increases due to internal wear.

The wear between sprocket and bushing during reverse travel is due to the sluing motion of the bushing on the tooth around the angular pitch at engagement (fig. 3), so that forward and reverse travel causes different and for the abrasion mechanism distinctive seperate contact surfaces. The sluing or rotating motion is the basis for the higher wear at reverse versus forwards travel. Systematic and in-depth studies [1] of the tribology between the sprocket and the track show the wear ratio for reverse versus forward travel for the bushing as 6:1 and for the tooth as 2.5:1. The abrasive material found at construction sites is also very determinant on the wear mechanism between sprocket tooth and bushing. The surface structures of the contact areas of the components are characterised by deep galling resulting from the relative motion between tooth and bushing under load, whereby reverse travel is more severe. From the knowledge of the kinematics and the wear mechanism between the sprocket and the chain, it is clear that the wear of the sprocket and bushing are dependent on the design and working environment.

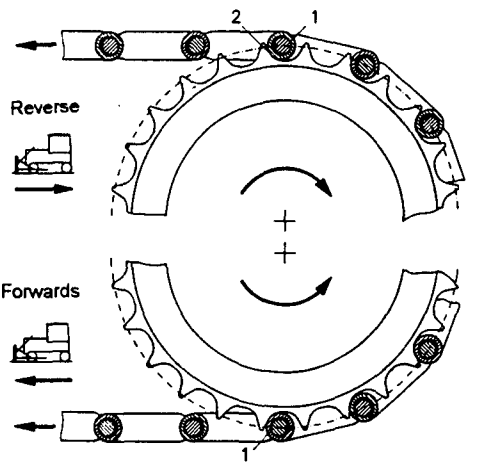

Fig. 2a: Engagement of Track in the Teeth of the Sprocket During Forward and Reverse Travel (acc. to [1, 2])
1. Friction Motion between Bushing and Pin
2. Friction Motion between Bushing and Tooth

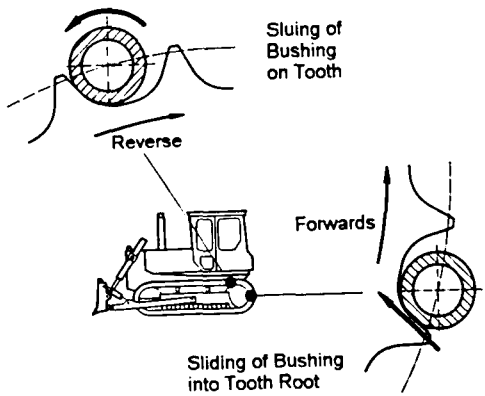

Fig. 2b: Sliding Motion between Bushing and Tooth as Cause of Wear (acc. to [1])

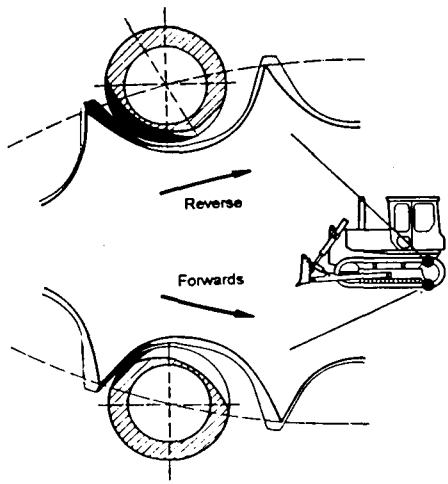

Fig. 3: Wear on the Bushing and Teeth Resulting from Different Kinematics of the Bushing Engagement During Forward and Reverse Travel (acc. to [1])

Within limits, the wear can be optimised by modifying the sprocket and tooth geometry [1]. The only way to achieve a decisive reduction in wear is through the use of materials that will stand up to the inherent kinematics and abrasive materials encountered by the machine at the work site.

It can be derived from the studies [1], that the present materials - primarily steel - used for sprockets and bushings in world-wide serial application (under simultaneous evaluation of the normal heat treatment) represent already the optimised wear solution, considering also economic factors. However, wear represents still a problem and there do not seem to be alternatives available in the area of metal materials. Therefore thought was given to the use of materials. Other than those in normally used for the bushings and sprocket teeth.

Special engineering of fine ceramics offers an alternative. Their potential suitability for the use on construction equipment was studied.

3 LOADS

The description of the function of the track kinematics shows, that under realistic field conditions of construction equipment, a load of the track bushing is not only applied through the track pull; additional shock loads are generated when the bushing is pulled into the sprocket. This load especially results from the accelerating status of the machine respectively to the different speeds of the sprocket and the track; that means when the track is pulled into the teeth of the sprocket, a shock load occurs between tooth and bushing which is caused by the different directions of the speed vectors of both components (fig. 4).

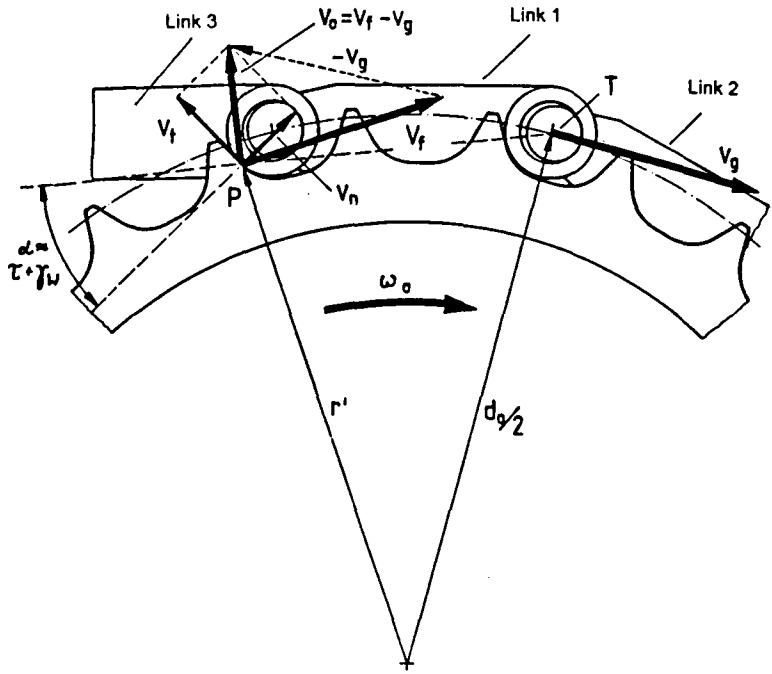

Fig. 4: Velocities of Bushing and by Engagement Impulse (Reverse Travel) (acc. to [3])

- p: Contact Point by Engagement Impulse
- T: Guide Point of the Engaged Track
- υ_g: Velocity of the Incoming Track Links
- υ_f: Velocity of the Contact Points of Bushing-Tooth
- υ_0: Relative Velocity Between Bushing and Tooth Shortly Before the Engagement Impulse
- υ_n: Vertical Component of υ_0 to Footh Flank
- υ_t: Tangent Component of υ_0 to Footh Flank
- d_0: Diameter of Reference Circle
- γ_w: Effective Flank Angle
- τ: Angular Pitch

Simultaneously with the impact, additional wear - not yet discussed in chapter 2 - takes place between tooth and bushing which is caused by impetuous surface damage and chain vibrations on the carrying run. These interrelations demonstrate the correlation of the acting wear mechanism with the mechanical problem field of the dynamic impact load during the pull-in phase of the track into the sprocket; consequently, the variations in time of the standard tooth force and friction force between sprocket tooth and track bushing as well as the impact acceleration have to be considered to understand the total problem.

In addition, in [1] as well as in [3] a complex calculation model was developed to meet these requirements. This model was the basis for the concept of a wear simulator [4] which was realized in connection with the before mentioned investigations [1 - 3] simulating the pull-in of the track bushing into the sprocket teeth as realistically as possible.

The test bench is driven by a test cycle which is in accordance with the calculation model of the variation in time for the standard tooth force and the torque angle in reverse (i.e. highest wear). In addition, for the calculation of the tooth's forces, the friction values between bushing and tooth even under abrasive conditions will be measured.

The in [1] and [3] recorded measurements of the pull-in impact from a separate running gear test bench show that the decay speed compared with the pull-in time is negligibly low which means that the static method can be used for the determination of the tooth force. As the variations in time for these measurements were only conditionally reproducible, an exact quantification of the impact strength was not possible. In addition, the simplified version of a running gear test bench would only give approximate values anyway, thus we have not obtained respective standards for the limit load of the bushings.

The breaking load values for the bushing made from the ceramic materials under investigation will have to be determined by practice oriented breaking tests (section 6). Their suitability for the use in tracks has to be evaluated in field tests.

4 Ceramic Application

Today, fine ceramics are applied as "state-of-the-art"-components for wear protection and for protection against corrosion. Few efforts are

known to introduce full-ceramic parts in applications with simultaneous tribological and mechanical stresses because they seem to be too brittle and have a too low of a room temperature strength compared to steels. The mechanical properties of some commercial ceramics available today contradict to this opinion as shown in table I.

Material	Strength [MPa]	Fracture toughness [MPa √m]	Elastic modulus [GPa]	Vickers-hardness [GPa]
SSi_3N_4 (EkaSin S)	~ 750+	7.0	275	15.4
GP-Si_3N_4 (SN235P)	~ 980+	6.7	306	14.5
SSiC (EkaSiC D)	~ 410+	3.2	410	28
GP-Si_3N_4 (HOE 120)	> 1200+	8 - 10	300	-
100Cr6H (AISI 52 100)	> 2000*	16 - 20	210	7.4
SAE15B15Cr	900 - 1300*	. / .	-	6.7 - 7.6
X155CrVMo121	. / :	23 - 27	215	6.5
C15 ISO 683 T 18	400 - 580*	-	-	1.5
GS37Mn5N	600 - 900*	. / .	-	2

+ = 4-Point-Bending-strength * = Tensile strength

Table I: Comparison of Mechanical Properties between Ceramics and Steels

As everybody knows, ceramic materials exhibit a high resistance against abrasive wear due to their high hardness, when the hardness of the abrasive particles (quarz sand = 750-1200 HV) is 20 % lower than the hardness of the structural ceramics ($Si_3N_4 \geq 1400$ HV) [10, 11].

If ceramic materials are suitable for abrasive-mechanical stressed applications, the running expenses can be lowered drastically. Typical examples of such branches and application are shown in table II.

Tribosystem	Abrasive	Branch
Mill and crush tools	Material to be ground	Cement plant, food and building material industry, Mining, road engineering
Track chains	Soil, moisture, minerals, silt	Tractors, loaders, excavators, Mining, agriculture
Pinion gears	powder dust	Conveyor, Cement and coal industry
Roller chain gears	powder dust	Mining, conveying systems
Hinge, link joints, pivoting bearings	Polluting particles, powder dust, silt	Tractors, loaders, agriculture, construction equipment.

Table II: Abrasive Wear in Production Plants

The bushings and sprockets of tracked tractors, loaders and excavators are typical parts, which are subjected to severe corner and bushing wear as well as to high peak loads.

Contractors are continually seeking larger machines that require less maintenance and repair, can bulldoze more material per pass, rip harder rock and push load a scraper with one tractor instead of two.

To contribute to these requirements, a servohydraulic test bench for abrasive wear with original D 6 or D 4 bushing was designed and built up at BAM. In this practically oriented test bench, new materials can be evaluated.

5 TEST CONDITIONS

5.1 Description of test bench

The working method and the operation are described in [1, 4] and illustrated by Fig. 5.

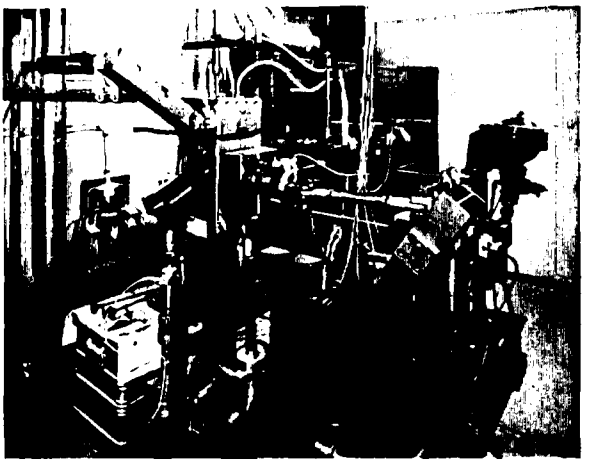

Fig. 5: Photograph of the Servohydraulic Bench for Abrasive Wear.

Original full-size components can be tribologically stressed outside of the application under defined test conditions giving reproducible results in a short time. Primarily, the force and the movement characteristics between bushing and sprocket of tracks can be simulated operationally and quarz sand can be added definitely. Normal and friction forces are beared uncoupled to avoid interdependencies. The main test conditions are the following.

Normal force	= 30 kN (increasing force)
Number of cycles	= 10.000
Simulated velocity	= 3 km/h
Swing angle	= 30°
Bushing D6D	= 69 mm outer diameter, 147 mm length

200 g/min fire dried quarz sand with a grain size distribution between 0.1 and 0.4 mm was added.

All experiments presented in this paper were performed as three-body abrasion and as unlubricated tests without abrasives. The reproducibility of the wear volume lies in the range of ± 5 %.

5.2 Materials

In this test program, conventional metallic material, like SAE15B15Cr, GS37Mn5N, 30MnB4 and 35MnCr5 as well as special steels of type 100Cr6 (AISI 52 100), 51CrMoV4 and X155CrVMo121 were tested.

Fig. 6 shows a full-ceramic and full-sized D6-bushing and a flat sample made of sintered Si_3N_4 compared to steel one. Two different types of Si_3N_4 were selected. EKaSinS is a sintered Si_3N_4 with around 8 weight-% of sintering additives and a gas pressure sintered Si_3N_4 (SN235P) with low content of sintering additives. The bending strength of SN235P with 1000 MPa is quite high. Some mechanical properties of the materials used, if they were accessible, are presented in table II. It is visible that the mechanical properties of ceramics today are close to those of steels.

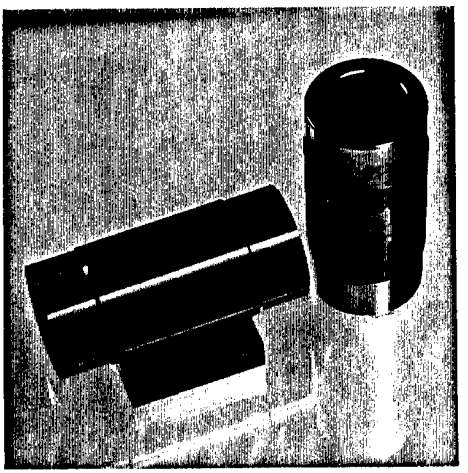

Fig. 6: Fullceramic D6D-Bushing and Flat Sample (sprocket) made in Si_3N_4

Bushings could not be manufactured in sintered SiC, because the bushing price in SiC will be too high and the strength and toughness are too low. Only flat samples in the dimensions 80x80x20 mm were used. SiC flat samples survived only tests with 10 kN, while they all failed at 20 kN and 30 kN. A similar situation occurred with D6-bushings made of the cheaper reaction-bonded SiC (SiSiC). These SiSiC bushings ran 10.000 cycles at 30 kN, but showed cracks after the tests.

6 TRIBOLOGICAL RESULTS

Figures 7 to 10 give a complete overview about the realized tests. The results are presented in two different wear specifications. First, the widely used wear volume per cycle and second, the volumetric wear factor [$mm^3/N \cdot m$], where N is Newton and m is sliding distance in meter, according to DIN 50 324. The description of the wear by the wear factor or wear coefficient enables the comparison to other results in different test systems with divergent normal forces and sliding distances.

6.1 Abrasive Wear

- Sintered Si_3N_4

Sintered Si_3N_4 bushings reduce the three-body abrasive wear by a factor of 6 compared to steel bushings, when the flat samples were steel. The greatest decrease in wear exhibits the full-ceramic couples, where no wear was detectable on the flat sample. The substitution of flat steel samples by sintered Si_3N_4 lowers the abrasive wear up to a factor of 8. The wear volume of the steel parts is unbiased by sintered Si_3N_4 substitution. The Figures 7 and 8 both illustrate an important wear reduction of the whole steel/Si_3N_4- or Si_3N_4/steel couples, compared to steel/steel couples.

Typical in practice, the abrasive wear volume of steel bushings is greater by a factor of 1.0 to 3.7 than this of the steel corners, similar to the results from the bench tests.

Sintered Si_3N_4 influences this relationship of wear in the combination sintered Si_3N_4 bushing/steel flat sample in the range from 0.6 up to 1.3 and in the combination steel bushing/Si_3N_4 flat sample in 8.8 up to 20.4. One has to remember that the total abrasive wear of both tribological partners is in any case lower with Si_3N_4.

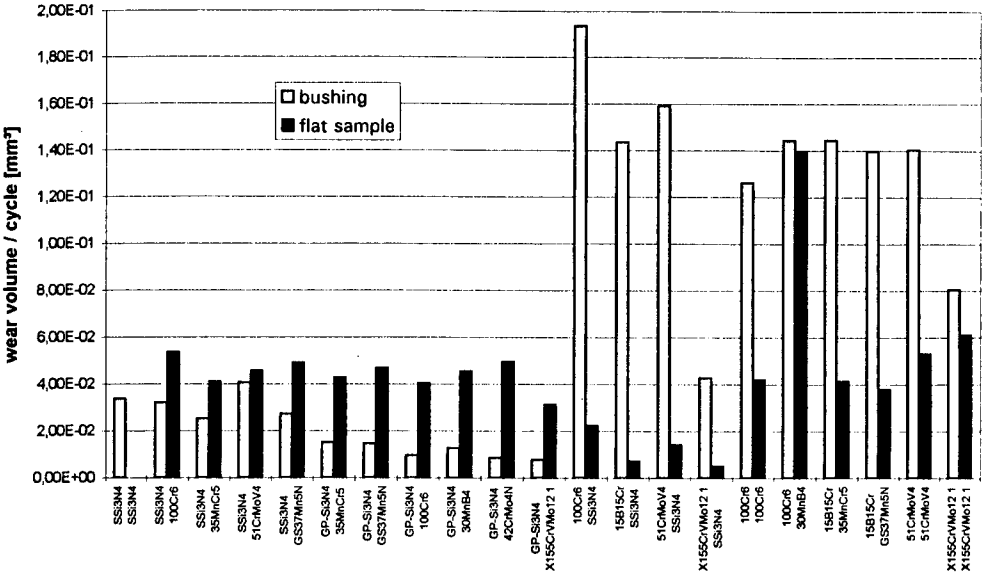

Figure 7: Wear Volume per Cycle [mm³] of Different Bushing and Flat Sample Materials with Quarz Sand

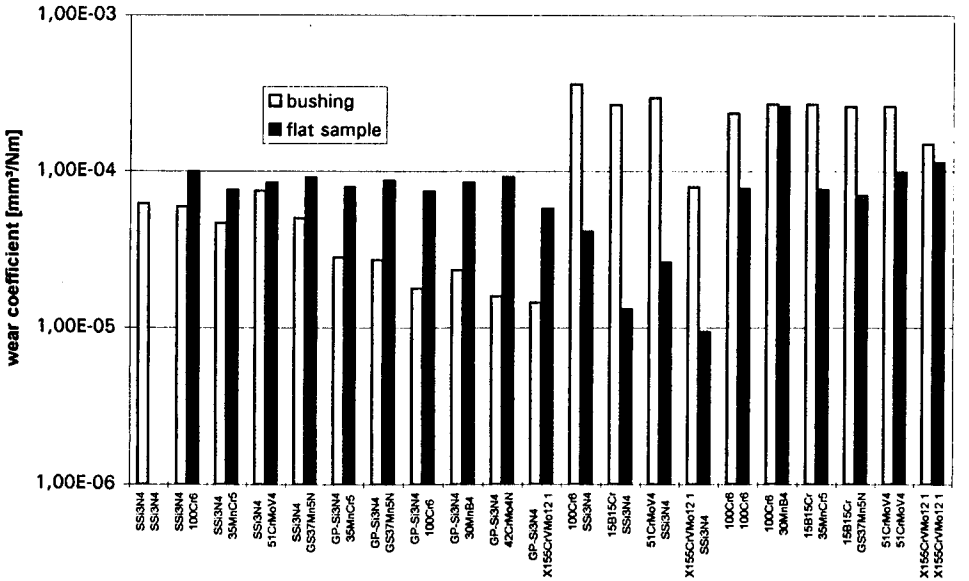

Figure 8: Wear Factor [mm³/(N·m)] of Different Bushing and Flat Sample Materials with Quarz Sand

- Gas-pressure sintered Si_3N_4

The reduction of abrasive bushing wear by the GP-Si_3N_4 is much higher than with the SSi_3N_4, as shown in Fig. 8. GP-Si_3N_4 tend to have by a factor of 2 to 3 lower wear coefficient under quarz sand than SSi_3N_4. By the substitution of SSi_3N_4 with GP-Si_3N_4, the wear of steels is not influenced. Table III summarises the global abrasive wear reduction by Si_3N_4. Another interesting remark from table III gives the combination SSi_3N_4/SSi_3N_4. The abrasive wear is reduced for the bushing by a factor of 5, but at the flat sample no wear could be measured!

bushing material	Wear ratio material/steel	flat sample material	wear ration material/steel
Steel	0.6 ... 1.5	Steel	1 ... 1/3
SSi_3N_4	1/8 ... 1/4	Steel	1 ... 0.75
GP-Si_3N_4	1/20 ... 1/8	Steel	1 ... 0.75
Steel	0.2 ... 1.6	SSi_3N_4	1/4 ... 1/2
SSi_3N_4	1/5	SSi_3N_4	n.m.

bushing 100Cr6H set = 1; Quarz sand; F_N = 30 kN; 10.000 cycles; n.m. = not measurable

Table III: Qualitative Comparison of the Global Abrasive Wear Reduction by Si_3N_4

6.2 Wear without abrasive

Sintered Si_3N_4

The level of the wear volume at the test without quarz sand is more than one order of magnitude lower, but Si_3N_4 did not in any combination with steels reduce the wear and thus improve lifetime (see figures 9 and 10) especially compared to the SAE15B15Cr-bushing/GS37Mn5N flat sample couple. Also, these tests reveal a widely known experience [12, 13] with self-mated Si_3N_4 couples under dry friction: they exhibit severe wear.

- Gas-pressure sintered Si_3N_4

As with abrasive, GP-Si_3N_4 performed under tests without abrasive (dry friction) better than SSi_3N_4.
The couple GP-Si_3N_4/X155CrVMo121 exhibited the greatest reduction in wear with a factor of 45 (see fig. 12), compared to steel.

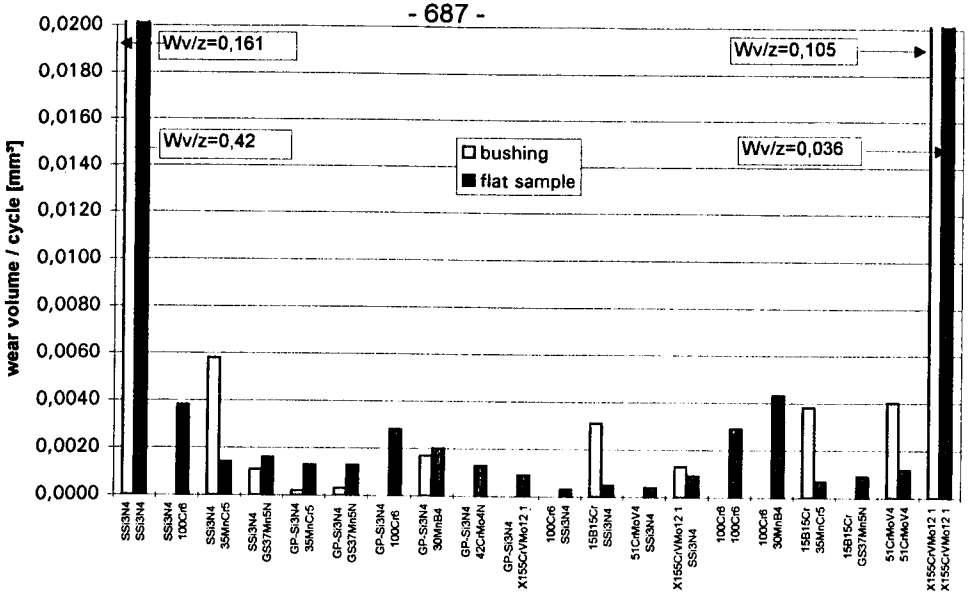

Figure 9: Wear Volume per Cycle [mm³] of Different Bushing and Flat Sample Materials under Dry Friction without Quarz Sand

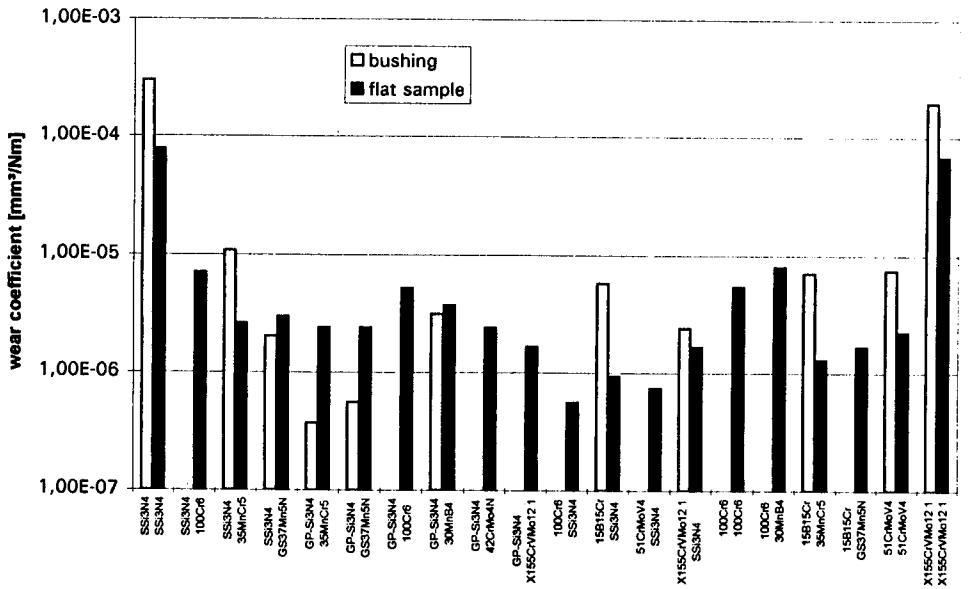

Figure 10: Wear Factor [mm³/(N·m)] of Different Bushing and Flat Sample Materials under Dry Friction without Quarz Sand

7 MECHANICAL PERFORMANCE

Beside the enormous reduction of the abrasive bushing wear by Si_3N_4, the question rises, if the fracture load of the ceramic bushing is high enough and the data from 4-point bending strength bars with 540 mm^3 can be transferred to bushings with 301.160 mm^3 stressed volume. The fracture loads were measured in a conformous contact with D6-bushings and increasing normal load at 10 kN/s (s. fig. 11).

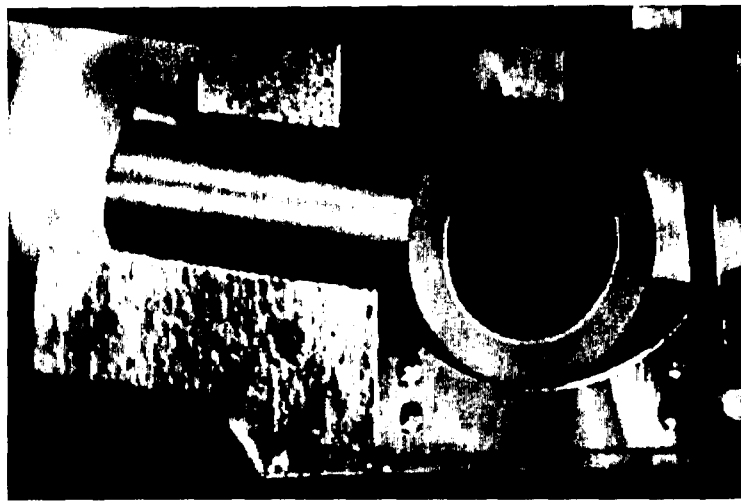

Figure 11: Photograph of the Configuration for Fracture Load Tests and with Fracture Initiation in Si_3N_4.

The results presented in table IV are quite high for GP-Si_3N_4 and reach the half of steels. It has to be kept in mind, that the ceramic bushings were stressed before between 50.000 to 80.000 cycles at 30 kN and than machined to tubes with 66.6 mm in outer diameter. The mechanical results revealed, that the strength data obtained by 4 point-bending-methods can not be transferred to bushings. The fracture load data of ceramics may not only be characterised with the average strength calculated from the Weibull statistic, but also must be seen in relation with the Weibull-modulus m, who gives an indication about the materials homogenity.

Material	σ 4-point bending[2] MPa	Weibulmodulus m[2]	Load to fracture[1) 3)] kN
S-Si_3N_4	750	17	102-103
ND-Si_3N_4	800	15	70-92
GP-Si_3N_4	1000	22	170-190
Si SiC	350	14	< 15
100Cr6H	-	-	> 600*
SAE15B15Cr	-	-	385-530

1) */Sample dimension: Ø : 66.6 mm, length: 150 mm
except* where Ø : 69 mm

2) Sample volume 540 mm³; 3) Bushing volume 301 100 mm³

Table IV: Fracture Load of D6-Bushings

8 MANUFACTURING AND ASSEMBLY OF TRACKS

There is no question about the fact that the operational aspect in relation to the function of the running gear components plays a major role in view of wear and loading if one starts to think about the use ceramic bushings in tracks. However, special consideration has to be given also to the aspect of manufacturing of the components and their assembly, because of the specific boundary conditions given by the different material characteristics. Especially in assembling the track (e.g., press fitting the links and bushings), the process technological accuracy has to be ensured. Because of the different coefficients of elasticity of steel for the link and of ceramic for the bushing, it becomes necessary to dimension the press fit between link and bushing in such a way that the operability of the track is guaranteed; simultaneously, it has to be avoided that additional tensile stresses are initiated in the ceramic components which would lead to early failures.

Therefore, it is necessary to evaluate the strength and the stress state of the press fit between the ceramic bushing and link. The press fit optimisation requires furthermore the proof of sufficient lifetime and

reliability. From this, investigations and conclusions result in the press fit optimisation.

Stress state in the ceramic bushing is estimated according to the theory of linear elasticity. As simplified model the press fit between two tubes was chosen. The axial-symmetric pressure stress in the fit is calculated under the assumption of plane strain. Additional FEM-simulation takes into account compression stress as radial load on the outer face of the bushing as well as axially fixed nodal points along the fit length.

Advanced ceramics are brittle materials. So one can neglect effects of yielding and use the principle of superposition to obtain stress distribution. This comes close to the real behaviour of the ceramic material, whereas the estimation for the link is of the safe side.

The simplified model of two tubes gives the well-known distribution of radial and cirumferential stress across the walls of the tubes:

$$\left.\begin{aligned} \sigma_\varphi(r)\big|_i &= c_{1_i} + \frac{c_{2_i}}{r^2}, \\ \sigma_\varphi(r)\big|_i &= c_{1_i} + \frac{c_{2_i}}{r^2}. \end{aligned}\right\} \qquad (1)$$

The index i characterises the ceramic bushing (inner tube) and link (outer tube). The constants c_{1i}, c_{2i} are calculated according to the geometrical excess of the press fit Δr. Thus, the formula of optimising the press fit reads as follows, [14]:

$$\Delta r = \frac{\sigma_r(r)\big|_i}{\left(\frac{c_{1_i}}{\Delta r} - \frac{c_{2_i}}{\Delta r \cdot r^2}\right)} \qquad (2)$$

The calculation was accomplished for the bushing D6D (see chapter 5), and the geometrical excess Δr = 0.35 mm. The materials are steel (link) and GP-Si_3N_4 (bushing). Essential material parameters are shown in table I.

The FEM-calculation considers axially fixed nodal points of the surface mesh on the bushing along the length of press fit. Thus, the state after pressing is simulated. The resulting stress distributions show a bending effect across the wall of bushing along the length of press fit; this bending effect cannot be determined by means of the elementary theory. The maximum of tension stress one obtains on the inner surface of the bushing, is:

$$\sigma_{bmax} \approx 200 \text{ MPa}.$$

This value linearly corresponds with the geometrical excess.

Now, the influence of this tension stress on lifetime and reliability, is estimated [15]. The SPT-diagram is the well-known scheme, which shows the relationship between strength (uniaxial stress), failure probability, and lifetime. The following formula is used:

$$\ln P_f = \frac{m}{n-2} \cdot \left[n \cdot \ln \sigma_c + \ln t_c - \ln\left(B\sigma_{ic}^{n-2}\right) \right] \qquad (3)$$

P_f-failure probability, m - WEIBULL modulus (material characteristic), t_c-theoretical lifetime, σ_n-nominal stress, n - material parameter, $\ln\left(B\sigma_{ic}^{n-2}\right)$-material parameter.

In case of mechanical loading a lot of experiences shows the possibility of design ceramic components with the help of the SPT-diagram with sufficient accuracy.

The following material parameters are estimated:

$$m = 20;\ n = 50;\ \ln\left(B\sigma_{ic}^{n-2}\right) = 312.$$

The corresponding SPT-diagram is shown in fig. 12. If a lifetime of 5 years is taken into account, then the pairs of nominal stress and failure probabilities summarized in table V, are obtained from equation (3).

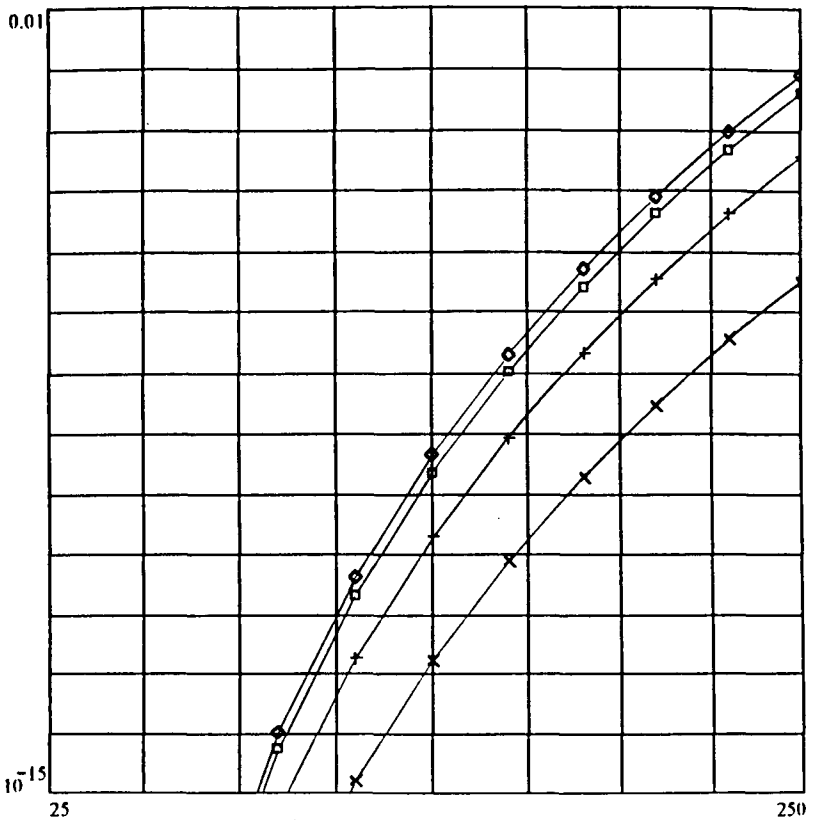

Figure 12: SPT-Diagramm
(failure probability Pf vs. nominal stress,
lines of equal lifetimes from bottom to top: 1s, 1d, 1a, 5a)

It is visible from table V, that the level of nominal stress (appr. 200 MPa) estimates the sufficient ratio: one failure of 100.000 bushings. However, caused by additional loading, the stress level can increase to 250 MPa. Then the failure probability increases to 8.21 of 10.000 bushings.
Thus, it is necessary in future investigations to consider additional time dependent loading histories of the press link.

Decreasing the bending strength in the bushing wall requires a decrease in pressure stress and geometrical excess, respectively. The following tasks have to be solved in future:

- Optimisation of geometrical excess considering quality management of the technology.
- Guarantee the functionally correct pressure stress in the press fit.
- Estimation of environmental and corrosion effects on crack growth in bushings.

nominal stress σ_n/MPa	log P_f	P_f
50	-17.6	
100	-13.38	
150	-7.71	1.96 E-08
200	-5.10	7.86 E-06
250	-3.09	8.21 E-04

Table V: Pairs of Nominal Stress and Failure Probability P_f, Lifetime 5 Years

9 REFERENCES

[1] Segieth, C.:
Verschleißuntersuchungen an Raupenlaufwerken von Baumaschinen.
VDI-Fortschrittsberichte, Reihe 1, Nr. 192.1990

[2] Segieth, C. und W. Poppy:
Verzahnungskräfte an Raupenlaufwerken.
Bericht im Rahmen des Forschungsvorhabens "Verschleißminderung und Lebensdauerverlängerung bei Raupenlaufwerken von Baumaschinen".
Technische Universität Berlin, Fachbereich Konstruktion und Fertigung, Institut für Maschinenkonstruktion, Fachgebiet Konstruktion von Baumaschinen. 1988

[3] Segieth, C.:
Messung des Einlaufstoßes beim Kettenumlauf an einem Raupenlaufwerk.
fördern und heben 39 (1989) 9, pp. 728-734

[4] Segieth, C. und W. Poppy:
Prüfstand zur Ermittlung von Gleitreibungszahlen unter Einwirkung abrasiver Zwischenstoffe.
Meßtechnische Briefe 27 (1991) 2, S. 43-49

[5] Müller, J. und M. Panas:
Schäden Vermeiden - Qualifizieren der Nutzungsdauer von hochbelasteten Rollenkettengetrieben.
Maschinenmarkt, 99 (1993) 4, S. 40-45

[6] Casemir, M.:
Das A und O der Laufwerkstechnik.
Sie & Wir - Fried. Krupp Hüttenwerke AG, Information 6/1980

[7] Ketting, M.:
Theoretical Principles to Optimize the Running Surfaces of Chain Links for Track Assemblies.
Proc. of 11th Int. Conference of the Int. Society for Terrain Vehicle Systems, Volume I. 1993, Lake Tahoe, Nevada, USA

[8] Woydt, M. und D. Steinmann:
Keramische Werkstoffe für umweltgerecht gestaltete Tribosysteme.
Metall 41 (1990) 9, S. 843-848

[9] Habig, K.-H. und H. Czichos:
Tribologie-Handbuch: Reibung und Verschleiß.
Publisher: Vieweg Verlag, 1992, ISBN 3-528-66354-8

[10] Uetz, H. (Editor):
Abrasion und Erosion.
Carl Hanser Verlag, München-Wien, 1986. ISBN 3-446-14215-0

[11] Hutchings, I.M.:
Tribology: Friction and Wear of Engineering Materials
Publisher: Edward Arnold, Div. of Hodde & Stoughton, London-Melbourne-Auckland. ISBN 0-340-56184-X

[12] Skopp, A.:
Tribological Behaviour of Si_3N_4 Materials under Dry Friction Between 22 °C and 1000 °C.
BAM-Research Report No. 197. N&W Verlag, 27511 Bremerhaven, Germany. ISBN 3-89429-400-0

[13] Woydt, M., A. Skopp and K.-H. Habig:
Unlubricated Sliding Friction and Wear of Various Si_3N_4 Materials Between 22 °C and 1000 °C.
Tribology International Vol. 23 (1990) No. 3, pp. 189-199

[14] Fischer, K.-F.:
Modell zur Bewertung von Buchsen für Gleisketten.
Forschungsbericht Projekt 0390-01, Institut für Festigkeit und Maschinendynamik, IAMT-Ingenieurgesellschaft für allgemeine Maschinentechnik, Plauen, Juni 1993

[15] Fischer, K.-F.:
Konstruktionskeramik.
Deutscher Verlag für Grundstoffindustrie, Leipzig, 1992

Off-Road Tyres with Emergency Capabilities

H. Haas

Missions given to wheeled armoured vehicles are numerous and with the light strike forces of today are ever increasing.

They perform such tasks as:

Reconnaisance
Personnel carriers
Material Transport
Anti Aircraft
Bridge construction
Missile carriers
Riot control
Fighting vehicles

In the gulf conflict where a number of countries served side by side many wheeled vehicles were utilised.

Reconnaissance and fighting vehicles included:

LAV 25	General Motors US (made under license from MOWAG-Swiss)
SAGAIE	Panhard France
AMX10RC	Giat Industries France
COMMANDO	Cadillac Gage (used by Saudi-Arabia manufactured in the US)

Among the personnel carriers used in the conflict were:

VAB	Renaults Vehicle Industry France
BMR	Pegaso Spain (used by Egypt)

Jeep type vehicles:

The Hummer	was also widely used

For the transportation of materials the US made 5 ton truck from BMY was a particularly well tried work-horse.

The U.S. also had the NBC Fuchs Vehicle manufactured by Thyssen on loan from the German Army.

All these vehicles without exception were fitted with a HUTCHINSON system.

Equipment currently being used in Somalia and Yugoslavia also includes wheeled vehicles.

Today in Europe industrie has been tasked to submit proposals for a new family of vehicles for use in the 21st century under the project headings tracer in the UK, and VBM in France. It would seem that various companies will offer wheeled armoured vehicles against track.

In the past the main obstacle to their use lay in a certain amount of hesitation regarding the suitability of wheeld vehicles fulfilling the necessary mobility requirements and in the vulnerability of tyres themselves.

In actual fact the main problem which a wheeled vehicle has to face is the constant risk of immobility due to a flat tyre. This can be caused by a bullet, shrapnel, or simply rough terrain, and is sufficient to prevent a vehicle from completing its mission. When a vehicle is neutralised there is a strong potential that it will be completely destroyed. One can imagine what would happen, if a number of vehicles were moving in convoy along a narrow and perhaps obstructed route and one of the leading vehicles is halted, they would all be exposed to air attack or other threat.

There are other occasions when wheeled vehicles are faced with having to cross soft or marshy terrains (mud, sand, snow). The consequences could be disastrous, if their progress is stopped or slowed by boggy ground.

We had evidence of this in the Falklands where vehicles could not move in the mud.

Wheeled vehicles, combat, light armoured, reconnaisance, armoured personnel carriers, logistic trucks all have one thing in common - the need to move in hostile and difficult terrains based on the effectiveness of the tyre and wheel assembly.

The importance of a safety device in the wheel now becomes obvious to give the vehicle a "get out" capability even when one, two or more tyres maybe punctured.

The problem has been identified and the solution must now be addressed. The following points were considered in HUTCHINSON's deliberations.

1. ON CROSS COUNTRY AND SOFT GROUND

A. Permit the vehicle to use the flexibility of the radial tyre.
B. Allow increase and decrease of tyre air pressure to improve mobility over various ground conditions

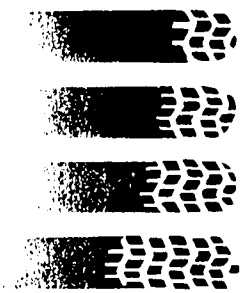

normal pressure	street, highway
middle pressure	piste, cross country
low pressure	snow, sand, mud
safety pressure	special and difficult terrain - muddy, sandy

C. Lock the beads of the tyre against the wheel rim
D. Eliminate tyre spinning on the rim
E. Prevent deterioration of the tyre at low pressure.
During a shock the internal face of the tyre may come into contact with the top of the run flat device.

If it is metallic, it will cut the tyre; if it is rubber, it will absorb the shock without damage to the tyre.

2. AFTER A PUNCTURE

A. Most important is to limit tyre collapse which reduces the deterioration rate and avoids damage to the gear box and differential. Also by limiting the collapse we keep the tyre and its tread in ground contact for running flat.

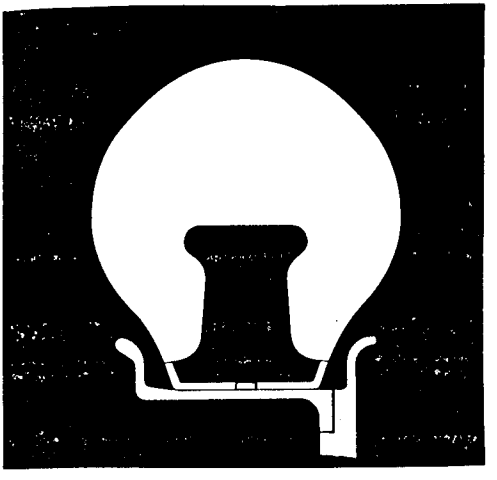

B. Support the vehicle load
C. Lock beads of the tyre against the rim and prevent separation of the wheel and tyre
D. Guarantee superior stability of ride and "get out" enhancement for several miles
E. Must meet the stringent standards of the european FINABEL 20 A5 and U.S. standards.

HUTCHINSON VFI/VPPV MOBILITY & SECURITY

Why is HUTCHINSON VFI/VPPV the best answer for a run flat device for military applications??

Description of VFI/VPPV

1. It is a device made of rubber - as previously determined rubber against the rubber of the tyre is the best solution.
It will not deteriorate the tyre when running at low pressure as a metallic system will do.
Will also ensure a smooth ride when running flat.

VFI

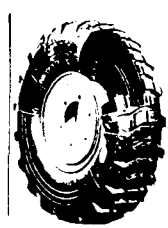

VPPV

2. Does not fill the entire tyre cavity.
The tyre is inflated normally.
No effect on tyre life duration
No speed limitation
No affect on acceleration
In actual fact the air pressure inside the tyre can be increased and decreased to suit the runnig conditions and increased mobility over various grounds.
It permits the vehicle to take advantage of the flexibility of the radial tyre.
When reducing air pressure the tyre foot print increases the tractive effect

and reduces the specific ground pressure. These are two elements for mobility.

3. The bottom of the VFI/VPPV acts as a beadlock.
The system locks the tyre beads against the rim and converts the output of the vehicles engine into tractive effort on the ground. It eliminates tyre spinning on the rim, avoids tyre separation from the rim and provides that the tyre bead seals airtight against the rim. This avoids entry of foreign matter such as sand, grit or stones inside the tyre.

4. The tooth or crown of VFI/VPPV limits the collapse of the tyre thus delaying rapid deterioration of the walls of the tyre.

What would happen to a flat tyre if it was not fitted with a HUTCHINSON insert?

It would not last very long.
It would be subjected to many destructive influences.
The diameter of a normal tyre is reduced from its usual dynamic operating size to a smaller diameter during flat running. The difference in circumferences between the tyre in the normal and flat running conditions leads to forced slipping and extreme crimping of the tyre support surface resulting in thermal overheating which may cause tyre failure (by burning for example).

The other cause to tyre failure leads to separation of the tyre coating from the carcass. The reason for this is that the wall of the tyre is folded outwards and pressed against the road surface.

This unavoidable contact with the road together with the friction of the side walls inside the tyre leads to their mechanical destruction.

With HUTCHINSON inserts the vehicle will proceed for a minimum of 50 kms or 30 miles keeping the tyre on the wheel.

<u>Our customers - market penetration - market share</u>

The exceptional advantages of our system are appreciated by all the major armoured vehicle manufacturers in the western countries. They consider HUTCHINSON VFI/VPPV an integral component of all their vehicles and fit them as a standard feature. You will find in the documents given to you a list, which is not exhaustive, of the vehicles clarified by makes and countries equipped with HUTCHINSON devices. We also attach a list of the armies in the world having in service vehicles equipped with HUTCHINSON devices.

BEADLOCK

1. Need for a beadlock

Wheeled armoured vehicles, combat vehicles and tanks need to be fed with ammunition, gasoline, etc.... The logistic vehicles may be whether on road or in the heart of the countryside.

To be able to proceed on soft ground it is sometimes necessary to reduce tyre pressure in order to achieve a longer foot print for better mobility.

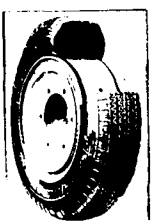

Beadlock

We know that wheeled armoured vehicles, being equipped with a run flat device, already have a beadlock - the bottom of the device.

For logisitc vehicles equipped or not equipped with C.T.I.S. a beadlock is compulsory.

2. The advantages of a beadlock

A. Allows to reduce tyre pressure for longer tyre footprint.
More contact with ground surface in soft soil, sand, mud and snow for better mobility.
B. Avoids tyre separation from rim.
C. Discourages tyres from spinning on the rims.
D. Provides that the tyre bead seal is airtight against the rim.
E. Keeps the bead against the side of the rim - even at 0 inflation.

HUTCHINSON is the sole supplier of beadlocks to the US army.

HUTCHINSON BEADLOCK = MOBILITY

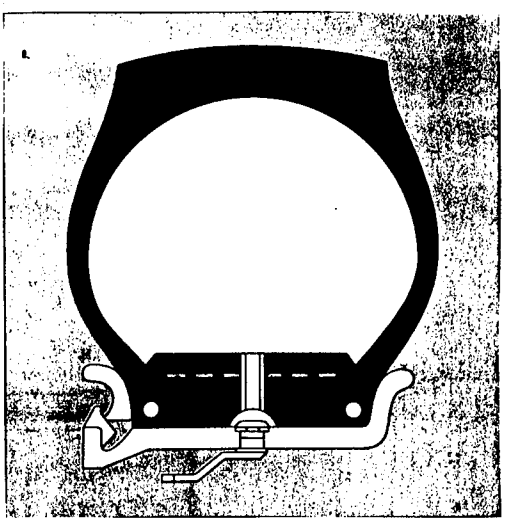

D.S.H.

All devices described until now are the best ones to use for military vehicles, because they block both beads of the tyre against the side of the rim which allow tyre pressure reduction in order to improve mobility when proceeding on soft grounds.

More so they are made of rubber and we know that it is better to have rubber device inside a tyre.
All these devices require a wheel with a flat rim, multi-piece and airtight.

There are some applications where the vehicle remains on the road (no cross-country requirement, no off the road mission). They are:

- Light military vehicles or logistic vehicle/jeep - TUL/TUM
- Police vehicles
- Anti riot vehicles
- Ambulances
- V.I.P. limousines
- Cash in transit, vans ...

These vehicles are generally equipped with a one piece wheel with a drop centre.

Taking advantage of our long experience in the run flat field, HUTCHINSON has developped and is marketing a new product.

1. What we were aiming at

- Easy to fit.
- Light in weight.
- Able to support the centrifugal force caused by high speed (VIP limousines).
- Preferably made by rubber.
- Ensure a good motricity.
- To be fitted on a standard one piece wheel.

2. What is motricity

When running flat, beads of the tyres will leave their seals. If the vehicle brakes or accelerates. If no motricity the tyre will spin on the wheel and the vehicle will either go out of control and have a crash or fail to move.

HUTCHINSON carried out a great deal of research and found that by keeping only one bead in position it was enough to make sure that the tyre will be blocked on the wheel, and therefore will never spin during braking or acceleration. Traction is maintained at all times.

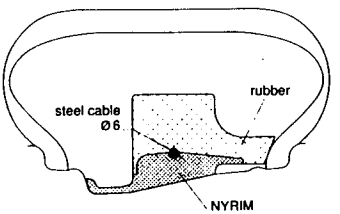

This is the major feature which separates HUTCHINSONS system from other "roller" type systems.

With more than 50 years experience in the run flat sector HUTCHINSON D.S.H. is our latest device. It permits vehicles fitted with the unit to run for long distances, at speed, with maximum safety after having had tyres punctured accidentally or through hostile aggression.

The D.S.H. consists of a single piece formed in a split ring and composed of a rubber tooth bonded to a base of Nyrim, which is a thermoplastic resin reinforced with glass fibre. The Nyrim base is molded exactly to the form of the drop centre wheel giving a perfect fit. One bead of the tyre is locked firm against the rim of the wheel by a rubber wedge which is integrated in the tooth of the device. This is an essential factor ensuring good motricity when braking and accelerating.

Other factors:

- Good ballistic resistance
- Good resistance to shock (when mounting the pavement)

The D.S.H. has simplified protective maintenance of vehicles:

- Easy assembly and dis-assembly
- Normal garage facilities
- Compatible with all commercial tubeless wheels

Following a tyre puncture the vehicle weight is supported by the rubber tooth. This absorbs shocks caused through rough ground or poor surfaces and ensures a greater comfort of ride in total security.

The Device Security HUTCHINSON (DSH) has been tested with great success by L'UTAC in the most severe conditions.

Harald Lach

HUTCHINSON
INDUSTRIE-PRODUKTE

HUTCHINSON INDUSTRIE-PRODUKTE GMBH
Postfach 12 09 62 D 68060 Mannheim
Hansastraße 66 D 68169 Mannheim
Telefon (06 21) 39 71 0 Fax (06 21) 39 71 2 06

NAZIONE	FABBRICANTE	TIPO DI VEICOLO	DISPOSITIVO HUTCHINSON IMPIEGATO	N.A.T.O. PART NUMBER
CANADA	GENERAL MOTOR	GRIZZLY LAV 25 PIRANHA 4X4 6X6	VPPV 11.00X16 TLMO VPPV 11.00X16 TLMO VPPV 11.00X16 TLMO VPPV 11.00X16 TLMO	2610.14.234.3029
CILE	CARDOEN	PIRANHA 4X4 6X6	VPPV 11.00X16 TLMO VPPV 11.00X16 TLMO	2610.14.234.3029
SPAGNA	ENASA	BMR	VPPV 13.00X20X8.50 TLMO	
FINLANDIA	SISU AUTO	XAPO	VPPV 14.00X20 TLMO	2610.14.351.1561
FRANCIA	GIAT	AMX 10 RC 155 TR	VPPV 14.00X20 TLMO B/L 14.00X20	2610.14.351.1561
	PANHARD	AML 60-90 ERC-SAGAIE M 3 VCR VLB ULTRAV	VPPV 11.00X16 TMLO VPPV 11.00X16 TLMO VPPV 11.00X16 TLMO VPPV 11.00X16 TLMO VPI 9.00X16	2610.14.234.3029 2610.14.234.3029 2610.14.234.3029 2610.14.234.3029 2610.14.449.7615
	RENAULT	VAB	VPPV 14.00X20 TLMO	2610.14.351.1561

NAZIONE	FABBRICANTE	TIPO DI VEICOLO	DISPOSITIVO HUTCHINSON IMPIEGATO	N.A.T.O. PART NUMBER
ITALIA	IVECO	A55F13/14	VPPV 7.50X16 TLMO	
		B1 (CENTAURO)	VFI 14.00X20 (41 KG)	2610.14.449.7619
		VM 90	VFI 9.00X16	2610.14.449.7615
		FIROS-MLRS	VFI 14.00X20 (41 KG)	2610.14.449.7619
UK	R.OF	FOX	VPPV 11.00X20 TLMO	
	GKN SANKEY	SAXON	VPPV 14.00X20 TLMO	2610.14.351.1561
GERMANIA	INTERMED	MILITARY HOSPITAL	VPPV 14.00X20 TLMO	2610.14.351.1561
	THYSSEN	TM 170-CONDOR		
		FUCHS	VFI 14.00X20 (53 KG)	2610.14.449.7618

NAZIONE	FABBRICANTE	TIPO DI VEICOLO	DISPOSITIVO HUTCHINSON IMPIEGATO	N.A.T.O. PART NUMBER
SVIZZERA	MOVAG	ROLAND 4X4	VP 9.00X20	
		PIRANHA 4X4	VPPV 11.00X16 TMLO	2610.14.234.3029
		PIRANHA 6X6	VPPV 11.00X16 TMLO	2610.14.234.3029
		PIRANHA 8X8	VPPV 11.00X16 TLMO	2610.14.234.3029
USA	AM GENERAL	HMMWV HUMMER	VFI 12.5X16.5X8.25	
	BMY	M939	B/L 14.00X20	
	OSHKOSH	PLS	B/L 14.00X20	
		HET	B/L 14.00X20	
	TELEDYNE	P23	B/L 14.00X20	

NATO PART NUMBER FOR HUTCHINSON RUN FLAT DEVICES

VFI 9.00 x 16 x 5.50	2610.14.449.7615
VFI 11.00 x 16 x 6.50	2610.14.449.7616
VFI 11.00 x 16 x 9.00	2610.14.449.7617
VFI 14.00 x 20 x 10.00/41kgs	2610.14.449.7619
VFI 14.00 x 20 x 10.00/53kgs	2610.14.449.7618
VFI 14.00 x 20 x 10.00/57kgs	2610.14.449.7620
VP 7.50 x 20 x 5	2610.14.243.741
VP 11.00 x 20 x 7.33	2610.14.346.1317
VP 8.50 x 20 x 6	2610.14.234.3032
VPPV 11.00 x 16 x 6.50	2610.14.234.3029
VPPV 14.00 x 20 x 10 TLMO	2610.14.351.1561
VPPV 14.00 x 20 x 10 Allégée	2610.14.374.6346

THE PREDICTION OF SOIL STRENGTH ON BASIS OF CLIMATIC DATA AS CRITERIA OF OFF-ROAD MOBILITY

Detlef Hinze *)

Institute of Automotive Engineering IKK
- Prof. Dr.-Ing. I.C. Schmid -
University of the Federal Armed Forces Hamburg, Germany

ABSTRACT

Terrain mobility of a vehicle on a given soil depends on the soil strength. The soil strength is influenced by the soil type and the soil conditions, which are the dry density and the moisture content. On natural soils the soil type and the soil density are nearly constant parameters for a defined area. In contrast to this the moisture content is not constant. The moisture content is decisive for the soil strength [1]. It is of importance in terrain vehicle evaluation, that the soil strength decreases with the increase of moisture content.

Till now soil strength has to be measured every day and couldn't be calculated, because of the most unknown parameter - the weather. This paper, orginated at the Institute of Automotive Engineering IKK - Prof. Dr.-Ing. I. Schmid - in Hamburg, deals with calculation of the moisture content in future, based on the known moisture content today and the development of the climatic data. In a physical and a mathematical model the correlation of soil strength and moisture content will be described. Further on the change of moisture content as a result of the weather situation will be discussed, too. So the relation climatic data moisture content - soil strength - off-road mobility is developed, mathematically described and on different soil types verified.

*) The author is professor at the Fachhochschule Hannover since October 1993.

1 INTRODUCTION

The off-road mobility depends on the soil strength. Further the soil strength is determined by the moisture content and the change of moisture content is a result of the weather situation. The weather determines with its precipitation and dryness the moisture content in the soil. Therefore it seems logical to assume, that moisture content can be derived from climatic data and that soil strength can be derived from moisture content. These algorithms to predict moisture content by climatic data and to predict soil strength by moisture content are described in the two models, named model A and model B. For a defined area it is possible on a 24 hour basis to calculate the development of moisture content and soil strength over every period.

2 MODEL A: PREDICABILITY OF THE MOISTURE CONTENT BY CLIMATIC DATA

For the balance of moisture content the following hypothesisses are necessary.

Hypothesisses:
- defined area
- constant soil type
- daily forecast
- constant soil density
- soil layer close to the surface of 10 cm (4 inches)

The daily variation of the moisture content is the result of the weather situation, of the water inflow and of the running off water, **figure 1**. These terms describe the water balance. So the moisture content w can be written as a daily development

$$w = w_1 + \Delta w \qquad (1)$$

w_1 measured or well known moisture content today
Δw daily variation the moisture content

The daily variation of moisture content Δw consists of two main parts. First the water inflow with precipitation N and capillary water GW, and second the running-off water with evapotranspiration V, surface run-off AB and gravitation water VS. So Δw in equation (1) can be written as

$$\Delta w = N + GW - V - AB - VS \qquad (2)$$

The parts of Δw will be examined in the following.

2.1 Water inflow - total soil moisture capacity

The discharge fluctuation is shown in **figure 2**. Described is the alterability of moisture content dependent on the hight above ground water. At first any dry condition has been considered. Moisture content increases with the increasing depth in regard to the soil surface, because capillary water increases from ground water. Above the ground water adjusts a closed (h_0, where all voids are filled with water) and an unsettled zone of capillarity. The distribution of water depends on the soil type. For every soil type exists a specific graph of the distribution of moisture content above ground water. For two soil types the graph is measured and calculated.

$$w = w_{saturated} * (h_0/h)^{\alpha} \qquad (3)$$

cohesionless soil	(sand)	$h_0 = 20$ (cm),	$\alpha = 1{,}66$ (-)
cohesion soil	(loam)	$h_0 = 5$ (cm),	$\alpha = 0{,}2$ (-)

The distribution of moisture content above ground water is a steady daily situation without precipitation. Superpose by precipitation a new moisture content will occur (curve 1 till 4 in **figure 2**). This behavior has to be described mathematically.

Rain water increases the moisture content. The moisture content increases as long as an upper limit of the moisture content w_{max} will be attained. The rise of moisture content happens so long till a highest value is reached, which the soil can tie up (curve 3). More rain water will percolate then (curve 4), but don't change the moisture content w_{max} in the soil layer close to the surface. More rain water increases the moisture content from the top to the ground water, where it drains off or increases the ground water. This influence is considered by the measured initial value w_1.

Figure 3 shows, that the precipitation N increases moisture content up to a maximum w_{max}. From that value more precipitation drains off or percolates. This running-off water will be especially considered, that an upper limit w_{max} consists, which couldn't be surpassed. That means everytime

$$w \leq w_{max} \tag{4}$$

Because the surface is critically for the off-road mobility, a soil layer of 10 cm close to the surface is important for the determination of the moisture content. In this zone it is to be remarked, that the moisture content varies between an upper and a lower limit. These limit values are depended on the soil type. Their difference defines the capability of the soil to store water in the pores. Generally in cohesive soils most of the voids are filled with water. If all voids are filled the system is saturated. In cohesionless soils there is a system, which is partly saturated. The voids are filled with air and water. Rain water can percolate quickly and don't change moisture content in the surface essentially. Dependend on the grain grade scale the soil belongs to a sand or a gravel.

The saturated moisture content can be described by

$$w_{saturated} = \frac{\rho_w}{\rho_d} - \frac{\rho_w}{\rho_s} \tag{5}$$

ρ_w water density ρ_d dry density ρ_s grain density

and then the upper limit of moisture content by

$$w_{max} = S_r * w_{saturated} \quad (6)$$

S_r saturation value

The upper limit w_{max} can be calculated or also can be measured after heavy precipitation.

The saturation value S_r depends on the grain size of the soil type. The soil type is described by his particle size distribution. Here the finest particle sizes determine the main soil property, because the finest particle have a bigger surface by the same mass than the bigger grain sizes. Kézdi [2] has shown the interdependence between saturation value and the effective grain size, **figure 4**. The effective grain size is the particle size by 10% of the grain size distribution. **Figure 5** shows the three curves of grain size distribution of the examined natural soils, where the effective grain size d_{10} is plotted, too.

The water inflow consists of two parts, precipitation and capillary water. The daily alterability of moisture content as a result of capillary water is neglectable and by this way it is included in the starting value w_1 of the general water balance, equation (1).

The running-off water consists of three parts. These are the percolation and the surface running off, which both don't change the moisture content in the soil layer close to the surface, and the evapotranspiration. Percolation and running-off are considered in the relation of equation (4). Evapotranspiration (evaporation and transpiration) are influenced by the weather, vegetable kingdom and soil type. They will be discussed in the following chapter.

2.2 Running-off water - climatic effects

As is well-known, only a limited amount of water vapour can be contained in a given quantity of air. This limit is determined by temperature. At very low temperatures only a small amount of water vapour can remain in the air; at very high temperatures a much larger amount is able to remain. Most of the time the air is unsaturated, because the humidity $F(T)$ of the air is less than 100%, **figure 6**. The difference between possible $F_{max}(T)$ and existing $F(T)$ will be introduced for the size of evaporation V and called characteristic evaporation value Vk. **Figure 7** shows an example for the determination of Vk.

$$Vk = F_{max}(T) - F(T) \quad (7)$$

The weather stations register temperatures, humidities and dew points (corresponding to $F(T)$, [3]) and can be easily called up or measured.

Evaporation is only possible if a difference is present between absolute $F_{max}(T)$ and relative $F(T)$ humidity. The difference determines and correponds to the evaporation V.

$$V = a * Vk \quad (8)$$

The proportionality factor a, soil influence factor, describes the influence of the soil to the evaporation and can be found by the best fit between measured and calculated points using the method of least squares.

As is known, increasing wind increases the evaporation. A wind influence factor f_v is determined by the wind velocity v in [m/sec]. The factor f_v can be found by literature and measurements of the weather stations.
This factor, shown in **figure 8**, follows the equation

$$f_v = 0{,}65 + v/10 \quad (9)$$

Just as the wind influences the evaporation, evaporation also changes with different kinds of flora. A larger surface of leaves increases the evaporation, then called evapotranspiration, and will be determined by a flora influence factor f_B. Experimental results in literature ánd own measured values show, that for grass the factor amounts $f_B = 2$ for example. Then the whole evaporation (evapotranspiration) is

$$V = a * Vk * f_v * f_B \quad (10)$$

2.3 Running-off water - soil influence

The soil influence factor *a* from the equations (8) and (10) will be analysed in this chapter.

At first own test results are shown, **figure 9a**. The water consumption about the course of evaporation for different soils and surface water is presented. The saturated soil samples had been dried over a long period under a constant weather condition *Vk*. While the evaporation from the surface water remains always the same, the water consumption of the soil samples decreases with additional days.

From the test results a mathematical model for water consumption is derived, **figure 9b**.

$$W_v = W_{vmax} * (1 - e^{-t/k}) \qquad (11)$$

It can be shown, that the soil influence factor depends on the weather situation, on the soil type, on the capability to store water and additionally it is time dependend [4].

$$a\,(t) = W_{vmax} * e^{-t/k} / (k * Vk) \qquad (12)$$

Remarkable is the large period of time for the same daily evaporation, **figure 9a**. It means, that in the daily water balance with running-off water and water inflow the daily soil influence factor *a* is a constant size and depends chiefly from soil type. This allowed to write

$$a\,(t) = a \qquad (13)$$

Because the character of soil type is described by small grain sizes, they have a bigger specific surface in relation to the same grain mass. Therefore the soil influence factor will be related to a small grain size, the effective grain size d_{10}. **Figure 9c** gives a proposal for the selection of factor a. It is developed from the best fit of measured and calculated data [4].

$$a = 0{,}5 / d_{10}^{1/3} \tag{14}$$

2.4 Water balance

Now the input data for model A to predict moisture content from climatic data are known. For a defined area the effective grain size, the dry soil density, the ground-water level and the flora will be assumed as nearly constant parameters. Dry soil density and effective grain size from the grain size distribution have to be measured. Based on this the soil influence factor a can be determined. Ground-water is considered by factor a and by the measured initial moisture content w_1. The climatic data can be called off from the weather stations. Otherwise temperatures (humidities) and precipitation are easily to be measured. Precipitation N had to be reduced by running-off water ΔN if $w \geq w_{max}$, following equation (4), and amounts

$$\Delta N = VS + AB \tag{15}$$

and

$$N_{eff} = N - \Delta N \tag{16}$$

Now the moisture content after a period of n-days can be calculated by

$$W_n = W_1 + \sum_{i=1}^{n-1} (N_i - \Delta N_i) - a * f_B * \sum_{i=1}^{n-1} Vk_i * f_{vi} \tag{17}$$

w_1 initial value, measured
N precipitation from weather station
Vk characteristic evaporation value
f_B flora influence factor
f_v wind influence factor
a soil influence factor

3 MODEL B: PREDICABILITY OF THE SOIL STRENGTH BY MOISTURE CONTENT

The pressure sinkage relationship depends on moisture content. Because in natural soils the pressure sinkage curve and the moisture content have a big range of scatter, it will be necassary to gather a great amount of data for developing regularities. So the off-road mobility - comparable with the soil strength - was measured with the cone penetrometer. **Figure 10** shows the measurment results and regression of the *CI* value and the moisture content for two soil types. Every point is the result of 36 CI values and of 10 moisture content values. The correlation between soil strength *CI* and moisture content *w* could be found by a linear regression.

$$CI = CI_0 - m * w \qquad (18)$$

The parameter CI_0 and *m* are given in **table 1**, part of **figure 10**. It is shown, that the variations of *CI* and *w* are bigger in the loam (cohesive soil), than in the sand (cohesionless soil). The effective grain size $d_{10} > 0.063$ mm is also a size for cohesionless soils.

Figure 11 shows the well-known coherence between soil strength *CI* value and off-road mobility expressed by the Vehicle Cone Index *(VCI* value). The difference *CI* between *VCI* decides in a simple, but experienced way about Go or No Go in the off-road mobility.

4 VERIFICATION OF THE MODELS A AND B

The use of models A and B will be shown for three natural soils about a long period of several calendar weeks. Soil-physical parameters as dry soil density, grain size distribution, soil type, grain densitiy and saturated soil are determined in situ or calculated of a defined area. The starting point value w_j was measured. Based on this all the other moisture content values are calculated by climatic data in a daily time. Climatic data as temperature, dew point for the present humitidy and precipitation are called up by a weather station, close to the test field. **Figure 12** shows an example for the given climatic data. These are the input data for the models A and B.

4.1 Verification of a sandy soil, Boberg

In the upper part of **figure 13** the climatic input data are plotted. The daily evaporation V is calculated by the equations (7) and (8). The course of time of moisture content is calculated by equation (17). The calculated curve compared to the measured points is shown. Both values agree well, even there are a good agreement with calculated and measured CI values in the lower part of **figure 13.**

Because the effective grain size is big, the percolation is high and the soil stores only a little bit of water. Therefore the moisture content w_{max} is less and the moisture content w varies in small limits. The upper part of **figure 13** confirms the statement, that the variation of moisture content has no influence to the size of the soil strength. In contrast to this in cohesive soils exist a significant dependence of the moisture content to the soil strength.

4.2 Verification of a cohesice soil (loam), Benstaben

These verification results of the models A and B are shown in **figure 14.** In the upper part the input climatic data of a period of four months are shown. In the middle part the comparison of predicted and measured moisture content is plotted. The lower part presents the comparison of predicted and measured CI values. The agreement of the measured and calculated points is always proper.

4.3 Verification of a second cohesive soil (loam), Reinfeld

Figure 15 presents the results of a second cohesive soil alike **figure 14**. Dry soil density is higher and w_{max} is less than for the first cohesive soil. The comparison of calculated and measured moisture content leads to comparable results. The comparison of soil strength is not so good. This is the reason of acting soil frost during the measurements. Slightly the results of soil strength are falsified by the soil frost.

5 CONCLUSIONS

Till now soil strength has to be measured every day and couldn't be calculated for the future time. Now with the two presented models, **figure 16**, soil strength can be calulated by climatic data. The new models are verified on three different natural soils successfully over a long and different period of time.

Hence it is possible to predict soil strength of a given soil without field measurements using only the development of climatic data.

REFERENCES

[1] BEKKER, M.G.:Introduction to Terrain - Vehicle Systems, Ann Arbor, The University of Michigan Press, 1969

[2] KÉZDI, A.: Handbuch der Bodenmechanik, Band 1, VEB Verlag für Bauwesen, 1969

[3] HINTZE, D.: The prediction of soil strength with the aid of climatic data, ISTVS 5th European Conference, Budapest 1991, Vol. 1

[4] HINTZE, D.: Ph. D.-Thesis "Einfluß der Witterung auf die Bodenfestigkeit als Kriterium der Geländebefahrbarkeit", Institut für Kraftfahrwesen und Kolbenmaschinen der Universität der Bundeswehr Hamburg, 1992

$$W = W_1 + \triangle W$$

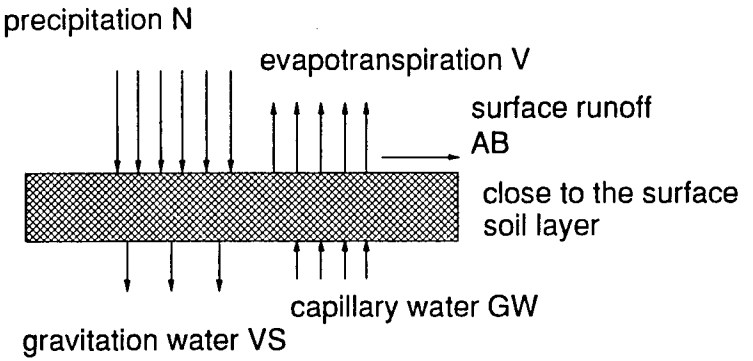

$$\triangle W = N - VS - AB - V + GW$$

Figure 1: Influences on the balance of moisture content

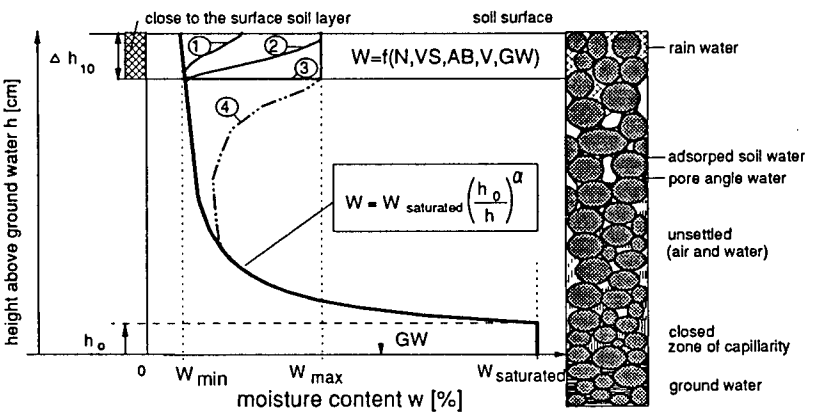

Figure 2: Distribution of water in the soil (soil profile)

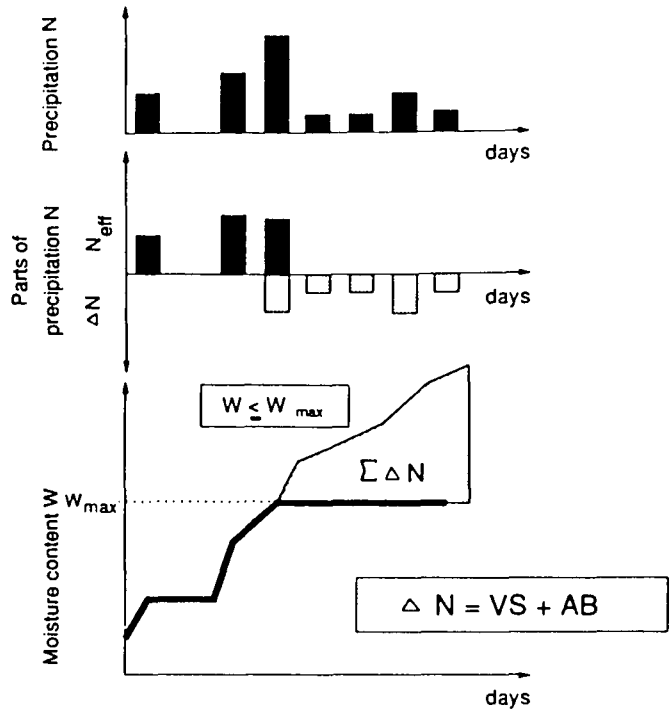

Figure 3: Parts of precipitation which are absorbed in soil, running-off and percolates

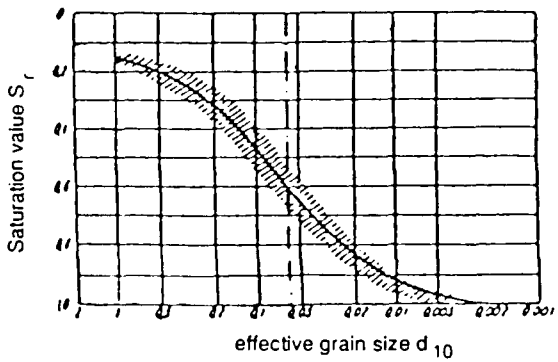

Figure 4: Saturation value depends on effective grain size, Kézdi [2]

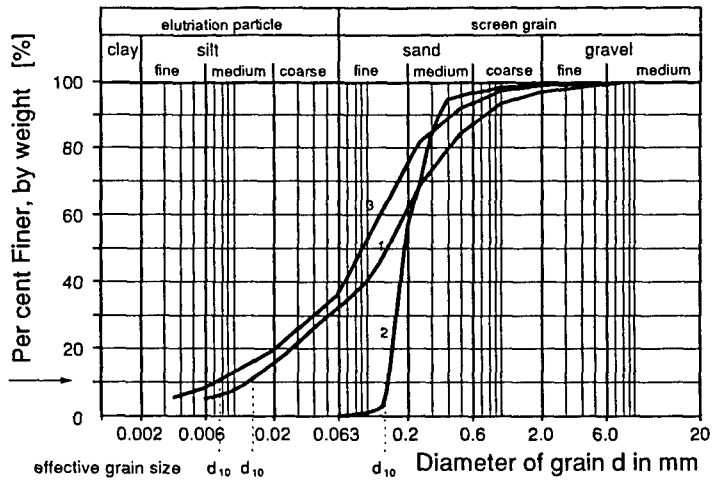

Figure 5: Grain size distribution of three tested natural soils
1: loam Benstaben; 2: sand Boberg; 3: loam Reinfeld

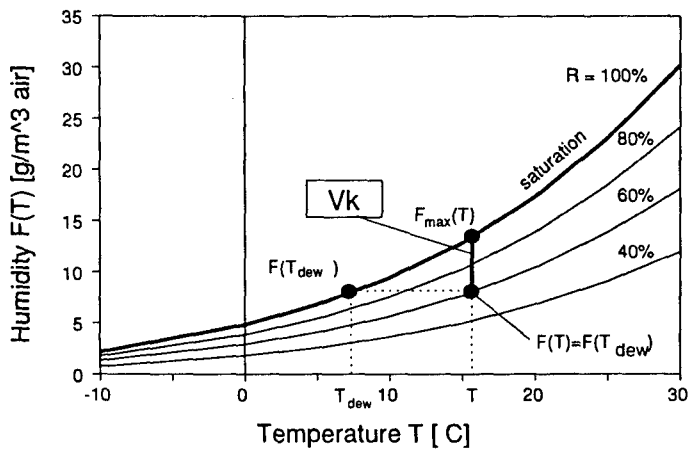

Figure 6: Calculation of the characteristic evaporation value Vk
by given temperature, dew point temperature and their humidity

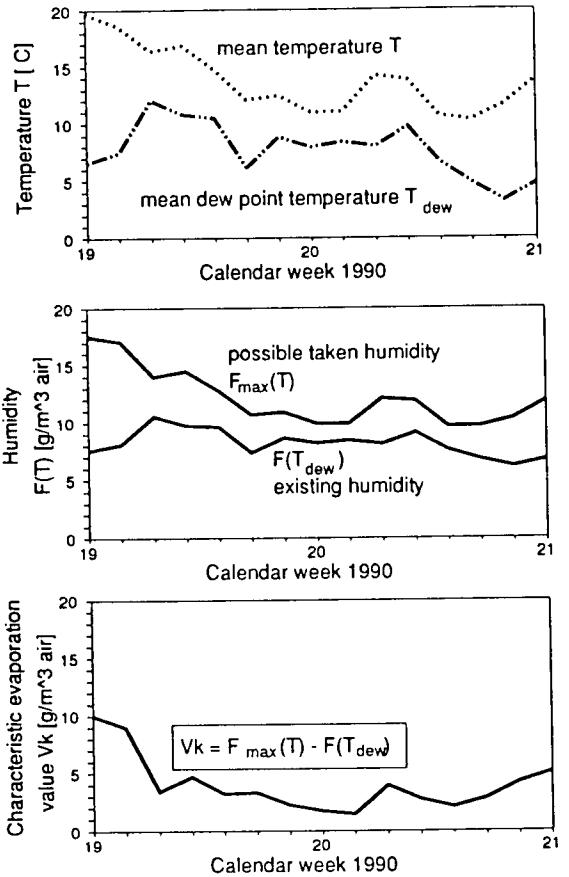

Figure 7: Example for the calculation of the characteristic evaporation value Vk

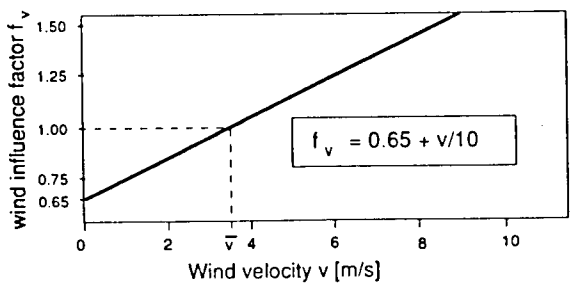

Figure 8: Determination of the wind influence factor

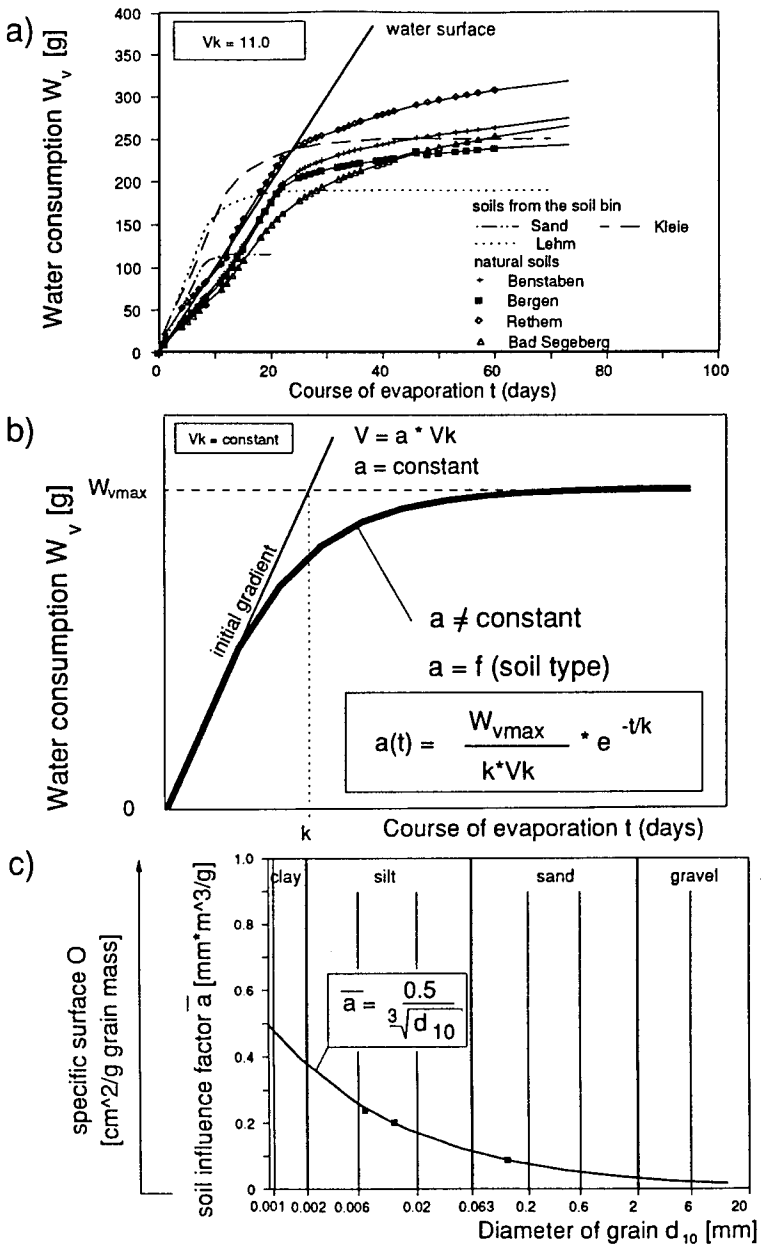

Figure 9: Influence of soil type on the lapse of evaporation
a) Measurements (laboratory); b) Model of measurements
c) Measurements and model based on field tests

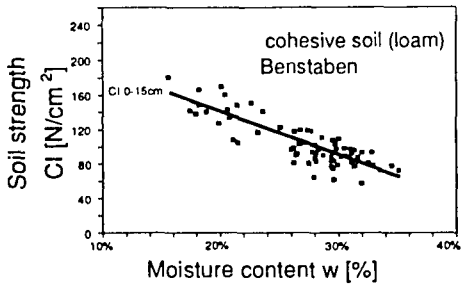

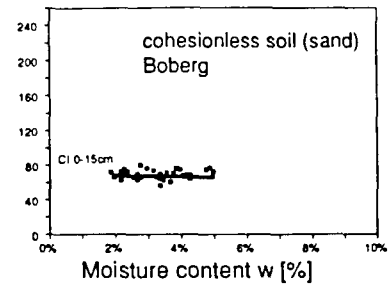

$$CI = CI_0 - m * w$$

Table 1: Parameter for the depth range 0-15cm

charac. values soil	d_{10} [mm]	CI_0 [N/cm²]	m [N/(cm²·%)]
Reinfeld	0.007	406	11.46
Rethem	0.009	210	4.47
Benstaben	0.013	242	5.03
Bergen	0.050	174	4.02
Boberg	0.160	69	0.58

Figure 10: Coherence between soil strength CI and moisture content w

single pass: $CI > VCI$ → GO

multi pass: $RCI = RI * CI > VCI$ → GO

Table 2: Remolding Index RI for different soils

	RI values [-]
Lehm	0.8
Sand	1.1

Table 3: Vehicle Cone Index VCI

	VCI values [N/cm²]
Spz Marder	16
Lkw 5t mil gl	33
Lkw 10t (6*4)	42

Figure 11: Coherence between soil strength CI and off-road mobilty expressed by Vehicle Cone Index VCI

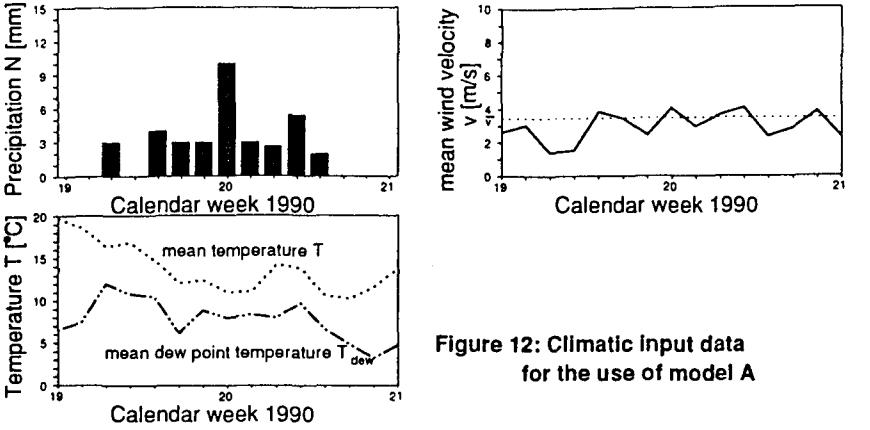

Figure 12: Climatic input data for the use of model A

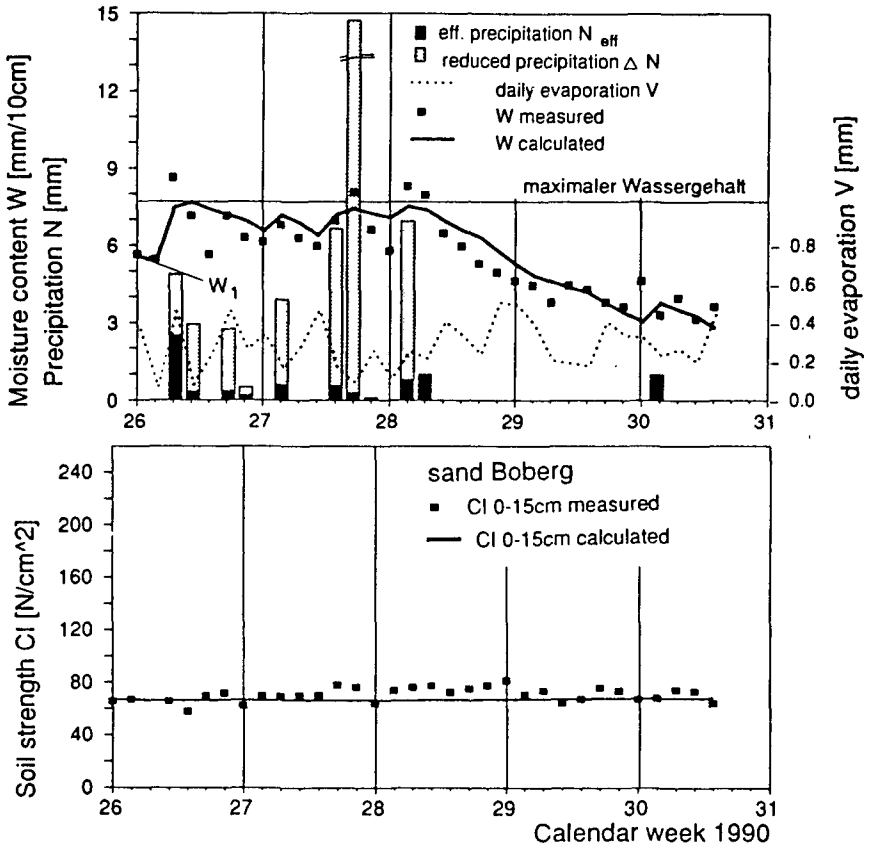

Figure 13: Verification of model A and B to a noncohesive (sandy) soil, Boberg

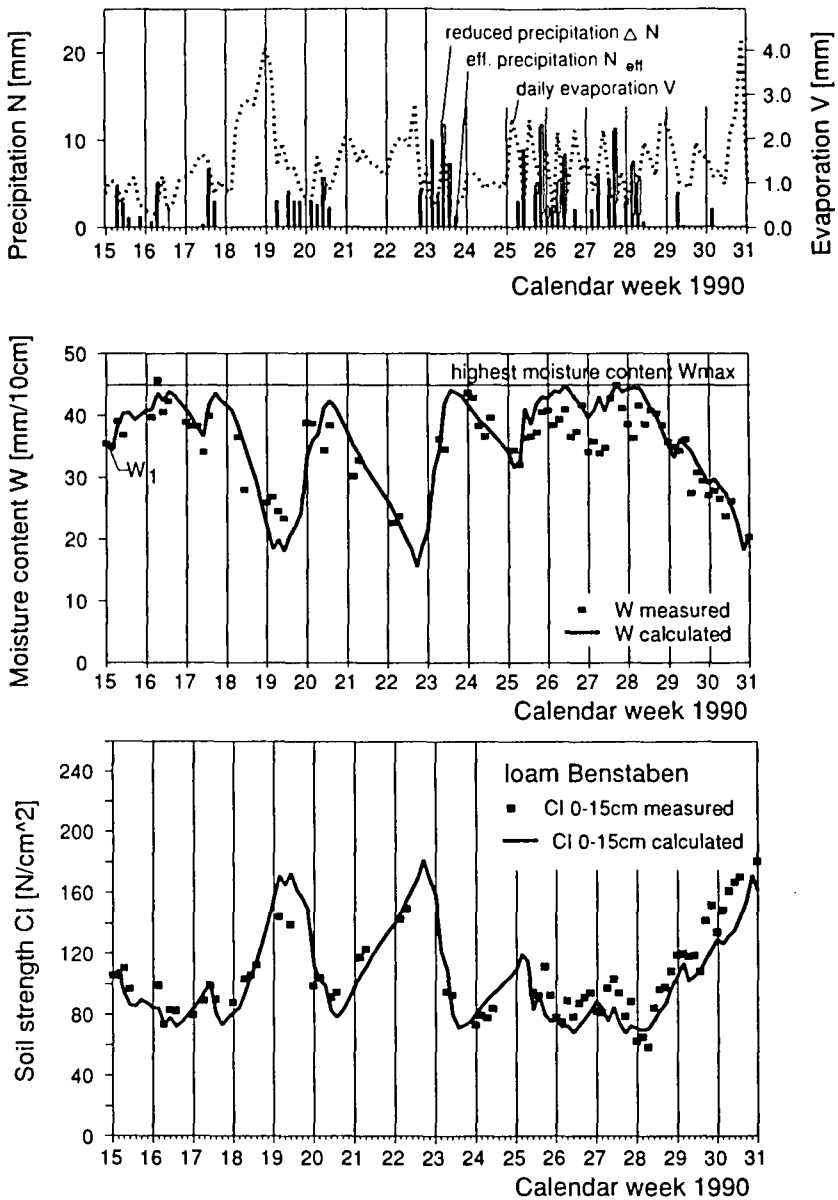

Figure 14: Verification of model A and B to a cohesive soil, loam Benstaben 1990

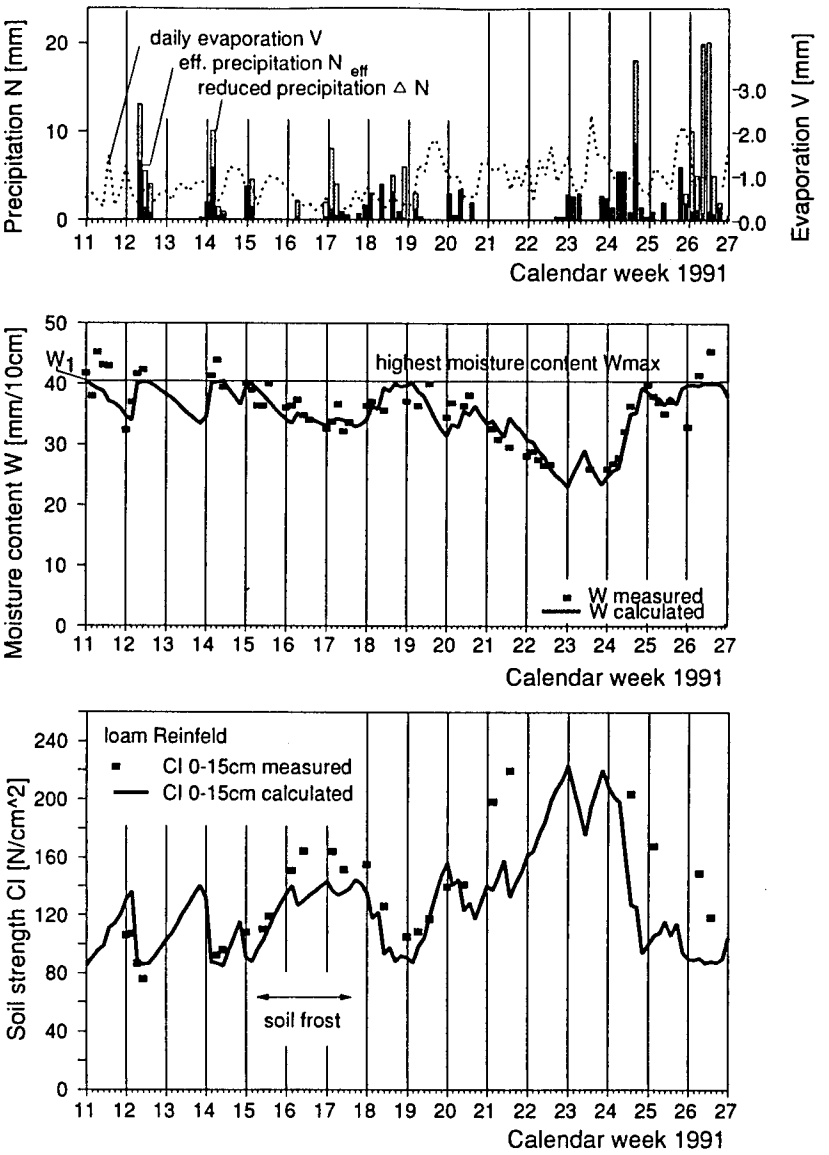

Figure 15: Verification of model A and B to a cohesive soil, loam Reinfeld 1991

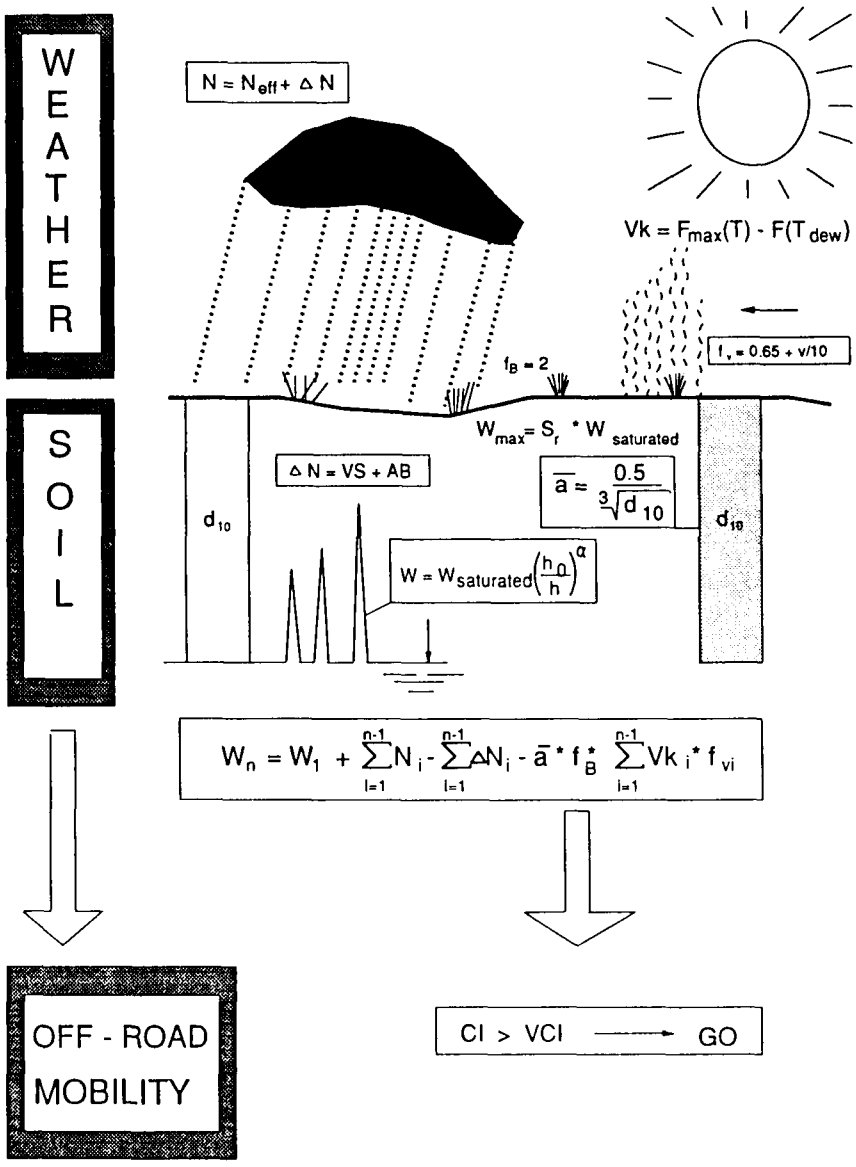

Figure 16: Coherences between weather, moisture content in soil and off - road mobility

EXPERIMENTAL AND THEORETICAL ANALYSIS OF A COHESIVE SOIL SHOVING PROCESS (THE OPTIMISATION OF THE PROCESS)

A.Jarzębowski, J.Maciejewski, D.Szyba, W.Trąmpczyński

1. INTRODUCTION

Earth moving processes due to construction works, realised by heavy machines such as loaders and excavators, are energetically very ineffective and their optimisation can save a lot of energy. Although it is earth cutting process itself which is the most important for this problem, it has no proper understanding and description until now.

A lot of effort was made to describe such a process within the theory of plasticity, where the problem of active pressure exerted by a rigid wall on a granular medium (under plane strain condition) can be assumed as a simplified model for soil shoving by heavy machine tools [1,2]. In such a case the method of characteristics was used [3,4,5,6] and several theoretical solutions (for static's and kinematics) were obtained under the assumption of rigid-perfectly plastic soil behaviour. Although a number of boundary value problems were solved in this manner, there exist several limitations in obtaining complete solutions or even the kinematically admissible ones [6] specially in the case of more advanced earth cutting processes.

Another approach, based on kinematically admissible mechanisms, was proposed later [2] and applied for the description of more advanced earth shoving processes [7-9]. Although it was shown that several experimentally observed effects can be described this way, more complex experimental investigations were not performed.

The aim of program summarised below was to execute experiments concerning the advanced stage of the earth shoving processes, to compare the obtained results with kinematically admissible solutions of the theory of plasticity and to propose the process optimisation.

2. EXPERIMENTAL DEVICE

A fully computer-controlled stand [10], was designed and built in the technical scale (Fig. 1). It

consists of a fixed container ($7.5 \times 1.3 \times 1.4$ [m]) having transparent walls to enable photographic recording of the material motion. The wall of various shape (1) moves within the box (which is partially filled with soil) in one plane by means of three hydraulic jacks providing its horizontal (2), vertical (3) and rotary (4) displacements (hydraulic jacks in such a configuration were chosen to simulate the kinematics of heavy machines). Motion of the jacks is fully computer-controlled through the electric, proportional valves and a hydraulic pump. Models of different machine tools are attached to a special movable frame (5, 6 - moved by the jacks mentioned above) through a set of loading cells (7) enabling the measurement of horizontal and vertical forces. Displacement of the tool is measured by two linear extensometers and one rotational. All the data obtained this way are elaborated (and stored) by the computer and used for the "on line" movement control.

The container was filled with especially prepared cohesive medium (modelling a clay) consisting of: cement 35% - 50%, bentonite - 20%, sand - 18% and white vaseline-12%, characterised by the following parameters: ϕ =24° (internal friction angle), γ=18.4 kN/m^3. Before each test the medium was mechanically preconsolidated by means of a special device, based on the idea of a certain mass dropped from different heights. Special compacting procedure allowed for obtaining uniform medium cohesion c=20 kPa.

3. EXPERIMENTAL RESULTS

Using the above described stand it was possible to perform a wide program of soil shoving processes with different model tools and working paths. A photograph showing a typical shoving process in the case of L-shaped tool is presented in Fig. 2a. The material deformation is realised as rigid zones sliding along the slip lines (well visible cracks) along which material changes its parameters (the initial cohesion c decreases to the residual value close to c_r=0). Force-displacement relation shows that horizontal force grows as process advances, but in unstable manner (Fig. 2b). The moment of reduction of the force coincides with creation of a kinematical mechanism originating from the rigid wall. Such mechanisms are created periodically.

4. KINEMATICALLY ADMISSIBLE SOLUTIONS FOR WALL PRESSURE PROBLEMS

As it was shown in [7,8,9,10], a process characterised in section 3 can be described within theory of plasticity, using kinematically admissible solutions taking into account changing of material parameters along slip lines.

Let us discuss the problem of rigid wall shoving presented schematically in Fig. 3. Assuming the material to be rigid-perfectly plastic and to obey the Coulomb-Mohr yield criterion

$$\tfrac{1}{2}(\sigma_1-\sigma_2)+\tfrac{1}{2}(\sigma_1-\sigma_2)\sin\phi - c\cos\phi = 0 \qquad (1)$$

where: c-material cohesion, ϕ - internal friction angle.

The flow rule takes the form:

$$\dot{\varepsilon}_{ij} = \dot{\lambda}\frac{\partial G(\sigma_{ij})}{\partial \sigma_{ij}} \qquad (2)$$

where $G(\sigma_{ij})$ represents a plastic potential.

In the case when potential is described by the yield criterion, (Eq. 2) describes the associated flow rule and when another function is taken, the flow rule is non-associated.

Using this approach and assuming a change of material parameters within the slip line (similar approach was used also in [11]), the different kinematically admissible solutions for a rigid wall shoving process can be proposed. Then, the solution predicting minimum energy is searched for (as kinematically admissible solution, we mean an arbitrary solution satisfying all kinematical constrains and the equation of the positive energy dissipation). Such an investigation is very subjective and needs a lot of experience (first of all due to small energetic differences between the mechanisms assumed - especially in more advanced stages of the process). Hence, the special computer program was prepared for this task.

Kinematically admissible solutions for different rigid wall shapes are presented and discussed in [7,8,9,10] for associated and non-associated flow rules. A typical solution for tool incipient motion and more advanced stage is presented in Fig. 3 for non-associated flow rule.

Using above -mentioned technique, quite good theoretical prediction for different tool shapes and different tool trajectories was found [7,8,9].

5. THE OPTIMISATION OF HEAVY MACHINE TOOLS FILLING PROCESS

As it was mentioned before, in the case of earth-moving process due to heavy machine tools, the material (cohesive soil) deforms as rigid zones sliding along the slip lines where material substantially changes its parameters (cohesion drops). Such behaviour can be described theoretically using kinematically admissible mechanisms of the theory of plasticity.

According to this observations, as soon as slip lines are created, the energetically most effective way of the tool filling is to follow previously created slip line by the tip of the tool. Such an idea was then checked experimentally (Fig. 4).

L-shaped tool (inclined with an angle 5° simulating the real process- Fig. 4a) was first pushed into slope inclined with an angle λ=20° (c=20 kPa), to a certain position(Fig. 4b). Then its tip was moved along three different straight lines (Fig. 4c), with simultaneous rotation of the tool (Fig. 4d) to have it filled with material. Those straight lines were inclined with an angle α=30° , 40° and 50°. The values α=40° and 50° are close to the inclination of slip lines created during the tool horizontal pushing process (Fig. 4c). It means, that in such a case the end of the tool was moved along the slip line, where material cohesion c substantially dropped as a result of material softening. Specific energy of such a process for three different preliminary horizontal displacement, denoted by s, related to amount of material left in the tool is shown in Fig. 5a, whereas related to amount of material displaced (Fig. 4c- KLAC for α=40°), is shown in Fig. 5b. One can see that in the case of α=30° the specific unit energy is much higher than for α=40° and α=50°. Hence, conducting the tool tip along line inclined with an angle equal or higher than the angle of slip lines inclinations, the specific energy of the earth-filling process can be significantly reduced. The amount of soil which remain within the tool after the process is higher for α=40° than for α=50°.

6. CONCLUSIONS

Presented results show that in the case of cohesive soil earth-moving process:

1. material deforms as rigid zones sliding along the slip lines where material substantially

changes its parameters (cohesion).

2. moving the machine tools along created previously slip lines one can substantially save energy used for earth-moving processes (tool filling). This observation is the basis of the optimisation of the filling process.
3. material behaviour, mentioned in section 1, can be described theoretically using kinematically admissible mechanisms of the theory of plasticity.

Acknowledgement. This research was sponsored by the Project 706-74 91 01 "Automatization of excavators", coordinated by Prof.J.Szlagowski, Warsaw Technical University.

REFERENCES

1. W.Szczepiński, Limit states and kinematics of granular media [in Polish], PWN 1974.
2. R.Izbicki, Z.Mróz, Limit states analysis in mechanics of soils and rocks [in Polish], PWN 1976.
3. W.Szczepiński, Mechanics of a granular body during the digging process by means of a loading machine [in Polish], Arch. Bud. Masz. 3, XVIII, 1971
4. W.Szczepiński, H.Winek, Experimental study of kinematics of granular media for certain boundary value problem [in Polish], Rozpr. Inż., 20, 1, 1972
5. W.Trąmpczyński, Experimental study of kinematics of soil shoving, Bull.Acad.Polon.Sci., vol.XXV, No 11, 1977.
6. W.Trąmpczyński, The analysis of kinematically admissible solutions for different shape wall movement [in Polish], Theor. and Appl. Mechanics, 1, 15, 1977
7. W.Trąmpczyński, J.Maciejewski, On the kinematically admissible solutions for soil-tool interaction description in the case of heavy machine working process, Proc. 5th ISTVS European Conference, Budapest 1991
8. W.Trąmpczyński, A.Jarzębowski, On the kinematically admissible solution application for theoretical description of shoving processes, Eng.Transactions, 39,1,75-96,1991.
9. Z.Mróz, J.Maciejewski, Post critical response of soils and shear band evolution, 3rd Workshop on localisation and bifurcation theory for soils and rocks, Aussois , France, September 1993
10. D.Szyba, W.Trąmpczyński, Experimental verification of kinematically admissible solutions for incipient stage of cohesive soil shoving process, Eng. Transactions (in press)
11. R.L.Michałowski, Strain localization and periodic fluctuations in granular flow processes from hoppers, Geotechnique, 40, 3, 389-403, 1990.

FIGURE CAPTIONS

Fig. 1. The fully automated stand for heavy machine tools investigation: 1. Model of tool, 2. Horizontal hydraulic jack, 3. Vertical hydraulic jack, 4. Rotation hydraulic jack, 5. Horizontal movable frame, 6. Vertical movable frame, 7. Loading cells.

Fig. 2. Typical deformation of cohesive soil in the case of the advance shoving process: a) a photo; b) horizontal force versus horizontal displacement diagram.

Fig. 3. Numerical simulation: a) initial stage; b) advanced stage; c) horizontal force versus horizontal displacement diagram.

Fig. 4. Experimental program performed: a) the model of the tool and a slope; b) initial stage of the process horizontal movement c) advanced stage of horizontal movement; d) the final stage of the process.

Fig. 5. Comparison of specific energy for different toll path: a) for the unit weight of material remained within the tool; b) for the unit weight of the material displaced during the process.

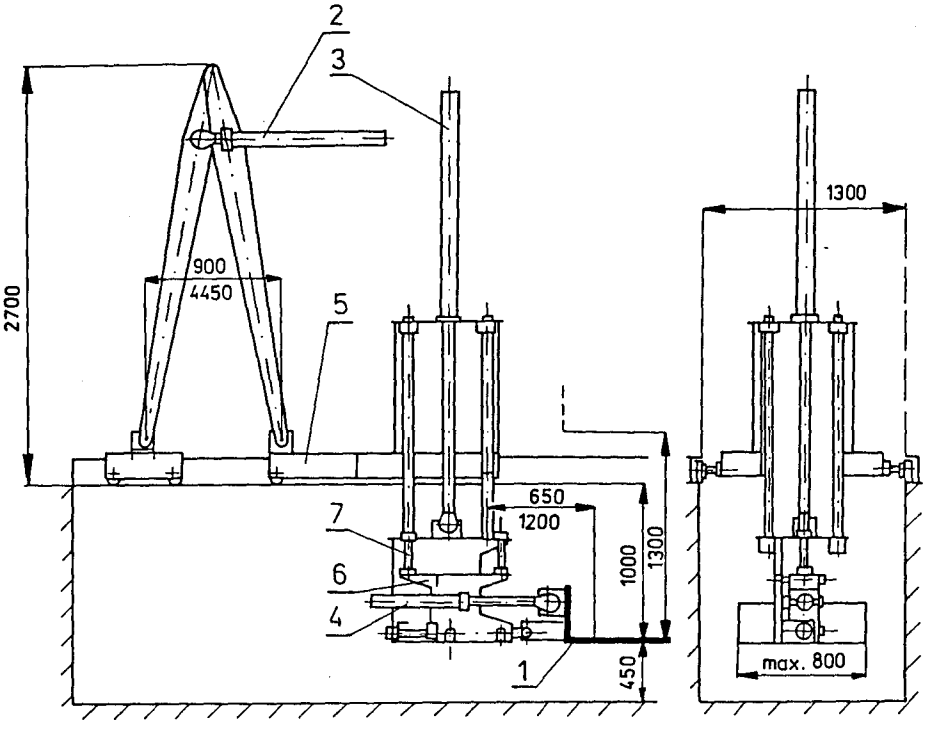

Fig. 1

a)

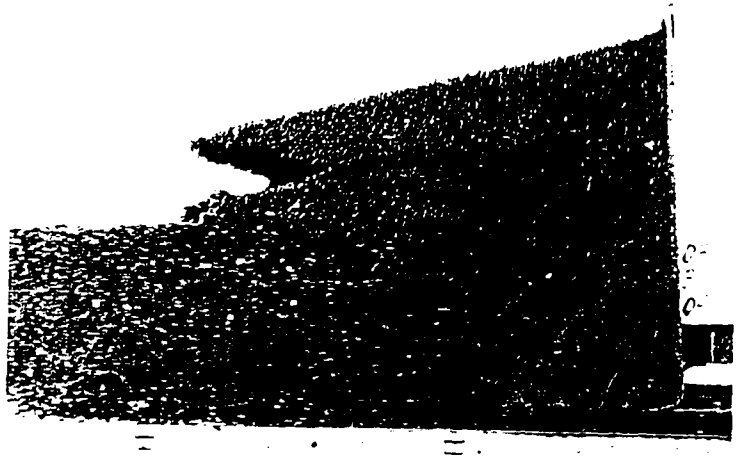

b)

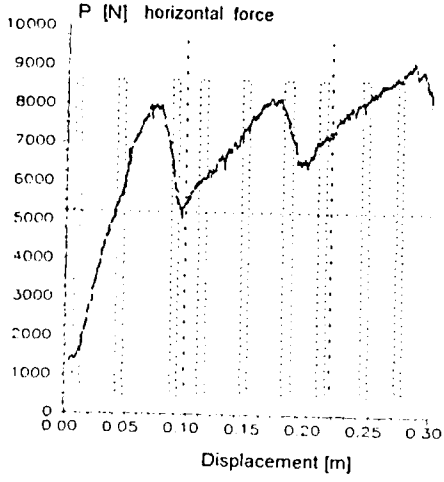
P [N] horizontal force
10000
9000
8000
7000
6000
5000
4000
3000
2000
1000
0
0.00
0.05
0.10
0.15
0.20
0.25
0.30
Displacement [m]

Fig. 2

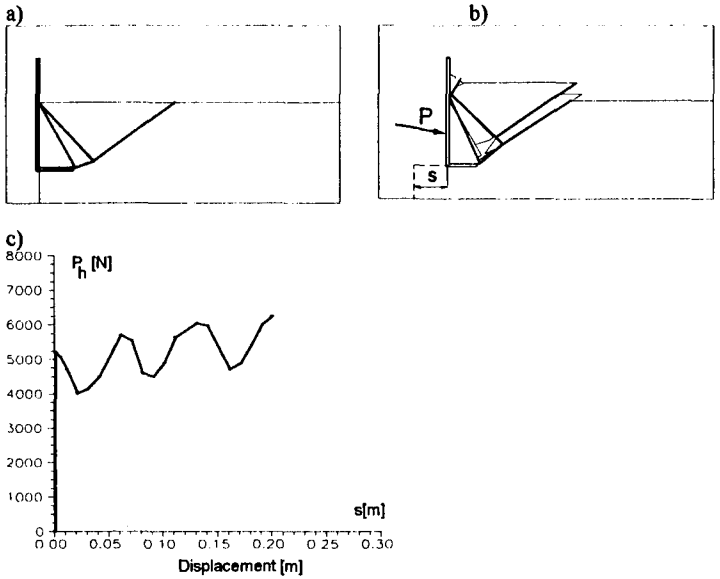
a)
b)
P
s
c)
P_h [N]
8000
7000
6000
5000
4000
3000
2000
1000
0
s[m]
0.00
0.05
0.10
0.15
0.20
0.25
0.30
Displacement [m]

Fig. 3

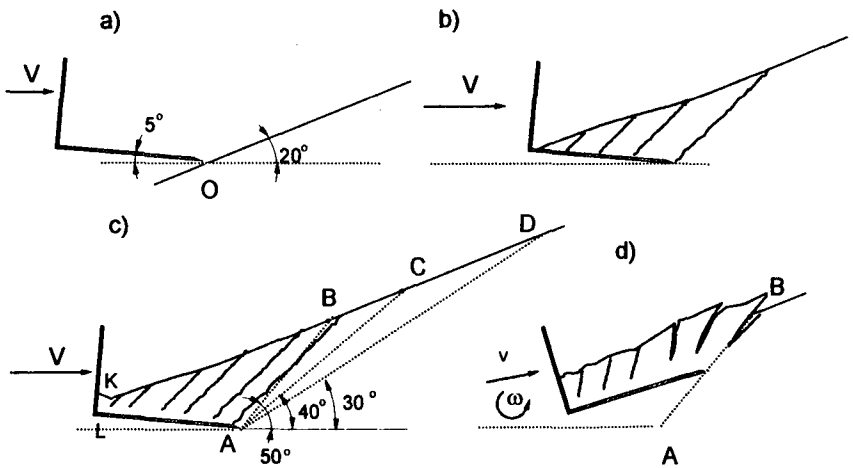
a)
b)
V
5°
20°
O
V
c)
D
C
B
V
K
40°
30°
L
A
50°
d)
B
v
ω
A

Fig. 4

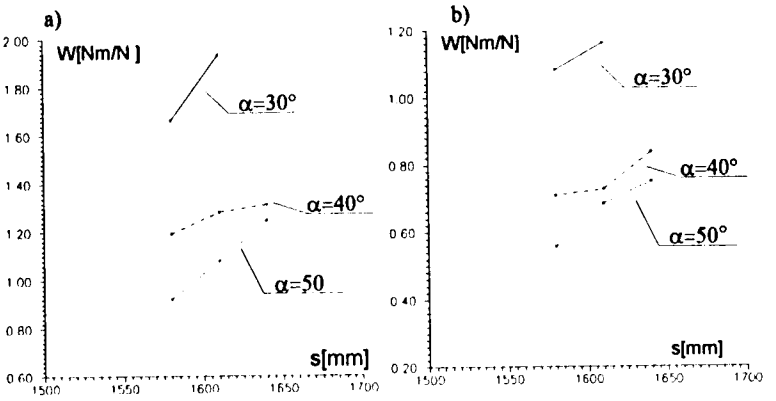
a)
W[Nm/N]
2 00
1 80
1 60
1 40
1 20
1 00
0 80
0 60
α=30°
α=40°
α=50
s[mm]
1500
1550
1600
1650
1700
b)
W[Nm/N]
1 20
1 00
0 80
0 60
0 40
0 20
α=30°
α=40°
α=50°
s[mm]
1500
1550
1600
1650
1700

Fig. 5

A NEW TYPE OF OFF—ROAD TIRE ——BIONIC CAMEL FOOT TIRE

Zhuang Jide, Qiu Xiding and Ji Xuewu
Department of Automobile Engineering,
Jilin Univercity of Technology, Chang Chun, China

ABSTRCT

Based on comprehensive study on the interaction of a camel foot and sand, this paper summaries the characteristics of the camel foot when walking in the desert, and presentes a new type of off—road tire——bionic camel foot tire(BCFT) which takes the virtue of the camel foot. The traction properties of BCFT and those of the conventional tire are also compared in this paper. The result showes that BCFT is more efficient than the conventional tire when walking in the desert.

INTRODUCTION

Desert coveres approximately one—seventh the land of the world. And there are rich natural resources such as oil and natural gas under the desert. In order to exploit these natural resources, desert vehicles are necessary for tansportation firstly. While conventional off— road vehicles are not suitable for usage in desert. Some of the reasons are that sand beneath the tire flows easily and the wheel sinks severesly.

As we know that camels can travel in desert freely. Study on the interaction of a camel foot and sand will give us some helpful indication. Based on comprehensive study on the intercation of a camel foot and sand , this paper summaries the characteristics of the camel foot when walking in the desert, and presentes a new type of off—road tire——bionic camel foot tire(BCFT) which takes the virtue of the camel foot.

Ref. [1][2] reported a type of camel shoe tire whose tread width is presented in a cantilever position compared to the rim width. This type of tire tread can make the stress beneath the tire more uniform (see Fig. 1). But it only considered the stress distribution along the lateral. Experiments have shown that stress in lateral beneath a tire is usually uniform especially under lower inflation pressure [3]. Therefore, some measures must be taken to change the stress distribution along the longitudinal in order to increase trafficability of a off—road vehicle.

BEHAVIOR OF A CAMEL FOOT WALKING IN DESERT

The camel foot is concave. And at the bottom of the concave, there is a layer of elastic cushion, and around is the hooked shell. When the camel is working in desert, the camel foot can restrict sand beneath the foot flowing.

The camel foot is parallel to sand surface when the foot plugs into sand at beginning. Before the foot leaves sand, it will rotates around the foremost point of the hoof. When the foot is pulling out of the sand, it is almost perpendicular to sand surface. Therefore, the camel foot disturbs the sand to a small extent when it plugs into and pulls out of the sand.

During bearing state, as the weight borne by the foot increases, the foot spreads and the contact area enlarges. When the foot is about to pull out of sand, the weight borne by the foot decreases and the foot recovers[4].

Fig. 2 showes the camel footprint left on sand. It can be seen that sinkage in the front of footprint is deeper than that in the rear of it. This indicates that the camel foot provides thrust by the horizontal component of sand reaction. In other words, the camel foot converts part of sand bearing capacity to thrust. This way of the camel foot steping on sand with foot inclined in sand is more efficient than that of a conventional tire treading on sand with the tread almost parallel to sand surface as to producing thrust[3].

CONCEPT AND COSTRUCTURE OF BCFT

As above mentioned, the camel foot has the following characteristics when walking in desert:

(1) converts part of the sand bearing capacity to thrust;

(2) restricts sand beneath the foot flowing;

(3) enlarges the contact area when bearing weight;

(4) disturbs the sand to a small extent when pluging into and pulling out of sand.

If a tire is of that four characteristics, it can be called BCFT.

According to the requirements above stated, following constructure can be adopted, see Fig. 3.

On the tread, there are right triangle wedges around the tire carcass (see Fig. 3a). The wedges can change the stresses distribution beneath them and make the forward horizental component of the normal stress increase. For a conventional tire, the horizontal component of normal stress beneath the contact area before B. O. C (bottom of center) is opposite to wheel moving direction, and provides resistance to the wheel. While for BCFT, the horizontal conponent of normal stress beneath the contact area before B. O. C is identical to wheel moving direction, and provies the wheel with thrust. In other words, the wedge can convert the sand bearing capacity to thrust.

From Fig. 3a, it can also be seen that in the fore part of contact area, the slope of point B on the wedge is smaller than that of the corresponding point A on the outer circle. While in the rear part of entact area, the slope of point C on the wedge is greater than that of the corresponding point D on the outer circle. Therefore, BCFT disturbs the sand more slightly than a conventional tire does when entering and leaving sand.

On the two outer sides of the tread, there are lugs inclined outwards in pairs, see Fig. 3b. The lugs and the wedges form concaves (see Fig. 3c), and restrict the sand flow, and increase the sand bearing capacity. Moreover, the lugs can spread when the tire bears much more weight.

PREDICTION OF THE TRACTION PROPERTIES OF BCFT

The inflation pressure is usually low when a vehicle is driving on dry loose sand. Experiments [3][5] have shown that the normal stress beneath a tire is uniform along the longitudinal when the inflation pressure is low. The normal stress can be expressed as:

$$p = p_i + \alpha W \tag{1}$$

where

p_i — —inflation pressure, KPa;

α — —emprical coefficient;

W — —load, KN.

Therefore, the model of interaction of tire — sand can be expressed as Fig. 4 shown, the contact area is devided into two parts. One is the arc AB, and the other is plane BC.

Similarly, the following assumptiopns can be made in the prediction of traction properties of BCFT:

(1) contact area of BCFT — sand consists of two parts, the arc AB and the plane BC (see Fig. 5);

(2) effect of the stresses acting on arc AB can be neglected;

(3) effect of the stresses acting on the lugs can aslo be neglected;

(4) the stresses beneath place BC are uniform along lateral;

(5) sand is isotropic and homogeneous.

Moreover, the normal stress beneath the wedges is uniform and can be expressed as eq. (1), and the tangential stress beneath the wedges can be expressed by Janosi's formula:

$$\tau = (c + p\tan\varphi)[1 - \exp(-j_h/k)] \tag{2}$$

where

c — —sand cohesive, KPa;

φ — —sand internal friction angle, rad;

j_h — —shear displacement of a point on hypotenuse of the wedge, m;

k — —sand shear displacement modulus, m.

The shear displacement j_h can be expressed by the shear displacement of a corresponding point on base of the wedge j_b:

$$j_h = j_b/\cos\beta \tag{3}$$

where β is the angle of hypotenuse relative to base. And j_b can be expressed as:

$$j_b = sR\cos^2\theta_2(\tan\theta_2 - \tan\theta) \tag{4}$$

where

s — —slip;

R — —radius of the tire, m;

θ_2 — —contact angle shown in Fig. 5.

Substituting eq. (3) and eq. (4) into eq. (2), the tangential stress can be rewritten as:

$$\tau = (c + p\tan\varphi)\{1 - \exp[-sR\cos^2\theta_2(\tan\theta_2 - \tan\theta)/\cos\beta]\} \tag{5}$$

According to the equilibrium of forces acting on the wheel, following eqations can be get:

$$W = 2RB\rho\sin\theta_2 - RB\cos\theta_2\tan\beta\int_{-\theta_2}^{+\theta_2}(1+\tan^2\theta)\tau d\theta \tag{6}$$

$$DP = 2RB\rho\sin\theta_2\tan\beta + RB\cos\theta_2\int_{-\theta_2}^{+\theta_2}(1+\tan^2\theta)\tau d\theta \tag{7}$$

Considering the symmetry of plane BC(see Fig. 5), the torque of normal stress p about the wheel axle center O can be expressed as:

$$T_n = NBH\rho(R\cos\theta_2 + H/2) + (2R\cos\theta_2 - NL)B\rho\tan\beta[R\cos\theta_2 + (2R\cos\theta_2 - NL)\tan\beta/2] \tag{8}$$

where

B——width of the tire tread, m;

N——numbers of the wedges in contact length;

H——hight of the wedge, m;

L——base length of the wedge, m.

The arm of tangential stress of a ponit on hypotenuse of the wedge is undefined. In order to define the torque of tangential stress τ, we first decompose τ into horizontal and vertical components τ_x and τ_y. And the arm of τ_x can easily be defined, the arm of τ_y can be taken as $(R\cos\theta_2 + H/2)$. Therefore, the torque of tangential stress can be expressed as:

$$T_\tau = BR\cos\theta_2(R\cos\theta_2 + H/2)\int_{-\theta_2}^{+\theta_2}(1+\tan^2\theta)\tau d\theta + BR^2\cos^2\theta_2\tan\beta\int_{-\theta_2}^{+\theta_2}(1+\tan^2\theta)\tan\theta\tau d\theta \tag{9}$$

The total torque can be get by plus eq. (8) and eq. (9):

$$T = T_n + T_\tau \tag{10}$$

Wheel sinkage which is the distance form sand surface to middle point of the wedge(see Fig. 5) can be calculated according to results of inclined plate-sinkage tests[4]:

$$p = (1 - 0.0073\beta)K(Z - H/2)^n \tag{11}$$

where

p——normal stress beneath tire, KPa;

β——angle between hypotenuse and base of the wedge, deg;

K, n——experimently determined sand parameters;

H——height of the wedge, m;

Z——sinkage, m.

Given the load, the angle θ_2 can be defined through eq. (6). And the drawbar pull, torque and sinkage can be defined through eq. (7) to eq. (11).

Fig. 6 showes the results of prediction of traction properties of BCFT and those of a conventional tire which has the same demension and is subjected to the same load as BCFT. It can be seen that BCFT has priority to the conventional tire in traction properties.

CONCLUSION

BCFT pesented in this paper takes the virtue of the characteristics of the camel foot when walking in desert, and its tractive performace is priory to that of conventional tires.

REFERENCES

1. P. F. J. Abeels, Pneus Classiques et Camel Shoe en Agriculture, Proc. of 6th. Int. Conf. of ISTVS, Vienna, Austria, 1978.

2. P. F. J. Abeels, Modelling of Off— Road Tyres and Soil for Improved Traction, Proc. of 8th. Int. Conf. of ISTVS, Cambridge, U. K., 1984.

3. Xu Peijun, Study on the Mechanism of Camels Walking in Desert and the Application to Legged Vehicle, Ph. D Dissertation of Jilin Univercity of Technology, 1992.

4. Ji Xuewu, Study on the Inetraction of Tire—Sand and the Key Technique of Bionic Camel Foot Tires, Ph. D Dissertation of Jilin Univercity of Technology, Unpublished.

5. Wang Qingnian, A Study of the Working State of a Driven Tire and Its Optimum Trative Performace on Soft Soil, Master Dissertation of Jilin Univercity of Technology, 1983.

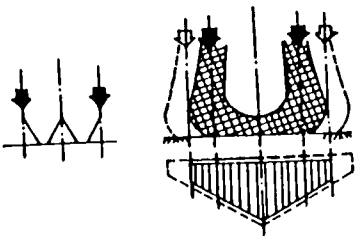

(a). conventional tire

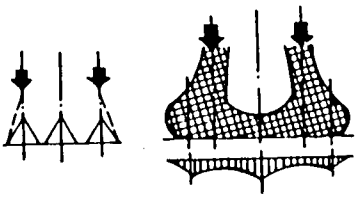

(b). camel shoe.

Fig. 1 normal stress distribution beneath conventional tire and camel shoe.

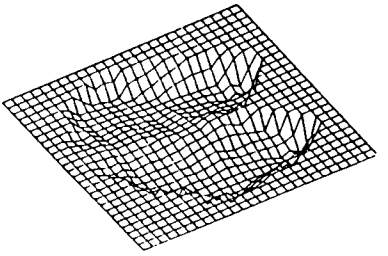

Fig. 2 camel footprint left on sand

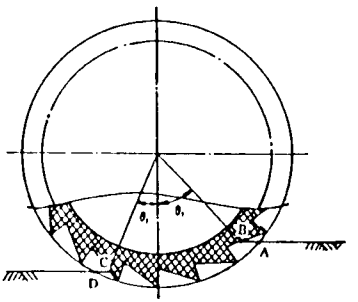

(a)

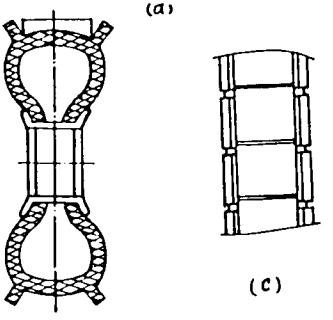

(b)

(c)

Fig. 3 constructure of BCFT

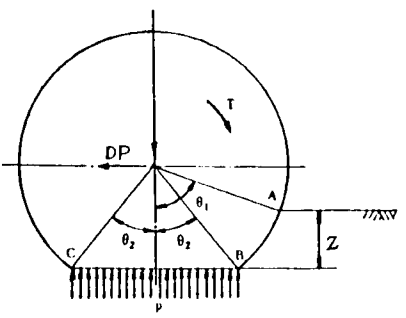

Fig. 4 interaction of a conventional tire and sand

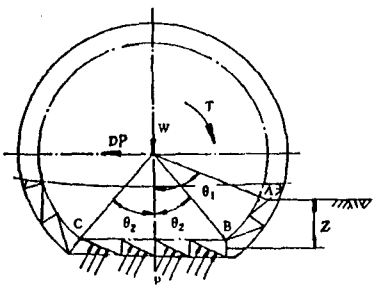

Fig. 6 Interaction of BCFT and sand

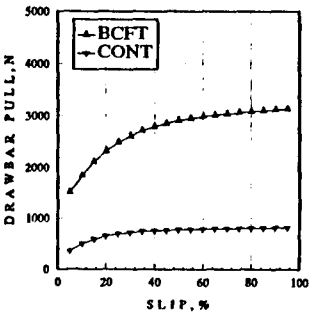

(a)

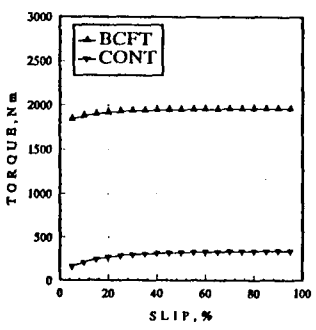

(b)

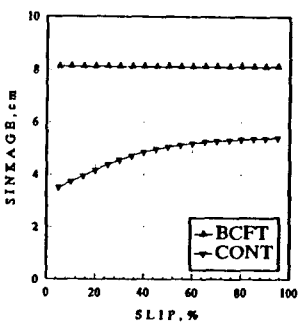

(c)

Fig. 6 tration properties of BCFT and a conventional tire

Numerical Simulation of the Dynamic Behaviour of Tractors

Dipl. Ing. C. Kaplick

Technical University of Berlin
Institut for Machinery Design
Department for Agricultural Engineering and Construction Machinery

Numerical Simulation Predictions - State of the Art

From the very beginning of numerical ride dynamics simulation of agricultural tractors, mainly two fields of problems proved to complicate reliable predictions concerning the vehicle behaviour. First of all, this is the definition of useful terms to describe and quantify the often quite abstract aims of optimization, i.e. "ride safety" and "ride comfort". From a number of experimental investigations it is known that measured values and the driver's subjective feeling sometimes differ remarkably. For the numerical simulation this still means that a compromise has to be made between the actually intended renunciation of prototypes and an in-time pre-assessment by man, before a project stage with perhaps irreversible decisions for the vehicle concept might be reached. The nearly unquantifiable human perception especially of "ride comfort" and the resulting definition of corresponding terms for ist description call for a critical awareness when interpreting simulation results, but in fact they are not a problem of simulation.

A much bigger problem is posed by the still unsatisfactory exactness of the predicted simulation results, which - in connection with the so far indisputable success of tractor simulation - may be surprising. But it has to be taken into account that in the past mostly tendencial statements were made concerning the effect of different optimization approaches and that they were accepted by the vehicle manufacturers as an important assistance. It was by comprehensive investigations on the effect of vehicle and cabin suspensions as well as absorber systems that the principal disadvantages of the standard tractor were uncovered and a process of rethinking of the manufacturers was provoked. The growing acceptance of TRAC vehicles as well as the presentation of corresponding concept studies is an unmista-

kable sign that this formerly very conservative market slowly started to move.

On the other hand, increasing research progress and more and more powerful hard- and software tools also led to an increased level of expectations on the manufacturers' side which is, looking to the severe situation of agriculture and the agricultural industry, an inevitable and legitimate development. The profitability of a new design respectively of a technical improvement is more than ever indispensable for the economic success of a company and has to become visible by a measurable sales increase or by putting through increased consumer prices. Concrete sales forecasts are only possible if the practical benefit of a design measure can be proved and quantified on the basis of known costs and consumer habits. In other words: development work and perhaps production changes on the basis of tendencial statements nowadays hold an economic risk that no manufacturer is ready or able to take. It is conspicious that the numerical methods wil have to face this challenge to cope with their claim being a very efficient and economic aid in industrial product development, also in the field of tractor ride vibration simulation.

Verification

In scientific work in the field of ride dynamics simulation, the verification of simulation results proves to be a central problem again and again. As a consequence, checking the computed results by measurements on the real vehicle still is indispensable. It is remarkable that the question of verification is neither limited to the investigation of wheeled vehicles nor to the vibration analysis of tractors, but it runs like a thread trough all technical disciplines

where mechanical or - more general - physical systems are described by mathematic models and analyzed by numerical methods.

Doing this, it is possible to describe the real system in many cases - depending on its complexity - more or less exactly by an appropriate model, but this usually demands an iterative model adaptation on the basis of parameters and properties determined on the real system. The input parameters for the simualtion which are determined this way often turn out to be plausible and obvious later, making forget that not knowing the result before might have led to a completely different approach.

That lack seems to be disregardable, at least as far as the optimization of the tractors´s vertical vibration behaviour is concerned. Recalling the meaning of the driver as a criterion of assessment for terms like "ride comfort" or the "nuisance" of vibrations, one might be firmly convinced that a comprehensive prototype development is indispensable anyway, assuring the existance of suitable test vehicles for parameter studies and verification in the future.

Upon closer examination this approach is wrong. Recalling the intention of numerical simulation methods, there are mainly two prime aims to be mentioned :

- a clear reduction of prototype and test stand development and of the test and measuring departments; instead of this: quick, cost-saving and weather-independant "test rides" at the computer monitor with a wide parameter spectrum and mainly automized optimization algorithms

- a drastic reduction of development costs by identical and bidrectionally associative data bases for design, simulation ("test") and production; reduction of development cycles with corresponding temporal and technological competition advantages.

The rather hesitant introduction of numerical simulation methods in the industrial tractor development therefore is an expression of different, admittedly unsolved problems, letting project-accompanying prototype investigations still be the only pragmatic way. On the other hand, it would be wrong intending to make permanant the status quo. From the scientific point of view the future of tractor ride vibration simulation has to be set up as a maximum demand if this research area wants to free from the reproach of an "end in itself".

Three basic demands can be deduced from this situation for the future succes of numerical simulation methods in tractor optimization :

- comprehensive qualitative and quantitative description of a vehicle´s behaviour under complete renunciation of the development of test vehicles,

- determination of parameters and system properties either from existing components or by means of CA-based methods, i.e. on the basis of design data,

- implementation of subjective human feeling and perception patterns in the vehicle model, e.g. using known and suitably implemented comparative cases.

It is certainly true that final statements concerning realization chances and times of correspondig software packages would be premature, but it also is obvious that this goal further on can only be reached by comprehensive prototype development and measurement in order to increase the often fragmentary knowledge about certain mechanisms and effects, e.g. the processes in the tyre. Nevertheless, it seems to be important to keep in mind the vision standing behind numerical simulation. The reduction of test-related development times and costs as a self-defined aim of computer simualtion of course reaches its most consequent interpretation in that moment when accompanying experimental investigation finally becomes superfluous.

Model Adaptation on the Basis of Comparative Experimental Investigations

At the moment, the "Tractor Simulation" project of the Department of Agricultural Engineering and Construction Machinery at the Technical University of Berlin is intensively investigating the improvement of the exactness of predicted numerical results. Special emphasis is placed on the development of a practical simulation environment as well as the drafting of design recommendations for the dynamic optimization of agricultural tractors.

During these works a new approach was found that might improve the often unsatisfactory agreement between measurement and simulation. The parameter supply of the vehicle models was considered as an essential problem so far. On the one hand, the reason for this problem is a backlog in the correct description of important effects in the tyres and the tractor

drive line. In addition to that, even the geometrical and kinetic parameters needed (vehicle dimensions, wheel-base, track, position of the centers of gravity, masses, mass moments of inertia etc.) sometimes turn out to be unknown or contradictory when trying to refer to manufacturer specifications.

Facing this problem again and again finally led to the reflection if it wouldn´t be easier and more useful not to supply the vehicle model with the "correct data", but with the data furnishing the "correct results" in the simulation, i.e. the results corresponding to the reality rsp. to the measurement. This idea may sound funny and it should be explained by an example. For many years, the final investigation of the effects in the contact zone between tyre and track - obviously being decisive for the dynamic behaviour - causes extreme difficulties; this is especially true for the tractor tyre. Trying to model these not even theorically penetrated effects and mechanisms by a suitable tyre model therefore doesn´t seem to be useful at the moment. Limiting oneself - as often usual anyway - to a single Voigt-Kelvin model, i.e. to the parameters "dynamic tyre stiffness" and "dynamic tyre damping" that are already known rsp. can be measured quite simply, an appropriate mathematic rule deduced from comparative measurements should be sufficient to adapt these tyre parameters in a way that an agreement between simulation and measurement can be assured.

This method finally could be carried out for the whole system "tractor", considering only the inputs (variation of vehicle parameters) and outputs (resulting vibration behaviour) of the real system and the physical model. In fact it should be sufficient to describe only the transmission behaviour in dependence on all numerically relevant parameters that are important for

the vehicle design, without ever modeling the underlying technical system.

As a matter of fact, the determination of the corresponding transmission functions of the model and the real vehicle is not the only problem, because an adaptation rule between those systems has to be found, of course depending itself on different vehicle and model parameters As a last step the universal validity of that rule has to be proven - at least for a certain class of tractors - or has to be assured by another transformation rule.

It is evident that a solution for this extremely multi-dimensional problem, if at all, will only be found falling back on structure-detecting and structure-examinating methods, i.e. by multi-variate analysis techniques. In case of success this would mean that tractor simulation would do a big step forward in the future, limiting oneself to a few known or quickly accessible vehicle parameters, intentionally "garbling" those pretendedly "correct" values according to a specific rule, inserting them into a vehicle model of rather low complexity - and getting the correct simulation results !

As a consequence of the novelty of this approach reaching an improved exactness of predicted numerical results by formulating adaptation rules to the reality and due to the volume of the underlying experimental and numerical data basis needed to assure the statistic relevance, final statements concerning the chances of this method cannot be made yet. Nevertheless, it can be proceeded from the assumption that the corresponding investigations on the parameter dependence of the tractor´s dynamic behaviour that are carried out at the moment and which - having in mind the intended purpose of the data - are especially systematic will at least be of great importance for the vehicle modeling.

ENVIROMENTAL FRIENDLY FUEL FOR DIESEL ENGINES IN OFF ROAD VEHICLES

Werner KIEHTREIBER
Altfettmethylester Produktions Ges.m.b.H

ABSTRACT

This paper presents the purpose, the manufactoring and the properties of an enviromental friendly fuel. Off-Road mobility should not only save the ground but also try to use fuels with high biodegradability and reduction of emissions at the exhaust to protect the enviroment especially in ecologically sensitive areas.

1. UTILIZATION OF THE FUEL

Off-Road mobility is necessary in many areas so as agriculture, forestry or military operations. Fleet tests of the Austrian Armed Forces as well as the Federal Institute for Agriculture have shown the applicability of Fatty acid methylesters under practical conditions as a very promising alternative to diesel fuel for all diesel engines. These test programs included the economical aspects as well as the technical performance from the production up to the utilization of the fuel under practical conditions and showed the usability of Fatty acid methylesters as a diesel fuel of full value. The fuel characteristics and the emission data are shown in table 1 and 2.

2. PRODUCTION AND FUEL CHARACTERISTICS

2.1. Raw material

Fatty acid methylesters can be produced from a wide range of raw materials

- unrefined vegetable oils (rape seet oil, sunflower oil, palm oil etc.)
- used cooking oils and fats collected from food industry, restaurants and households.

Used cooking oils have to be filtered mechanically by the collecting organization to prepare them for the production.

2.2. Production

The production of Fatty acid methylesters is a new continuous transesterification process, developed in Austria and patented all over Europe (see Fig. 1). At the end of the process the rough methylester is distilled under high vacuum to reach the highest possible purity and quality. This is the presupposition for a long-term running on diesel engines without disturbance. The continuous manufactoring process with a short catalytic reaction time guarantees efficient production.

2.3. Fuel characteristics

In accordance to the high purity the fuel shows very good test results in comparison to the Austrian standard ÖNORM C 1190 (see table 1) for rape seed methylester.
As can be seen, the main specific fuel data are quite similar to those of diesel fuel. In comparison, a higher flame point, a higher cetane number and a significant lower sulphur content are advantageous. Viscosity and carbon residue are comparable with diesel fuel. The most important characteristic is a biodegradability of more than 99 % within three weeks.

3. PERFORMANCE AND ENGINE BEHAVIOUR

In comparison to diesel fuel Fatty acid methylesters show us some interesting measured values on engines without modification at the injection unit.
As a result of the reduced caloric power, less performance (approximately 5 %) must be expected if the injection unit is not modified. However, the performance deficit can easily be compensated by increasing the full load injection rate. Excessive full load soot is not to be expected.
The changes in the exhaust emission values and fuel consumption can be seen in tab. 2. Accordingly, on the specific test engine, increased fuel consumption, unchanged NOx emissions, decreased CO and HC emissions and significantly reduced soot blackening and particulates were observed.

4. CONCLUSION

Fatty acid methylester seems very promising as an alternative bi-product to diesel fuel. The 2 to 3 % of diesel fuel which can be substituted (under Austrian conditions) appears relatively low, but the Fatty acid methylester is, due to its rapid biodegradability, an excellent bi-product for use in ecologically sensitive areas,especially for Off-road mobility. Additionally, the exhaust emissions are lower than those of diesel fuel.

5. LITERATURE

(1) Lenz, H.P.; Demmelbauer-Ebner, W.: Untersuchungen von Altsspeiseölmethylester (AME) VITA DIESEL 2000 an einem direkt-einspritzenden Nutzfahrzeugdiiselmotor. Bericht des Institutes für Verbrennungs-kraftmaschinen und Kraftfahrzeugbau der TU Wien. B2054 (1993).

Measured value		ÖNORM C 1190	Typical value	Diesel fuel
Density at 15°C	g/cm³	0,87 - 0,89	0,88	0,84
Flashpoint	°C	> 100	170	71
CFPP				
Summer	°C	max. 0	-2	-19
Winter	°C	max. -15	-20	
Viscosity at 20°C	mm²/s	6,5 - 8,0	6,8	4,2
Sulphur	% mass	max. 0,02	0,001	0,14
CCR	% mass	max. 0,05	0,01	0,03
Ashe	% mass	max. 0,02	0,003	
Cetan number		> 48	52	50
Neutralizations number	mg KOH/g	max. 0,8	0,06	
Methanol	% mass	max. 0,20	0,02	
Free glycerol	% mass	max. 0,02	0,001	
Total glycerol	% mass	max. 0,20	0,05	
Phosphorous	mg/kg	max. 20	0,5	

Tab. 1 : Fuel characteristics

	[ ]	DF	f AME	LIMIT
CO Carbon Monoxide	g/kWh	1,34	1,22	4,90
HC Unburned Hydrocarbon	g/kWh	0,60	0,49	1,23
NO2 Nitrogen Oxide	g/kWh	7,06	7,26	9,00
Formaldehyde (in 4 Load Points)	ppm	3,50	3,70	-
PM Particle Mass	g/kWh	0,48	0,23	0,70 (0,4 since 1.10.93)
SZ Soot Blackening Number	-	1,21	0,50	-
Be Specific Fuel Consumption	g/kWh	233,60	264,90	-

Tab. 2 : Emission and Fuel Consumption

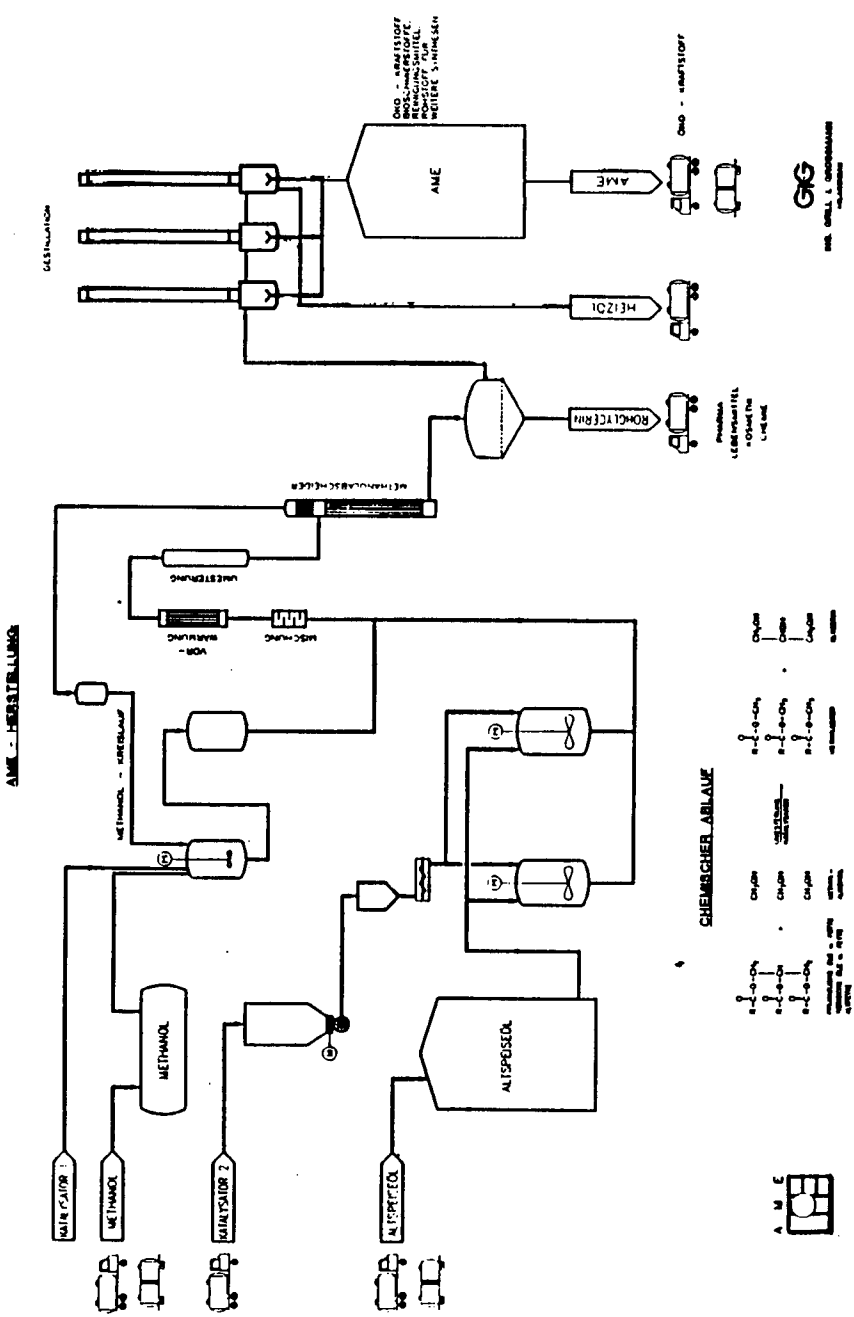

Fig. 1 : Production process

STATE OF ART REPORT OF THE MOBILITY RESEARCH IN HUNGARY

Lajos Laib
associate professor

University of Agricultural Sciences, Gödöllő, Hungary
Department of Automotive and Thermal Technology

ABSTRACT

The author publishes for the first time the detailed description of the Hungarian Army Mobility Model (HAMM). Different organizations and authorities have increasingly used the model during the past few years in support of the replacement of their vehicle fleets. The paper describes the model and, in the addition, it shows its application for the evalution of the performance of a few vehicles.

1. Background

In the early 1980s, following the example of NATO, the Hungarian Army developed its own cross-country model. It is Known as the Hungarian Army Mobility Model or HAMM. (The NATO model is called the NATO Reference Mobility Model or NRMM.) [1.:2.]

Earlier the existence of HAMM "hindered" Army experts in the process of procuring new vehicles, because they had to "select" vehicles which they were given by the Warsaw Pact regardless of any other consideration.

Howerer, after the recent political reforms HAMM has become an important tool. Today every vehicle offered to the Hungarian Army must be examined by means of HAMM. The model's output is a very important factor in arriving at a final decision, but it is by no means the only one.

In this study I describe the detailed flow of computations as well as the equations and formulas comprising the model. It should be noted that we are not fully satisfied with every aspect of HAMM and, therefore, work has begun to further improve it.

The detailed description of the model is followed by the presentation of an example in which we analyzed a number of vehicles in the 4x4 3/4 ton weight class and ranked them according to their predicted performance.

The Hungarian Army specified a so called "reference terrain-area" whose mobility related terrain data are well known by us. Moreover we know how these data vary as a function of variations in weather and seasonal changes. Each vehicle was evaluated with respect to this reference terrain.

2. The Hungarian Army Mobility Modell

Terrain-vehicle relationship research began with the investigation of the structural characteristics of the soil. The first results consisted of the determination of the bearing capacity of the soil. The investigation of the mobility of cross-country vehicles began about 20-25 years ago. The NATO Reference Mobility Model was established first and, subsequently, improved versions were developed, first of all on the basis of the work by TACOM and by WES.

A common feature of all mobility models is that they determine the traction force once the rolling resistance is calculated on the basis of running gear soil interaction research. The Cone Index is the basic parameter employed. An important factor of every mobility model is the acceleration due to shock and vibration caused by uneven terrain which affect the driver and the occupants. These accelerations may limit the speed of the vehicle significantly.

This paper describes the computional flow of the mobility model developed in Hungary for the H.D.F and, subsequently, presents a method for computing accelerations.

The program calculates the speed of the vehicle which is determined or limited by vibrational accelerations. To this end we needed the following formula:

$$y=((int(b/x+a)100)+0.5)/100$$

which is obtained via regression analisys from $V_L=f(\sigma_x^2)$, where

V_L [km/hour] is the vehicle speed and

σ_x^2 [m²] is the variance of the terrain profile.

The independent variable σ_x^2 is an input parameter. Next we discuss these functions together with pertinent theoretical considerations.

2.1 The Mobility Model

The input data of the model consist of parameters and relationships concerning the terrain, the vehicle and the driver. Output data are: the time needed to complete the mission, the average speed, fuel consumption and the go/ no go map.[1]

FIG. 1. shows the input-output data of the model and the flow of computation is depicted in FIG. 2.

The formulas and the list of variables are as the follows.

Vehicle related input data:

P_n [kW] = nominal engine performance

P_{op} [kW] = maximum engine operating performance

B_{tmax} [dm³/h] = fuel consumption at nominal engine performance

Mo [kg] = mass of the vehicle

Mp	[kg]	=	mass of the trailer
M_L	[kg]	=	payload
B	[in]	=	tire width
D	[in]	=	tire diameter
C1	[-]	=	constant needed to determine fuel consumption
C2	[-]	=	constant needed to determine fuel consumption
A	[m2]	=	cross section measured perpendicularly to the air stream
Cw	[-]	=	form factor
η_{atl}	[-]	=	power train efficiency
m	[-]	=	number of wheels

Terrain related input data

dv/dt	[m/s2]	=	attainable acceleration. (recommended value = 0.8 [m/s²])
L	[km]	=	length of terrain segment
E	[-]	=	slope of terrain given as a decimal fraction
σ_x^2	[m2]	=	variance of the terrain profile
CI	[lbs/in²]	=	cone index
Gy	[-]	=	frequency of acceleration. Recommended value=0.3

Constants built into the program

δ	[-]	=	reduction factor of the rotating masses

Terrain parameters (constants)

For all wheel drive λ=1.0,

For two wheel drive λ is as follows:

λ = 0.68 for lose sand

λ = 0.73 for sand stubble

λ = 0.76 for medium firm soil

λ = 0.78 for firm soil

K is an empirical factor

K = 1.5 for loose sand soil

K = 1.0 for sand stubble field

K = 0.6 for medium firm soil

K = 0.4 for firm soil

n is an exponent; it is an empirical factor

n = 0.45 on loose sand

n = 0.50 on sand stubble field

n = 0.55 medium firm soil,, firm stubble field

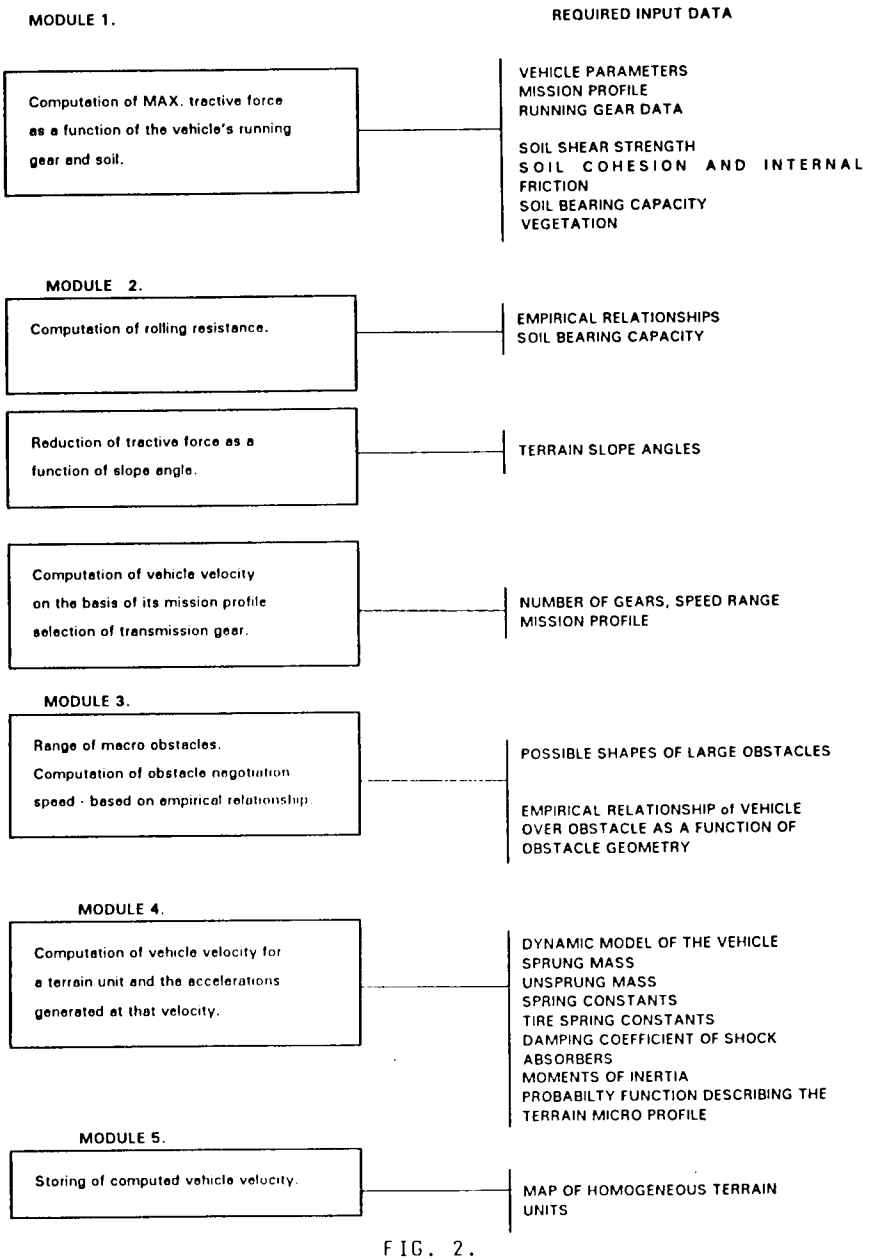

FIG. 2.

Flow of the computation of HAMM

Output Data:

CN	[kN]	=	rolling resistance
RO	[-]	=	specific rolling resistance
Mu	[-]	=	coefficient of adhesion
FG	[N]	=	force required to overcome the rolling resistance
FE	[N]	=	resisting force due to slope
FK	[N]	=	peripheral force
SV	[%]	=	slip
VV	[m/s²]	=	acceleration at 10 % slip
V9	[km/hour]	=	speed at 10% slip
V1	[km/hour]	=	stationary speed
V2	[km/hour]	=	dynamic speed
VA	[km/hour]	=	average speed
VL	[km/hour]	=	speed limited by vibrational acceleration
PA	[kW]	=	average performance (power)
BT	[lit/hr]	=	fuel consumption
ET	[-]	=	power efficiency (power utilization coefficient ratio)
T	[hour]	=	time needed to cover the prescribed path or distance
SB	[liter]	=	fuel consumption

The following formulas are used in the algorithms:

Summing of masses:

$$M_o + M_L = M_j \qquad [kg]$$

$$M_j + M_p = M \qquad [kg]$$

Computation of the rolling resistance:

$$CN = \frac{(CI \cdot B \cdot D \cdot m)}{M_j}$$

$$\varrho = \left(\frac{1.2}{CN}\right) + 0.04$$

Traction needed to overcome the rolling resistance:

$$FG = M \; g \; \varrho$$

Traction needed for acceleration:

$$FGY = M \frac{dv}{dt} \delta \qquad [N]$$

Traction needed to negotiate a slope:

$$FE = M \; g \; E \qquad [N]$$

Total traction required:

$$FT = FG + FE + FGY \qquad [N]$$

The coefficient of adhesion:

$$\mu = \frac{FT}{\lambda M_j g}$$

Slip:

$$s = \mu \frac{1}{n} K + 0.015$$

Computation of the acceleration available at 0.1 slip:

$$\mu = \left(\frac{0.1}{K}\right)^{n}$$

$$FT^{0.1} = \mu M_j g \lambda \qquad [N]$$

$$FGY = FT^{0.1} - FG - FE = \delta M_j \frac{dv}{dt} \qquad [N]$$

$$a = \frac{dv}{dt} = \frac{FGY}{\delta M} \qquad \left[\frac{m}{s^2}\right]$$

If the dv/dt = 0 than the HAMM yields a "NO GO" for the mobility of the vehicle.

The maximum attainable vehicle speed under dynamic and/or static conditions:

$$(FG+FE+FGY+FL)\frac{V}{3600\eta_{dtt}(1-s)} = P_a \qquad [kW]$$

$$F_L = \frac{1}{2} A C_w \varrho_{air} \left(\frac{V}{3.6}\right)^2 \qquad [N]$$

To be solved for the following conditions:

$P = 0.6\ P_{operational}$ or $P = 0.8\ P_{operational}$

If dv/dt = 0.8 → V2 And

dv/dt = 0 → V1

Then VA = 1/2 GY V2 + (1-GY)V1 [km/h]

VA << VL, V = VA

VA >> VL, V = VL

Power requirement:

$$P = \frac{(FG + FE + FL + GY \cdot FGY) \cdot V}{3600 \eta_{atl} (1 - s)} \qquad [kW]$$

Required fuel consumption:

$$\eta_t = \frac{P}{P_{op}}$$

$$B = (C1 \eta_t + C2) \frac{s}{V} \qquad [dm^3]$$

Time needed to cover the distance:

$$T = \frac{s}{V} \qquad [h]$$

The flow of computation is shown in Fig.3.

Fig.4. shows an example for tables of input/output data

VEHICLE	FOUR WHEEL
NOMINAL PERFORMANCE	TWO WHEEL
MAX OPERATIONAL PERFORMANCE	DRIVE
(L/H) FUEL CONSUMPTION	
MASS OF VEHICLE	SOIL TYPE
TRAILER	
PAYLOAD	LOOSE SAND
WIDTH OF TIRE	
DIA OF TIRE	MEDIUM

CONSTANTS	
ENGINE CONSTANS C1	CONSTANS B1
ENGINE CONSTANS C2	CONSTANS B2
AREA OF THE V. FACE A=	AVERAGE EFFICIENCY=
SHAPE PARAMETER CW=	NO OF TIRES M=

ACTUAL RUNNING PARAMETERS		
DV/DT	DT=	VARIANCE OF TP. σ_x^2
DISTANCE [KM]	L=	CONE INDEX=
SLOPE	E=	ACCELERATION FACTOR=

OUTPUT DATA

SOIL TYPE:MED.FIRM DISTANCE COMPLETED		
ROLLING RESIST.	CN=	
ROLLING RESIST.	RO=	
ADHESION COEFF.	MU=	
ROLLING RESIST.	FG=	
SLOPE RESIST.	FE=	
PERIPHERIAL FORCE	FK=	
SLIP	SY=	
ACCEL. AT 10% SLIP	VV=	
SPEED AT 100 % SLIP	V9=	
STATIONARY SPEED	V1=	
DYNAMIC SPEED	V2=	
AVERAGE SPEED	VA=	
SPEED DEPENDING ON THE ACC.	VL=	
AVERAGE PERF	PA=	
FUEL CONSUMPTION	BT=	
PERF. UTILIZATION FACTOR	ET=	
TIME REQUIRED TO COVER THE DISTANCE	T=	
AMOUNT OF REQUIRED FUEL	SB=	

FIG 4.

INPUT-OUTPUT MASK OF THE MODEL

2.2 Computation of vehicle speed limited by vibrational acceleration:

The goal of the computation is the determination of the function $V_L=f(\sigma_x^2)$ for specific vehicles at constant acceleration.[4]

The power spectral density of the terrain profile is calculated first. Next a polynomial is fitted to the PSD. The profile is characterized by three parameters: (σ_x^2), λ, L

Three road profile categories were defined for this study and the following functions were established:

$$\lambda = f(\sigma_x^2)$$

$$L = f(\sigma_x^2)$$

This relationship is used as an excitation function and the maximum attainable speed is calculated by means of the 3 dimensional model of the vehicle assuming constant allowable maximum acceleration at the driver's position.

This method is discussed in more detail in the following.[3]

THE MATHEMATICAL APPROACH APPLIED FOR THE PROBLEM

The amplitudes of the road profile are available from profile measurements.It is assumed that the profile is stationary and ergodic.

In Fig. 5. H is the length of travel, h is the profile sampling interval, m is the number of profile data points considered.(We use 2048 points in order to satisfy Fast Fourier Transformation FFT- requirements.)The
average velocity is:

$$V=\frac{mh}{t} \qquad [\frac{m}{s}]$$

where t is the time needed to cover distance H. The first step is the statistical analysis of the samples. The mean is:

$$\overline{X}=\lim\frac{1}{m}\sum_{i=1}^{m} x_i$$

Transferring to the horizontal(mean) axis we get the vertical deviation from the mean:

$$X_i=x_i-\overline{X}$$

The approximate variance is:

$$\sigma_x^2 = \lim_{m \to \infty} \frac{1}{m} \sum_{i=1}^{m} (x_i - \bar{x})^2$$

The next step is the computation of the correlation function:

$$R(\zeta) = \lim \frac{1}{m} \sum_{i=1}^{m} x_i \cdot x_{i+k}$$

where $\zeta = kh$

R(ς) is sometimes called the autocovariance.

The maximum value of k is 1/3-d of the length of the profile.(k=0, k=1, k=2,..k=1/3* H)

To compute L, we first normalize the auto correlation function with respect to the variance:

$$R_x^*(\zeta) = \frac{1}{\sigma_x^2} R_x(\zeta)$$

Integrating this function gives L, which is the scale parameter of the road segment, a statistical measure of the profile. (Fig. 6.)

$$L = \int_0^{\infty} R_x^*(\zeta)\, d\zeta$$

L defines the distance within which the function may be considered homogeneous; it may be called the correlation distance.

The third step is the computation of the power spectral density by means of Fast Fourier Transformation (FFT) of $X_i(h)$.

The formula is as follows:

$$G_x(\frac{k}{mh}) = \frac{h}{m}\sum_{i=1}^{m-1} |X_i \exp(-j2\pi \frac{k_i}{mh})|^2$$

where

$$n = \frac{k}{mh}$$

The result is the power spectral density of the displacement $G_x(n)$ which is bounded. (See Fig.7.). We may approximate this function by an expression having a negative exponent:

$$G_x(n) = \sigma_x^2 \frac{4L}{(1+\frac{4}{\alpha-1}Ln)^{\alpha}}$$

and α is a constant depending on the type of road surface.

Once road surface characteristics α, L and σ_x^2 are known we have a relatively simple method to establish the excitation caused by the road. Table 1 shows the values of these constants for some important road surfaces.

Converting the spatial spectrum to the frequency domain is an important step. This is necessary for computing the acceleration spectrum $G_a(f)$ for various vehicle speeds.

The time step is obtained by:

$T = L / V$ or $L = V T$

where V is the constant vehicle speed.

The power spectral density in the frequency domain is:

$$G_x(f) = \sigma_x^2 \frac{4T}{(1 + \frac{4}{\alpha - 1} Tf)^{\alpha}}$$

As mentioned earlier we measured and analyzed three road surfaces as follows:

- smooth hard road,
- cobble stones,
- dirt road.

In order to simplify the computations a functional relationship was established between α, L and σ_x^2.(Fig.8.)

The next step was the computation of the acceleration at the drivers's location. For a given vehicle VL = f (σ_x^2) was established, which is the vehicle speed vs. road profile variance relationship, for 0.5g and 0.3g driver location accelerations. (See Figs. 9.) This figure shows several cross country vehicles of different types. As stated before 0.3g and 0.5g maximum accelerations were allowed at the driver's location.

The curves shown in Fig. 9. can be approximated by a function of the form:

$$VL = ((\frac{b}{\sigma_x^2} + a)100 + 0.5)/100$$

The values for a and b depend on the vehicle-type. When the variance of the road profile and the type of the vehicle are known one can predict the velocity which is limited by the maximum acceleration allowed at the driver's position.

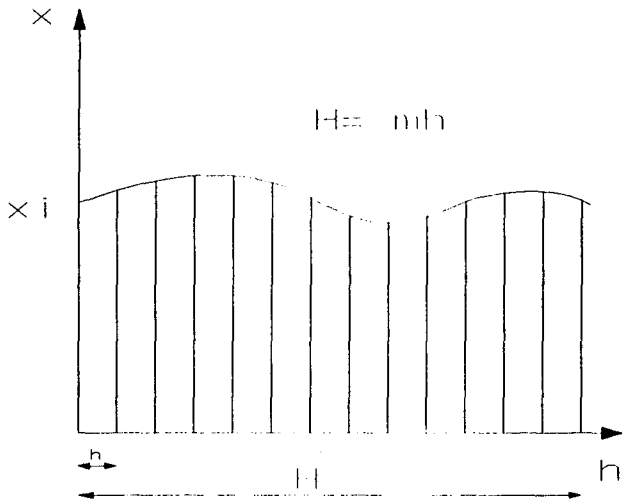

Fig.5
Signals of the Terrain Profil

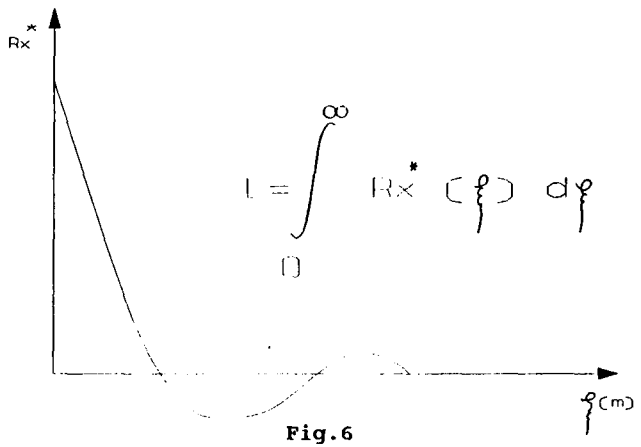

Fig.6
Correlation function of the terrain profil

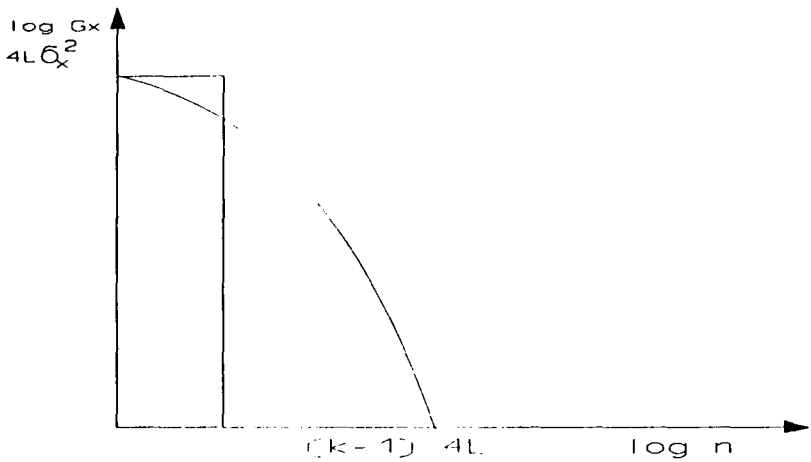

Fig.7.
Power spectral density of the terrain profil

TABLE 1.

VARIANCES, SCALE PARAMETERS AND EXPONENTS
FOR VARIOUS ROAD SURFACES

Type of ROAD	σ_z^2[cm^2]	σ_z[cm]	L[cm]	α[-]
Secondary road	49.9	7.35	102.6	2.642
Autobahn	1.38	1.175	49.6	2.174
Cobble stone	23.76	4.875	1.77	4.256
Concrete covered with asphalt	1.966	1.402	135.1	1.61
Asphalt road	10.002	3.2	44.5	2.068
Runway	3.894	1.973	52.2	2.125
Small cobble stone	5.038	2.245	2.91	2.844
Very good asphalt-concrete	0.648	0.805	38.09	2.434
Good cement concrete	0.447	0.669	18.2	2.09
Medium macadam	3.368	1.835	52.2	2.101
Medium cobble stone	1.729	1.315	53.6	1.545
Medium dirt-road	33.44	5.783	14.4	2.463
Meadow	16.1	4.01	21.6	2.091
Smoothed plough field	23.6	4.86	21.8	2.491

We modeled the vehicle means of a three dimensional dynamics model. This model is presented in figs. 10 and 11. I show the input data in table 2.

The damping coefficient and the spring constant of the tire were obtained from a diagram received from the manufactuer. It is a characteristic of the model that the vehicle can undergo pitching and yawing motion around the axis which runs across the center of mass. We assumed that the spring and damping elements behaved in a linear fashion within the range of operation and, in addition, we neglected the frictional forces within the leaf springs.

Most of the input data were furnished by the manufactuer. The inertia of the independent suspension was obtained by swinging the wheel as a pendulum and we measured the system's period.

We considered the damping effect of the lateral and longitudinal stabilizers. The equations of motion were solved by means of the Runge-Kutta iteration method.

The output of the computation is function

$$VL = F(\sigma_x)'$$

Which is shown in Fig. 9. and Fig. 12.

3.Engine Coefficients

We determined engine coefficients C_1 and C_2 in accordance with the third item in the experimental program. These are required as input data for the mobility model for the purpose of computing the fuel consumption of the engine on the basis of power requirement and load coefficient.

DESCRIPTION OF THE TEST:

We determined fuel consumption and exhaust gas temperature simultaneously for different vehicle loads. The data of these test are illustrated in Fig. 13. and table 3.

Function B_t (dm^3/h) = F (HT/HU) Was approximated by fitting a straight line using linear regression. The equation of the straight line is as follows:

$$B_t = C_1 \ (\ HT/HU \ ) + C_2(\ dm^3/h \ )$$

We determined the engine load efficiency factor.

$$\eta_t = (\ B_t - B_{tmin} \ ) \ / \ \Delta B$$

where:

B_{tmin} = fuel consumption for lower RPM (dm^3/h)

$\Delta B = B_t - B_{tmin}$ (dm^3/h)

Substituting:

$$\eta_t = (\ C_1 \ (\ HT/HU \ ) + C_2 - B_{tmin} \ ) \ / \ \Delta B$$

Dividing each term, we obtain:

$$\eta_t = (\ C_1/\Delta B \ ) \ (\ HT/HU \ ) + (\ C_2 - B_{tmin} \ ) \ / \ \Delta B,$$

and we determined constants (C_1, C_2) for each vehicle.

This concludes the determination of all data needed for the program. All vehicle data are shown in table 4.

4. Analysis of different vehicles by means of HAMM

The hungarian army assigned a terrain unit which was judged to be suitable for military vehicle mobility evaluation. We divided this unit into smaller units, each being nearly uniform as far as mobility impediments were concerned. We "mapped" these units in great detail. We determined the cone index of the soil, its moisture content, its density, slope angle and the length of each segment. We surveyed the profile at 10 cm intervals and we computed the variance of the profile. Important terrain data are show in table 5.

Vehicle speed and fuel consumption data are show by themselves in table 6 and 7. A comparison of the velocities and fuel consumption of the six vehicles is presented in Figs. 14 and 15.

The computations show that on the same terrain type "D" 35.5% faster than type "F" slower than type "C" 27.4% slower than type "B".

I show a bar graph in Fig.16. This depicts the combined ranking of vehicles according to velocity and fuel consumption.

5.The obstacle performance function

5.1. Obstacle conditions of Hang-UP Failure (HUF)

The "DR" circle defines the amount of obstacle encroachment which occurs between the wheels and huf will take place if H=0. The definition of hang-up diameter (DR) makes it possible to determine vehicle failure quantitatively. Huf is basically defined by a twoplane obstacle. [5]

The vehicle will fail if

$$HG=0.5((D+DR)-\sqrt{(D+DR)^2-L^2})$$

where

"HG" is the longitudinal ground clearance (M)

"L " is the wheel base (M)

"DR" is the longitudinal vehicle ground clearance diameter (M)

"D " is the wheel diameter (M)

5.2. Obstacle conditions of Nose-IN Failure (NIF)

The nose-in failure will occur if

$$\frac{D}{2\sin(\beta_2+\alpha)} = L_1 - L$$

Where "α" is the slope vehicle's longitudinal axis at the moment of failure.

In the particular case, where the bottom of the obstacle is horizontal ($\beta_2=0$) and ($\alpha=\beta_1$, the condition of nif is

$$\frac{D}{2\sin\beta_1} \leq L_1 - L$$

or

$$\frac{D}{2\sin\beta_1} + B\cos\beta_1 \leq L_1 - L$$

the critical height:

$$H_{crit} = \frac{D}{2} + L\sin\beta_1 - \frac{D}{2}\cos\beta_1$$

The vehicle-slope-elevation (VSE) function defines the relationship between depth of descent "H" and slope "β" at the moment of vehicle failure. It serves as a basis for comparing canal-crossing performances.

Figure 17. summarizes the geometric relationship between the vehicle and the descending portion of the obstacle for "NIF" and "HUF".

6. Discussion

The Hungarian Army Mobility Model has provided useful information during the past 10 years for the user. In recent years it significantly helped our experts involed in the decision making process. The accuracy of the model is ±10% when compared to actual data obtained on the reference terrain-area. Although this should be considered as good agreement we can expect futher improvement by employing more accurate input data. HAMM, as well NRMM, simulate the tire-soil interaction by means of a host of empirical factors. Therefore we have concentrated on defining terrain and soil input data as accurately as possible. These data were determined as a function of weather conditions and seasonal effects. Consequently the analytical results computed for vehicles moving over the reference terrain yield realistic comparisons for different vehicle types.

After considerable delays we have undertaken further development of the model. We are investigating the relationship between terrain-profile and the vehicle mass, which will enable us to develop a more accurate tire-soil interaction model.

The reference area is also being expandedd by including loose sandy and "stony" units. We are in the process of developing subroutines to compute the location of the vehicle's center of mass and its displacement time-history as the vehicle rides over a given terrain-unit.

REFERENCES

1/ LAIB L.: Off-Road Mobility of Military Vehicles. Research Report 1983-86. pp. 1050 (in Hungarian)

2/ LAIB L.: Vehicle mobility modelling. Haditechnikai Szemle 1985 Vol. 3. pp. 3-8. (in Hungarian)

3/ LAIB L.- GEDEON J.: Analysis of the motion of crosscountry vehicles. Járművek és Mezőgazdasági Gépek 1989 Vol.36.No.8. pp. 285-289.

4/ MISCHKE J.: Dynamik der Kraftfahzeuge. Springerverlag. 1979. 237.p.

5/ BEKKER M.G.: Introduction to terrain vehicle systems. Published by The University of Mechigen Press, Ann Arbor, 1968 386.p.

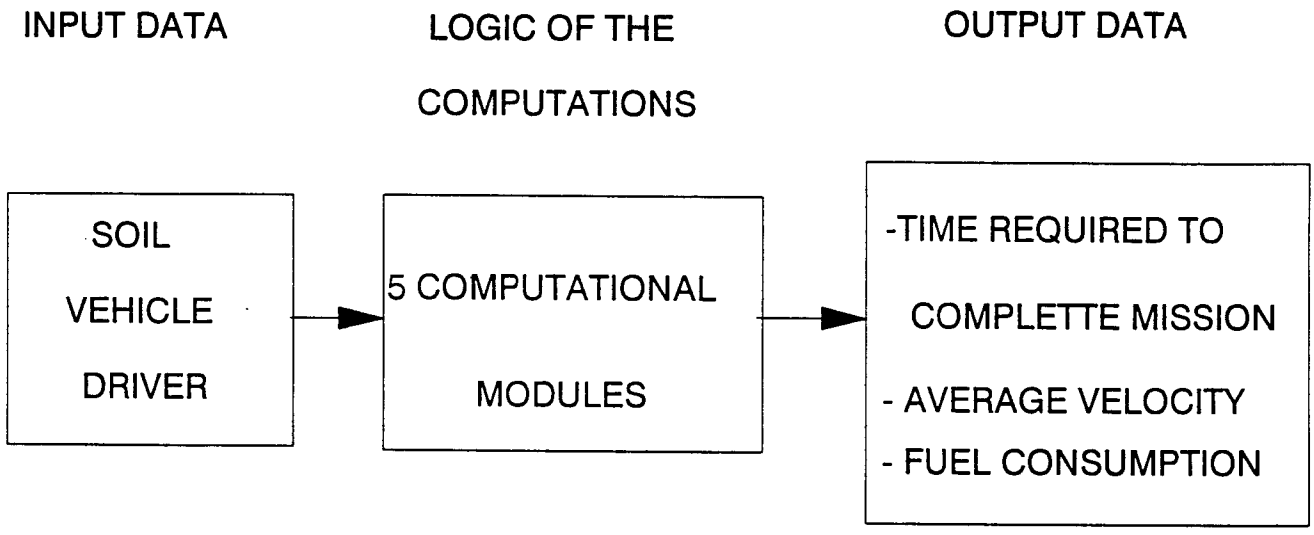

FIG. 1.

INPUT-OUTPUT DATAS OF THE MODEL

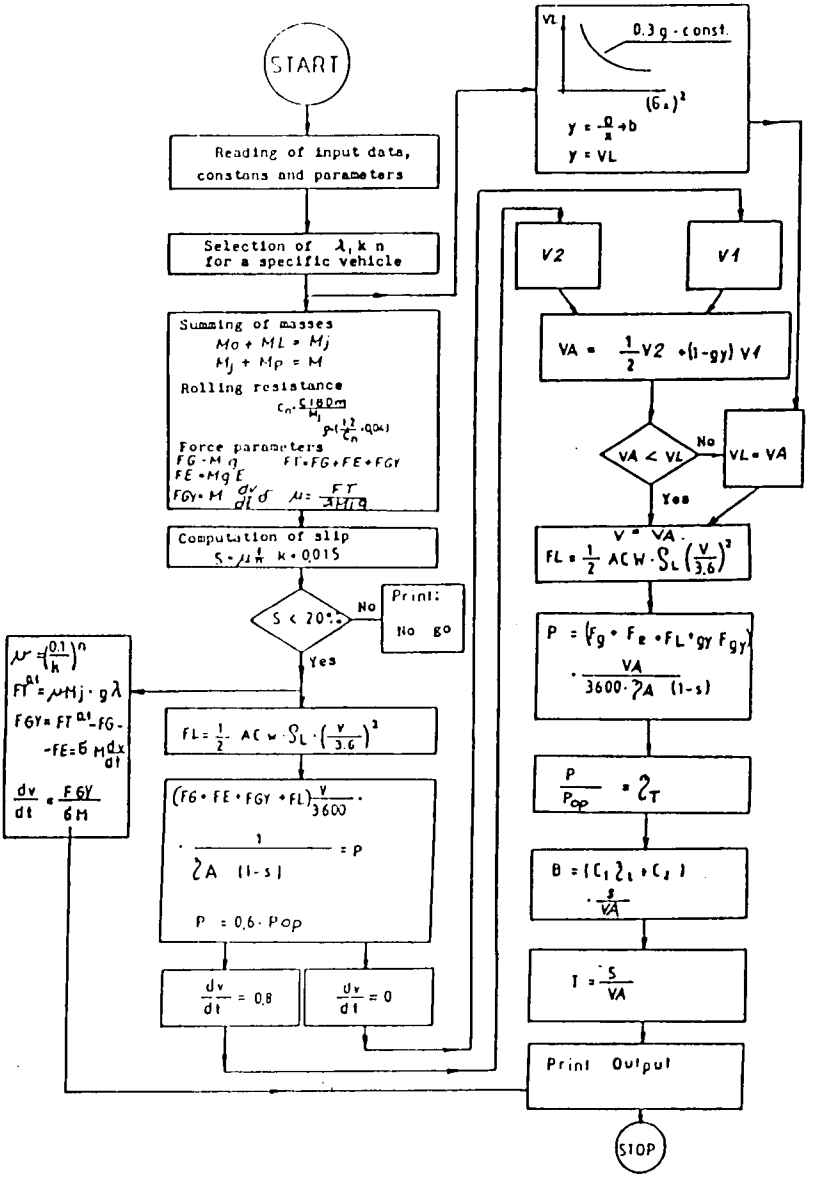

Fig. 3

The flow of computation of HAMM

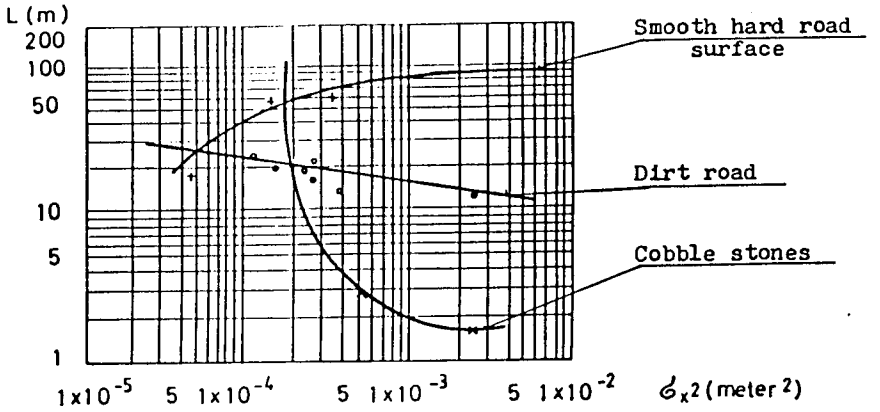

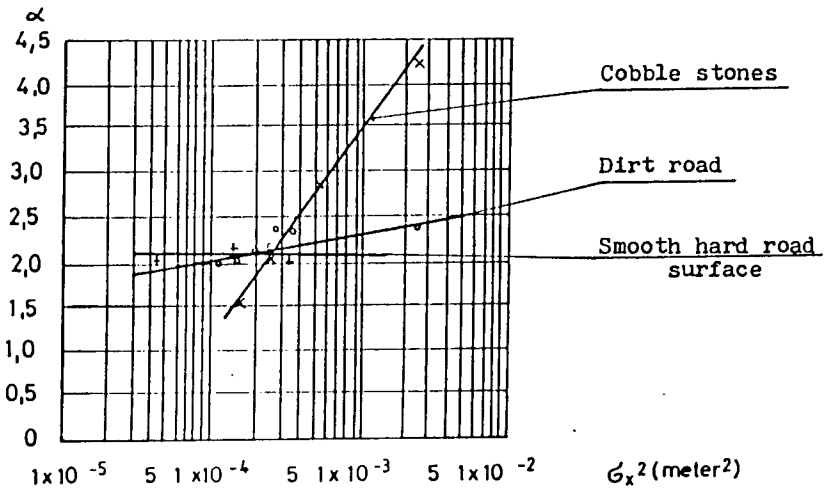

Fig. 8

Relationship between "α"-"L"- and σ_x^2

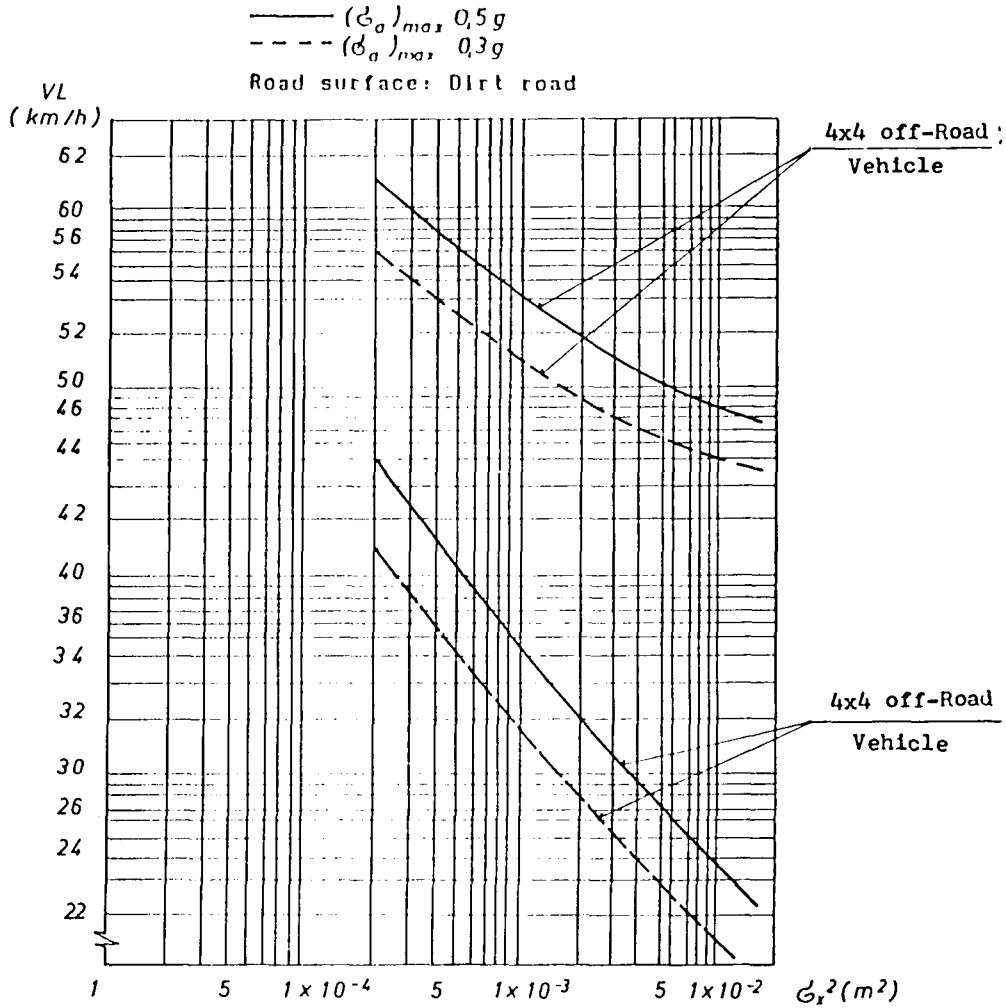

Fig. 9

Relationship between vehicle velocity and the variance of road profile function

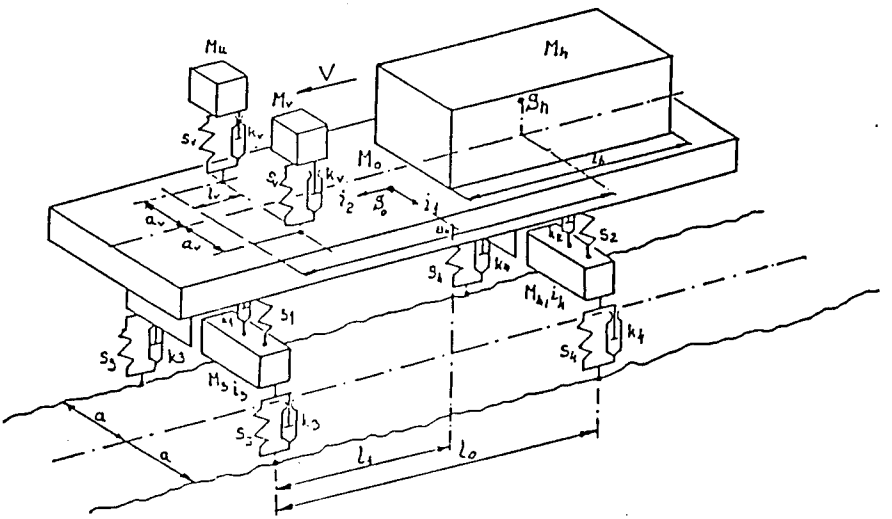

Fig. 10

Three Dimensional Dinamics Model of the Vehicle

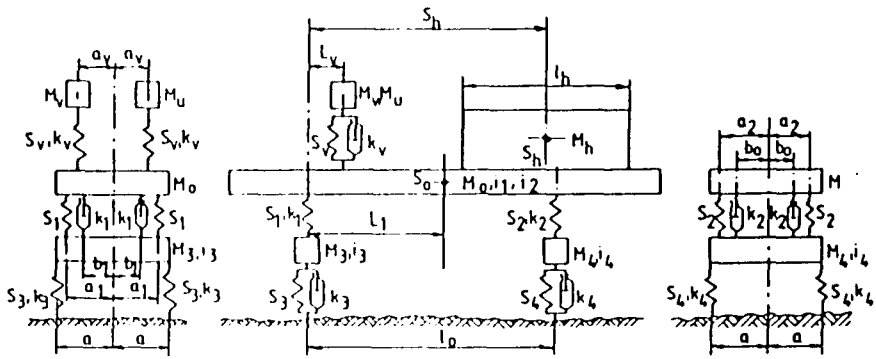

Fig. 11

Three Dimensional Dynamics Model of the Vehicle

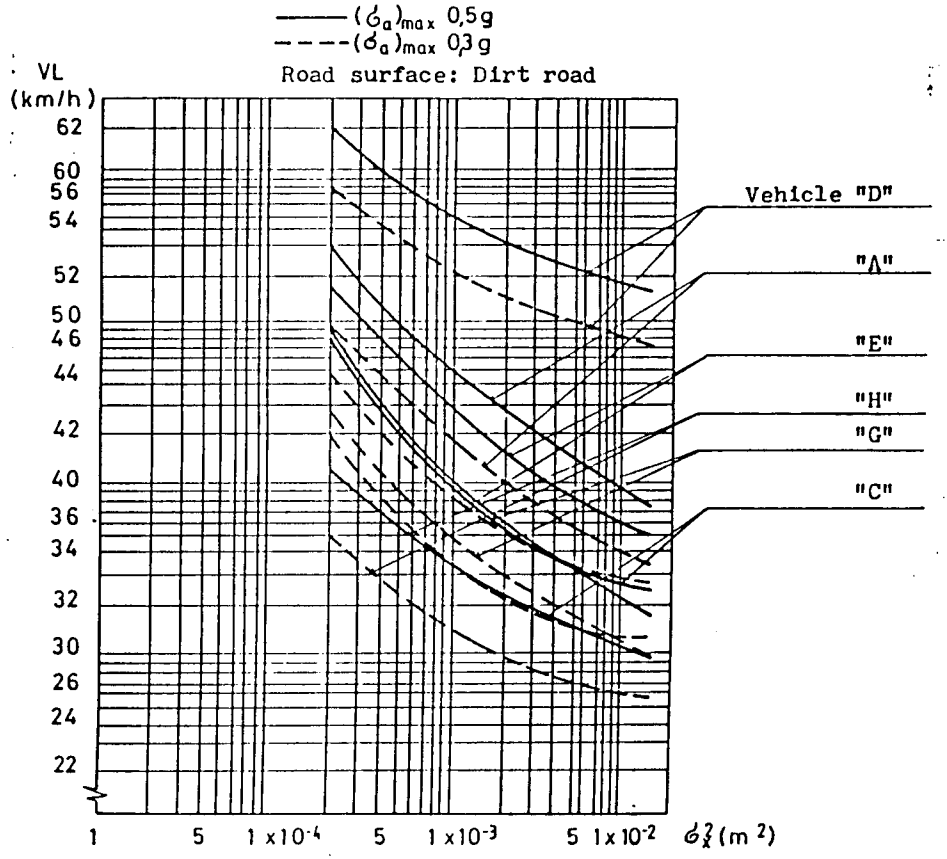

Fig.12

Relationship between vehicle velocity and the variance of road profile function

Type of vehicles:		"B"
P_{op}	= 72 kW	73 kW
B_{tmax}	= 21,07 dm³/h	14,96 dm³/h
B_{tmin}	= 0,51 dm³/h	0,50 dm³/h
ΔB	= 20,56 dm³/h	14,46 dm³/h

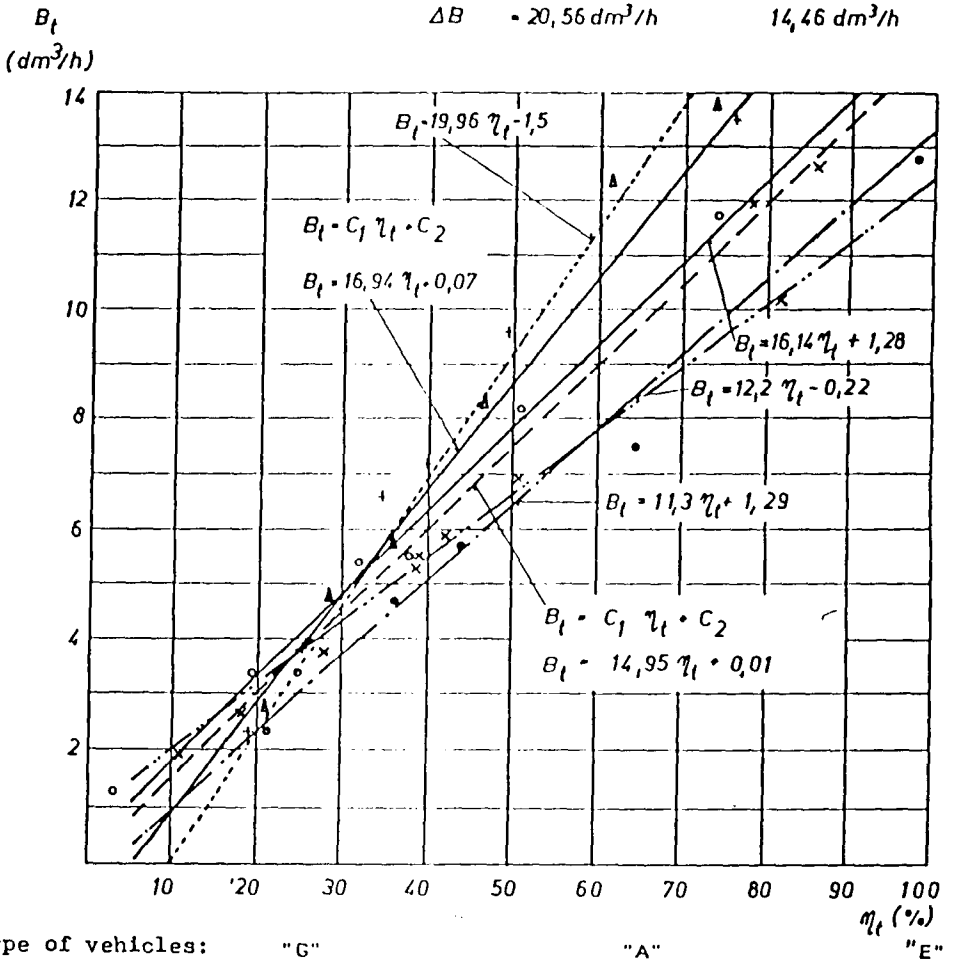

Type of vehicles:	"G"	"A"	"E"
P_{op}	= 59 kW	66 kW	55,2 kW
B_{tmax}	= 13,78 dm³/h	17,6 dm³/h	17,16 dm³/h
B_{tmin}	= 0,77 dm³/h	0,92 dm³/h	0,74 dm³/h
ΔB	= 13,01 dm³/h	16,68 dm³/h	16,42 dm³/h

Fig. 13.

RELATIONSHIP OF THE FUEL-CONSUMPTION AND AVERAGE-LOAD OF THE ENGINE FOR THE ABOVE VEHICLES

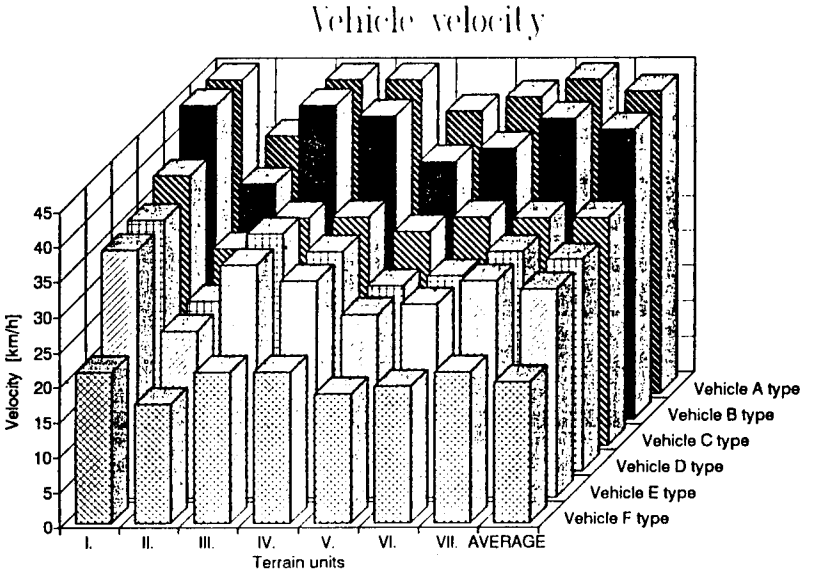
Vehicle velocity
Velocity [km/h]
45
40
35
30
25
20
15
10
5
0
I.
II.
III.
IV.
V.
VI.
VII.
AVERAGE
Terrain units
Vehicle A type
Vehicle B type
Vehicle C type
Vehicle D type
Vehicle E type
Vehicle F type

Fig 14.

Table 7.

COMPARISON OF PREDICTED FULL CONSUMPTION OF THE SIX VEHICLES

TERRAIN	VEHICLE FULL-CONSUMPTION (DM3/H)					
UNITS	C TYPE	D TYPE	B TYPE	F TYPE	A TYPE	E TYPE
I.	6.19	9.96	6.78	7.06	8.28	6.47
II.	7.71	9.74	6.73	8.04	10.15	6.37
III.	6.52	9.92	6.78	7.42	9.35	6.46
IV.	7.07	9.88	6.78	8.08	9.28	6.44
V.	7.74	9.78	6.75	8.08	10.16	6.39
VI.	7.76	9.81	6.76	8.11	10.15	6.41
VII.	7.03	9.88	6.78	8.01	9.90	6.44
AVERAGE	7.15	9.85	6.77	7.83	9.61	6.43

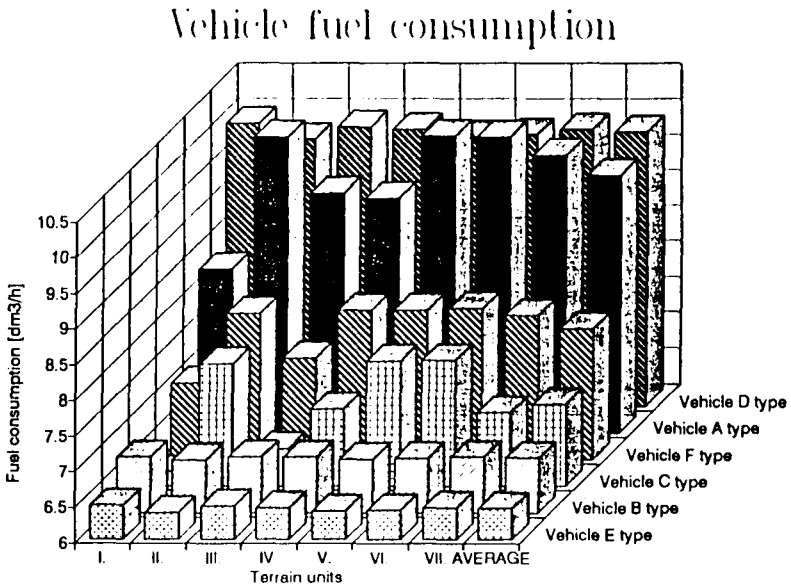

Fig 15

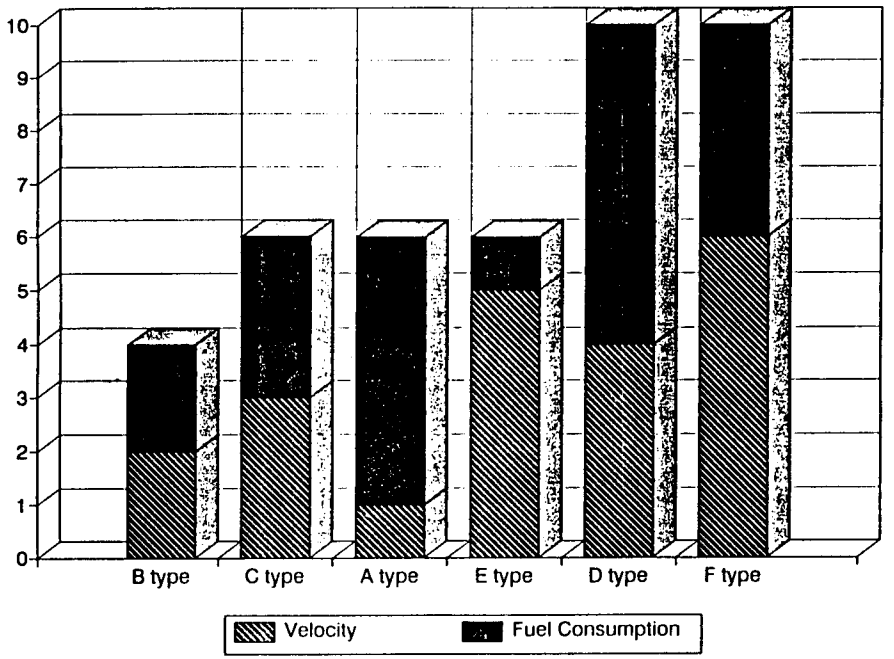
10
9
8
7
6
5
4
3
2
1
0
B type
C type
A type
E type
D type
F type
Velocity
Fuel Consumption

FIG.16

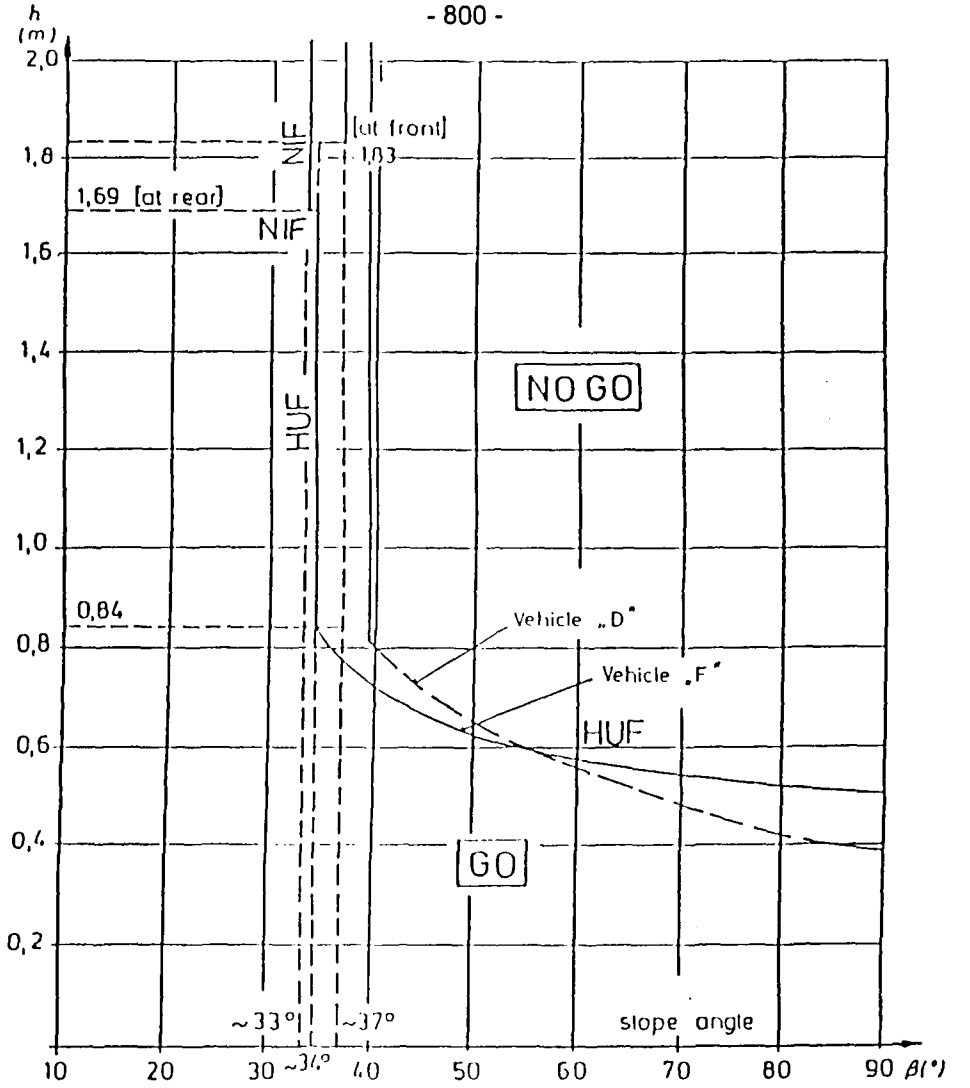

Fig. 17

SLOPE - DESCENT DEPTH RELATIONSHIP OF THE ABOVE VEHICLES

TABLE 2.

Vehicle dynamics input data for the Dynamics Analyses.

SYMBOL	NOMENCLATURE	DIM.
M(0)	MASS OF THE VEHICLE	KG
i1	INERTIA RADIUS FOR PITCH	M
i2	INERTIA RADIUS FOR YAW	M
M3/R,L		
M4/R,L	UNSPRUNG MASS PER WHEEL	KG
	HALF TRACK OF WHEELS	M
MV	MASS OF THE DRIVER'S SEAT WITH THE DRIVER	KG
I3,I4	INERTIA RADIUS OF INDEPENDENT SUSPENSION PER WHEEL	M
S1	FRONT SPRING CONSTANT	N/M
K1	FRONT DAMPING COEFFICIENT	NS/M
S2	REAR SPRING CONSTANT	N/M
K2	REAR DAMPING COEFFICIENT	NS/M
S3,S4	FRONT AND REAR SPRING CONSTANT OF THE TIRES	N/M
K3,K4	FRONT AND REAR DAMPING COEFFICIENT OF THE TIRES	NS/M
SV	DRIVER'S SEAT SPRING RATE	N/M
KV	DRIVER SEAT DAMPING COEFFICIENT	NS/M
L1	DISTANCE OF C. G. FROM THE FRONT AXLE	M
LO	WHEEL BASE	M
LV	LOCATION OF DRIVER'S SEAT IN THE LONGITUDINAL DIRECTION	M
A1	HALF TRACK OF THE FRONT SPRINGS	M
B1	HALF TRACK OF THE FRONT SHOCK ABSORBERS	M
A2	HALF TRACK OF THE REAR SPRINGS	M
B2	HALF TRACK OF THE REAR SHOCK ABSORBERS	M
SH	DISTANCE BETWEEN THE FRONT AXLE AND THE C. G. OF THE CARGO	M
A	HALF TRACK OF THE WHEELS	M
AV	DRIVER SIDE WARD DISPL.	M
	LENGTH OF THE TIRE FOOTPRINT	M
SK1;SK2	TORSIONAL SPRING CONSTANT OF THE FRONT/REAR STABILIZER	NM/RA
KK1;KK2;	TORSIONAL DAMPING RATE OF THE REAR STABILIZER	NM/RA
LH	LENGTH OF THE CARGO	M

TABLE 3.

FUEL CONSUMPTION
AND ENGINE LOAD COEFFICIENT DATA

VEHICLE: D type

Pmax: 77kW
Bmax: 22.86 dm3/h

Operational Condition	Load Coefficient γ_t	Fuel Consumption Per Hour [dm3/h]
LOW RPM OF ENGINE	0.05	1.07
OFF-ROAD AND ON-ROAD	0.35	5.58
HIGHWAY	0.55	8.32
OFF-ROAD WITHOUT CARGO	0.41	6.50
OFF-ROAD WITH CARGO	0.70	13.80

TABLE 4.

TECHNICAL DATA OF THE VEHICLES

TYPE OF THE VEHICLE
NOMINAL ENGINE PERFORMANCE PN (KW)
MAXIMUM OPERATING ENGINE PERFORMANCE Pop (KW)
FUEL CONSUMPTION AT THE NOMINAL ENGINE PERFORMANCE Btmax (DM3/H)
MASS OF THE VEHICLE (KG)
PAYLOAD MR (KG)
TIRE WIDTH (")
TIRE DIAMETER (")
POWER TRAIN EFFICIENCY
CONSTANS NEEDED TO DETERMINE FUEL CONSUMPTION
C1
C2
CROSS SECTION MEASURED PERPENDICULARLY TO THE AIR STREAM A (M2)
FORM FACTOR Cw
REDUCTION FACTOR OF THE ROTATING MASSES
NUMBER OF WHEELS

TABLE 5.

AVERAGE PARAMETERS OF TERRAIN UNITS

Terrain units						
No.	slope	L[km]	CI	RCI	x[%]	ρ[g/cm^3]
1.	0.01	0.725	133.4	149.4	17.73	1.93
2.	0.056	0434	148.1	179.2	15.63	1.79
3.	0.02	0.442	158.9	200.1	14.93	1.82
4.	0.02	0.711	117.3	140.76	16.68	1.89
5.	0.042	0.694	131.56	168.3	16.83	2.04
6.	0.035	0.677	127.1	155.09	18.65	2.05
7.	0.025	0.670	141.08	181.9	13.64	2.03

Table 6.

COMPARISON OF PREDICTED VELOCITIES OF THE SIX VEHICLES

TERRAIN UNITS	VEHICLE VELOCITIES											
	C TYPE		D TYPE		B TYPE		F TYPE		A TYPE		E TYPE	
	MEASURED	COMPUTE	MEASURED	COMPUTE	MEASURED	COMPUTE	MEASURED	COMPUTE	MEASURED	COMPUTE	MEASURED	COMPUTE
I	36.80	38.47	33.26	35.85	47.20	48.90	20.60	21.60	44.38	45.71	34.61	35.25
II	26.90	28.04	21.96	24.20	32.30	33.60	16.20	17.03	36.90	36.86	22.81	23.81
III	30.90	32.43	31.67	33.77	45.10	46.02	20.02	21.58	46.25	45.69	31.96	33.13
IV.	31.00	32.44	30.20	31.27	42.50	43.35	19.98	21.59	46.25	45.69	29.67	30.87
V.	27.90	30.48	25.40	26.44	35.20	36.78	17.50	18.54	41.00	40.36	25.66	26.06
VI.	31.20	32.44	26.65	27.85	36.80	38.70	18.10	19.51	43.63	42.46	26.48	27.46
VII	32.00	32.40	30.26	31.28	44.02	43.04	20.50	21.56	46.24	45.67	29.67	30.77
AVERAGE	30.96	32.39	28.49	30.09	40.45	41.48	18.99	20.20	43.52	43.21	28.69	29.62

TRACTIVE PERFORMANCE OF A FOUR-WHEEL DRIVE VEHICLE MOVING UP A SLOPED WEAK TERRAIN

Tatsuro MURO
Prof. of the University of Ehime
Faculty of Engineering
3 Bunkyo-cho, Matsuyama, Japan (790)

ABSTRACT

The mechanism of tractive performance of a 5.88 [kN] weight, two-axle, four-wheel drive vehicle moving up a sloped weak sandy terrain is theoretically analysed. For the given dimensions of the vehicle and the given terrain-wheel system constants, the relations among tractive effort of the vehicle, amount of sinkage of the front and rear wheels and slip ratio were analysed by use of a simulation method. The optimum height of application of force and the eccentricity of the center of gravity of the vehicle to obtain the largest value of maximum effective tractive effort of the vehicle can be explained with the analytical simulation program. Results of this study showed that the optimum eccentricity e_{opt} for the application height $H=14$ [cm] should be always controlled to be -0.20 and -0.25 for the slope angle $\beta=\pi/36$ [rad] and $\pi/18$ [rad] respectively. The optimum height of application of force H_{opt} of the vehicle should be always controlled to be 14 [cm] for the eccentricity of the center of gravity $e=-0.20$, and for the slope angle $\beta=\pi/36$ [rad].

1. INTRODUCTION

Several wheeled construction machines are used in many earth moving sites, excavating a sandy soil, pulling or pushing other vehicles. For an example, tyres of four-wheel drive motor scraper are forced to drive forward to penetrate a cutting blade into a hard sandy terrain. The axle load at the rear tyre reduces sometimes due to the occurrence of large vertical excavation resistance acting on the cutting blade. Then, the effective tractive effort of the

motor scraper A drops down suddenly in accompanying with the excessive slippage of the rear tyre. At that time, another motor scraper B is necessary to help the excavation. The position of the center of gravity and the position of application height of the pulling force of the scraper B should be controlled to be set on each optimum position respectively, to obtain the largest value of the maximum effective tractive effort on the scraper A.

In this paper, the mechanism of traffic performance of a 5.88 [N] weight, two-axle and four-wheel vehicle moving up a sloped weak sandy terrain was theoretically analysed for both rear-wheel drive vehicle and four-wheel drive vehicle. For given dimensions of the vehicle and given terrain-wheel system constants, the relations among effective tractive effort, effective driving force, locomotion resistance and slip ratio and the relations among amount of sinkage of front and rear wheels and slip ratio were analysed by use of a simulation analytical program.

The maximum tractive effort of the vehicle varies with the position of the center of gravity and the height of application of force. The optimum eccentricity of the center of gravity and the optimum height of application of force to obtain the largest value of the maximum effective tractive effort could be determined for various slope angles of the terrain, in the case of rear-wheel drive vehicle and four-wheel drive vehicle respectively.

After that, the center of gravity position control system and the application height control system of the four-wheel drive vehicle moving up a sloped weak terrain will be robotized soon to obtain the largest value of maximum effective tractive effort on the sloped terrain.

2. TRAFFIC PERFORMANCE OF A FOUR-WHEEL VEHICLE

2.1 REAR-WHEEL DRIVE VEHICLE

The mechanism of traffic performance of a rear-wheel drive vehicle moving up a loose sandy sloped terrain is considered as the combination of an effective braking force [1] of the front wheel during pure rolling state and an effective driving force [2] of the rear wheel during driving action.

Fig.1 shows the vehicle dimensions and forces acting on the rear-wheel drive vehicle moving up a sloped terrain of angle β [3]. The vehicle weight W acts vertically on the gravity center G of the vehicle, and the front axle load W_f and the rear axle load W_r act normally to the terrain surface, and the slope resistance $W_f \tan\beta$ and $W_r \tan\beta$ act in parallel to the terrain surface, on the front axle O_f and the rear axle O_r respectively. The position of the center of gravity G is located on the amount of eccentricity eD from the central axis of the vehicle and on the height h_g perpendicular to the line $O_f O_r$. D is the

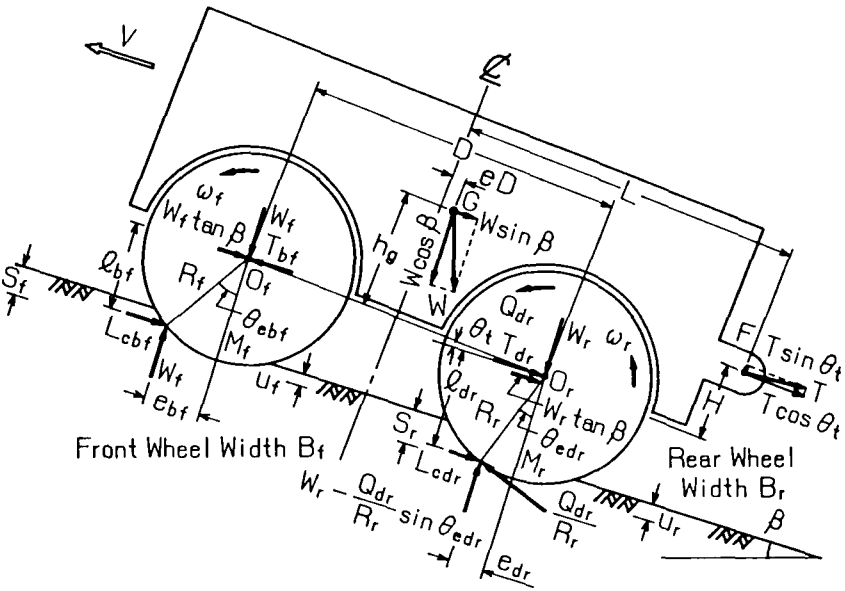

Fig.1 Vehicle dimensions and forces acting on a rear-wheel drive vehicle running on a sloped terrain

wheel base from the front wheel axle to the rear one, R_f and R_r is the radius of front and rear wheels respectively. The driving torque Q_{dr} acts around the rear axle O_r. The position of the application point F of the effective tractive effort T is located on the distance L from the central axis of the vehicle and on the application height H from the line $O_f O_r$. The effective braking force T_{bf} acts on the front axle O_f in parallel to the terrain surface, and the effective driving force T_{dr} acts on the rear axle O_r in parallel to the terrain surface, as shown in this figure. The vehicle trim angle θ_t is defined as the angle between the line $O_f O_r$ and the terrain surface. For the amount of sinkage s_f at the bottom-dead-center M_f of the front wheel and for the amount of sinkage s_r at the bottom-dead-center M_r of the rear wheel, the vehicle trim angle θ_t is calculated as follows;

$$\theta_t = \sin^{-1} \frac{R_f - u_f + s_r - R_r}{D} \tag{1}$$

where u_f is the amount of recovery of the terrain at the front wheel.
On the forward contact part of the front wheel, the pure rolling resistance i.e. compaction resistance L_{cbf} in parallel to the terrain surface and the normal

ground reaction W_f act at a distance of amount of eccentricity $e_{bf}=R_f \sin\theta_{ebf}$ and $\ell_{bf}=R_f \cos\theta_{ebf}$. On the forward contact part of the rear wheel, the compaction resistance L_{cdr} in parallel to the terrain surface, the tangential driving force Q_{dr}/R_r, and the normal ground reaction $W_r - Q_{dr}\sin\theta_{edr}/R_r$ act at a distance of amount of eccentricity $e_{dr}=R_r \sin\theta_{edr}$ and $\ell_{dr}=R_r \cos\theta_{edr}$. B_f and B_r are the front and rear wheel widths respectively.

For the vehicle speed V, the angular velocity ω_f and ω_r of the front and rear wheel, the skid i_{bf} of the front wheel and the slip ratio i_{dr} of the rear wheel are expressed as follows;

$$i_{bf}=\frac{R_f\,\omega_f}{V}-1 \tag{2}$$

$$i_{dr}=1-\frac{V}{R_r\,\omega_r}\quad(=i_d) \tag{3}$$

From the force equilibrium in parallel and normal direction to the terrain surface,

$$T_{dr}=\frac{Q_{dr}}{R_r}\cos\theta_{edr}-L_{cdr}-W_r\tan\beta \tag{4}$$

$$T_{bf}=-L_{cbf}-W_f\tan\beta \tag{5}$$

$$T=T_{dr}+T_{bf}=\frac{Q_{dr}}{R_r}\cos\theta_{edr}-L_{cdr}-L_{cbf}-W\sin\beta \tag{6}$$

$$W\cos\beta=W_f+W_r \tag{7}$$

are obtained.

From the momental equilibrium around the rear axle O_r,

$$W_f D\cos\theta_t+L_{cbf}D\sin\theta_t-W\cos\beta\{\frac{D}{2}-(eD+h_g\tan\theta_t)\}\cos\theta_t+HT\cos\theta_t-(L-\frac{D}{2})T\sin\theta_t+W\sin\beta[\frac{h_g}{\cos\theta_t}+\frac{D}{2}-(eD+h_g\tan\theta_t)\}\sin\theta_t]=0 \tag{8}$$

is obtained.

The effective tractive effort T (Eq.(6)) can be calculated from the compaction resistance L_{cbf}, the effective driving force T_{dr} and the slope resistance. The relations among T and i_d, T_{dr} and i_d, and T_{bf} and i_d, the relation between Q_{dr} and i_d, and the relation between s_f, s_r and i_d are determined by means of the analytical simulation program.

2.2 FOUR-WHEEL DRIVE VEHICLE

The mechanism of the traffic performance of a four-wheel drive vehicle moving up a loose sandy sloped terrain is considered, as the combination of an effective driving force of the front wheel and that of the rear wheel, during driving action. **Fig.2** shows the vehicle dimensions and forces acting on the four-wheel drive vehicle. The driving torque Q_{df} acts around the front axle O_f and the driving torque Q_{dr} acts around the rear axle O_r. The effective driving force T_{df} acts in parallel to the terrain surface on the front axle O_f and the effective driving force T_{dr} acts in parallel to the terrain surface on the rear axle O_r, as shown in this figure.

On the forward contact part of the front wheel, the compaction resistance L_{cdf} in parallel to the terrain surface and the tangential driving force Q_{df}/R_f, and the normal ground reaction $W_f - Q_{df} \sin\theta_{edf}/R_f$ act at a distance of amount of eccentricity $e_{df} = R_f \sin\theta_{edf}$ and $\ell_{df} = R_f \cos\theta_{edf}$. On the other hand, the compaction resistance L_{cdr} in parallel to the terrain surface and the tangential driving force Q_{dr}/R_r, and the normal ground reaction $W_r - Q_{dr} \sin\theta_{edr}/R_r$ act on the forward contact part of the rear wheel at a distance of amount of eccentricity $e_{dr} = R_r \sin\theta_{edr}$ and $\ell_{dr} = R_r \cos\theta_{edr}$.

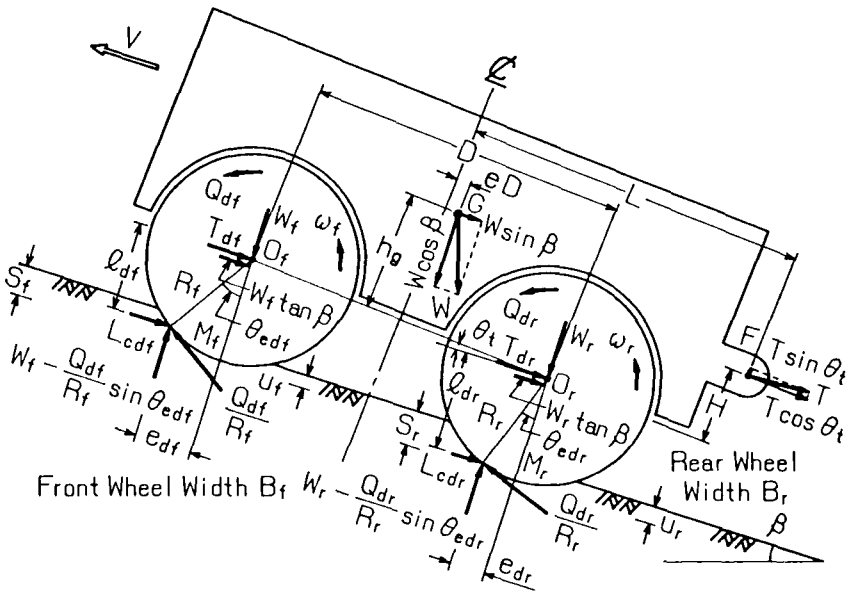

Fig.2 Vehicle dimensions and forces acting on a four-wheel drive vehicle running on a sloped terrain

For the vehicle speed V, the angular velocity ω_f and ω_r of the front and the rear wheels, the slip ratio i_{df} of the front wheel and the slip ratio i_{dr} of the rear wheel are expressed as follows;

$$i_{df}=1-\frac{V}{R_f\,\omega_f} \tag{9}$$

$$i_{dr}=1-\frac{V}{R_r\,\omega_r}\quad(=i_d) \tag{10}$$

From the force equilibrium in parallel and normal direction to the terrain surface,

$$T_{df}=\frac{Q_{df}}{R_f}\cos\theta_{edf}-L_{cdf}-W_f\tan\beta \tag{11}$$

$$T_{dr}=\frac{Q_{dr}}{R_r}\cos\theta_{edr}-L_{cdr}-W_r\tan\beta \tag{12}$$

$$T=T_{df}+T_{dr}$$

$$=\frac{Q_{df}}{R_f}\cos\theta_{edf}+\frac{Q_{dr}}{R_r}\cos\theta_{edr}-(L_{cdf}+L_{cdr})-W\sin\beta \tag{13}$$

$$W\cos\beta=W_f+W_r \tag{14}$$

are obtained.
From the momental equilibrium around the rear axle O_r,

$$W_f D\cos\theta_t-T_{df}D\sin\theta_t-W\cos\beta\{\frac{D}{2}-(eD+h_g\tan\theta_t)\}\cos\theta_t$$
$$+HT\cos\theta_t-(L-\frac{D}{2})T\sin\theta_t+W\sin\beta[\frac{h_g}{\cos\theta_t}+\frac{D}{2}$$
$$-(eD+h_g\tan\theta_t)\}\sin\theta_t]=0 \tag{15}$$

is obtained.
The effective tractive effort T (Eq.(13)) can be calculated from the summation of the effective driving force T_{df} acting on the front wheel and the effective driving force T_{dr} acting on the rear wheel.
The relations among T and i_d, T_{df} and i_{df}, and T_{dr} and i_{dr}, the relation between Q_{df} and i_{df}, Q_{dr} and i_{dr}, and the relation between s_f, s_r and i_d are determined by means of the analytical simulation program.

3. VEHICLE DIMENSIONS AND TERRAIN PROPERTIES

As an example, the traffic performance of a 5.88 [kN] weight and four-wheel

vehicle was simulated. The vehicle dimensions are shown in **Table 1**, and the terrain-wheel system constants at the site of front and rear wheel are shown in **Table 2**, respectively. The average line pressure of the wheel is 0.147

Table 1 Dimensions of two-axle and four-wheel vehicle

Vehicle weight	W	5.88 [kN]
Wheel base from front to rear wheel axle	D	50 [cm]
Radius of front wheel	R_f	16 [cm]
Radius of rear wheel	R_r	16 [cm]
Width of front wheel	B_f	10 [cm]
Width of rear wheel	B_r	10 [cm]
Line pressure of front wheel	$W/4B_f$	0.147 [kN/cm]
Line pressure of rear wheel	$W/4B_r$	0.147 [kN/cm]
Eccentricity of center of gravity	e	$-0.30 \sim 0.35$
Height of center of gravity G	h_g	50 [cm]
Distance between central axis of vehicle and point F acting effective tractive effort	L	30 [cm]
Application height of effective tractive effort	H	20 [cm]
Peripheral speed of rear wheel	$R_r\ \omega_r$	7.07 [cm/s]

Table 2 Terrain-wheel system constants

Plate loading and unloading test	
Front wheel	Rear wheel
$k_{c1} = 28.93$ [N/cm$^{n_1+1}$]	$k_{c1} = 28.93$ [N/cm$^{n_1+1}$]
$k_{\phi 1} = 8.41$ [N/cm$^{n_1+2}$]	$k_{\phi 1} = 9.68$ [N/cm$^{n_1+2}$]
$n_1 = 0.450$	$n_1 = 0.445$
$k_{c2} = 48.10$ [N/cm$^{n_2+1}$]	$k_{c2} = 48.10$ [N/cm$^{n_2+1}$]
$k_{\phi 2} = 31.12$ [N/cm$^{n_2+2}$]	$k_{\phi 2} = 35.83$ [N/cm$^{n_2+2}$]
$n_2 = 0.394$	$n_2 = 0.389$
$\lambda = 0.35$	$\lambda = 0.40$
$\kappa = 1.55$	$\kappa = 1.60$
$V_0 = 0.035$ [cm/s]	$V_0 = 0.035$ [cm/s]
Plate traction and sinkage test	
Front wheel	Rear wheel
$c_a = 0$ [kPa]	$c_a = 0$ [kPa]
$\tan\phi = 0.442$	$\tan\phi = 0.444$
$a = 2.05$ [1/cm]	$a = 2.51$ [1/cm]
$c_0 = 5.275 \times 10^{-3}$	$c_0 = 2.035 \times 10^{-3}$
$c_1 = 0.887$	$c_1 = 0.984$
$c_2 = 0.523$	$c_2 = 0.500$

[kN/cm]. To determine the terrain-wheel system constants at the front wheel and the rear wheel, the plate loading and unloading test, the plate traction and sinkage test were executed for the fresh loose sandy soil and for the compacted sandy soil after one pass of the roller having the same line pressure, respectively.

3.1 REAR-WHEEL DRIVE VEHICLE

Fig.3 shows the relations among the effective tractive effort T of the vehicle, the effective driving force T_{dr} of the rear wheel and the slip ratio i_{dr} of the rear wheel, for the rear-wheel drive vehicle moving up the sloped terrain of angle $\beta = \pi/36$ [rad]. These simulation results are obtained for the eccentricity of the center of gravity $e = 0.00$ and the application height $H = 14$ [cm]. The difference between T_{dr} and T is given as the summation of the compaction resistance L_{cbf} and the slope resistance $W_f \tan\beta$ acting on the axle of front wheel O_f as mentioned previously in Eq.(4)(5) and (6). In this case, the rear-wheel drive vehicle could not move up the slope because the effective tractive effort T of the vehicle takes always a negative value for the whole range of the slip ratio. On the other hand, the effective driving force T_{dr} of the rear wheel changes at $i_{dr} = 2$ [%] from a negative value to a positive

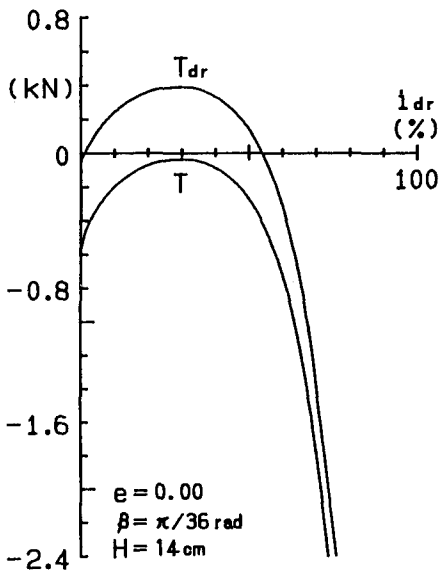

Fig.3 Relations among effective tractive effort T, effective driving force T_{dr} and slip ratio i_{dr} for a rear-wheel drive vehicle

one, and it takes a maximum value 0.404 [kN] at $i_{dr}=30$ [%]. After that, T_{dr} decreases remarkably with the increment of slip ratio i_{dr} due to the increasing amount of slip sinkage of the rear wheel.

3.2 FOUR-WHEEL DRIVE VEHICLE

Fig.4 shows the relations among the effective tractive effort T of the vehicle, the effective driving force T_{df} of the front wheel, the effective driving force T_{dr} of the rear wheel and the slip ratio $i_d=i_{df}=i_{dr}$ of the front and rear wheel, for the four-wheel drive vehicle moving up the sloped terrain of angle $\beta=\pi/36$ [rad]. These simulation results are obtained for the eccentricity of the center of gravity $e=-0.20$ and the application height $H=14$ [cm]. The effective tractive effort T is given as the summation of the effective driving force T_{df} and the effective driving force T_{dr}, as mentioned previously in Eq.(13). In this case, the effective tractive effort of the four-wheel drive vehicle takes a maximum value 0.840 [kN] at $i_d=33$ [%], while the effective driving force of front wheel takes 0.448 [kN] and the effective driving force of rear wheel takes 0.392 [kN]. After that, T decreases remarkably with the increment of slip ratio i_d due to the increasing amount of slip sinkages of the front and the rear wheel.

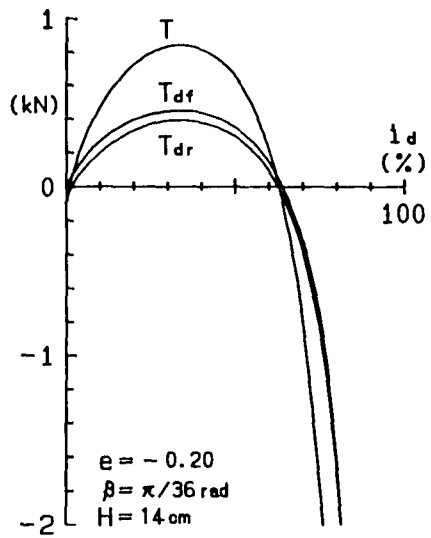

Fig.4 Relations among effective tractive effort T, effective driving force force T_{df}, T_{dr} and slip ratio i_d for a four-wheel drive vehicle

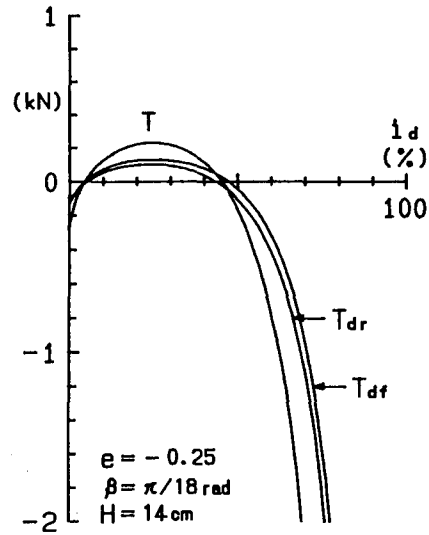

Fig.5 Relations among effective tractive effort T, effective driving force force T_{df}, T_{dr} and slip ratio i_d for a four-wheel drive vehicle

Fig.5 shows the relations among the effective tractive effort T of the vehicle, the effective driving force T_{df} of the front wheel, the effective driving force T_{dr} of the rear wheel and the slip ratio i_d for the four-wheel drive vehicle moving up the sloped terrain of angle $\beta = \pi/18$ [rad]. These simulation results are obtained for the eccentricity of the center of gravity $e = -0.25$ and the application height $H = 14$ [cm]. In this case, the effective tractive effort of the four-wheel drive vehicle takes a maximum value 0.232 [kN] at $i_d = 24$ [%], while the effective driving force of front wheel takes 0.130 [kN] and the effective driving force of rear wheel takes 0.102 [kN]. After that, T decreases remarkably with the increment of slip ratio i_d due to the increasing amount of slip sinkages of the front and the rear wheel.
The effective tractive effort T of the four-wheel drive vehicle decreases gradually with the increase of slope angle β.

4. OPTIMUM ECCENTRICITY OF CENTER OF GRAVITY

4.1 REAR-WHEEL DRIVE VEHICLE

Here, the effect of the position of the center of gravity of the vehicle $e\,D$ on the effective tractive effort T was analysed when the two-axle rear-wheel

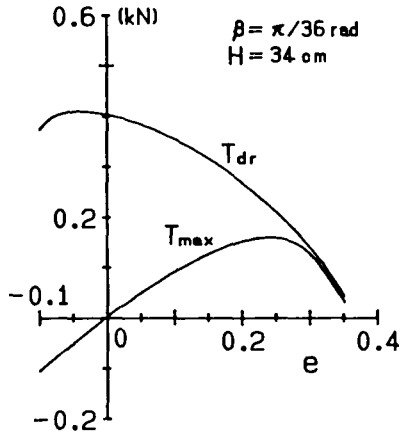

Fig.6 Relations among maximum effective tractive effort T_{max}, effective driving force T_{dr} and eccentricity of center of gravity e for a rear-wheel drive vehicle

drive vehicle is operating on a loose sandy sloped terrain to pull other construction machinery. The optimum amount of eccentricity of the center of gravity to obtain the largest value of the maximum effective tractive effort can be determined for the rear-wheel drive vehicle, of which the front wheel is in a pure rolling state and the rear wheel is in a driving state.

Fig.6 shows the relations among the maximum effective tractive effort T_{max} of the rear-wheel drive vehicle, the effective driving force T_{dr} of the rear wheel and the eccentricity e of the center of gravity [4]. These simulation results are obtained for the slope angle $\beta = \pi/36$ [rad] and the application height $H = 34$ [cm]. In this case, the maximum effective tractive effort of the rear-wheel drive vehicle takes a largest value 0.159 [kN] at $e = 0.25$, while the effective driving force of the rear wheel T_{dr} decreases gradually with the increment of the eccentricity e of the center of gravity. In these cases, the skid i_{bt} of the front wheel is maintained from -3 [%] to -4 [%] for the pure rolling state.

So, it is clarified that the optimum eccentricity e_{opt} is determined as 0.25 for this rear-wheel drive vehicle moving up the sloped terrain of angle $\beta = \pi/36$ [rad].

4.2 FOUR-WHEEL DRIVE VEHICLE

The effect of the position of the center of gravity of the vehicle e_D on the effective tractive effort T of the two-axle four-wheel drive vehicle was analysed when the vehicle is moving up the loose sandy sloped terrain to pull

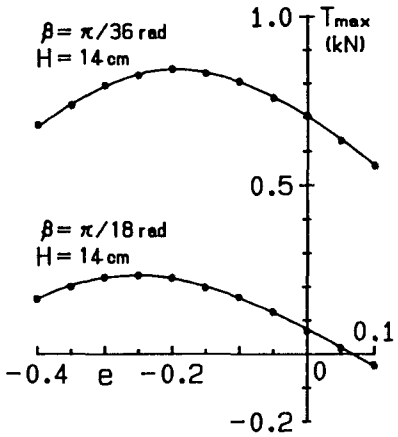

Fig.7 Relations between maximum effective tractive effort T_{max} and eccentricity of center of gravity e for a four-wheel drive vehicle

other construction machinery. The optimum amount of eccentricity of the center of gravity to obtain the largest value of the maximum effective tractive effort can be determined for the four-wheel drive vehicle, of which the front and rear wheels are in a driving state.

Fig.7 shows the relations between the maximum effective tractive effort T_{max} of the four-wheel drive vehicle and the eccentricity of the center of gravity e. These simulation results are obtained for $H=14$ [cm] and for the slope angle $\beta=\pi/36$ [rad] and $\beta=\pi/18$ [rad] respectively. For the slope angle $\beta=\pi/36$ [rad], the maximum effective tractive effort T_{max} of the four-wheel drive vehicle takes a largest value 0.840 [kN] at the optimum eccentricity $e_{opt}=-0.20$. For the slope angle $\beta=\pi/18$ [rad], the maximum effective tractive effort T_{max} takes a largest value 0.232 [kN] at the optimum eccentricity $e_{opt}=-0.25$.

So, it is clarified that the optimum eccentricity e_{opt} of the center of gravity of the four-wheel drive vehicle depends slightly on the slope angle β, that is, $e_{opt}=-0.20$ for $\beta=\pi/36$ [rad] and $e_{opt}=-0.25$ for $\beta=\pi/18$ [rad].

Establishing a position control system of the eccentricity e of the center of gravity which should be set up to the optimum eccentricity e_{opt}, the maximum effective tractive effort of the four-wheel drive vehicle can be automatically controlled to maintain the largest one.

5. OPTIMUM APPLICATION HEIGHT

5.1 REAR-WHEEL DRIVE VEHICLE

Here, the effect of the application height H on the effective tractive effort T was analysed, when the two axles and rear-wheel drive vehicle is operating on the loose sandy sloped terrain to pull other construction machinery. The optimum application height to obtain the largest value of the maximum effective tractive effort can be determined for the rear-wheel drive vehicle, of which the front wheel is in a pure rolling state and the rear wheel is in a driving state.

Fig.8 shows the relations among the maximum effective tractive effort T_{max} of the rear-wheel drive vehicle, the effective driving force T_{dr} of the rear wheel and the application height H of the tractive effort. These simulation results are obtained for the slope angle $\beta = \pi/36$ [rad] and the eccentricity of the center of gravity $e = 0.05$. As a result, the largest value of the maximum effective tractive effort $T_{max} = 0.055$ [kN] is obtained at $H = 24$ [cm] in this case.

So, it is clarified that the optimum application height H_{opt} is able to determine as 24 [cm] in this rear-wheel drive vehicle moving up the sloped terrain of angle $\beta = \pi/36$ [rad].

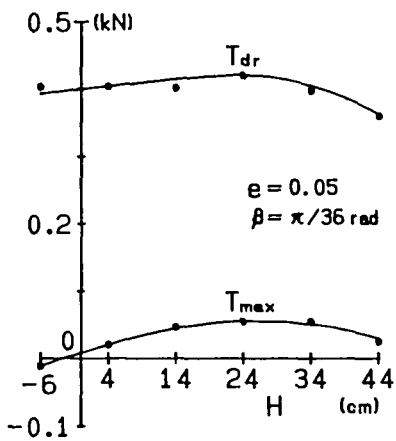

Fig.8 Relations among maximum effective tractive effort T_{max}, effective driving force T_{dr} and application height H for a rear-wheel drive vehicle

5.2 FOUR-WHEEL DRIVE VEHICLE

The effect of the application height H on the effective tractive effort T of the two-axle and four-wheel drive vehicle was analysed when the vehicle is moving up the loose sandy sloped terrain to pull other construction machinery. The optimum application height to obtain the largest value of the maximum effective tractive effort can be determined for the four-wheel drive vehicle, of which the front and rear wheels are in a driving state.

Fig.9 shows the relations between the maximum effective tractive effort T_{max} of the four-wheel drive vehicle and the application height H. These simulation results are obtained for $e=-0.20$ and $\beta=\pi/36$ [rad] and for $e=-0.25$ and $\beta=\pi/18$ [rad]. For the slope angle $\beta=\pi/36$ [rad], the maximum effective tractive effort T_{max} of the four-wheel drive vehicle takes a largest value 0.840 [kN] at the optimum application height $H_{opt}=14$ [cm]. For the slope angle $\beta=\pi/18$ [rad], the maximum effective tractive effort T_{max} takes a largest value 0.232 [kN] at the optimum application height $H_{opt}=14$ [cm].

So, it is clarified that the optimum application height H_{opt} of the effective tractive effort is 14 [cm] for both cases of $e=-0.20$, $\beta=\pi/36$ [rad] and $e=-0.25$, $\beta=\pi/18$ [rad].

Establishing a control system of the application height H which should be set up to the optimum application height H_{opt}, the maximum effective tractive effort of the four-wheel drive vehicle can be expected to be automatically controlled to maintain the largest one.

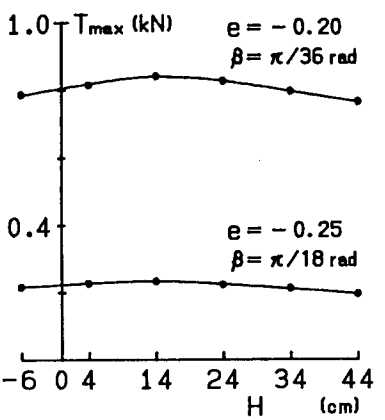

Fig.9 Relations between maximum effective tractive effort T_{max} and application height H for a four-wheel drive vehicle

6. SLOPE ANGLE

In general, the maximum effective tractive effort of a four-wheel drive vehicle is larger than that of a rear-wheel drive vehicle, when a two-axle and four-wheel vehicle is moving up a loose sandy sloped terrain. Here, the maximum slope angle of the terrain on which the four-wheel drive vehicle or the rear-wheel drive vehicle is able to move up the loose sandy sloped terrain was analysed by use of the simulation program, when the four wheel vehicle is moving up the slope at each optimum eccentricity of the center of gravity and at each optimum application height of the effective tractive effort. **Fig.10** shows the relation between the maximum effective tractive effort T_{max} and the slope angle of the terrain β for the four-wheel drive vehicle and rear-wheel drive vehicle, respectively. Generally speaking, the maximum effective tractive effort T_{max} decreases gradually with the increment of the slope angle β.

For the rear-wheel drive vehicle, T_{max} is 0.672 [kN] for the flat terrain $\beta = 0$ [rad] at $e_{opt} = 0.20$ and $H = 34$ [cm], T_{max} is 0.159 [kN] for the slope angle of terrain $\beta = \pi/36$ [rad] at $e_{opt} = 0.25$ and $H = 34$ [cm], and T_{max} is -0.278 [kN] for the slope angle of terrain $\beta = \pi/18$ [rad] at $e_{opt} = 0.20$ and $H = 34$ [cm]. In this case, it is clarified that the maximum slope angle of the terrain β_{max} to carry up other construction machinery is about 0.038π [rad].

For the four-wheel drive vehicle, T_{max} is 1.446 [kN] for the flat terrain $\beta = 0$ [rad] at $e_{opt} = -0.15$ and $H = 14$ [cm], T_{max} is 0.840 [kN] for the slope angle

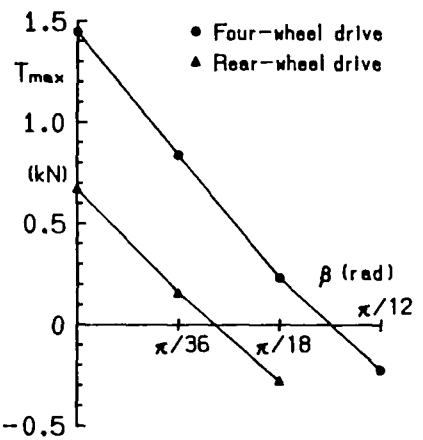

Fig.10 Relations between maximum effective tractive effort T_{max} and slope angle β for both rear-wheel drive vehicle and four-wheel drive vehicle

of terrain $\beta = \pi/36$ [rad] at $e_{opt} = -0.20$ and $H_{opt} = 14$ [cm], T_{max} is 0.232 [kN] for the slope angle of terrain $\beta = \pi/18$ [rad] at $e_{opt} = -0.25$ and $H_{opt} = 14$ [cm], and T_{max} is -0.224 [kN] for the slope angle of terrain $\beta = \pi/12$ [rad] at $e_{opt} = -0.30$ and $H = 14$ [cm]. In this case, it is clarified that the maximum slope angle of the terrain β_{max} to carry up other construction machinery is about $5\pi/72$ [rad].

7. CONCLUSION

The maximum effective tractive effort of a two-axle, four-wheel drive vehicle moving up a loose sandy sloped terrain varies with the position of the center of gravity and the application height of effective tractive effort. So, the tractive performances of a 5.88 [kN] weight, rear-wheel drive vehicle and four-wheel drive vehicle were simulated by use of terrain-wheel system constants. Especially, the optimum eccentricity of the center of gravity and the optimum application height of the effective tractive effort should be determined to obtain the largest value of the maximum effective tractive effort.

Several analytical results are summarized as follows;

[1] For a given four-wheel vehicle moving up a sloped terrain having a given soil properties, the optimum eccentricity of the center of gravity $e_{opt} = 0.25$ is obtained for the rear-wheel drive vehicle at the sloped angle $\beta = \pi/36$ [rad], $e_{opt} = -0.20$ is obtained for the four-wheel drive vehicle at $\beta = \pi/36$ [rad], and $e_{opt} = -0.25$ is obtained for the four-wheel drive vehicle at $\beta = \pi/18$ [rad].

[2] The optimum application height $H_{opt} = 34$ [cm] is obtained for the rear-wheel drive vehicle at the sloped angle $\beta = \pi/36$ [rad], and $H_{opt} = 14$ [cm] is obtained for the four-wheel drive vehicle at $\beta = \pi/36$ [rad], and $\pi/18$ [rad].

[3] The maximum effective tractive effort of a four-wheel drive vehicle is larger than that of a rear-wheel drive vehicle, when a two-axle, four-wheel vehicle is moving up a loose sandy sloped terrain. The maximum slope angle of the terrain on which the rear-wheel drive vehicle or the four-wheel drive vehicle is able to move up the loose sandy sloped terrain is about 0.038π [rad] for the rear-wheel drive vehicle, and about $5\pi/72$ [rad] for the four-wheel drive vehicle.

REFERENCES

[1] MURO, T. : Braking Performances of a Towed Rigid Wheel on a Soft Ground Based on the Analysis of Soil-Compaction, SOILS AND

FOUNDATIONS, Vol.33, No.2, pp.91-104, June, 1993.

[2] MURO, T. : Tractive Performance of a Driven Rigid Wheel on Soft Ground Based on the Analysis of Soil-Wheel Interaction, Journal of Terramechanics, Vol.30, No.5, pp.351-369, Sep., 1933.

[3] MURO, T. and FUKAGAWA, R. : Application Height Control System of a Wheeled Vehicle Running on a Loose Sandy Soil, Proc. of the 11th Int. Sympo. on Automation and Robotics in Construction, Brighton, UK, pp.495-502, May, 1994.

[4] MURO, T. and FUKAGAWA, R. : Application Height and Eccentricity of Gravity Center Control System of a Rear-Wheel Drive Vehicle Moving up and down a Sloped Weak Terrain, Proc. of the 4th Sympo. on Construction Robotics in Japan, July, 1994.

TERRAMECHANICAL EXPERIMENTS IN SOIL BINS

THE ISTVS PUBLICATIONS' REVIEW (1984 - 1994)

Marek M. Poncyliusz, Artur Mastalinski

Warsaw University of Technology, Warsaw, Poland.
Institute of Cranes and Heavy Machinery Eng.

ABSTRACT

The role of soil bin filled with loose soil was presented as main part of research stands. These stands were used in laboratory experiments described in ISTVS issues, basicly in bimonthly Journal of Terramechanics as well as in proceedings of International and European Conferences.

In this analysis the last eleven years were taken into account with over 700 papers well-known to authors. They chosen from that group about 100 papers connected with experiments in soil bins briefly describing them.

1. INTRODUCTION

The role of experiments in terramechanics was always outstanding. In spite of continuous development of the theoretical description of interaction processes between deformable ground and vehicles (mobile or towed) or between this and working tools, terramechanical laboratory is still irreplaceable. Even more and more intensive contribution of the newest software in the mentioned above description oes not change this state of affairs.

Because of existing in interaction's processes a lot of unstable factors very often being interdependent, prediction of their influence for investigated variable is not always possible in an accurate way.

We observe a numerous simplifying assumptions but theirs influence for faithfulness of acquired results is not quite clear.

However, because of widely known ground's heterogeneity as well as complicated character of ground- vehicle (tool) interaction, experimental verification of obtained theoretical solutions allows for evaluations of value of compatibility of accepted assumptions or predicted parameter's values with reality.

Terramechanical experiments may refer to recognition of fundamental phenomena occurring in natural or artificial soil medium during shearing, compacting, shoving, water saturation, etc. in average and extremal environmental conditions.

These experiments may also concern phenomena being found in the zone of interaction of machines or theirs working tools with ground while mining or excavating of it either relocating over it (rarely inside ground half space).

These research processes should be carried out in natural environment i.e. "in situ" or by means of laboratory stands providing among others significant repeatability of " a priori " predicted course conditions.

Some tendencies are still observed in selection of research technologies and in using of experimental environments. The authors decided to analyse these trends, fixing attention on soil bins. They considered universality of them as well as relatively frequent application for example on Polish technical universities.

Having this analysis in view authors used papers as well as conference's materials published by ISTVS (International Society for Terrain Vehicle System = the forum assembling outstanding terramechanicians) either in its bimonthly " Journal of Terramechanics " or in numerous conference's proceedings. The query included a period of eleven years (1984 -1994), but the last year partially. Besides, because of absence of participants from Poland on some far - away conferences information gathered until now is incomplete, but the query still goes on.

To some extent similar analysis were presented in [1, 2, 3]. The scope of data didn't comprise investigated subject, but only following problems :

- structure of existing soil bins and chanels as well as technique of soil preparing before investigation ([1] - into the world, [2] - in Poland) ;
- research environment and methodology [3].

2. THE ISTVS PUBLICATIONS' REVIEW

In the period of 1984 - 1994 over 900 papers and conference's materials were published and authors gathered 709 of them. During analysis 96 works connected with researches carried out in soil bins were separated.

The name " soil bin " used in quoted papers we understand here as follows :

- filled with loose medium cubicoidal or toroidal fixed reservoir, in which investigative model complex move regarding this medium ;
- small mobile cubicoidal bin in which the relative movement phenomenon occurs in a reversible way i. e. the model is fixed ;
- soil channel that means large cubicoidal pit in floor with dimensions achieving ten or even more meters, allowing researching of prototypes or serial machines as well as theirs details in the scale of 1 : 1.

The basic data regarding studies with soil bin's utilisation were listed in table1. This listing consists of serial number, author's name, title of paper, kind of ground filling the bin and lastly main subject of analysis.

Some abbreviations were prepared and shortly below explained to keep table clear. From the same reason a source of each paper was emphasised.

KIND OF GROUND

SAN - sand
SAL - sandy loam
LOA - loam
CLL - clay loam
BWM - bentonite - water mixture
KAC - kaolin clay
CLA - clay
SAC - sandy clay
SIL - silty loam
PAF - paddyfield
MAP - magnetic powder
SNO - snow (MAS - manufactured, NAS - natural)
LOE - loess

SUBJECT OF ANALYSIS

F - traction efforts
DP - drawbar pull
R - soil resistance
R_t - tangential soil resistance
R_n - normal soil resistance
p / z - pressure / sinkage ratio
p_x - stress distribution on contact area
ER - energy consumption
j - soil deformation
Tq - torque
SF - shear force
ADF - adhesive force
F_{st} - steering forces
SSCA - shape and size of contact area
TIP - tire pressure
LCC - load carrying capacity
STC - strength characteristics
ADC - adhesive characteristics
PSD - particle - size distribution
SOC - soil compaction
W - humidity
L - displacement
φ - angular displacement
V - velocity
i - slip
H - depth
N - number of tested objects
D - diameter

TABLE 1

JOURNAL OF TERRAMECHANICS

No	AUTHOR/No	TITLE	KIND OF GROUND	SUBJECT OF ANALYSIS
1	Zhidang Wang 1/84	A RECENT APPLICATION- THE DRIVEN DISC CUTTER	SAN	R(i) ER(i)
2	Zhidang Wang et al. 4/84	THE PERFORMANCE OF FREE ROLLING RIGID AND FLEXIBLE WHEELS ON SAND	SAN	DP z L
3	T. Paul 2/85	OPTIMIZATION OF TANDEM WHEEL SPACING FOR TRAFFICABILITY IN SAND	SAN	STC
4	M. A. Sargana et al. 2/85	A DYNAMIC EQUATION FOR THE PRESSURE-SINKAGE RELATIONSHIP IN SATURATED CLAY SOILS	SAL	p/z
5	M. Spektor et al . 3/85	EXPERIMENTAL STUDY OF FRONTAL RESISTANCE FORCE IN SOIL CUTTING	LOA	R(v)
6	Kyeong Uk Kim et al. 4/85	MODELING MOTION RESISTANCE OF RIGID WHEELS	SAL	R(i,p)
7	James H. Taylor et al. 3/87	TOTAL AXLE LOAD EFFECTS ON SOIL COMPACTION	SAC,LOA	$p_x(H)$
8	J. G. Hetherington et al. 4/87	THE ROLE OF MEAN MAXIMUM PRESSURE IN SPECIFYING CROSS-COUNTRY MOBILITY FOR ARMOURED FIGHTING VEHICLE DESIGN	SAN	$p_x(N,D)$
9	V. M. Salokhe et al. 4/88	MODES OF WET CLAY SOIL BEHAVIOUR UNDER A SINGLE CAGE WHEEL LUG	LOA	j(z,i)
10	P. A. Dudzinski 1/89	DESIGN CHARACTERISTICS OF STEERING SYSTEMS FOR MOBILE WHEELED EARTHMOVING EQUIPMENT	lack of data	lack of data
11	Ashenafi T. Abebe et al. 2/89	SOIL COMPACTION BY MULTIPLE PASSES OF A RIGID WHEEL RELEVANT FOR OPTIMIZATION OF TRAFFIC	SAL	R j
12	V. M. Salokhe et al. 3/4/89	TECHNOLOGY SHOWCASE APPLICATIONS OF ENAMEL COATING IN AGRICULTURE	LOA	SU Z,i
13	V. M. Salokhe et al. 3/4/89	LIMITATIONS OF PASSIVE EARTH PRESSURE THEORY FOR CAGE WHEEL LUG AND TINE FORCE PREDICTIONS	LOA	R j(φ)
14	Tatsuro Muro 3/4/89	TRACTIVE PERFORMANCE OF A BULLDOZER RUNNING ON WEAK GROUND	LOA, SIL	z(i,p)
15	V. M. Salokhe et al 1/90	PULL AND LIFT FORCES ACTING ON SINGLE CAGE WHEEL LUGS	LOA	R_t, R_n z,φ
16	V. M. Salokhe et al. 2/90	STUDIES ON EFFECTS OF SURFACE COATING ON FORCES PRODUCED BY CAGE WHEEL LUGS IN WET CLAY SOIL	LOA	R_t, R_n z,φ
17	T. C. Thakur et al. 4/90	THE MECHANICS OF SOIL CUTTING BY A ROTATING WIRE	SAL, LOA	R_t, R_n Tq(φ)
18	J. M. Fielke et al. 1/91	THE UNIVERSAL EARTHMOVING EQUATION APPLIED TO CHISEL PLOUGH WINGS	SAL	DP

TABLE 1 (continued)

No	AUTHOR / No	TITLE	KIND OF GROUND	SUBJECT OF ANALYSIS
19	H. Raheman 1/91	A LABORATORY INVESTIGATION INTO THE EFFECTS ON PRESSURISED AIR ON THE EROSION OF WET SOILS BY AIR CUSHION VEHICLES	lack of data	j
20	J.G.Hetherington 1/91	ELECTRIC, ALL-WHEEL-DRIVE, TRACKED VEHICLES	SAN	DP(i)
21	D. A. Crolla 2/3/91	SOIL TANK MEASUREMENTS OF TYRE LATERAL AND LONGITUDINAL FORCES	SAL	F(i)
22	Y. Nohse et al. 4/91	A MEASUREMENT OF BASIC MECHANICAL QUANTITIES OF OFF-THE-ROAD TRAVELLING PERFORMANCE	SAN	R, Tq p_x, L φ, z
23	O. A. Adebiyi et al. 4/91	COMPACTION CHARACTERISTICS FOR THE TOWED AND DRIVEN CONDI -TIONS OF A WHEEL OPERATING IN AN AGRICULTURAL SOIL	SAL	p_x
24	A. Boccafogli et al. 1/92	EXPERIMENTAL EVALUATION OF CUTTING DYNAMIC MODELS IN SOIL BIN FACILITY	lack of data	SF
25	S. Shibusawa 1/91	FRACTALS IN CLODS FORMED WITH ROTARY TILLAGE	CLL	PSD
26	G. Rajaram et al. 1/92	DEFORMATION OF SAND CAUSED BY TINE IMPLEMENTS	SAN	R
27	H. Murakami et al. 1/92	A MATHEMATICAL MODEL FOR SPATIAL MOTION OF TRACKED VEHICLES ON SOFT GROUND	SAN	SSCA
28	E. Canillas et al. 2/92	PERFORMANCE OF COATED FLOATS IN DIFFERENT SOILS	SAN, CLA, SAL	R
29	J. G. Hetherington 2/92	THE USE OF SCALE MODEL TESTS TO VERIFY EARTH ANCHOR DESIGN PREDICTIONS	SIL	R
30	V. M. Salokhe et al. 2/93	MODELLING SOIL COMPACTION UNDER PNEUMATIC TYRES IN CLAY SOIL	SAL	p_x R
31	K. Watanabe et al. 2/93	EXPERIMENTAL CHARACTERIZATION OF DYNAMIC SOIL-TRACK INTER-ACTION ON DRY SAND	SAN	p/z SF
32	T. Niyjamapa et al. 6/93	LABORATORY INVESTIGATIONS INTO SOIL FAILURE UNDER VIBRATORY TILLAGE TOOLS	SAL	R Tq
33	Yu Gu et al. 1/94	DYNAMIC LOAD DISTRIBUTION AND TRACTIVE PERFORMANCE OF A MODEL TRACTOR	CLL	F, i
34	Yang Quinsen et al.	A SOIL - TOOL INTERACTION MODEL FOR BULLDOZER BLADES	LOE	V, R
	3th European ISTVS Conf. Warsaw, Poland 1986			
35	Ronal M. Djordie	QUANTITATIVE ANALYSES OF COMPACTED SOIL PROFILE UNDER THE TRACTOR WHEELS	LOA+CLA	z
36	Alessandro Orlandi et al.	WHEEL-GROUND CONTACT PHENOMENA IN THE PRESENCE OF VIBRATIONS	SAN	DP, L Tq,φ
	5th European ISTVS Conf. Budapest, Hungary 1991			
37	Wang Qingnian et al.	BEARING CAPACITY AND SINKAGE MECHANISM OF LOOSE SAND	SAN	p/z

TABLE 1 (continued)

No	AUTHOR/No	TITLE	KIND OF GROUND	SUBJECT OF ANALYSIS
38	Yao Jian Shao et al.	ADVANCED STUDY ON THE PERFORMANCE OF LUG CONFIGURATION AND ARRANGEMENT FOR POWERED WHEEL OF POWERED TILLER IN PADDYFIELD	SAL, CLA	Tq DP φ, i
39	P. J. Wagner	THE CALCULATION OF PRESSURE-SINKAGE CURVES BASED ON SHEAR STRENGTH MEASUREMENTS	lack of data	p/z
40	Zhuang Jide et al.	THE WAYS TO IMPROVE THE TRAFFIC-ABILITY OF VEHICLES ON SAND	SAN	p/z i
41	H. Schwanghart	SOIL PRESSURE AND COMPACTION UNDER AGRICULTURAL TIRES	SAL	SSCA TIP
42	Dj. M. Ronai et al.	ONE SIMPLE LABORATORY METHOD FOR RELATIVE ESTIMATIONS OF TRACTOR TYRES PERFORMANCES	lack of data	DP SSCA
43	G. Dörfler	TRAFFICABILITY OF DEEP-SEA FLOOR	BWM	DP
44	M. M. Poncyliusz	IMPROVED METHOD OF SIMPLE CALCULATION OF THE TRACKED VEHICLE PERFORMANCE	SAN	DP(i)
8th Int. ISTVS Conf. Cambridge, England 1984				
45	P. Boonsinsuk et al.	SOIL COMPLIANCE INFLUENCE ON TYRE PERFORMANCE	lack of data	DP,Tq, SSCA
46	Tej Paul	PERFORMANCE PREDICTION OF PNEUMATIC TYRES ON SAND	SAN	F
47	Dj. M. Ronai	EFFECTS OF SLIP ON ENERGY DISTRIBUTION BETWEEN TYRE AND SOIL	SAL	DP, Tq, φ, TIP
48	J. Swiech	TRACTION FORCES OF DRIVE TYRE ON THE COMPACTED SOIL	SAN,SIL, CLA	DP,Tq, SSCA
49	A. Mierzwicki	THE DEPENDENCE OF SOIL BEARING CAPACITY AND DRAWBAR PULL ON THE SPACING BETWEEN TRACK PLATES	SAN	DP
50	M. M. Poncyliusz	ANALYSIS OF GROUND PRESSURE DISTRIBUTION BENEATH TRACKED MODEL WITH RESPECT TO EXTERNAL LOADING	SAN	DP(i)
51	R. N. Yong et al.	EFFECTS OF HITCH POSITIONS ON THE PERFORMANCE OF TRACK/GROUSER SYSTEMS	KAC	DP i
52	Deng Zhuorong et al.	AN INVESTIGATION OF THE DRIVING WHEEL THRUST OF PADDY FIELD TRACTORS	PAF	j i φ
53	S. X. Wu et al.	BEHAVIOUR OF SOIL UNDER A LUGGED WHEEL	SAN,LOA	j(i)
54	M. Yamazaki et al.	PREDICTION ACCURACY OF THE TORQUES FOR ROTARY TILLAGE BY AN ANALOG TOOL	SAN+SIL	R Tq
55	Tai Ling Zhang et al.	THE ANALYSIS ON THE DYNAMIC PERFORMANCE OF A SINGLE LUG	PAF	R_t R_n
56	I. Bolling	PRESSURE TESTS IN SOIL BELOW TIRES OF AGRICULTURAL VEHICLES	SAL	p_x
57	S. Hata et al.	QUALITY CONTROL IN SOIL COMPA-CTION BY BEHAVIOURS OF EXCITER	SAN	STC LCC

TABLE 1 (continued)

No	AUTHOR/No	TITLE	KIND OF GROUND	SUBJECT OF ANALYSIS
58	James H. Taylor et al.	FLOTATION TIRES AND SUBSURFACE COMPACTION	SAL,LOA	p_x
59	D. Gee-Clough et al.	MEASUREMENT OF SOIL PROPERTIES IN DRYLAND AND WETLAND CONDITIONS	SAL,LOA	R
9th Int. ISTVS Conf. Barcelona, Spain 1987				
60	C. Holm et al.	THE INFLUENCE OF SHAPE AND SIZE OF A PENETRATION BODY ON THE PRESSURE-SINKAGE RELATIONSHIP	SAN,LOA, CLA	p/z
61	M. Grahn	INVESTIGATION OF THE INFLUENCE OF PENETRATION VELOCITY ON THE PRESSURE-SINKAGE RELATIONSHIP	SAL	p/z V
62	G. W. Heiming	STATISTICAL PROCEDURES FOR EVALUATION OF TERRAIN MEASURING DATA	LOA	$p_x(H)$
63	A. J. J. M. Schoenmakers et al.	MEASURING TRAFFIC-INDUCED STRESSES AT THE INTERFACE OF SOIL LAYERS OF CONTRASTING STIFFNESS	lack of data	$p_x(L)$
64	Hua Zhong Lu et al.	EXPERIMENTAL RESEARCH ON THE SOIL FLOW AND SOIL REACTION BENEATH LUGS OF POWERED WHEEL	PAF,SAN, LOA	F j
65	Xu Da	A RESEARCH OF THE DYNAMIC PERFORMANCE OF THE PADDLE DRIVING WHEEL WORKING ON SOFT TERRAIN	lack of data	F(D)
66	V. M. Salokhe	STUDIES ON EFFECT OF LUG SURFACE COATING ON SOIL ADHESION OF CAGE WHEEL LUGS	LOA	ADC
67	Shoiro Hata et al.	DETERMINATION OF LIFT HEIGHT IN SOIL COMPACTION	SAL	SOC W
68	Alessandro Orlandi et al.	EFFECTS OF VIBRATION ON ROLLING RESISTANCE	SAN	DP
69	J. K. Agarwalla et al.	STEERING FORCES ON CAGE-WHEELS AND TYRES IN PUDDLED CLAY SOIL	LOA	F_{st}
70	Liu Shuxue et al.	EXPERIMENTAL RESEARCH OF GEO-METRIC SHAPE AND ITS WORKING RESISTANCE OF LOADER BUCKET	SAN	R
71	Jiang Chongxian	THE TEST STUDY ON MORPHOLOGY AND PARAMETERS OF DRIVING WHEEL OF BOAT-TRACTOR	PAF	F
10th Int. ISTVS Conf. Kobe, Japan 1990				
72	Cong Qian et al.	RESEARCH ON REDUCING ADHESION RESULTS OF SOIL ELECTRO-OSMOSIS AND ITS AFFECTING FACTORS	CLA	ADF
73	M. S. Xiong et al.	EXPERIMENTAL STUDY ON SIMULATING BEHAVIOUR OF NATURAL SOIL WITH MAGNETIC POWDER	MAP	STC
74	Irwin G. J. et al.	PREDICTION OF LOAD CARRYING CAPACITY OF DEEP SNOW BY RAMMSONDE HARDNESS	SNO (MAS & NAS)	LCC

TABLE 1 (continued)

No	AUTHOR/No	TITLE	KIND OF GROUND	SUBJECT OF ANALYSIS
75	Jiang Chong-Xiau et al.	THE STUDY OF PENETRATION PERFORMANCE OF PADDY SOIL UNDER PLATE	PAF	p/z
76	Shen Jie et al.	PRESSURE-SINKAGE-TIME EQUATION FOR WET SOIL	CLA	p/z
77	Eddie C. Burt et al.	TIRE DYNAMIC LOAD EFFECTS ON SOIL-TIRE INTERFACE AND SOIL PROFILE STRESSES	SAL,LOA	p_x
78	Yu Qun et al.	A NEW METHOD FOR MEASURING SHAPE AND SIZE OF TIRE-SOIL CONTACT ZONE	SAC	SSCA
79	H. Schwanghart	MEASUREMENT OF CONTACT AREA, CONTACT PRESSURE AND COMPACT-ION UNDER TIRES IN SOFT SOIL	SAL	SSCA p_x
80	Randal K. Wood et al.	TIRE THRUST AS AFFECTED BY DYNAMIC LOAD	SAL,LOA	TIP
81	V. M. Salokhe et al.	THE MEASUREMENT OF FORCES UNDER MULTIPLE CAGE WHEEL LUGS	LOA	$R(\varphi)$
82	A. Oida et al.	THREE DIMENSIONAL STRESS DISTRIBUTIONS ON TIRE-SAND CONTACT SURFACE	SAN	p_x
83	T. Hiroma et al.	ANALYSIS OF NORMAL STRESS DISTRIBUTION UNDER A WHEEL USING A VISCOELASTIC MODEL OF SOIL	SAL	p_x
84	M. Ueno et al.	A DEVELOPMENT OF ANALYZING SYSTEM FOR STRAIN AND STRESS OF SOIL UNDER THE WHEEL	SAN	$j(\varphi)$
85	M. M. Poncyliusz	SIMPLIFIED METHOD OF CALCULATION OF THE TRACKED VEHICLE THRUST	SAN	DP(i)
86	M. Grahn	PREDICTION OF SINKAGE AND ROLLING RESISTANCE FOR 0F-THE-ROAD VEHICLES CONSIDERING PENETRATION VELOCITY	SAC	p/z
87	Kenji Cho	RESEARCH ON RUNNING PERFORMANCE OF CRAWLER TYPE VEHICLE AND DEVELOPMENT OF NEW SHAPE CRAWLER SHOE	SAL	R
88	Y. Nohse et al.	A MEASUREMENT OF BASIC MECHANICAL QUANTITIES OF OFF-THE-ROAD TRAVELLING PERFORMANCE	SAN	R,Tq p_x φ,z
89	Larry G. Wells et al.	FACTOR AFFECTING BULK DENSITY OF RECONSTRUCTED PRIME FARMLAND SOILS	SAC	j
90	Hisahi Horio	A NEW LOCOMOTIVE SYSTEM; STEERING, PROPELLING AND SUPPORTING VEHICLE BODY BY ROLLING BOWLS	CLA, SIL	R j L
91	A. Boccafogli et al.	EXPERIMENTAL EVALUATION OF DYNAMIC CUTTING MODELS IN SOIL BIN FACILITY	lack of data	F(V,i)
92	S. Shibusawa	FRACTALS IN CLODES FORMED WITH ROTARY TILLAGE	SAN+CLA	PSD
93	V.K.Sharma et al	SOIL-TOOL INTERACTIONS IN SAND	SAN	R

TABLE 1 (continued)

No	AUTHOR/No	TITLE	KIND OF GROUND	SUBJECT OF ANALYSIS
94	Yin Yongguang et al.	A NEW CALCULATION METHOD OF INSERTING OF LOADER SHOVEL	lack of data	R
95	Y. Matsumoto et al.	AN EXPERIMENTAL STUDY ON THE MULTI-CIRCULAR FACE SHIELD -THE STEERING CONTROL	lack of data	R_n R_t Tq
96	Y. Matsumoto et al.	AN EXPERIMENTAL STUDY ON THE MULTI-CIRCULAR FACE SHIELD -THE EXCAVATABILITY AND THE FACE STABILITY	lack of data	Tq DP
11th Int. ISTVS Conf. Lake Tahoe, USA 1993				
SORRY, UP TO DEADLINE, PROCEEDINGS WERE NOT DESCRIBE SCIENTIFICALLY				

3. CONCLUSIONS

On the base of the above listing we were able to draw the following conclusions :

- a percentage of researches with application of the soil bins amounted about 15 - 20 % of the overall number of terramechanical experiments ;
- the soil bins were applicable in investigations concerned with various problems, especially with evaluation of the traction parameters ;
- these laboratory appliances were often used for carrying out of parametric analysis ;
- the soil bins were very useful for verification of computer simulation of complicated models of terrain - vehicle interaction as well as description of dynamics of the new type of undercarriages ;
- the research methodology based on using of the soil bins secured real repeatability of measurement but soil preparation was still a problem ;
- modelling methodology was fundamental but we found some models with partial disregarding of occurring distortion ;
- only a few soil bin's stands were located outside (on open air) ;
- most of researches used natural soils usually put to the homogenising treatment except magnetic powder (73) and manufactured snow (74).

4. REFERENCES

[1] WISMER R. D. **Soil Bin Facilities ; Characteristics and Utilization.** Proc. of 8th Int ' l Conference ISTVS. Cambridge 1984.

[2] KARCZEWSKI T **Research in Soil Bins**. Proc. of 3rd European Conferences ISTVS. Warsaw 1986 .

[3] PONCYLIUSZ M. M. **The Analysis of the External Loads on the Drawbar Pull of Track - Type Undercarriages**. Unpublished Ph. D. Thesis. Faculty of Automobiles and Heavy Machinery Engineering of Warsaw University of Technology. Warsaw 1987, (in Polish).

Besides, the authors used the annual sets of Journal of Terramechanics (1984 - 1994) and proceedings of works from five International and European ISTVS Conferences (listed in table 1).

THE TURNING RESISTANCE OF TRACKED VEHICLES; INFLUENCED BY LATERAL ELASTICITIES OF THE RUNNING GEAR AND THE TRACKS

Stefan Pott

Institute of Automotive Engineering IKK

- Prof. Dr.-Ing. I.C. Schmid -

University of the Federal Armed Forces Hamburg, Germany

ABSTRACT

When a tracked vehicle is driving in a curve the turning resistance is added to the motion resistances of straight ahead motion. Previous analytical models to describe the turning resistance do not consider the complex friction phenomenon that occurs during a turning manoeuvre. These former models are based either on the principle of isotropic Coulomb's friction or on empirical statements

MEMOKET, a new developed mechanical model at the Institute of Automotive Engineering, does not use empirical measurements carried out with the complete tracked vehicle. Design parameters of the running gear, such as the real friction behaviour of the rubber track pad and especially the lateral elasticities of the rubber, the tracks, the rocker arms and the track rollers, are included. The variation of the design parameters concerning the reduction of the turning resistance can be discussed.

SIMKET, another analytical model for kinematic and dynamic studies, uses the multibody method ADAMS.

By using MEMOKET as well as by using SIMKET field measurements with a complete vehicle can be avoided.

1. INTRODUCTION

Tracked vehicles are characterized by high mobility even in rough terrain. Besides slope- and acceleration-capability the turning behaviour is very important. The impact of the turning resistance onto the propulsion system is of primary interest [1]. During cornering the torques on the sprockets can be about 20 times higher than in straight ahead motion. The cornering capability of a tracked vehicle must therefore be considered in the design stage of a vehicle as well as in the testing procedure.

In order to minimize the turning resistance the knowledge of the physical basics of a cornering manoeuver is necessary. The influence of the design parameters of the running gear is also very important.

2. FIELD MEASUREMENTS AND EXISTING MODELS

Fig. 1 shows the frictional forces acting on a turning tracked vehicle. The tracks slip laterally across the hatched area. Longitudinal slip is not regarded. Based on the frictional behaviour of a rubber track, frictional forces occur opposed to the sliding direction. They cause the turning resistance torque M_w around the center of gravity. To steer the vehicle, this torque must be overcome by a propulsion force K_a acting on the track of the outer side of the curve and a braking force K_i on the inner track. These track forces are produced by sprocket torques. HOCK [2] described the turning resistance torque M_w as

$$M_w = \frac{1}{4} m g l \mu_w \qquad (1)$$

with μ_w : turning resistance coefficient
m : vehicle mass
l : ground contact length of the tracks

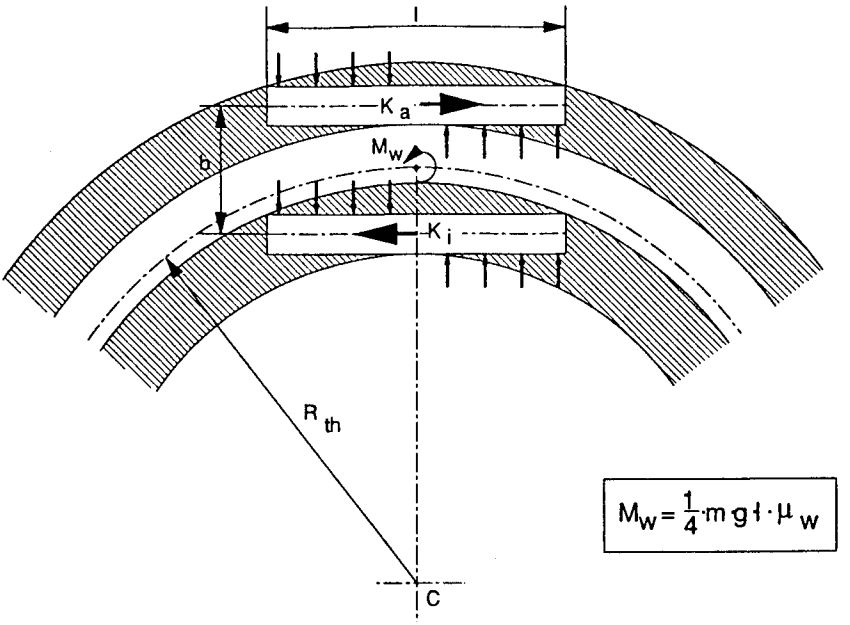

Figure 1: Forces Acting on a Tracked Vehicle during a Curve

The turning coefficient can be determined by measuring the sprocket torques in steady-state curves:

$$\mu_w = \frac{2b}{m\,g\,l\,r_k} * (M_a - M_i) \qquad (2)$$

with $M_{a,i}$: sprocket torques
b : track base
r_k : radius of the sprockets

At the Institute of Automotive Engineering comprehensive measurements were carried out to determine the sprocket torques of a tracked vehicle [3, 4, 5]. A 26tons tank JAGUAR was used as a test vehicle. The most important results of the measurements on a concrete road surface can be seen in fig. 2. It shows the measured torques at the sprockets versus the theoretical radius of the curve R_{th}, which is calculated from the rotational velocities of the two sprockets. The real radius R_g is larger. However, its enlargement is nearly independent from the velocity and the radius. It amounts to the radius enlargement factor f_v = 1.9. At the outer side of the curve a

(positive) propelling torque and at the inner side a (negative) braking torque are necessary to overcome the turning resistance. These torques achieve their maximum value for pivot steering. It can also be seen, that the curve for speed range 1 with the lowest speed envelopes all the curves at higher speed. This shows that the centrifugal force at higher speeds supports the turning behaviour of the tracked vehicle.

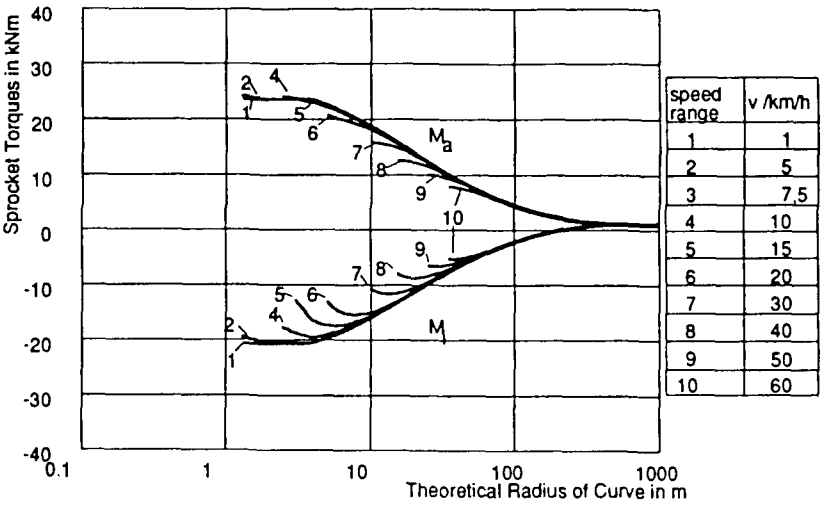

Figure 2: Measured Sprocket Torques of the Test Vehicle JAGUAR [3]

These results were used by EHLERT [3] to verify and improve analytical models of the turning resistance formulated by HOCK [2], the IABG [6] and KITANO [7]. The latter models take the influence of centrifugal forces and longitudinal slip into consideration. The models modified by EHLERT are worked out and presented in [5], so they won't be explained here. EHLERT improved HOCK's theory

$$\mu_w = f(R_{th}) \qquad (3)$$

by a better empirical description. Fig. 3 shows the modified turning resistance coefficient depending on the real radius R_ε. The target of EHLERT's investigation was the simulation of the motion-dynamics of tracked vehicles on the PAISI test plant [8]. The sprockets are the points of intersection

between the vehicle and the test stand. His analytical models are integrated in the PAISI-simulation. It was adequate to base the models on empirical statements. However, it was not clarified, how the sprocket torques depend on the interaction of track and ground and on the influence of design-characteristics of the running gear. The physical elements of the turning resistance of tracked vehicles were not worked out.

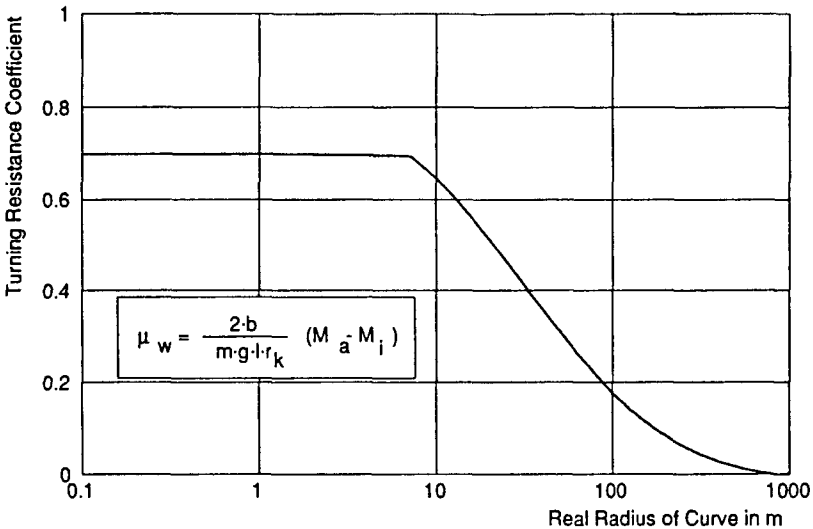

Figure 3: Calculated Turning Resistance Coefficient from Field Measurements

The friction behaviour of the tracks is of primary importance for the dynamics of motion of tracked vehicles. KAR [9] mentioned, that the analytical prediction of track forces or sprocket torques of tracked vehicles is more accurate when the relationship between the coefficient of lateral friction and the slip velocity is taken into consideration.

Some authors [10, 11] proposed another mathematical description of the friction behaviour of the tracks (fig.4a). The coefficient of lateral friction differs from the one of longitudinal friction. Measurements taken with a real rubber track pad (fig.4b) show the independence of the friction behaviour from the direction of movement between track and ground surface.

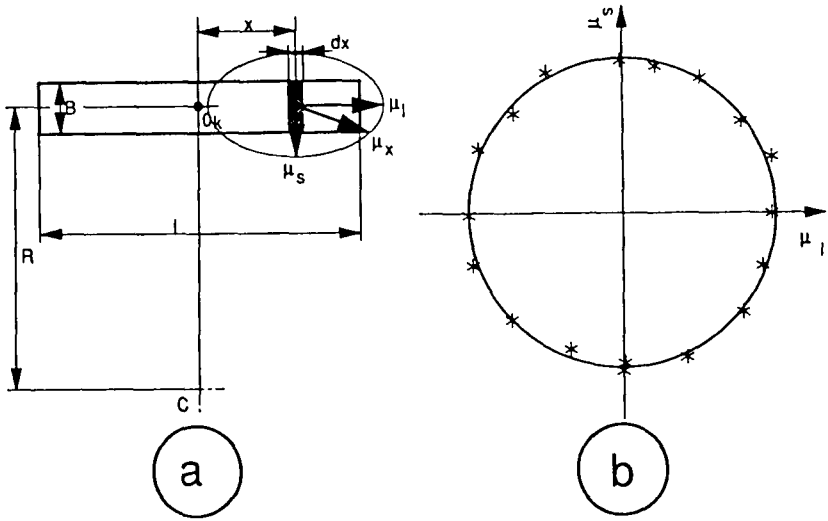

Figure 4: Proposed [11] and Measured Friction Coefficients of Rubber Pads

The models presented in this paper put the turning resistance on an entirely new basis. They are planned to examine the physical elements causing the turning coefficient. Two models with different methods have been developed. At first MEMOKET, a mechanical model, describes the transfer of force in a track and a running gear of a tracked vehicle. It uses the principle of a deflection beam, which is a substitute for the track. The target of this model is to examine the influence of elasticities in the running gear on the turning resistance. SIMKET, the second model, has been programmed using the multibody simulation software ADAMS [12]. The multibody simulation offers the examination of both: the dynamics and the kinematics of the computed model. These two models avoid the empirical description of the turning resistance.

Based on the real friction behaviour between a rubber track pad and the ground surface the models are developed to explore the basis of the regarded turning resistance of tracked vehicles. Design parameters of the tracks and the running gear must be taken into account.

4. MEASURED FORCES IN THE CONTACT AREA BETWEEN GROUND SURFACE AND TRACKS

A test stand was developed to examine both the lateral deformation of a rubber track pad and the friction behaviour in the contact area between the tracks and the ground [13].

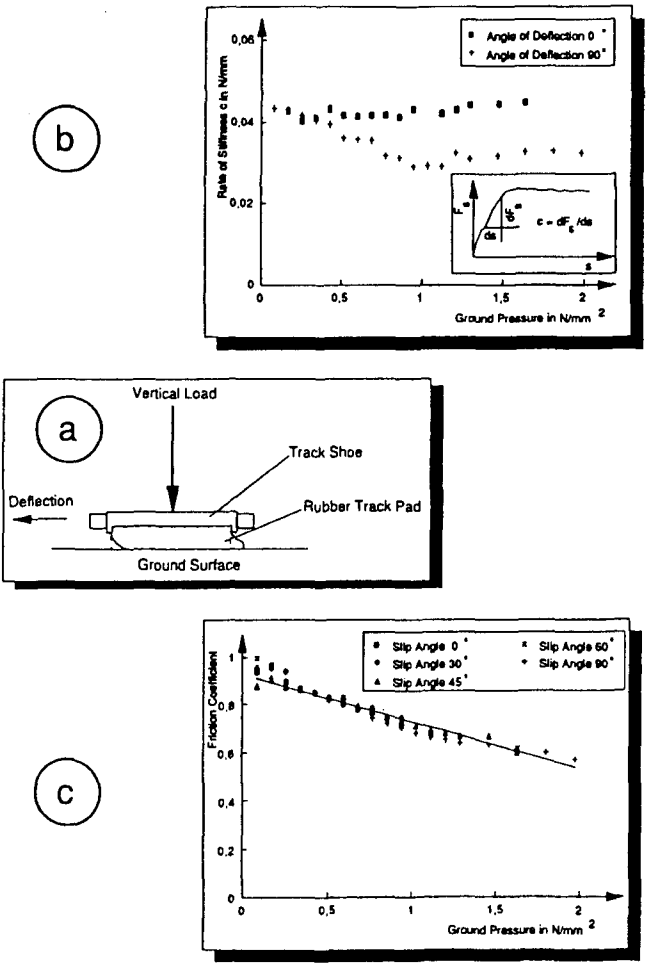

Figure 5: The Friction Behaviour of a Rubber Track Pad

A summary of the test procedures and the test results is represented in fig. 5. The track shoe, which is loaded with a vertical force, is standing on an element of the road. This element is displaced laterally by means of a hydraulic cylinder (fig. 5a). Measured values are the vertical load and the horizontal force, the stroke and the lateral deflection as well as the slip velocity.

In the range of small deflections (fig. 5b) there is only elastic deformation of the rubber track pad without any sliding movement between the rubber and the ground surface. The rate of stiffness depends more on the angle of deflection and less on the ground pressure. The measurements show, that elastic deformations of a rubber track pad at a ground pressure of 1.2 N/mm^2 or a vertical load of 2.5 tons can reach values up to 30 mm, before the pad starts sliding.

Sliding movements between the track and a ground surface occur, when the horizontal deflection exceeds the deformation capability of the rubber. The coefficient of friction (fig. 5c) declines in a linear way depending on the ground pressure. It also depends on the slip velocity and on the quality of ground surface, but it is independent of the direction of slip.

These results are the inputs for the analytical models described in the following.

The relationship between the horizontal force F_s and the lateral deflection s of the rubber track pad is mathematically described for a vertical load F_z under consideration of slip velocity and direction of slip:

$$F_s(s) = \frac{-F_{se}}{s_e^2} s^2 + 2\frac{F_{se}}{s_e} s \qquad \text{for } s \leq s_e$$

and (4)

$$F_s(s) = (F_{se} - \mu F_z)\, e^{\left(\frac{-(s - s_e)^2}{k}\right)} + \mu F_z \qquad \text{for } s > s_e$$

with
- s_e : maximum of elastic deformation
- F_{se} : $F_{se} = F_s(s_e)$
- F_z : vertical load
- μ : $\mu = \mu_o - a^* F_z$
- k : decay constant

5. MEMOKET: A MECHANICAL MODEL DESCRIBING THE TURNING COEFFICIENT

The real running gear of the tracked vehicle JAGUAR is compared to the modelled substitute in fig. 6. The model examines the transfer of force in the running gear in lateral direction. This intention and the design of the examined running gear result in the following conditions:

- The track is replaced by a deflection beam with the bending resistance $E*I_y$. The bearing of the beam is given by the track length between the tensioning wheel and the sprocket.
- The sprocket is replaced by a support fixed in longitudinal direction.
- The tensioning wheel is replaced by a support.
- The upper part of the track and the supporting rollers are not modelled.
- The road wheels are represented by linear spring tensions. In this way the lateral elasticity of the road wheel suspension can be considered.

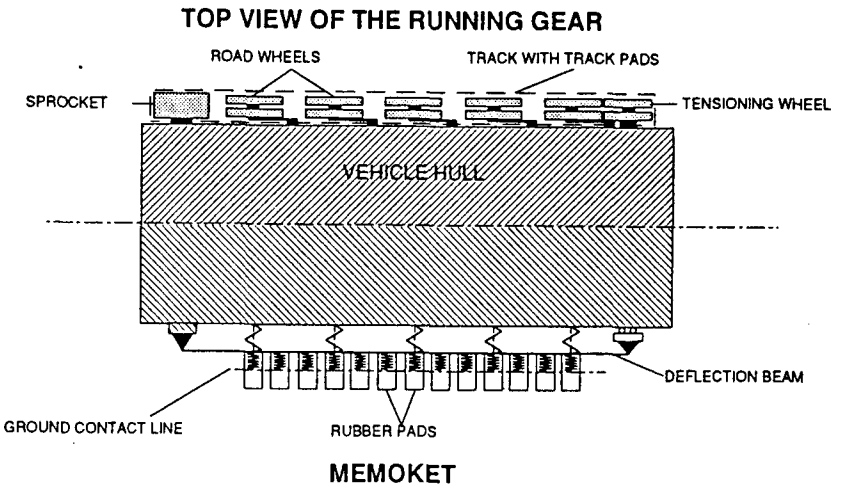

Figure 6: MEMOKET Compared to the Test Vehicle JAGUAR

Frictional forces between the rubber track pads and the ground surface as well as the supporting forces of the road wheels are considered as the beam loads. The lateral displacement of the rubber track pads is decisive for the amount of the forces between the rubber track pad and the ground.

Fig. 7 shows a track pad during a curve. Beneath the first road wheel

it gets in contact with the ground at the radius R (point x_0). In addition to the bending w of the track, the contact area of the pads is displaced sidewards due to the lateral elasticity s_e of the rubber pad. As long as the total displacement of the pad due to bending and lateral deformation of the rubber can follow the curve deviation s_d, the pad contact lies on the curve trace.

At this point x_1 there is no sliding motion and the lateral force is an elastic force. However, in that case, where the lateral deformation $w + s_e$ of track and pad is smaller than the deviation s_d of the curve (point x_2), the pad must slip laterally. In this point the slip length can be determined as

$$s = s_d - w - s_e \tag{5}$$

and consequently a lateral force is acting on the pad.

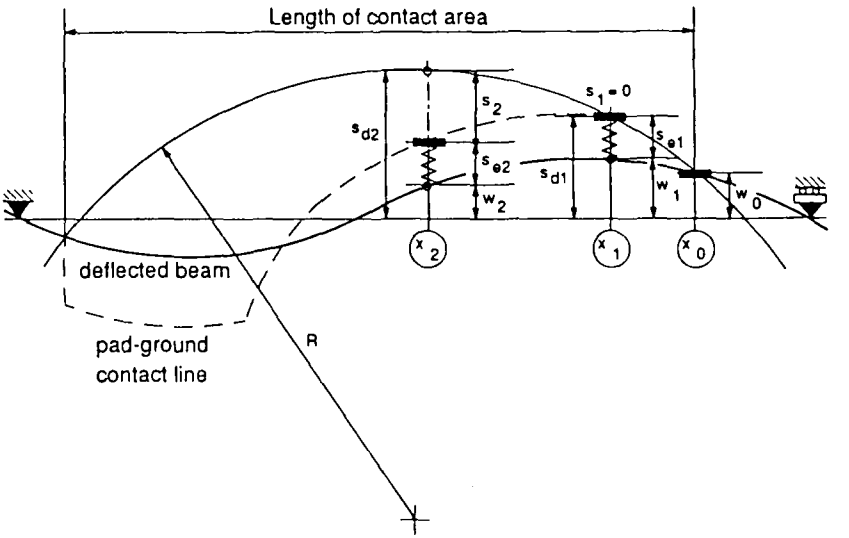

Figure 7: Lateral Deflections of a Track in a Curve

In general the bending line w is described as:

$$E*I_y*w'''' = q \tag{6}$$

$$E^*I_y^*w'' = - M \qquad (7)$$

with E^*I_y = const : bending resistance

q : line load

M : bending moment

The principle of superposition is used to calculate the resulting lateral bending of the modelled track. The bending caused by the frictional forces q and the bending caused by the supporting forces of the road wheels F_i are added:

$$w_g(x) = w(q) + \sum w_i(F_i) \qquad (8)$$

The supporting forces of the road wheels depend in a linear way on the bending :

$$F_i(x_i) = c_L^* w_g(x_i) \qquad (9)$$

with c_L: linear elasticity of the road wheel suspension

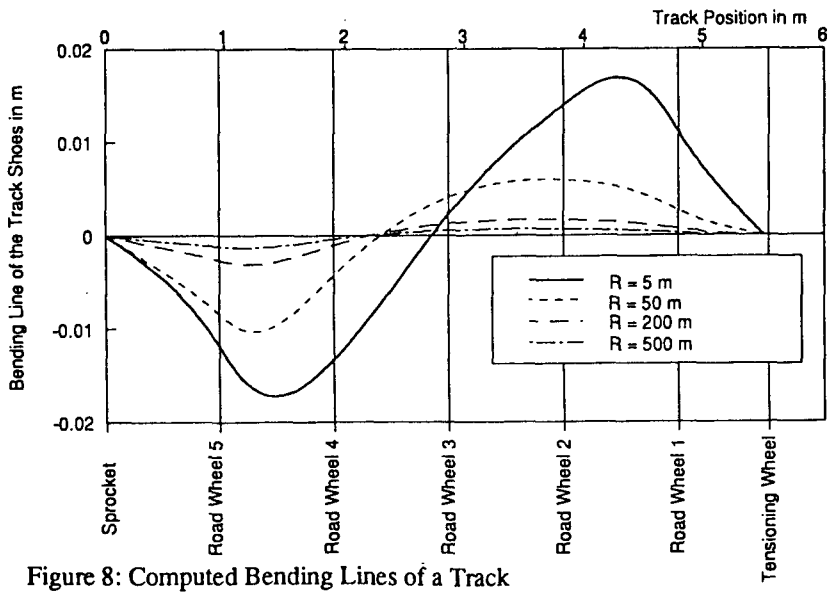

Figure 8: Computed Bending Lines of a Track

There is a set of equations to solve the unknown forces F_i and the bending line w. They influence each other. So the equations are solved using computed iterative algorithm.

Fig. 8 shows the result of the computed bending line at different radii. The deflection of the beam depends on the radius of the curve. And so by the deflection different lateral contact forces between ground and track are induced.

This model examines the driving behaviour of a tracked vehicle in a curve at low speed (no lateral acceleration). During this steady-state-moving there is no centrifugal force acting. The supporting forces of the road wheels and the reaction forces of the supports are inner cutting forces of the total model of the vehicle. Only the frictional forces at both tracks q_a (outer track) and q_i (inner track) build up the turning moment M_w:

$$M_w = \int q_a(x)\,dx + \int q_i(x)\,dx \qquad (10)$$

The turning moment is overcome by a couple of circumferential track forces. These forces influence the frictional connection between the rubber track pads and the ground surface. For the calculation this fact must be taken into consideration.

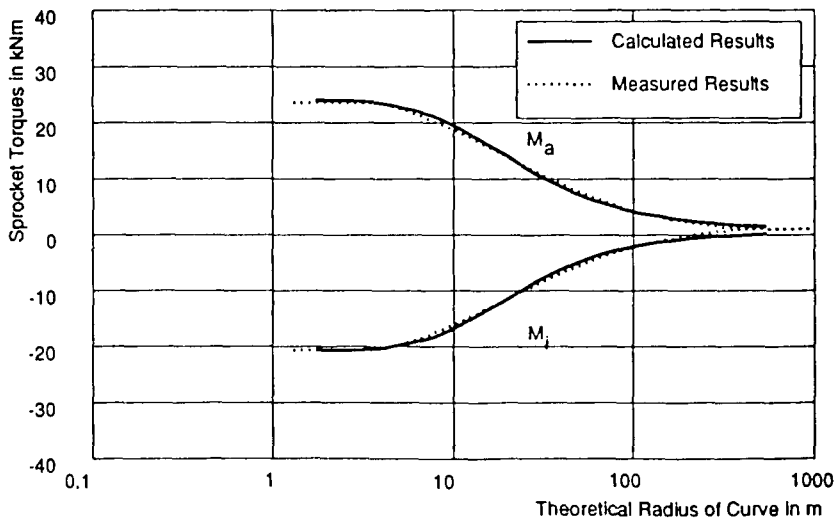

Figure 9: Calculated Sprocket Torques of the JAGUAR by MEMOKET

In fig. 9 the sprocket torques are plotted versus the theoretical radius: the unbroken line represents the results computed with the mechanical model, the dotted lines mark the results from field measurements with the test vehicle on a hard road surface at low rolling speed. As it is to be seen, MEMOKET is able to simulate the real conditions very well.

6. SIMKET: A MULTIBODY SIMULATION OF THE CORNERING OF A TRACKED VEHICLE

SIMKET is a model using the multibody system analysis software ADAMS. So it is a developed and supplemented ADAMS-Model of the test vehicle JAGUAR (fig. 10). ist setup is explained in [14].

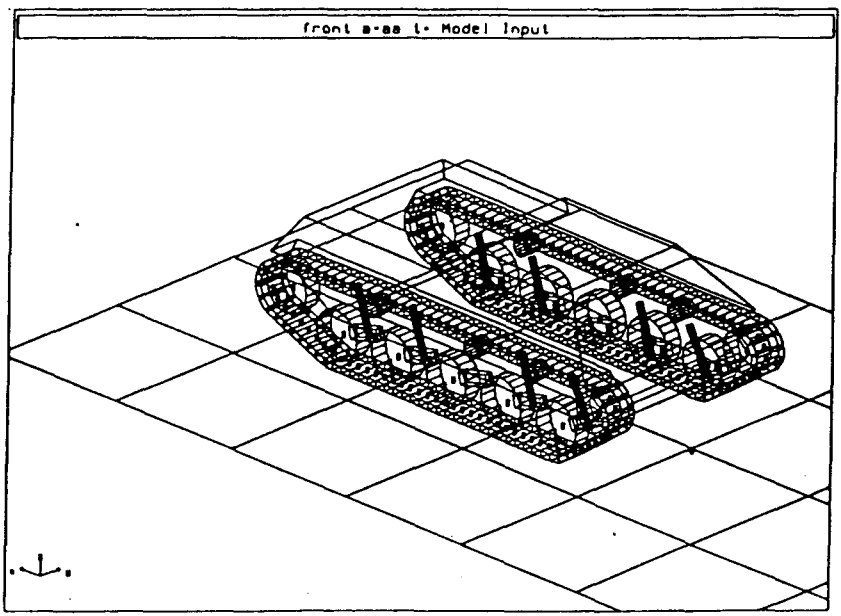

Figure 10: Simulated Test Vehicle JAGUAR in ADAMS

Results of this simulation are as well the distances, velocities and accelerations of each body and all forces and torques. In the following only steady-state motions will be regarded. They have to be compared to the results of the field measurements with the original test vehicle.

Besides the examination of the forces and torques the vehicle kinematics can be examined. As mentioned above the field measurements

show that the enlargement of the real radius is constant. Fig. 11 shows the radius enlargement factor versus the theoretical radius at a speed about 10 km/h. The simulated factor f_v is also independent of the radius, f_v reaches values about 2.

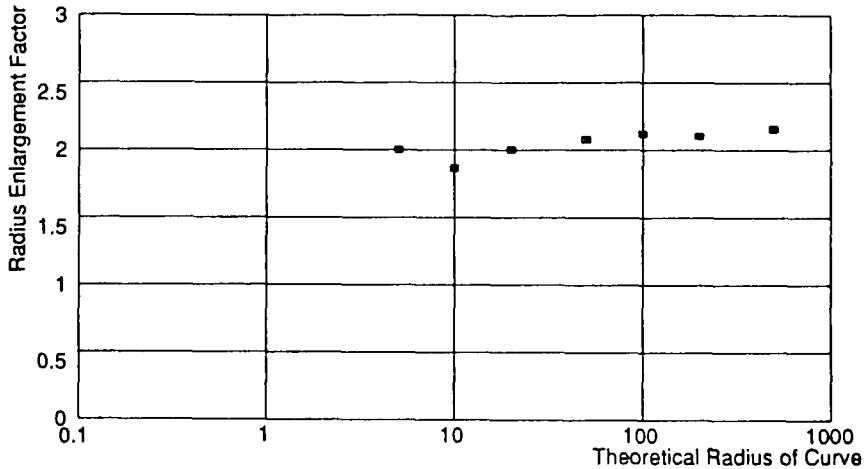

Figure 11: Radius Enlargement Factor Calculated by SIMKET

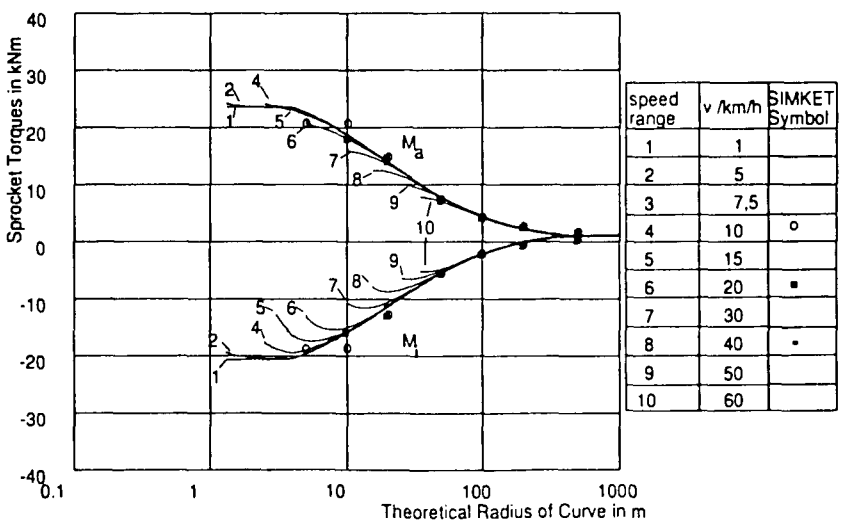

Figure 12: Sprocket Torques Calculated by SIMKET Compared to Field Measurements

Fig. 12 shows the sprocket torques versus the theoretical radius. The lines are the results of the field measurements, the symbols are the results of the calculation by SIMKET. Not only curves at low speed have been examined. Also high-speed-driving has been calculated in this model. In comparison with experimental results it can be seen, that the sprocket torques are simulated very well. Even the influence of the centrifugal forces on the sprocket torques can be regarded in the computed results as well as in the field measurements.

It can be stated, that the simulated model calculates not only the kinematics of the cornering of a tracked vehicle but also the dynamics sufficiently.

7. HOW TO MINIMIZE THE TURNING RESISTANCE

The turning resistance coefficient can be determined from eq.(1), if M_w has been calculated in one of the models:

$$\mu_w = 4*M_w/(m*g*l)$$

This coefficient will be useful in the discussion of the demands on the propulsion system during a curve. Some design parameters of a running gear are

- the vertical load of the tracks (number of road wheels),
- the friction behaviour of the rubber track pads (shape and composition of the rubber track pads),
- the elasticity of the rubber (composition and design of the rubber track pads),
- the bending resistance of the tracks and
- the elasticity of the road wheel suspension.

In fig. 13 some examples of the calculated turning resistance coefficient versus the real radius are plotted for different design parameters. The unbroken lines in both pictures represent the results computed with the original rate of stiffness of the rubber and friction coefficient, the design parameters are not varied.

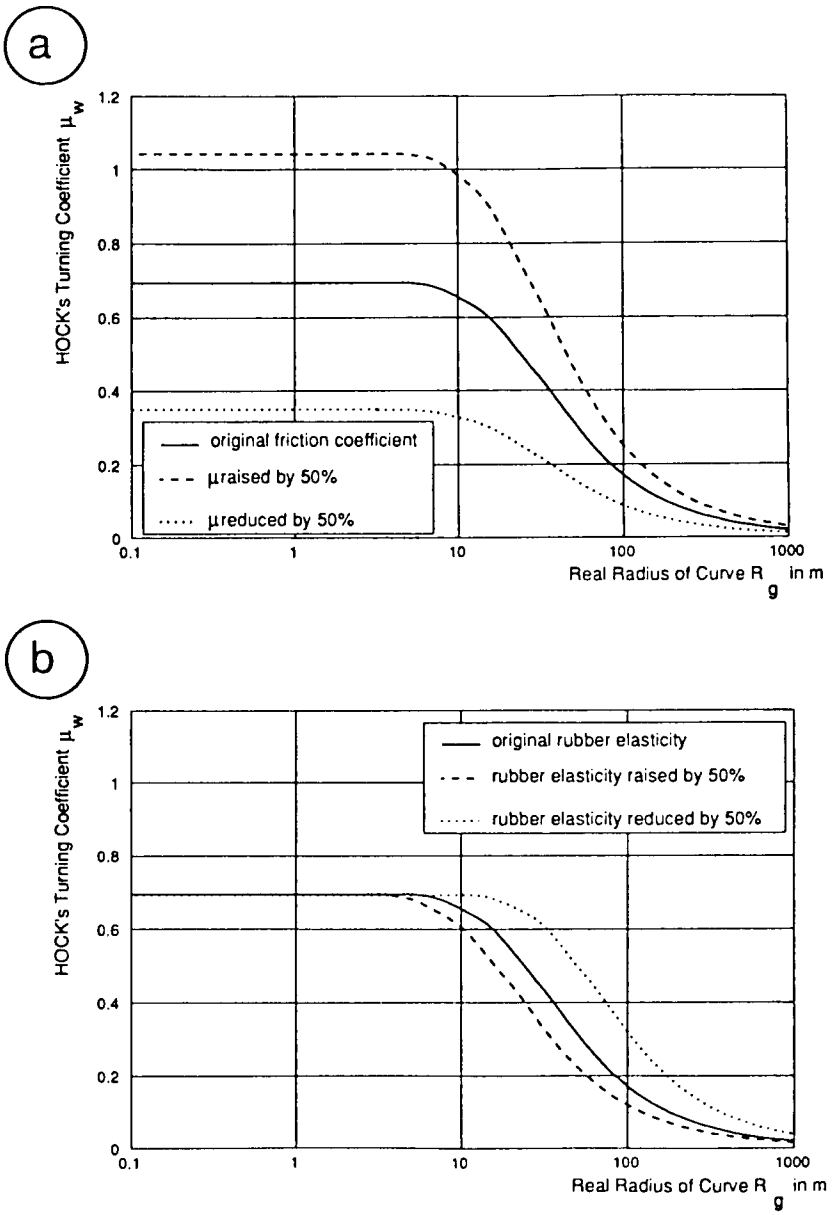

Figure 13: Calculated Turning Coefficients under Different Design Parameters

Fig. 13a shows the computed variation of the friction behaviour of the rubber track pads. The broken line is the result of an increasing of the friction coefficient μ by 50%, the dotted line shows the result of a reduced value of m. As is to be seen, the expected effect occurs: an increasing of the turning coefficient is caused by a higher friction coefficient. So reducing the friction coefficient leads to a lower demand on the propulsion system.

The friction coefficient depends on the frictional relationship between a rubber track pad and the ground surface. Reducing the turning coefficient in this way is in contradiction to the demand of having a good traction, which also depends on the friction coefficient.

Fig. 13b gives an example of variation of the rubber elasticity.The broken line is a result of raising the rubber elasticity, the dotted line shows the reduction of the elasticity. In the range of very narrow radii the rubber elasticity has no effect on the turning coefficient, all the rubber pads of the tracks are slipping. But in the range of medium radii between 10 and 200 m an increase of the elasticity leads to a clear reduction of the turning coefficient and so it would reduce the sprocket torques. In this way the influence of the turning resistance could be minimized.

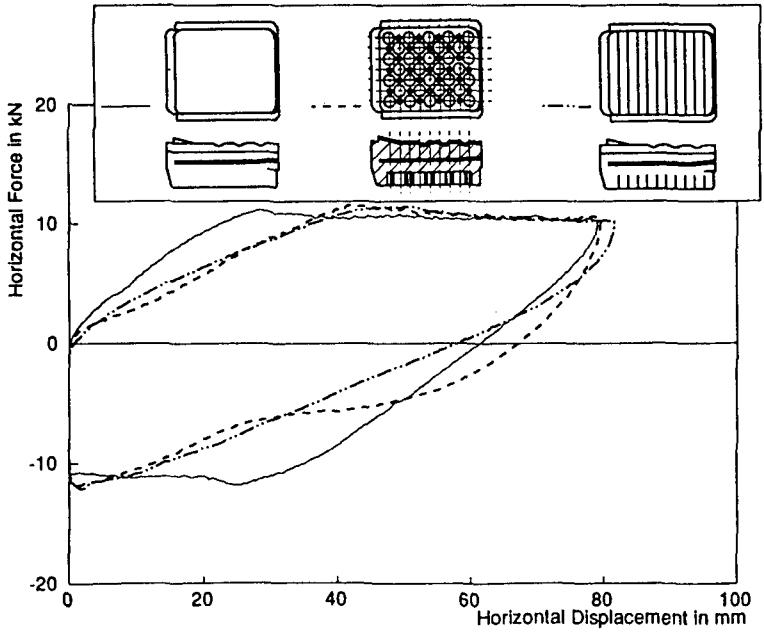

Figure 14: The Friction Behaviour of Different Rubber Shapes

There are two possibilities to vary the elasticity of the rubber pad. At first the designer can choose another composition of the rubber to get it more elastic. But generally this leads to greater abrasion and it means a significant change in the friction behaviour. The second possibility is to vary the shape of the rubber pad. An example of this variation is given in fig. 14. The original rubber pad has only half the elasticity of the rubber pad with the cicular hole pattern or the one with longitudinal cuts at the same ground pressure.

8. SUMMARY AND CONCLUSIONS

When a tracked vehicle is driving in a curve the turning resistance is added to the motion resistances of straight ahead motion. Previous analytical models to describe the turning resistance are based either on the principle of isotropic Coulomb's friction or on empirical statements. So the turning resistance coefficient is won by field measurements. In this paper two models have been described to overcome the empirical statements. Both models base on the lateral elasticity and the real friction behaviour of a rubber track pad. The presented mechanical model MEMOKET, which is based on the theory of a deflection beam, includes design parameters such as the elasticities in the running gear. SIMKET, a rigid body simulation in ADAMS, includes the masses and the inertias of every part of the tracked vehicle. Both models have been proven by comparison with steady-state field measurements. The simulated results correspond with the measurements in the description of the outer motion resistances.

As it has been shown, the presented models could be a helpful tool in designing the running gear of tracked vehicles. Studies of designed parameters are possible. These studies can minimize the turning resistance and running gear resistance of tracked vehicles. This is decisive for designing the propulsion system of tracked vehicles. Especially SIMKET is of great interest, because it isn't as limited in the calculation of the turning resistance coefficient as the mechanical model is. Using a rigid body simulation for computing the driving behaviour of a tracked vehicle offers both: a general model for the turning of the complete vehicle and a detailed look on the behaviour of each part of the vehicle.

Further studies will extend and improve the models. So a model of a single track including its running gear will be developed based on data of the model of the complete vehicle. This is of great importance in regard to the internal running gear resistances, which cause the wear and the abrasion of the

tracks, the sprockets and the road wheels. Besides the steady-state-behaviour of a tracked vehicle dynamic motions must be simulated. In the future simulations concerning the off-road-behaviour should be possible.

Another field of interest is the powerflow in the drivetrain of tracked vehicles. Now being able to calculate the physical basics of the turning resistance, SIMKET offers the opportunity to minimize the losses in the runnig gears and also to examine the losses in the drivetrain and to optimize the powerflow during a curve by detailed extensions of running gears and gear boxes.

REFERENCES

[1] I.C. Schmid, W. Ehlert, St. Pott: Mobility of Tracked Vehicles and Simulation of the Dynamics of Motion on the PAISI Test Plant, XXII. FISITA-Congress, Dearborn, 1988, Technical Papers SAE-P-885114, pp. 2.170 -2.181

[2] J. Hock: Lenkgetriebe für Kettenfahrzeuge, Firmenschrift, ZF Friedrichshafen, 1970

[3] W. Ehlert: Simulation der Fahrwiderstände von Gleiskettenfahrzeugen auf dem Prüfstand, insbesondere bei Kurvenfahrt, Dissertation, Universität der Bundeswehr Hamburg, 1991

[4] W. Ehlert, St. Pott: Bodenmechanische Einflüsse auf den Wendewiderstand von Gleiskettenfahrzeugen, IKK-Bericht Nr. 89-19, Universität der Bundeswehr, Hamburg, 1989

[5] W. Ehlert, B. Hug, I.C. Schmid: Field Measurements and Analytical Models as Basis of Test Stand Simulation of the Turning Resistance of Tracked Vehicles, 10th International Conference of the ISTVS, Kobe, 1990, Proceedings, pp. 601 - 612

[6] IABG, not published

[7] M. Kitano: Dynamics of Tracked Vehicles, Vortragsmanuskript, 1. Tagung Geländegängige Kraftfahrzeuge, Universität der Bundeswehr, Hamburg, 1982

[8] I.C. Schmid: A Tracked Vehicle Test Plant for the Simulation of Dynamic Operation, 8th International Conference of the ISTVS, Cambridge, 1984, Proceedings

[9] M.K. Kar: Prediction of Track Forces in Skid-Steering of Military Tracked Vehicles, Journal of Terramechanics, 1987, Vol. 24, No. 1, pp. 75 - 86

[10] N. Ito: Practical Method of Improving the Turnability of Terrain Vehicles, 10th International Conference of the ISTVS, Kobe, 1990, Proceedings Volume III, pp. 687 -696

[11] H. Kondo, N. Tanaka, N. Sugiyama: A Study of the Steering Resistance of Tracked Vehicles, 1st Asian-Pacific Conference of ISTVS, Beijing, 1986, pp. 681 - 691

[12] Mechanical Dynamics Inc.: ADAMS User's Manual 5.2.1, Ann Arbor, 1989

[13] St. Pott: Friction between Rubber Track Pads and Ground Surface with Regard to the Turning Resistance of Tracked Vehicles, 5th European Conference of the ISTVS, Budapest, 1991, Proceedings Vol. I, pp. 105 - 112

[14] St. Pott: The Turning Resistance of Tracked Vehicles - ADAMS-Simulation Compared to Field Measurements and Analytical Models, 8th TEDAS News-Conference, München, 1992, Proceedings

BUCHER

6th EUROPEAN ISTVS CONFERENCE 1994

THE BUCHER DURO
A VEHICLE CONCEPT FOR THE FUTURE

A. Sasse
BUCHER-GUYER AG, Zurich, Switzerland

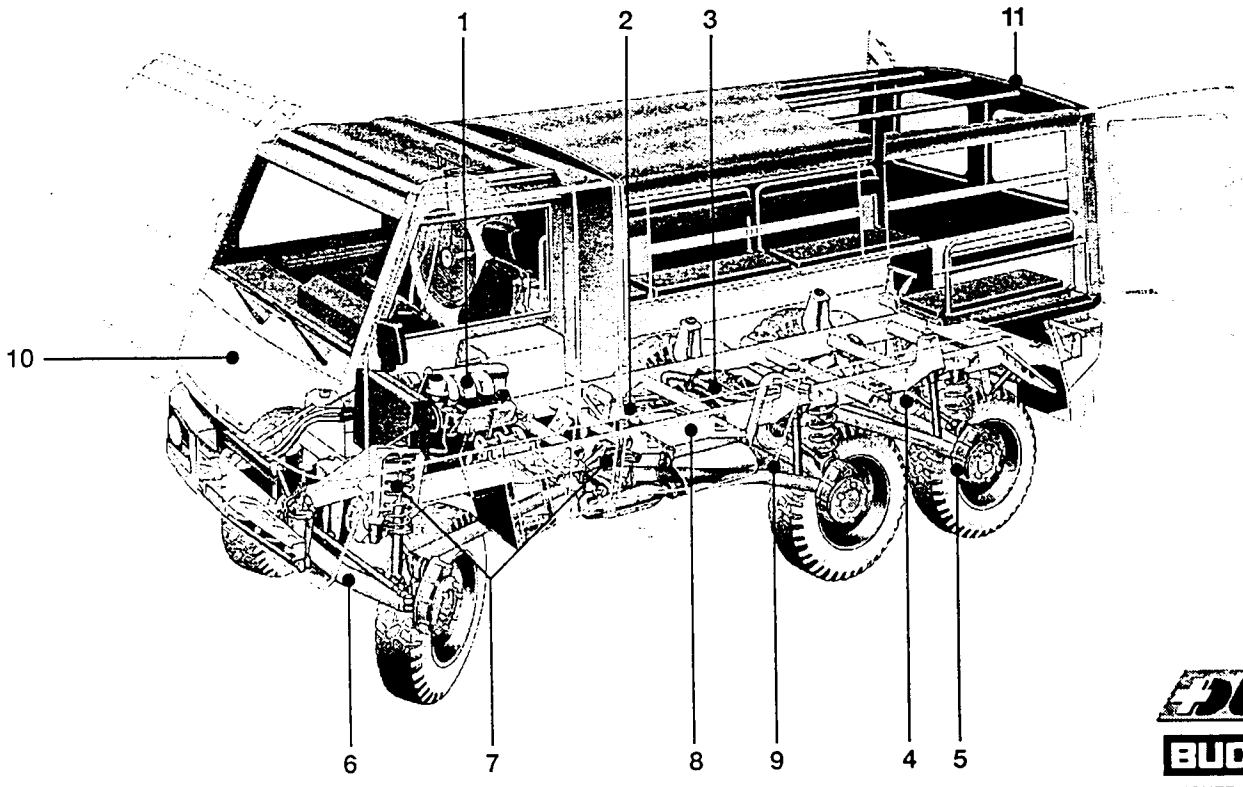

EURO
BUCHER
BUCHER-GUYER LTD
8166 Niederweningen Switzerland
Phone +41-1-857-22-11
Fax +41-1-857-22-49

BUCHER

<1> ENGINE

Diesel engine VM EP 638 LI
110 kW at 4,000 rpm
320 Nm at 2,200 rpm
6-cylinder, 3,749 cm^3
Exhaust gas turbocharging with charge air cooler

A mid-engine arrangement behind the front axle and beneath the driver's cab was selected with the objectives of balanced weight distribution to the axles, of sufficient space for three places in the cab and of achieving a low center of gravity. The modular construction - engine and transmission separate - additionally permits highest flexibility with regard to the installation of components.

<2> TRANSMISSION

4-speed automatic transmission MB W4A028,
hydraulically controlled, parking position.

For the purpose of optimum weight distribution the automatic transmission is arranged at a distance from the engine and together with the transfer gearbox in front of the rear axle. The engine and the transmission are therewith located near the axles, resulting in an excellent ramp angle.

<3> TRANSFER GEARBOX

BUCHER 2-speed reduction gearbox,
synchronized, electro-hydraulically pre-select shifting,
permanent all-wheel drive with TORSEN interaxle differential,
integral power output for 3rd axle (6x6).

The automatic transmission, transfer and axle gearboxes are arranged as an easy-to-install coherent assembly in front of the rear axle. This concept precludes top-heaviness, and affords stable tracking on panic braking, even in the otherwise dynamically critical unloaded condition. To achieve an appropriate ground clearance, these gearboxes were arranged as low as possible. Various superstructures with a lowered loading surface can be mounted on the free upper side of the frame.

BUCHER

<4> AXLE GEARBOXES FRONT AND REAR

BUCHER axle gearboxes with TORSEN differential and inboard, ventilated disc brakes.
In different assembly configurations the same gearbox can be installed in all three axles (6x6).

The use of self-locking TORSEN differentials simplifies the task of an unpracticed driver coping with difficult situations. The inboard brakes permit visual inspection and changing of the linings without removal of the wheels. The same discs and calipers are used on all wheels.

<5> HUB REDUCTIONS

BUCHER hub reductions

Hub reductions provide greater ground clearance underneath the axles, and lower torques in the drive train. Logistic advantages can be realized through drives of the same type, as well as through identical homokinetic drive shafts for all wheel.

<6> AXLES

BUCHER De-Dion axles for front and rear axles

The dynamic behavior of the De-Dion axles was improved substantially by shifting the brakes to the sprung mass. As a result of inboard brakes, despite axle gearboxes a smaller kingpin offset was realized. In this way, on braking in μ-split situations a stabilizing counter-steering torque can build up. Due to a low disturbing force leverage the sensitivity to shocks and imbalance was also reduced. Exact wheel guiding via the long spring travels is achieved via the long drawbar guides and the Watt linkage.

BUCHER

<7> SUSPENSION / SHOCK ABSORPTION / STABILIZER

At the front: progressive helical springs and gas-pressure shock absorbers acting together as spring strut, additional Cellasto springs.
Rear: Progressive miniblock springs with integrated additional springs and gas-pressure shock absorbers.
BUCHER stabilizer acting on front and rear axles.

On the one hand a high swing capacity or adaptation of the axles to the terrain was achieved by means of long spring travels and a low roll stiffness.
On the other hand, the patented stabilizer prevents the simultaneous, one-sided compression of the axle springs during road travel, while permitting alternating compression of the axle springs free of stabilizer forces.

<8> FRAME

Ladder-type frame, main construction of welded hollow steel sections

The long spring travels permit a torsionally rigid design of the frame, with the advantage of being able to mount various superstructures and even to connect the cab functionally without encountering problems.

<9> SIDE GUARD

The side guard according to EEC guideline 89/297 contributes to passive safety.

BUCHER

<10> DRIVER'S CAB / ROLLOVER PROTECTION

Tilting cab of aluminum sections and cast connecting elements, combined with plastic paneling.
Floor, windshield, roof panel, rear wall and their windows are glued to the cab frame.
2 - 3 seats.
The aluminum rollover guard accommodates the heater for the superstructure and the spare wheel. The vehicle with personnel carrier superstructure has successfully passed the ECE-R 66 rollover test.

The aluminum construction used saves weight, increases the life and with regard to investments is ideal for medium series sizes. For the purpose of partner protection and to keep accident repair costs minimal the front paneling is of "soft nose" design, as well as being removable for the purpose of carrying out repairs on the cab.

<11> SUPERSTRUCTURES

Personnel carrier *with tarpaulin and hinge-up lengthwise benches for up to 16 persons or up to 6 pallets.*
Command and control shelter *with plastic hardtop and side doors, 3 radio operator stations and table for 4 further persons.*
Insulated ***box-type superstructure*** *with inside height of 1.9 m with a vehicle height of less than 3 m.*
Bolted aluminum platform construction.
Time requirement for superstructure change approx. 20 minutes.

The superstructures are of modular construction and are based on a uniform aluminum platform of extruded sections connected with CO-BOLT fasteners. The floor is integrated low in the chassis to ease climbing in and out by the personnel, to afford transport of personnel and materials with a favorable center of gravity and with a small raised roof to provide a comfortable standing height. The platform upper and lower load surfaces are dimensioned for standard pallet sizes.

THE NEW DORNIER FOLDABLE BRIDGE DOFB

Peter Schmidt, Siegfried Bäumel
Eurobridge, Mobile Brücken GmbH

ABSTRACT

Troop mobility is a critical point in all phases of a military operation. The mobility requirements to be fulfilled by the vehicles employed have continously increased. However even for modern vehicles, high mobility becomes useless when natural or man-made gaps and destroyed bridges cannot be overcome. For this reason, bridging equipment such as mobile bridges have to be taken into consideration when planning military missions.

Basically, it can be stated that tactical requirements with regard to the mobility of transportable bridges, on the road and in the terrain, have become increasingly important. The same applies to the requirements with regard to shorter construction times because of the troops' increased moving speed.

The example of the Dornier Foldable Bridge (DoFB) system described in the following shows how the two requirments, high mobility of the bridge system and short launching time, which initially appeared to be contradictory, could be fulfilled by optimizing the bridge components. At the same time, the mobility-increasing features of the bridge are represented.

1. INTRODUCTION

In the early 80s, the German engineer forces actively aimed for the replacement of an obsolete bridge which, in addition to other disadvantages, required too much time and too many persons for launch and recovery.

A modern concept, the so-called "Bridges of the 80s", had overcome these disadvantages. The launch of this bridge type was rapid and largely automated. The advantages, however, were achieved at the expense of mobility on roads and in the terrain on account of large dimensions and heavy weight, which required special vehicles. Numerous bridge construction sites could not be reached at all for this reason.

The Dornier foldable bridge DoFB represents a solution which offers the advantages of the concepts mentioned above without the associated drawbacks.

2. THE STARTING SITUATION

2.1 The conventional design

Military bridging equipment is characterized mainly by two trackways which bear the tracks of a tank. The trackways are connected by cross bracing yokes. This leads to a bridge width of max 4 m with a gap between the trackways.

Cantilevered launching of this type of bridge is possible up to a span of 26 m. This is the limit for the counterbalance moment of the launching vehicle. The critical counterbalance moment situation for longer bridges was overcome by a launching nose, a light auxiliary beam which reaches the opposite bank and supports the bridge for the remaining construction phase of the bridge.

2.2 The critical analysis

Analyzing the main criteria of the bridge system, i. e. mobility and launching time, shows that conventional solutions optimized either the mobility or the requirement launching time/personnel.

Example no. 1: Medium girder bridge, **Fig 2.2.1**

Advantage:	High mobility on roads and in the field on account small components
Disadvantage:	Long launching time with high personnel and large bank space requirements

Example no. 2: Bridges of the 80s and "Langer Leguan", **Fig 2.2.2**

Advantage:	Short launching time with few persons on account of large components
Disadvantage:	Low mobility on roads and in the field, there by limitation of possible bridge construction places

The problems of known, already established solutions for mobile, rapid-launch dry support bridges are thus characterized by the relations:

Short launching time in the bank area $\rightarrow$ large components

High mobility on roads and in the field $\rightarrow$ small components

The objectives for component dimensioning are thus contradictory:

Short construction time $\leftrightarrow$ high mobility

The analysis reveals that the two objectives correspond to completely different configurations:

Short construction time $\rightarrow$ bridge construction

High mobility $\rightarrow$ bridge transportation

This means that a dry support bridge concept that shall fulfill both objectives must cope with the following requirements:

- Large components for construction
- Small components for transportation

together with

- Lowest possible requirements with regard to time, personnel, and space for the change from the transportation configuration to the launching configuration at the bridge construction site

This resulted in a completely new concept, the DoFB foldable bridge, which is characterized by an integral deck without trackways and by a foldable, closed roadway (**Fig. 2.2.3**) as described in the following paragraphs.

3. DESCRIPTION OF THE DORNIER FOLDABLE BRIDGE DOFB

3.1 Operational requirements

The requirements which are important for a modern bridge equipment are as following:

Autonomous mobility to reach any place where the bridge is needed, which requires

- smart transport units featured by dimensions reasonable in width, length and hight,
- light weight bridge components,
- transport vehicles with good on and off road properties.

Rapid assembly to enhance the advance of the forces and to reduce the vulnerability of the bridge by enemy attacks which requires

- launching without bank preparation,
- small number of components to be launched,
- mechanized launching and retrieval of the bridge with a small crew and without physical strain on the crew,
- robust launching system to ensure a reliable and trouble free launching process.

High Crossing capabilities to enhance the mobility and manoeuverability of the forces on mission which requires

- wide and closed bridge roadway deck with ramps of low inclination to enable the crossing of any kind of vehicle with relatively high velocity,
- stiff bridge structure and stable bank support to enable the vehicles crossing the bridge centric or eccentric even on transversal inclination of the bridge resulting from the bank conditions,
- bridge components which are self adapting to global and local bank conditions,
- launching of the bridge from hidden places and from restricted bank space at the gap,
- modularity of the bridge to launch the proper bridge span with respect to the width of the gap,
- launching of the bridge on permanent bridges to increase their load capacity or to overcome distroyed parts,

3.2 Technical Description

System components

The standard 40 m DoFB bridge system shown in **Fig. 3.2.1** comprising the bridge sections, the traversing beam sections and the bank beams as shown in **Fig. 3.2.2.** To launch the bridge the launching vehicle with the launching system attached is required (**Fig 3.2.3**). The launching system comprises mainly the system frame as a torsion free platform to carry the hydraulic vehicle outriggers, the launching beam, the crane, the hydraulic supply, the electronic control and an auxilary power unit. For transportation of the bridge components five standard transport trucks of the type shown in **Fig. 3.2.4** are required.

Launching procedure

The bridge launching is done in two steps. First the traversing beam will be launched cantilevered. Secondly the bridge then is traversing on the traversing beam to the far bank. The launching sequence for both is depicted in **Fig. 3.2.5 a, b**

As soon as the bridge construction site is reached, the launching vehicle will be positioned at the bank and stabilized with the hydraulic outriggers.

To increase the counterbalancing moment of the launching vehicle against tilting while launching the traversing beam, the home bank beam will be attached to the launching beam to act temporarely as an additional support leg. The traversing beam sections are then fed into the launching beam, coupled and travelled towards the far bank. First the ramp section with the far bank beam attached at the tip followed by three further inner sections and the home bank ramp section (**Fig. 3.2.6**) until the far bank is reached. With the traversing beam spanning the gap the bridge launching starts subsequently. The transport truck carrying the folded bridge sections is positioned within the reach of the launching system crane as it is most conveniened with respect to the site access (**Fig. 3.2.7**).

The unfolding from transport width 2.7 m to the full operational width of 4.4 m is done by gravity while lifting the section with the crane hoisting gear from the transport truck (**Fig. 3.2.8**). The unfolded bridge section is then placed onto the traversing beam. First section is the far bank bridge ramp section. Before the next section will be launched the ramp section is to be travelled forward on the traversing beam to provide the space required for a bridge inner section. Ones the inner section is in place and linked to the ramp section both will be coupled at the lower and upper chords (**Fig. 3.2.9**).

The procedure will be repeated for another 3 bridge inner sections and the home bank ramp section until the bridge reached the bank beam positions.

At a last step the climbing ramps will be attached to the bank beams either by crane or by hand (**Fig 3.2.10**).

After approximately one hour by a crew of six the bridge is ready to use.

The retrieval of the bridge in reverse order is possible from either side of the gap. The bridge modules are folded back again by the crane, using different hoisting points.

Design Features

The modularity design of the bridge and the traversing beam (**Fig. 3.2.11**) provides two advantages, first to adapt the bridge extremely well to the gap width to avoid problems as shown in (**Fig. 3.2.12**), and secondly there is nothing which is protruding in the depth of the bank site while launching the bridge from very narrow bank sites as it is shown in Fig. 3.2.7.

The advantage of the the bank beam is to provide a well defined and ridgid bridge support at the bank, which compensates the stability problems for the bridge caused by slopes, steps, soil conditions or by uneven surface at the bank. The bank beam is provided with a special shoulder on which the sliding shoes of the bridge are resting (**Fig. 3.2.13**) to avoid the well known shifting of the bridge towards the gap by the deflection under the crossing load. Further it accommodates the movement of the bridge caused by braking forces.
The launching beam with the traversing beam ramp section still engaged can be swivelled so to enable the downhill or uphill launching of the traversing beam to the far bank (**Fig 3.2.14**). The bank beam is attached with a joint to the traversing beam to provide freedom for the adaptation to the two main directions of a bank slope.

The climbing ramp design with its finger like beams is ideal to adapt to uneven and sloped ground (Fig. 3.2.13), with the low inclination when emplaced, they facilitate the access to the bridge for the approaching vehicles.The exceptional wide and closed deck ensures safe crossing even with higher crossing speed (**Fig. 3.2.15**).

These features provide the important tactical advantage of an increased number of potential launching places to deploy the bridge and to enhance the crossing capacity for any kind of wheeled and tracked vehicle.

Main performance data

The DoFB is designed in accordance with the "Trilateral Design and Test Code for Military Bridging and Gap Crossing Equipment" and on German Army requirements especially concerning the load class to be born by the bridge and the bridge life.

The main data are summarized in **Table 3.2.1.**

Additionally to these data given in the Table the DoFB has the following remarkable features:

- Air and rail transportable without dismantling the bridge components and quick disconnection of launching system and launcher base truck (**Fig. 3.2.16**).
- Easily adaptable to the most truck makes.
- High mission reliability by conventional robust design and components proven in technical and troop tests, redundant components for vital functions, optimized man / machine interfaces and control, simple fault detection and exchange of parts.
- Beyond the 40 m standard DoFB the 46 m extented version is available without external reinforcement.
- Conversion for civil use with a ramp of lower inclination and with attachable footwalks and handrails is possible.

The DoFB has the German Army qualification by technical testing and troop testing which resulted in the certificate of suitability for the German Army use. Procurement will start in 1994.

Medium Girder Bridge MGB

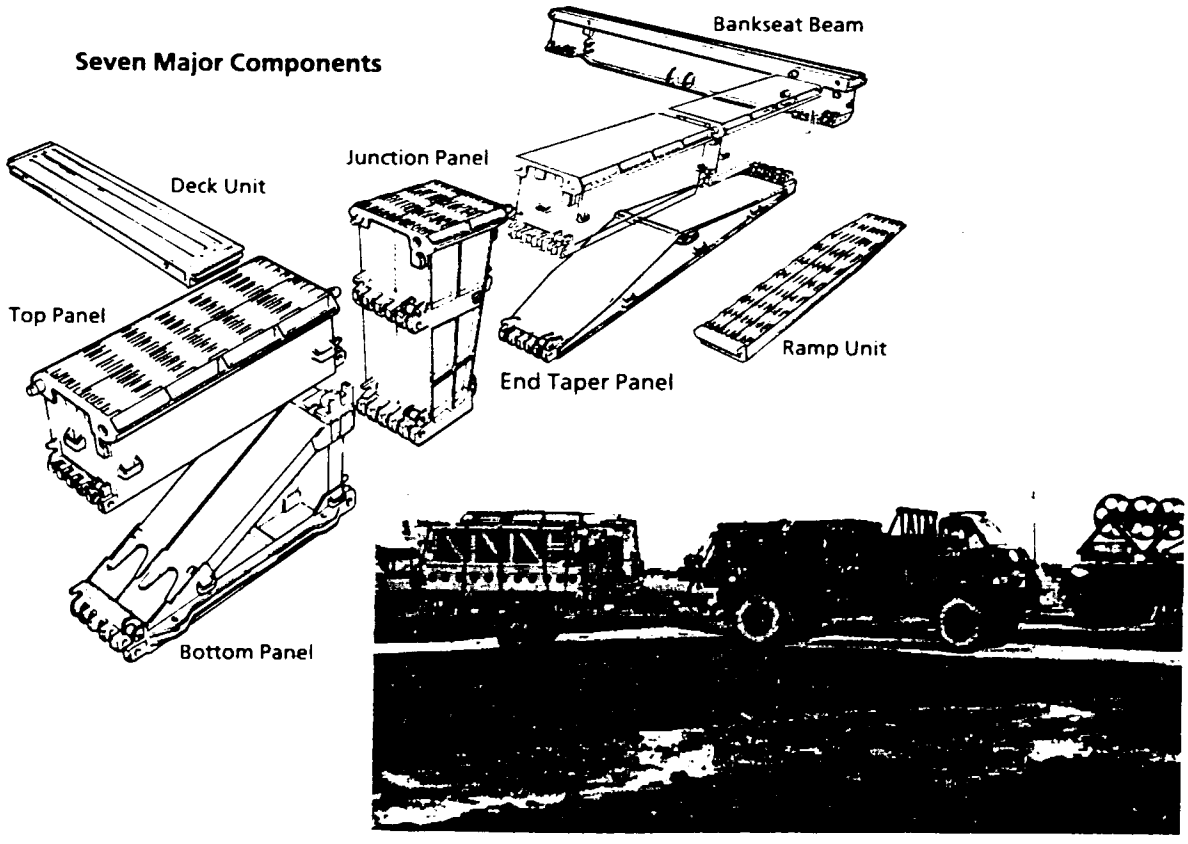

Fig. 2.2.1

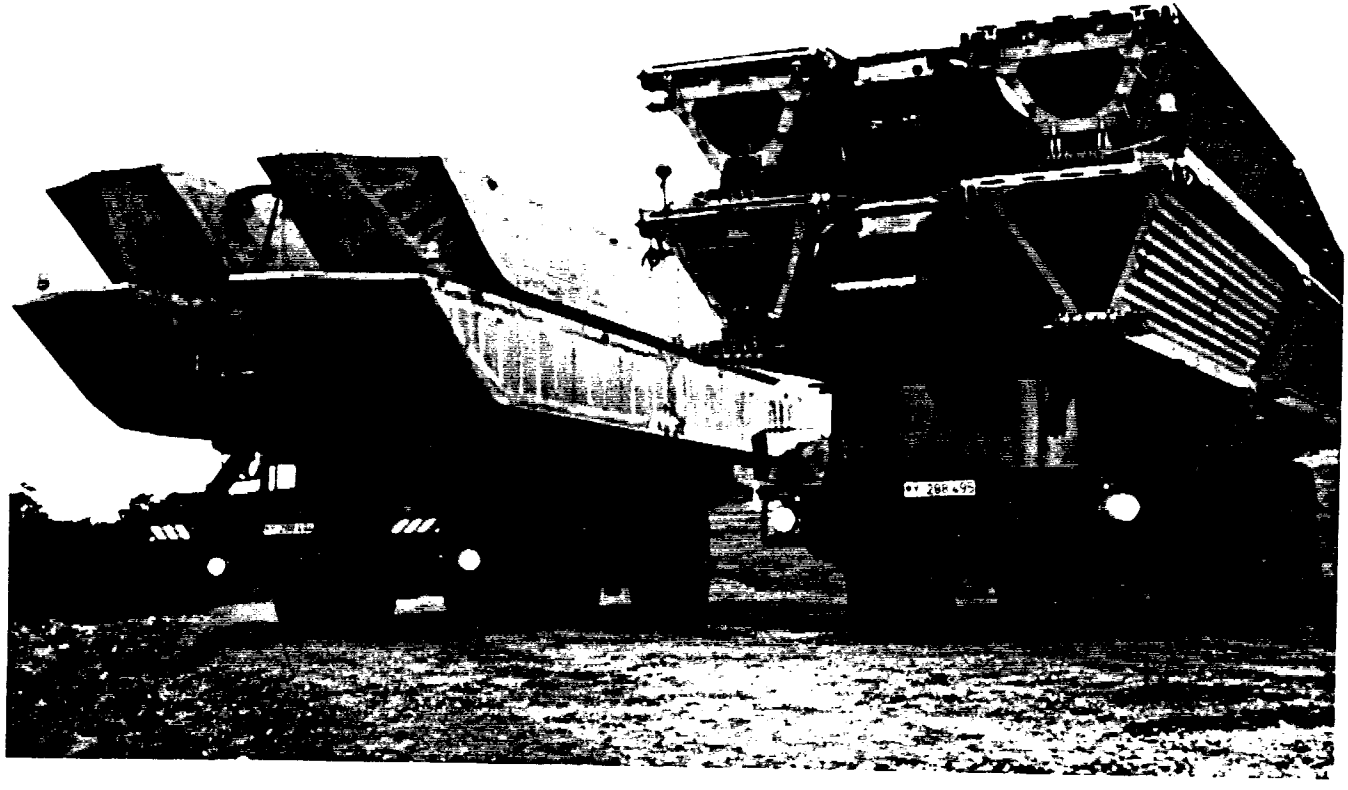

Fig. 2.2.2

DoFB Folding Principal

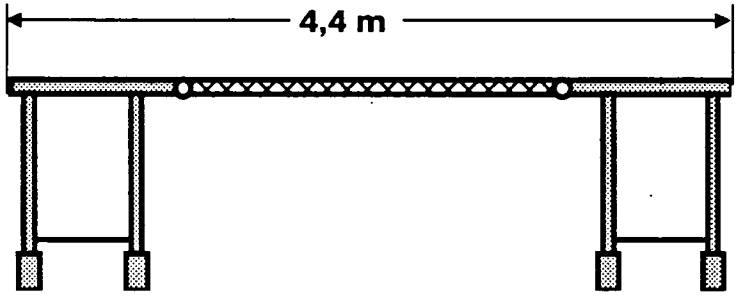

Bridge deployed

Folding and unfolding by crane

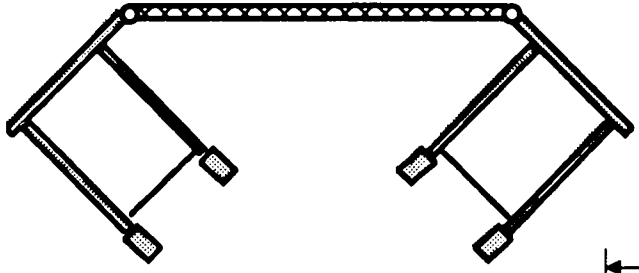

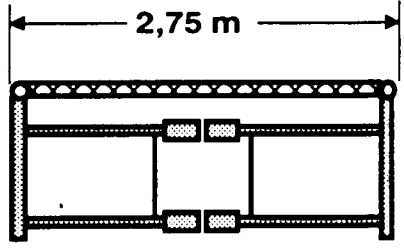

Transport package

Fig 2.2.3

Dornier Foldable Bridge DoFB

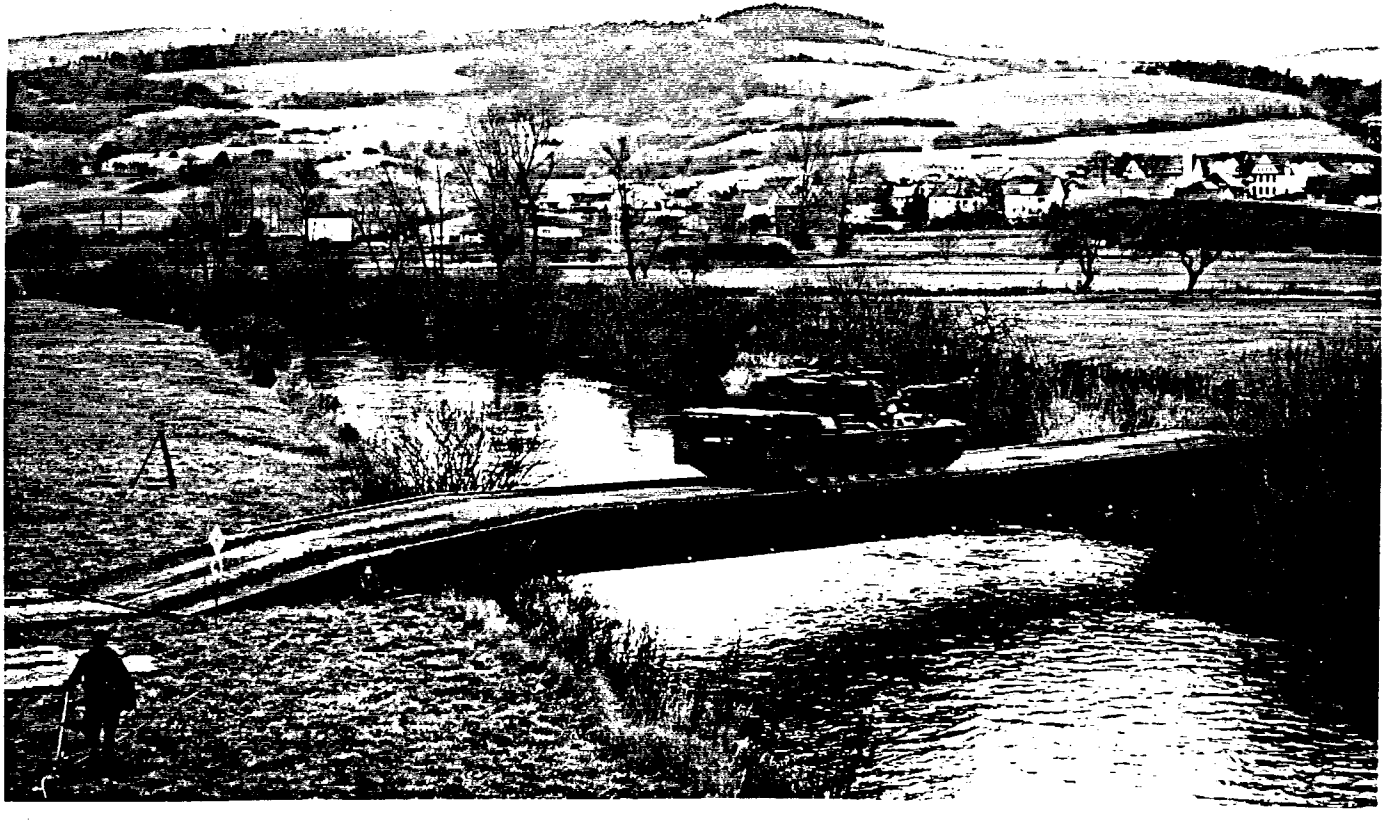

Fig. 3.2.1

DoFB Main Bridge Components

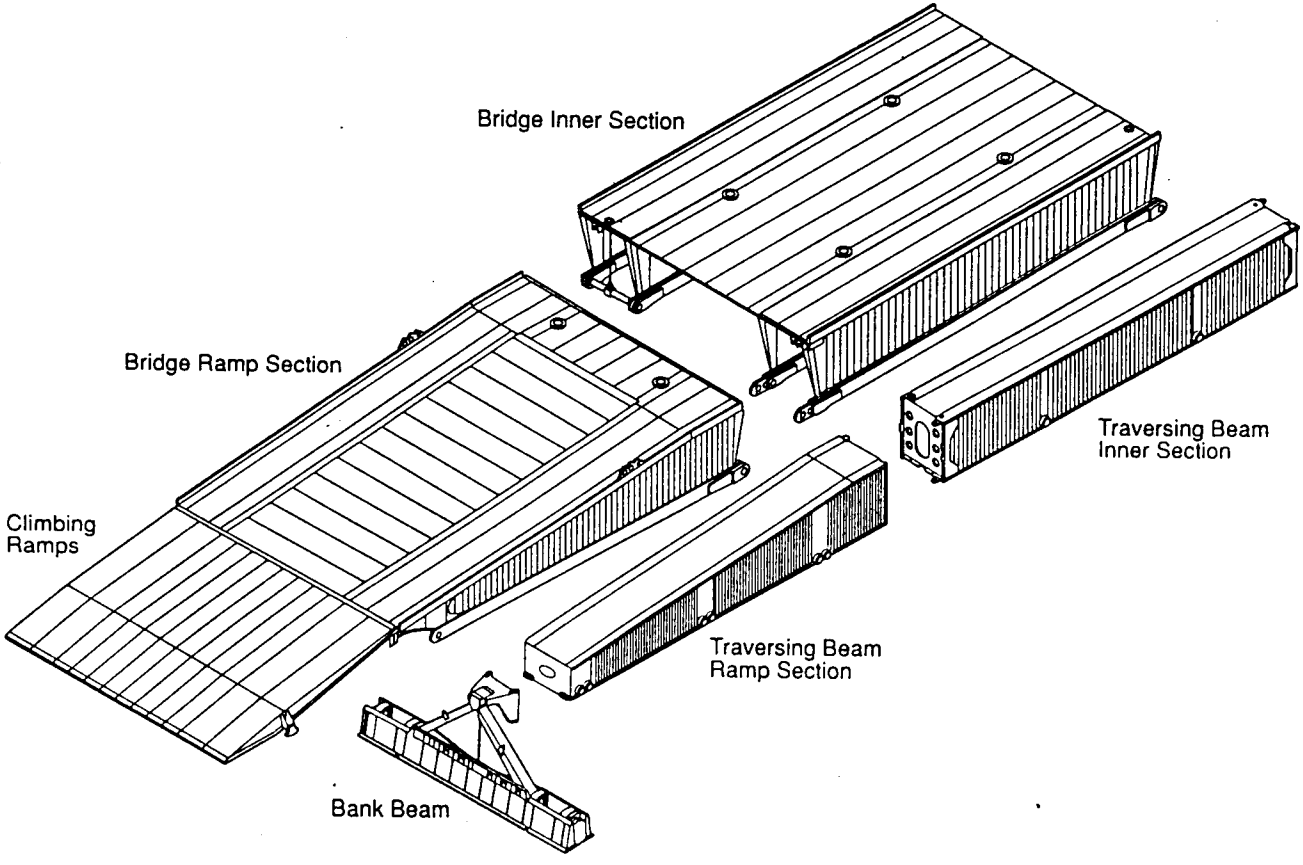

Fig. 3.2.2

DoFB Launching Vehicle 8x8

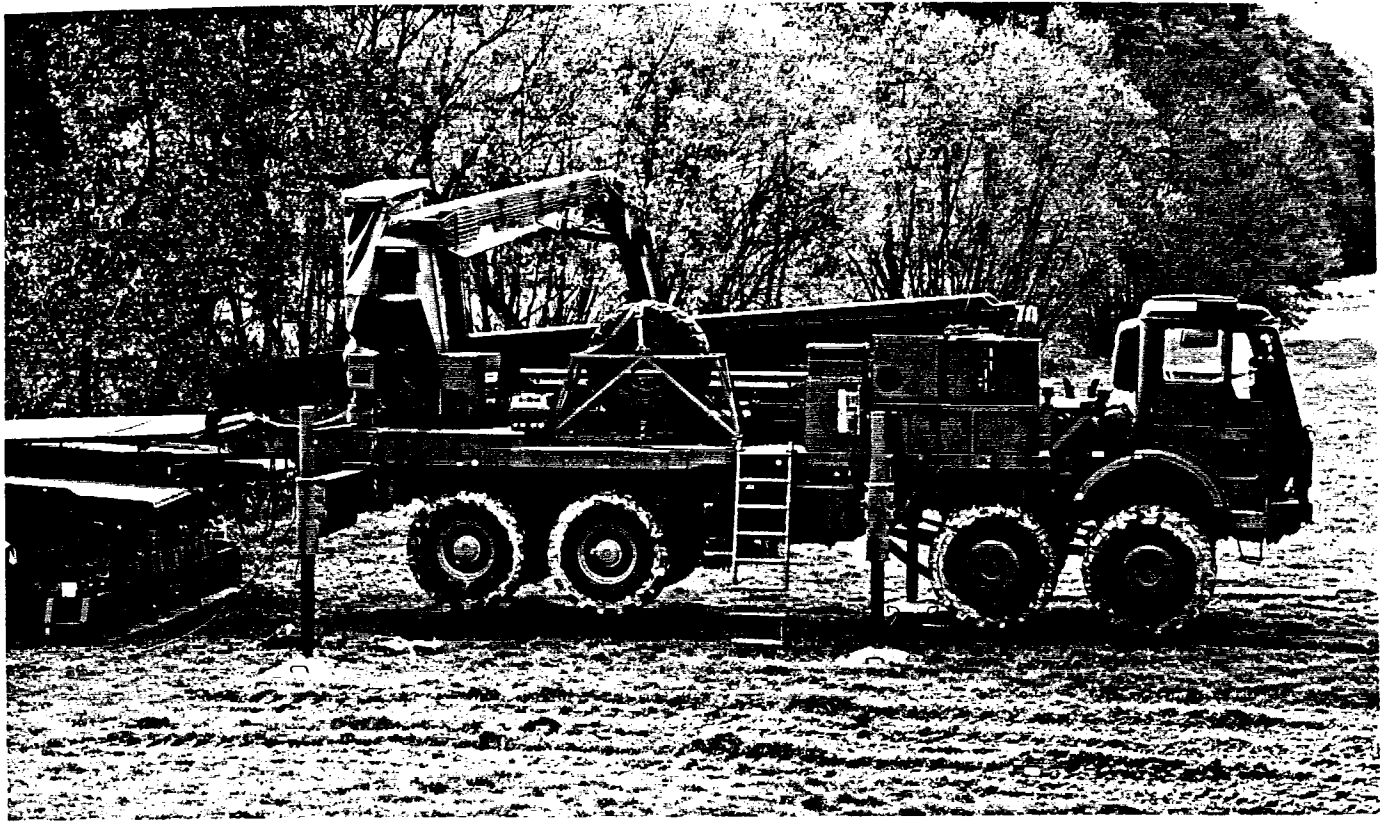

Fig. 3.2.3

DoFB Transport Truck 6x6

Fig. 3.2.4

DoFB Traversing Beam Launching

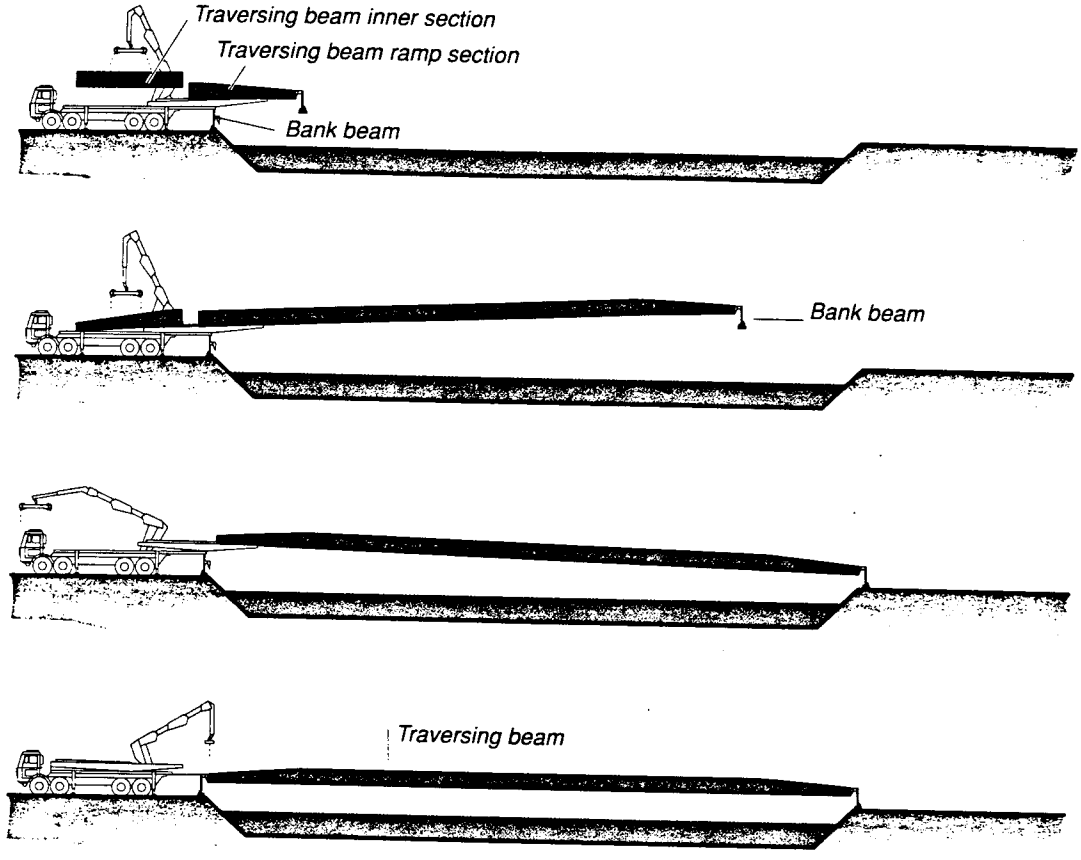

Fig. 3.2.5 a

DoFB Bridge Launching

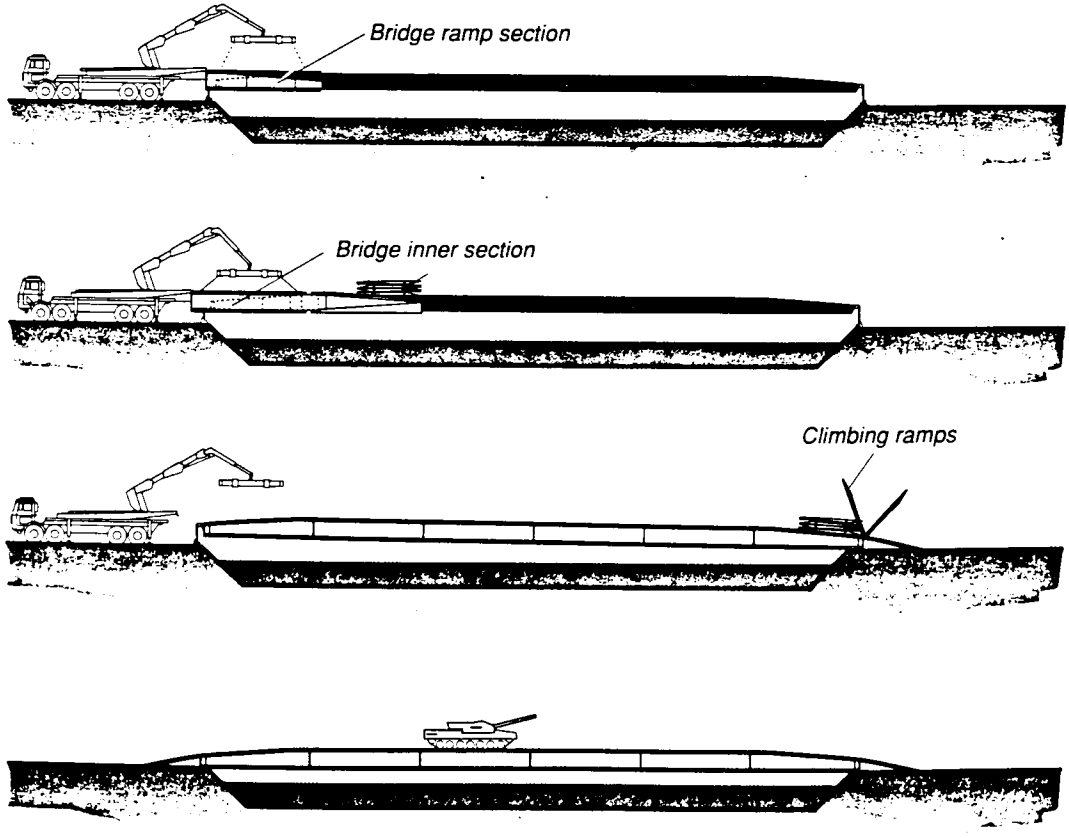

Fig. 3.2.5 b

DoFB Traversing Beam Launching

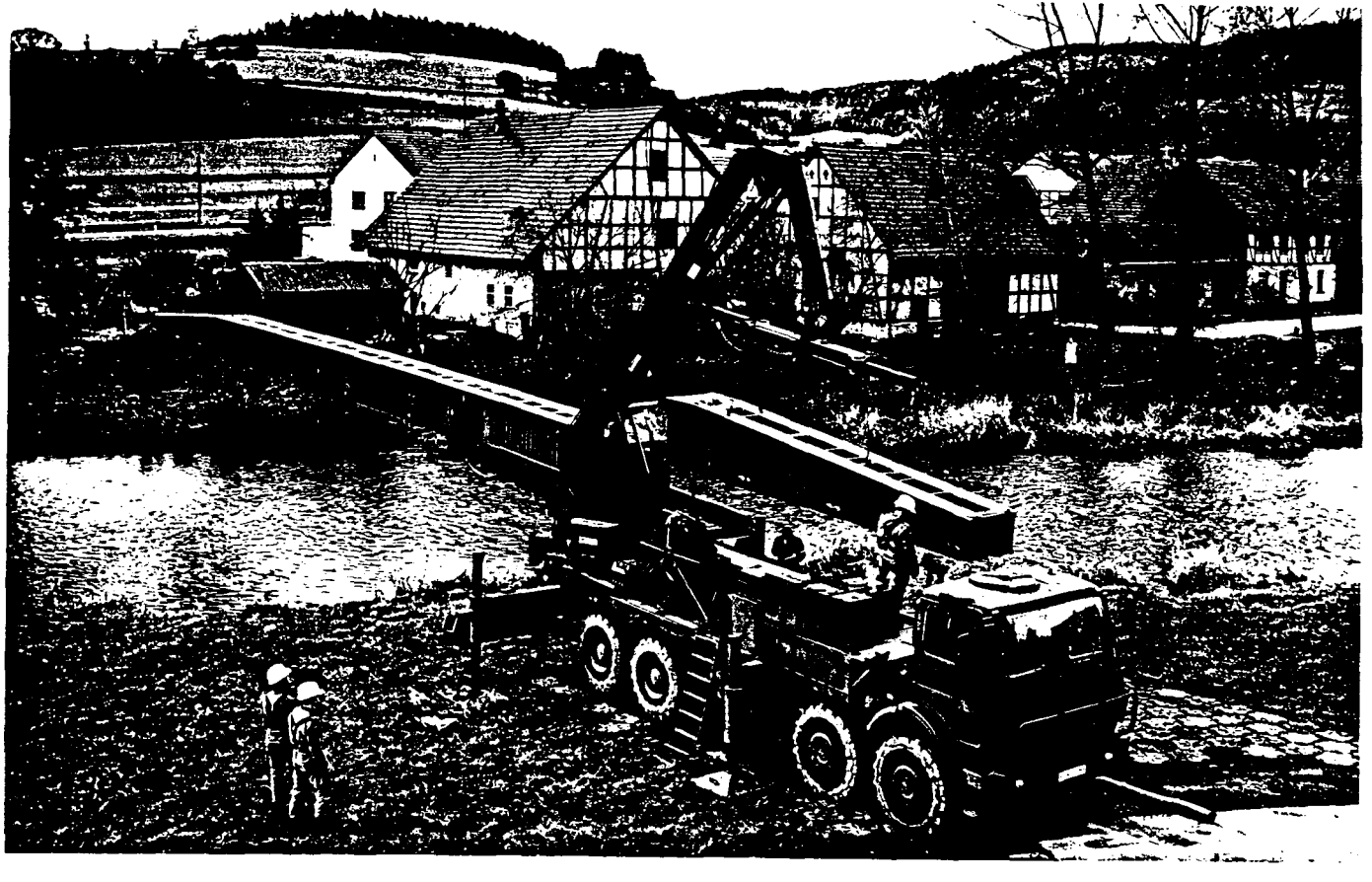

Fig. 3.2.6

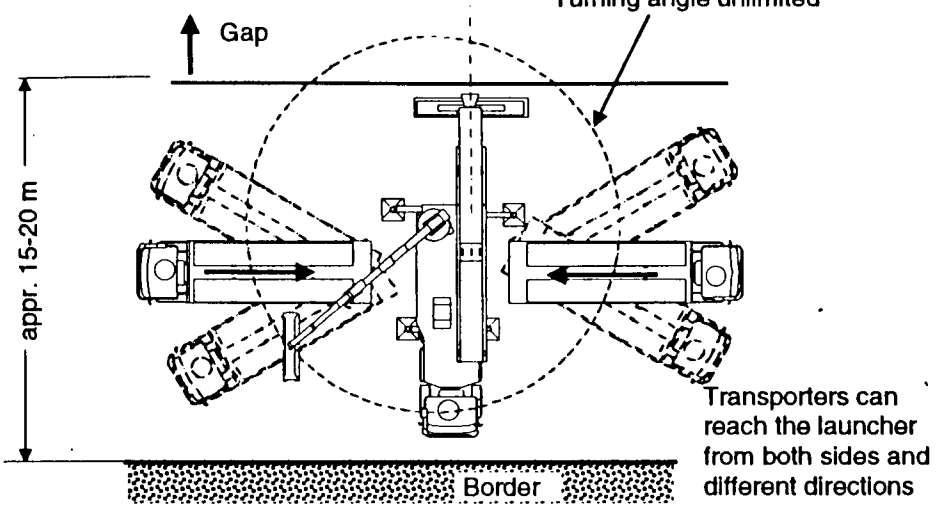

DoFB, construction site, required space at the bank if transporters can approach parallel to the bank

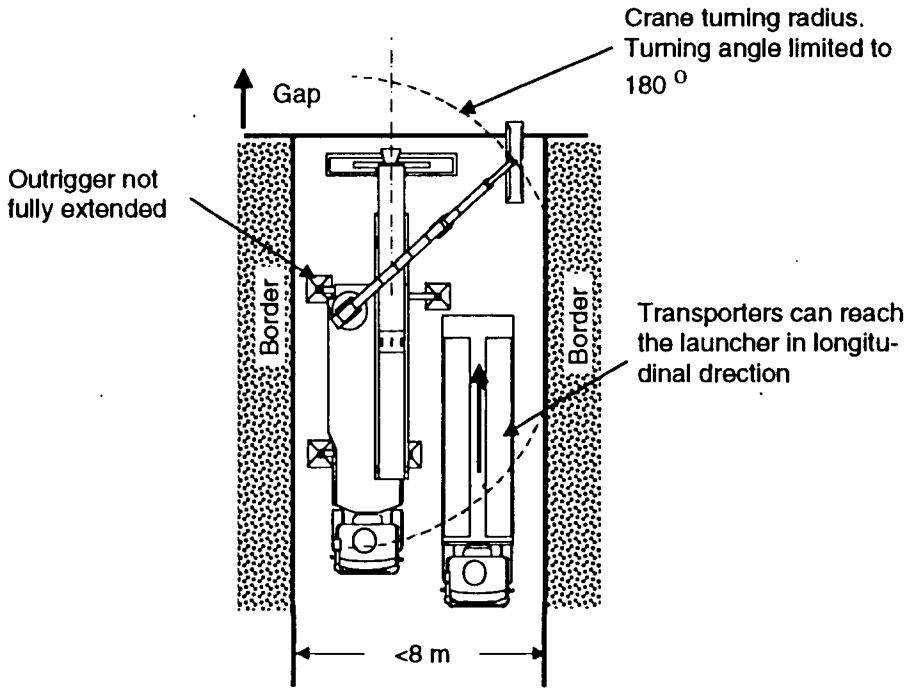

DoFB, narrowest construction site if the transporters can approach parallel to the launcher

Fig. 3.2.7

DoFB Bridge Section Unfolding by Crane

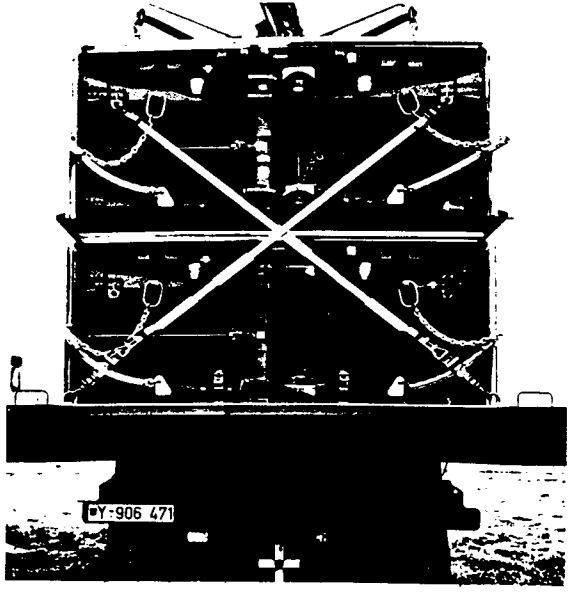

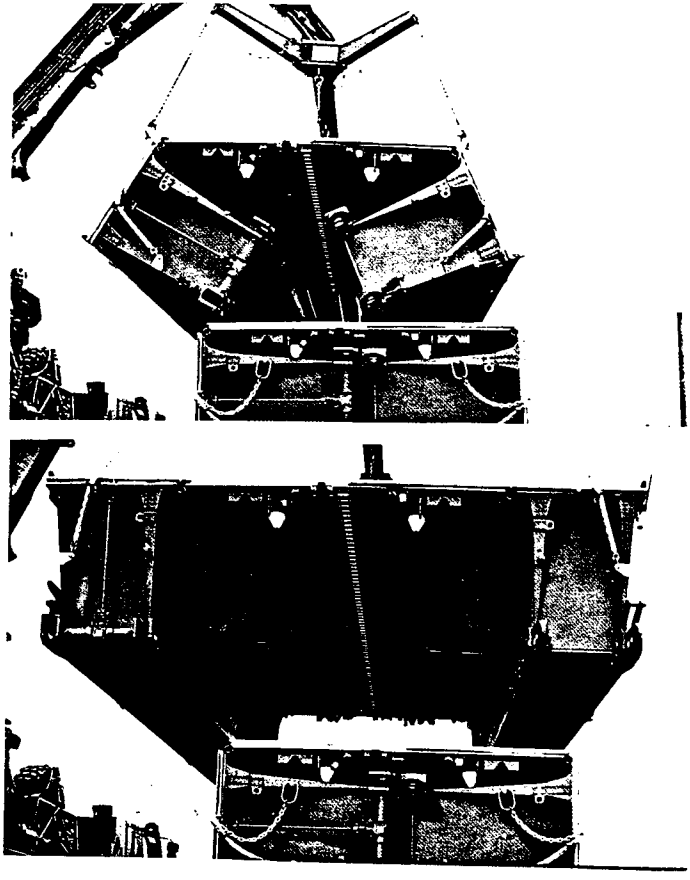

Fig. 3.2.8

DoFB Bridge Launching

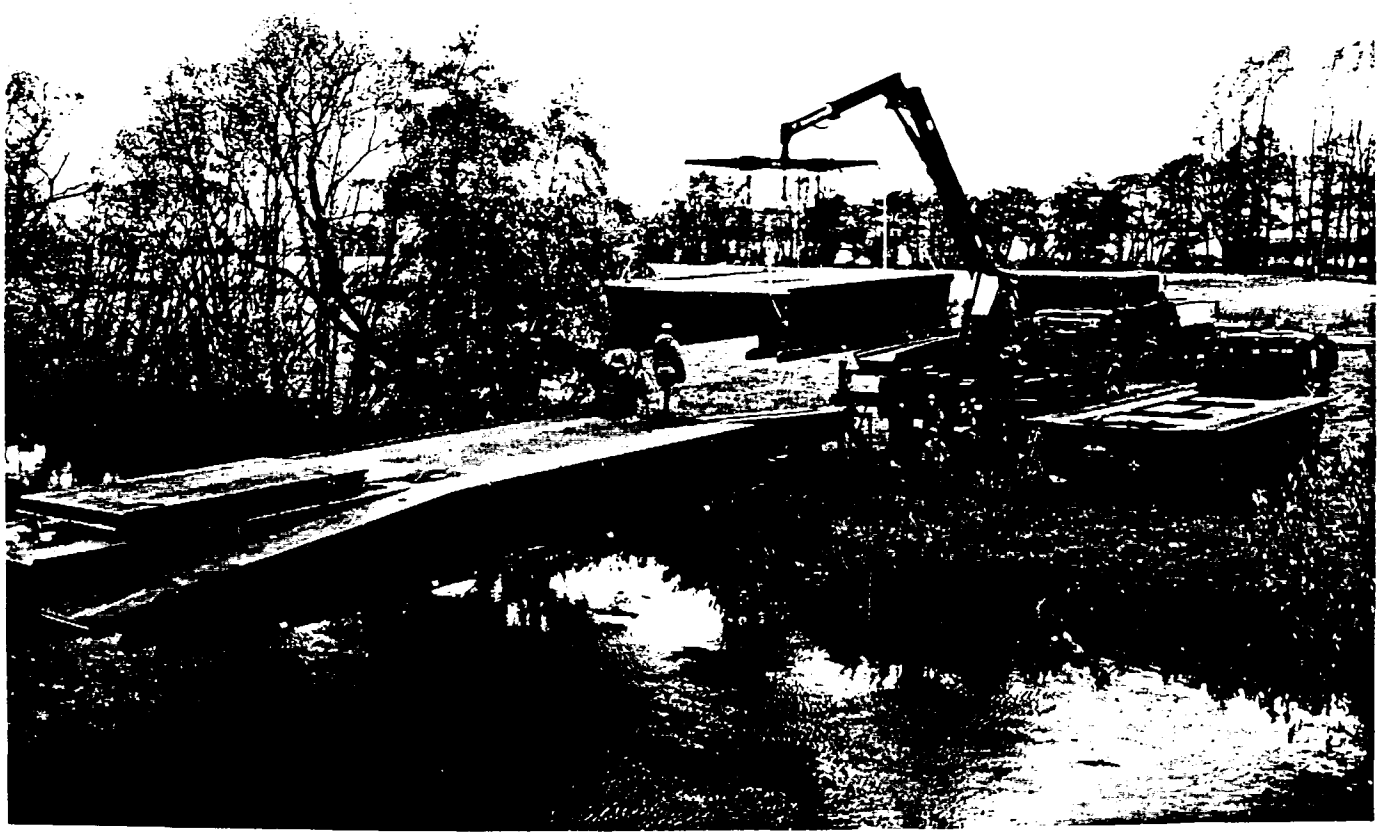

Fig. 3.2.9

DoFB Climbing Ramp Assembly

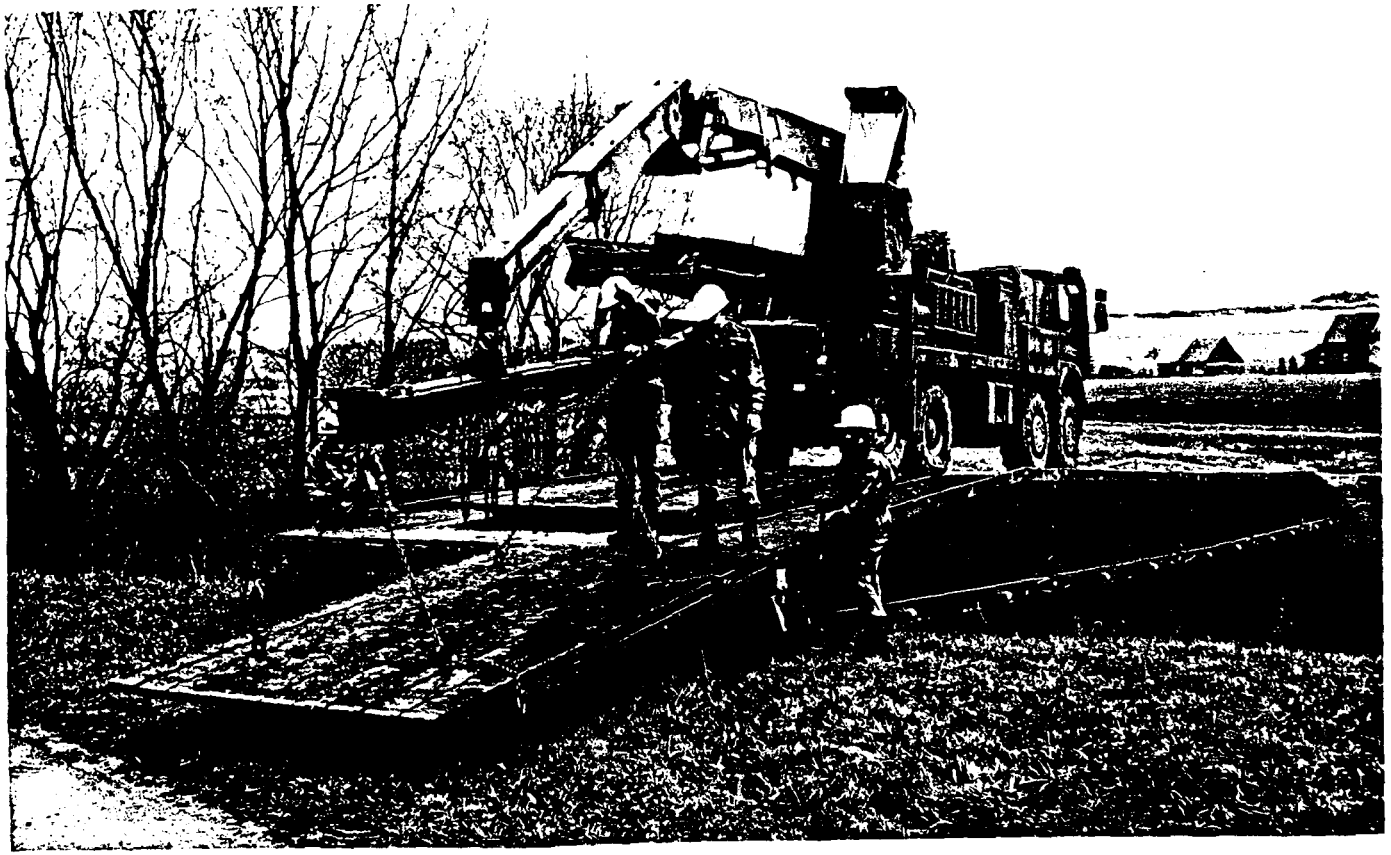

Fig. 3.2.10

DoFB Modular Concept

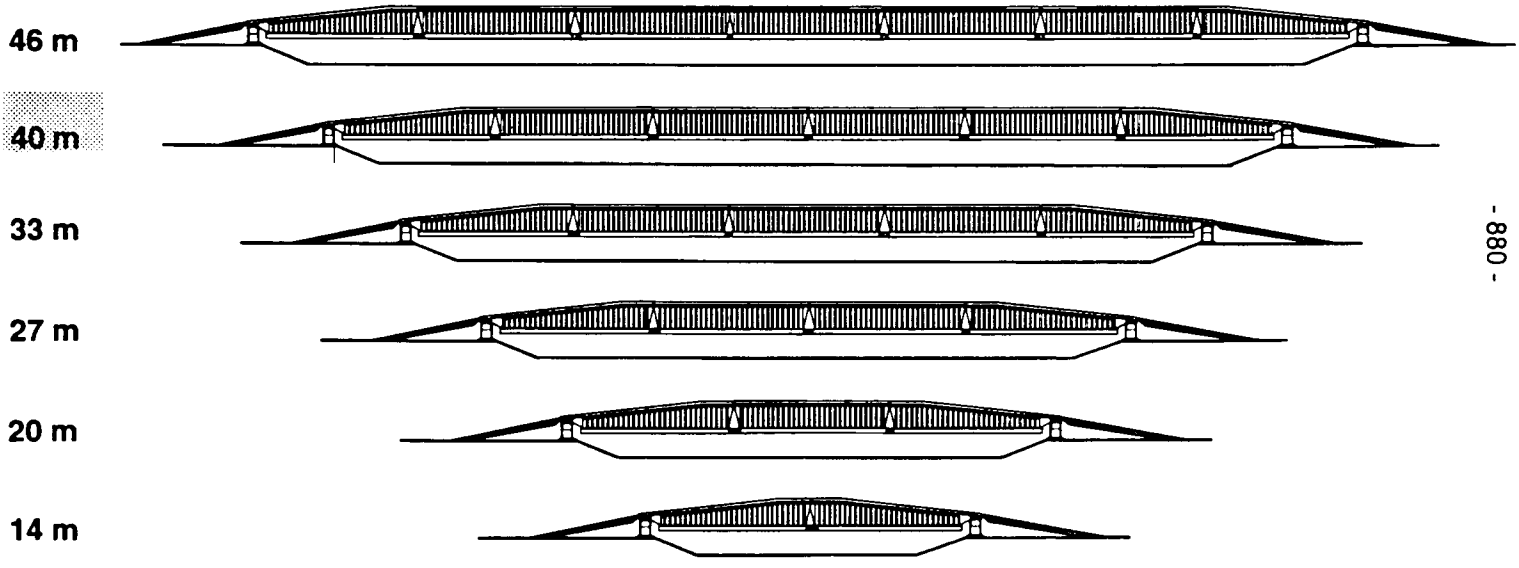

Fig 3.2.11

Standard Bridge 40 m DoFB

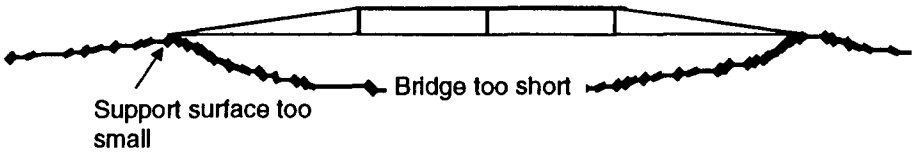

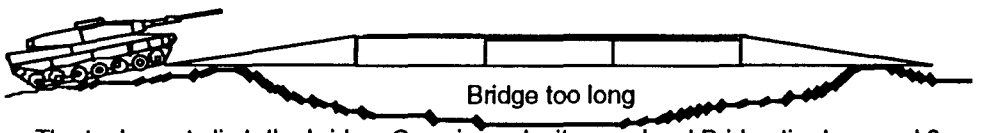

The tank must climb the bridge. Crossing velocity very low ! Bridge tip damaged ?
Crossing impossible for small wheeled vehicles. --> Support preparation necessary !

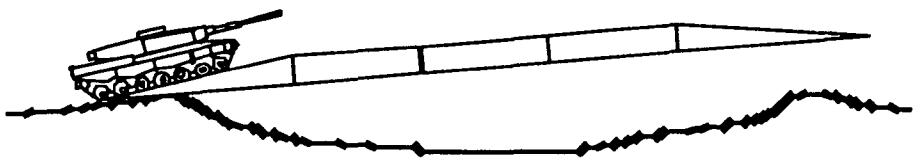

The Bridge tilts. Crossing velocity very low! Bridge tip damaged?
-- > Support preparation necessary!

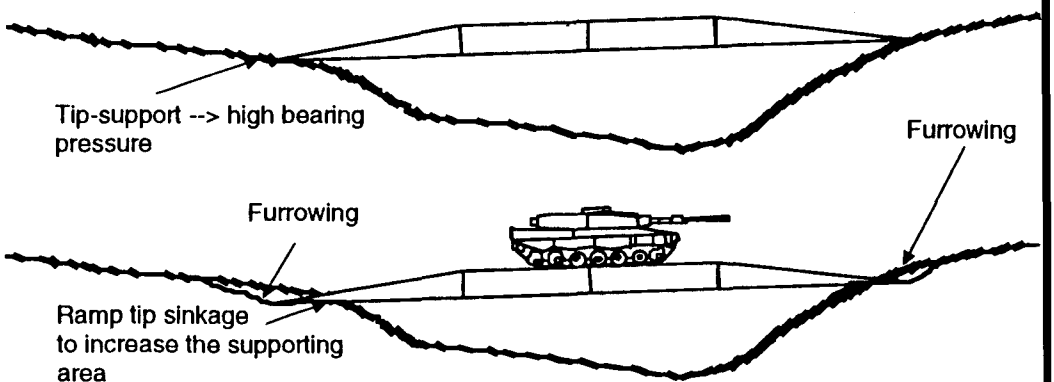

Bridge <u>without</u> bank beams, adaptability to gaps and bank conditions

Fig. 3.2.12

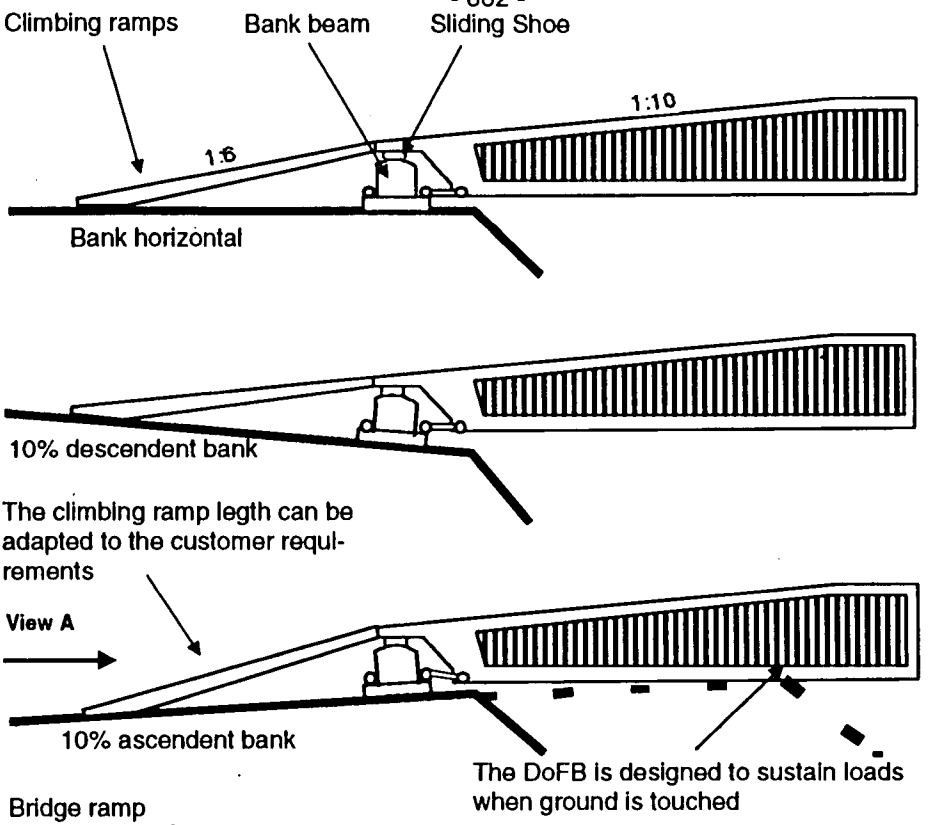

DoFB, adaptability to gaps and bank conditions

Fig. 3.2.13

DoFB Traversing Beam Up-hill Launching

Fig. 3.2.14

DoFB Roadway

Fig. 3.2.15

DoFB Separation of Launching Vehicle and Launching System

Launching vehicle with launching system in transport configuration ①

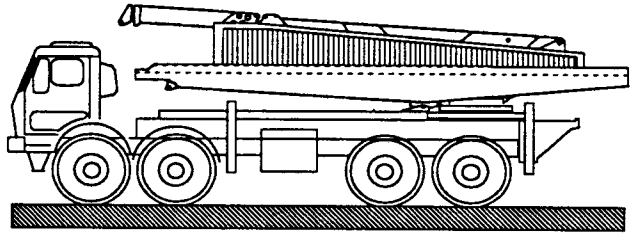

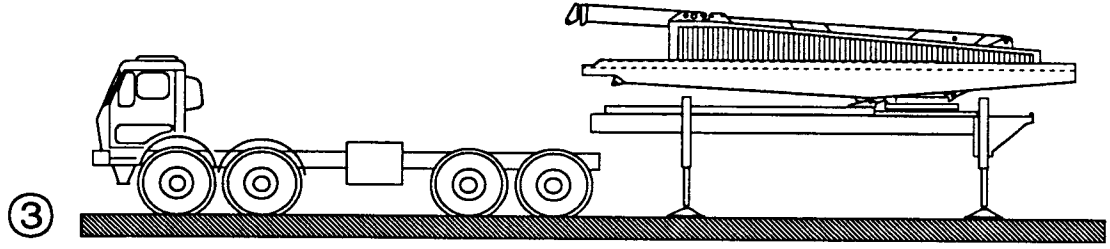

③ Launching system detached, truck ready to move,

Launching system ready to be lowered down

② Disconnection of cardan shaft,fuel hose for auxiliary Diesel unit, electric plugs, clamps to truck base frame.

Launching system jacked up by hydr. outriggers, integrated in the launching system frame, powered by the auxilary diesel engine of the launching system.

Fig. 3.2.16

Main Performance Data

Normal load	MLC 70
Max. load capacity	110 to, for the crossing of two MLC 70 tanks, one towing another, connected with a 5 m towrod; Tank transporter semitrailer laden with a MLC 70 tank
Bridge length modular	14 m, 20 m, 27 m, 33 m , 40 m, 46 m, (standard bridge 40 m)
Width	4.4 m, closed roadway
Ramp inclination	Climbing ramp 1:6 on 3,9 m, bridge ramp section 1:10 on 5,8 m or 1:10 on 13,6 m
Launching crew	5 to 6 men
Launching time	1 hour (40 m bridge)
Bank space	15 -20 m bank depth (depending on type of vehicle), 7 - 8 m bank width (when approaching the gap perpendicular)
Bank conditions	Steps up to ± 3 m betwen home bank and opposite bank; ±5% transversal bank slope; ±10% longitudinal bank slope; uneven ground with local resets of 150 mm
Crossing speed	25 km/h
Transport	1 Launching vehicle 8x8, MLC 30 standard chassis, 5 Series production transport trucks 6x6, MLC 18
Transport dimensions on vehicles	2.75 m width, < 4 m hight, 11 m length depending on type of vehicle
Life	10000 MLC 70 crossings plus 3000 launchings and 3000 retrievals

Table 3.2.1

STEYR 8090 & SEPPI M. MINIFORST ASSEMBLY IN SILVICULTURAL WORK

D. Horvat, K. Jelčić, S. Sever

ABSTRACT

The pedunculate oak forests are the most valuable stands in Croatia. For this reason special attention is given to their natural regeneration and silviculture. In the times of economic, social and other changes, lack of labour is a reason for mechanization of many silvicultural operations in giving shape to new oak forests. The paper deals with the application of a special assembly on one segment of silvicultural work. Two main components of the assembly are Seppi M. Miniforst mulching flail mower as a working machine, and prime mower Steyr 8090 tractor as the power engine.

Key words: *silvicultural pass and trail, mechanized silvicultural work, mulching flail mower, prime mower*

1. INTRODUCTION

The level of mechanization in Croatian silviculture is considerably lower than the one reached in forest exploitation. The only exception is the nursery production consisting of a small portion of silvicultural operations whose mechanization is almost equal to the agricultural production.
Special efforts are taken to replace manual work by machines when it is dealt with precious stands such as Croatian pedunculate oak forests. Several facts have accelerated the work on mechanization of some silvicultural activities: availability of working machines with adequate prime mowers; obvious lack of labour due to the war; short terms of completing the jobs; dependency of the fellings upon the termination of the required silvicultural operations, etc.

2. SUBJECT AND AIM OF INVESTIGATION

In many cases the existing vegetation over large forest areas or rides of various widths should be cut up. Depending on the type, thickness, species, etc. of the vegetation, these jobs can be done with flail shredders in a short time. The appearance of the mulching machines has enabled their further use in forest soil preparation for seeding and planting of seedlings. Furthermore, mulching flail mower may be used for cutting through fire breaks; restoration of the neglected farmlands; cleaning the land from plant residues; maintenance of forest roads, etc. In the lowland forests of the pedunculate oak similar jobs must be done particularly

- after unsuccessful regeneration felling followed by excessive weed growth;
- in the case of excessive growth of unfavourable brush and tree species due to forest dieback;
- when efficient systems of silvicultural tracks, roads etc. are introduced;
- when carrying out mechanized sowing right after soil preparation by scattering the acorn and covering it with cut plants mixed with soil, which is a future project for widening the use of the mulching flail mower.

The choice of the mulching flail mower Seppi m. miniforst and the prime mower Steyr 8090, a tractor adapted to the work in silvicultural operations - by the built-in crawling speed, double steerage (forward and backward), rpm of power take-off) - has resulted in an aggregate whose possibilities of use had yet to be defined.

The exploitation test was accelerated by the problems that had occurred in the transmission of the tractor, the coupling power take-off.

In addition, optimal speeds, number of passes, height/depth of the machine reach had all to be standardized for the characteristic working conditions.

3. WORKING METHOD AND DESIGN OF FIELD EXPERIMENTS

The field tests were planned according to the aims. Two different ways of applying the aggregate have so far been defined:

1. **Building and maintenance of silvicultural trails** which provide for finer internal division of the young stand and, at the same time, form a transportation net within it. In a young stand at a distance of 35 m, 3 m-passages are cut; and at every 5 m of the production area 1,5 m-silvicultural lanes are made along the former wider passages. Both

elements of thus created transport net enable equal attention, possibilities and intensity of silvicultural work upon each square meter of the production area.

2. **Soil preparation in natural regeneration of stands** provides the contact and also covering of the seed (acorn) with soil and cut-up biomass, the so-called mulching. It also involves chopping and removing the small stumps to reduce the coppice vigour of unwanted species. In this case the flail of the machine breaks the root neck by penetration of the blades 2 to 3 cm into the soil where it chops up the meristem cells.

The mentioned technological tasks may be performed in three basic ways:

A1 - By mulching the stand above certain height from the soil surface (e.g. 20...30 cm) on the first pass. In case of greater heights of the undergrowth, this passage is always done by backward drive with raised protection lid of the machine.

A2 - By final soil preparation on the second pass; by mulching with root system destruction at certain depth below the soil surface (e.g. 2...3 cm) -it is characteristic of soil preparation for natural regeneration of areas covered with plants of larger diameters.
In this gear (A2) the tractor moves forwards with lowered protection lid.

B - By mulching the seedling stand down to the soil surface - typical at building silvicultural lanes.

C - By seedling stand mulching with simultaneous soil preparation on a single pass - the same as A but for areas covered with plants of smaller diameters. Skid trails can be partly restored in this way.

As to the working machine, all tests were made without safety clutch, along with the checkings with the safety centrifugal clutch built in the belt-pulley of the final transmission of the mulching flail mower.
In order to eliminate the impact of the tractor and driver, all tests were done with the same tractor with all new blades.
A special attention was paid to the classification of the working conditions. Eight characteristic conditions were eventually selected, three in the natural stand and five in the preserve. As a rule, at double passing the first was always backwards, the second and last forwards. In this case the biomass was cut up first at 20 to 30 cm above the ground, in the second the rest and perhaps 2 to 3 cm of the soil. At maintaining the lane net, the flails are not entering the soil but the plants are cut up at the ground level.

With the given motor rpm and the control of the mulcher rpm, the torque on the mulching flail mower's shaft was measured. For every condition the real aggregate speed was measured.
The cut biomass was determined by sampling the number and tree species; dimensions; plant coverage of the soil; average diameter at the height of 30 cm and of small stumps; plant heights, etc.

4. SOME RESULTS OF THE RESEARCH

All results are given separately:

- of silvicultural lanes (Experimental plot "Slavir"), and
- of soil preparation (field area "Otočke šume"), and

of the described basic work methods (A1, A2, B and C). By means of experience or experiment, possible speeds of the aggregate are determined. The average torque of two working machine types - with and without the centrifugal safety clutch - was taken as the unit of transmission load. This paper gives the review of only some research results.

4.1 Building of silvicultural trails

Table 1 shows some of the research results.

TABLE 1 - Field area "Slavir" - building of silvicultural trails

	STAND CONDITIONS										
	VERY HARD		HARD			MEDIUM		LIGHT		VERY LIGHT	
	SPEED, m/s										
WORKING METHODS	0,076	0,186	0,093	0,145	0,2	0,214	0,328	0,23	0,78	0,15	0,885
	Torque mean values, Nm										
A1	202	358		228	282	200	344				
A2	297	516		300	517	470					
B						511	389				
C			470	470			367	475	336	250	257

It says that under the hardest conditions the work must be done in two passages (A1 and A2); under the lightest working conditions and accelerating speed of work, only one passage (C) is sufficient.
A survey of measuring the torque of the first aggregate pass (A1) together with the description of the stand characteristics defined as "very hard" with two working speeds are shown in the diagram of Figure 1. The torque significantly depends on the moving speed of the aggregate. This is even more obvious during the second pass (A2), and is shown in the diagram of Figure 2.

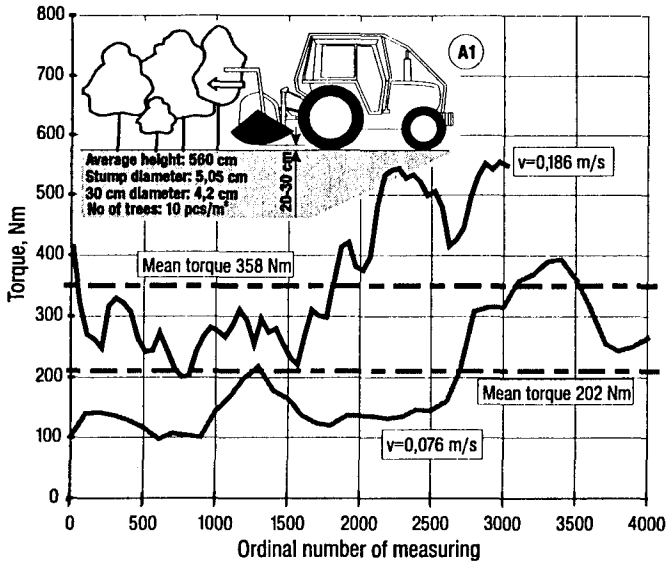

Fig. 1 Torque change depending on the speed in very hard stand conditions - A1

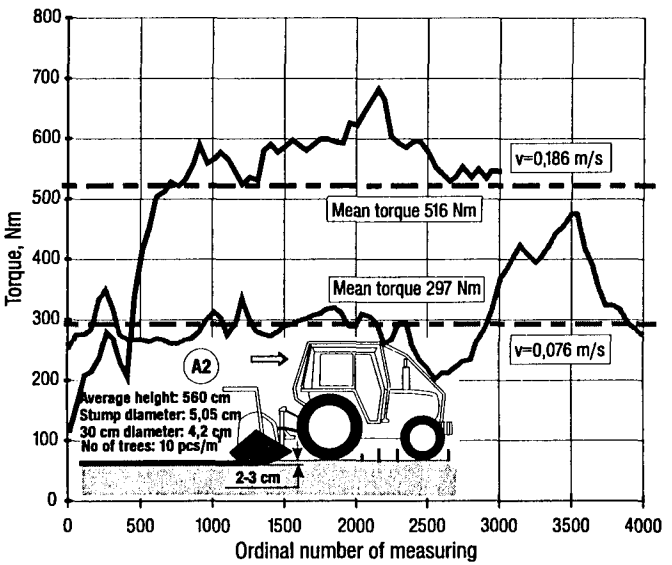

Fig. 2 Torque change depending on the speed in very hard stand conditions - A2

In very light conditions the aggregate was able to work in one pass (C), which is shown in the diagram of Figure 3. The similarity of the realized torques at both speeds is explained by deeper penetration of the shredder into the soil at lower speed, due to deeper penetration of the tractor wheel. This is also seen at higher speeds at the end of the experiment.

Fig. 3 Torque change depending on the speed in very light stand conditions - C

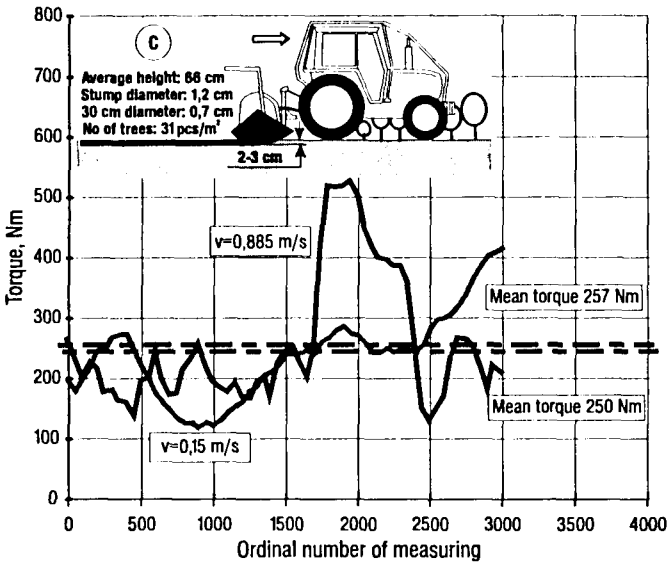

4.2 Preparation of the stand

Table 2 is a review of some results of the research on soil preparation.

TABLE 2 - Field area "Otočke šume", soil preparation

WORKING METHODS	STAND CONDITIONS							
	VERY HARD		MEDIUM		LIGHT		Skid trail restorat.	
	SPEED, m/s							
	0,103	0,152	0,145	0,286	0,308	0,678	0,14	0,308
	Torque mean values, Nm							
A1	300	358	135	150	100	131		
A2	440		305	383	415			
B								
C							300	490

Figure 4 shows the torque movement. At the second pass (A2) and already at small speeds, big torques are achieved, so that in this kind of work the protection of the tractor's transmission is necessary. Besides, in the first pass (A1) a more uneven torque is realized. The tips coincide with the approach of the shredder onto the individual small tree.

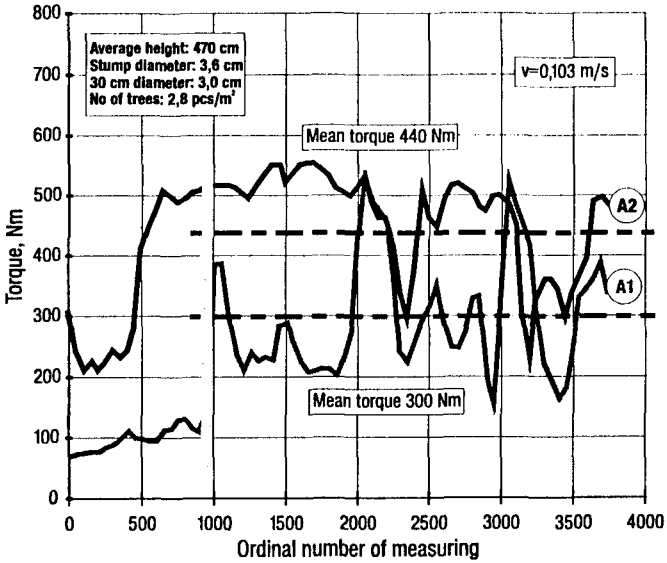

Fig. 4 The change of the torque as depending on the pass (A1 or A2) at hard stand conditions.

Due to frequent defects of the tractor's shaft, shredders with safety centrifugal clutch have lately been applied. Torque measuring at switching on the clutch proved the advantage of having the clutch. However, when the aggregate is working, especially under high load, no satisfying torque reductions were noticed. The diagram of Figure 5 shows the work of the aggregate in the conditions of partly regenerated surface layer of the ride. The shredder without the clutch was continually under peak load (490 Nm); the shredder provided with a clutch was slightly less loaded (420 Nm), though the torque reduction at the end of the experiment ended up with stopping the tractor.

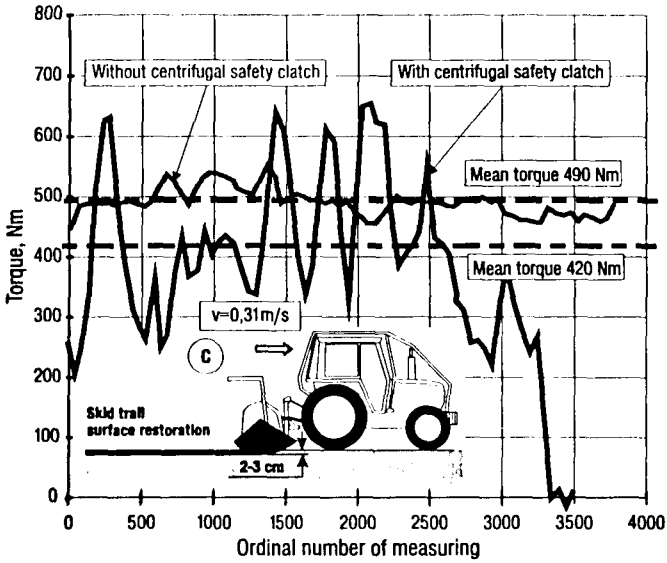

Fig. 5 Torques in ride improvements, with and without the clutch on the shredder drive system

5. CONCLUSIONS

Depending on the working conditions and methods, it may be generally concluded that

- lighter working conditions allow operation at significantly higher speeds;
- regardless of the pass (first or second), high torques occur on the penetration of the mulcher's tool into the soil;
- on the penetration of the mulcher's tool into the soil, the torques depend significantly on the moving speed of the assembly set;
- the tractor transmission is not protected from the peak loads by building in a centrifugal safety clutch.

6. LITERATURE:

1. Anon (1994): Forstmulchgeräte, KWF-Gruppenübersichten - technische Daten von Forstmaschinen, KWF, Gross-Umstadt
2. .....Tvornički podaci proizvoditelja Seppi m. Miniforst i traktora Steyr 8090
3. Krolin (1977): Traktori za pogon teških rotacijskih sjekača za čišćenje, Mehanizacija šumarstva Vol. 2, br. 5-6, str. 162-172
4. Kulaš (1983): Unapređivanje njege mladika primjenom staza, ZO, p. 607-612
5. Sever, D. Horvat, V. Golja (1983): Prilog proučavanju rada rotosjekača, ZO p. 653-663

The authors wish to express their thanks to the Vinkovci Forest Management and their offices Otok and Spačva for the given help and active contribution to the field research.

Authors' addresses:

1. Dr. Sc. Dubravko Horvat and Professor Dr. Sc. Stanislav Sever, Faculty of Forestry, University of Zagreb, Svetošimunska 25, 41000 Zagreb, Croatia

2. Dipl. Ing. Krunoslav Jelčić, Public Corporation "Croatian Forests" Zagreb, Vukotinovićeva 2, 41000 Zagreb, Croatia

A Single Track Module in Multi-Body Systems Sense for Simulation of Steering of a Vehicle on Hard Ground

M. Sc., Ph.D. candidate Dag Thuvesen
Machine and Vehicle Design
Chalmers University of Technology
S-412 96 GÖTEBORG, Sweden

ABSTRACT

Recently available Multi-Body Systems (MBS) software has opened new and powerful opportunities for analysis of transient and nonlinear vehicle dynamics. Thereby a module for a single track has to be created, which is the tyre model for road vehicles, in order to enable versatile simulation of steering dynamics of tracked vehicles.

The track module must take into account the instantaneous normal load, both its magnitude and the point of resulting action, which may vary along, but not necessarily across, the track. The load distribution along the track has been given a realistic default shape, which, however, may be modified. In a first step a module has been developed for flat, rigid ground. The track - ground interface is then modelled by consistent constitutive equations, allowing for anisotropic Coulomb friction.

The 2D relative motion between track and ground, interpreted in terms of rotation about a specified spin pole, is the motion related input to the module. This gives rise to 2D frictional forces, the resulting action of which is a single force, acting along some line. The force magnitude and its action line location/orientation are the output quantities from the module.

Algorithms have been developed and evaluated for the above mentioned type of analysis, especially fitted to interact with MBS software, such as ADAMS or DADS.

This paper will be published in an appendix to the proceedings

EFFECT OF THE WAY THE LOAD APPLIES ON THE BEARING CAPACITY OF DRY-LOOSE SAND

Ji Xuewu, Zhuang Jide and Qiu Xiding
Department of Automobile Engineering,
Jilin Univercity of Technology, Chang Chun, China

ABSTRCT

The bearing capacity of dry loose sand is one of the key problems considered for a vehicle walking in desert. And it is affected by the way the load applies. Based on plate—sinkage tests, the effect of two different ways the load applies on the bearing capacity of dry loose sand is studied. One way is that the plate is horizontal while the angle of the load relative to the plate normal is varied from 0 to 30 degrees, and the other is that the load is always perpendicular to the plate while the angle of the plate relative to sand surface is varied from 0 to 30 degrees. The results indicate that the bearing capacity of dry loose sand in the former case is higher than that in the latter one.

INTRODUCTION

Soil bearing capacity under vertical load is widely studied by using Bevameter[1][2] and the likes. Based on the vertical load—sinkage relation, it is always assumed that the soil reaction was purely radial in analysing the forces acted on the wheel and in predicting the traction properties of a off— road vehicle. For a towed wheel, the assumption is reasonable because in general the tangential stress is so small that it can be neglectable. However, for a driven wheel, the tangential stress is so large that it can not be neglected, and the assumption becomes unreasonable. Because no better method is available, the assumption is usually used as an expedient.

On the view of force composition, the resultant of the normal and the tangential stresses beneath a wheel must angulate with the normal stress. And if the inclined load—sinkage relation is adopted, the precision of the prediction of a wheel traction properties can be increased.

As we know that the camel can pass through a desert easily, while in general a tired vehicle can not do as easily as the camel can. This indicates that some differences must exist between the interaction of camel foot—sand and that of tire—sand. Ref. [3] indicated that camel foot can restrict the sand flow to some extent by the camel hoof, and that the camel foot will spread when it acts on sand and bears part of the weight. Further investication into the interaction of camel foot— sand, it can be found that the camel foot angulately acts on sand when it provides traction. While a tire especially under lower inflation pressure condition acts on sand almost horizontally [4].

In order to increase the precision of predicting the vehicle traction properties and to discover the differences between interactions of camel foot — and tire — sand, two types of plate — sinkage tests which simulate the two above mentioned interactions are conducted. This research will provide a base for the design of new type of off — road vehicle tires.

TEST PROCEDURE AND DATA PROCESSING

The dry loose sand is taken from one of the world famous deserts — Takelamagan Desert in Sinklang Uighur Autonomous Region in the northwest of China. Its grain size distribution is shown in Fig. 1, and its main characteristics are as follows:

D_{10}(10% by weight diameter) = 0.08 mm;

D_{60}(60% by weight diameter) = 0.14 mm;

D_{60}/D_{10}(coefficient of nonhomogenious) = 1.75;

φ (angle of internal friction) = 31.4°;

e_{max}(maximum void ratio) = 0.835;

e_{min}(minimum void ratio) = 0.583;

γ_d(dry density) = 14.65 KN/m^3.

The tests were conducted on the indoor soil bin test rig shown in Fig. 2. Different sinkage rates can be get by adjusting the flow regulator of the hydrolic system (which is not shown in Fig. 2). The angle of the load relative to the plate normal can be changed by the holed bar. The load appling on the plate and the plate sinkage were measured though force — and displacement — transducer respectively. The soil bin dimension is 2400 × 720 × 700 (length × width × height) in mm.

Two types of tests were conducted. One is that the plate is horizontal while the load changes its direction with inclination to the plate normal varied from 0 to 30 degrees, and the other is that the load is always perpendicular to the plate while the plate is inclined to sand surface with inclination varied from 0 to 30 degrees.

In order to strengthen the friction between the plate and sand in the former case, carborundum whose grain dimension is similar to sand's was stuck on the plate. Before each of the tests, some pretreatment such as turning updown the sand and scraping the sand surface level must be done. Tests under the same condition were repeated 5 to 7 times.

A personal computer is used to sample and process the data. A computer program was so designed that after each set of the tests under the same condition all the load — sinkage curves of this set and the soil parameter values were shown on the sreeen directly.

A weighted least squares method was adopted. The weighting factor is taken as $w_i = p^2$[5], where p is the average pressure beneath the plate.

TEST RESULTS AND ANALYSIS

The results of tests conducted under different sinkage rates indicate that sinkage rates have little effect on load — sinkage relation in both cases. This is identical to Bekker's conclusion[1] which was drown from vertical load — sinkage tests. Accordingly, the tests can be conducted

under the same sinkage rate. In this paper, the sinkage rateis taken approximately as 15mm/s in all the other tests.

Fig. 3 showes the sinkage curves of tests in case 1. It can be seen that plate sinkage under the same load increases as the inclination of load applied increases. This indicates that a increase of load inclination causes a decrease of the bearing capacity of dry loose sand. Sinkage curvers of tests in case 2 is shown in Fig. 4. Also, a increase of the plate inclination causes a increase of the plate sinkage and a decrease of the bearing capacity of dry loose sand.

From Figs. 3 and 4, it can be seen that sinkage in case 1 is large than that in case 2 under the same load. This indicate that the bearing capacity of dry loose sand in case 1 is lower than in case 2.

As to the bearing capacity of dry loose sand under vertical load, Bekker gave the following emprical equation[1]:

$$\begin{cases} p = K \cdot Z^n \\ Q = p \cdot A \end{cases} \tag{1}$$

where

p——average pressure beneath the plate in the direction of load, KPa;

K, n——exprimentally determined sand parameters, K, $KN/m^{(n+2)}$, n, dimensionless;

Z——plate sinkage in direction of load, m;

A——plate area, m^2;

Q——load applied, KN.

Similarly, in case 1 and 2, eq. (1) can be rewritten as:

$$\begin{cases} p = K_\alpha \cdot Z^{n_\alpha} \\ Q_\alpha = p \cdot A \end{cases} \tag{2}$$

and

$$\begin{cases} p = K_\beta \cdot Z^{n_\beta} \\ Q_\beta = p \cdot A \end{cases} \tag{3}$$

respectively, where

p, Z, A——as in eq. (1);

K_α, n_α——exprimentally determined sand parameters in case 1;

Q_α——load applied in case 1;

K_β, n_β——exprimentally determined sand parameters in case 2;

Q_β——load applied in case 2.

Variation of sand parameters K_α and n_α with angle α which is the angle of load inclination to the plate normal are shown in Fig. 5. It can be seen that K_α decreases with the increase of angle α almost in line, while n_α is barely varied with α.

By linear regress, the relation of the ratio K_α/K and the angle α can be expressed as:

$$K_\alpha/K = 1 - 0.0157 \cdot \alpha \tag{4}$$

where K is sand parameter in eq. (1).

Similarly, n_β does not vary with angle β which is the angle of plate relative to sand surface,

and K_β decreases with increase of angle β, see Fig. 6. And the relation of the ratio of K_β/K and β can be expressed as:

$$K_\beta/K = 1 - 0.0073 \cdot \beta \tag{5}$$

From eq. (1) to eq. (5), following equations can be gained:

$$Q_\alpha/Q = 1 - 0.0157 \cdot \alpha \tag{6}$$

$$(Q_\alpha/Q_\beta)|_{\alpha=\beta} = (1 - 0.0157 \cdot \alpha)/(1 - 0.0073 \cdot \alpha) \tag{7}$$

Variation of Q_α/Q and Q_α/Q_β with α is shown in Fig. 7 and Fig. 8 respectively.

Eq. (6) indicates that the bearing capacity of dry loose sand under inclined load is lower than that under vertical load, and that if the inclined load—sinkage relation is used in the prediction of a vehicle traction properties, a preciser result can be gained.

Eq. (7) indicates that the bearing capacity of dry loose sand under inclined plate is higher than that under inclined load. Accordingly, camel foot is more efficient than conventional tires when walking in desert. How to make a tire be of "inclined plate" constructure would be the key technique of a bionic camel foot tire.

CONCLUSION

1. Sinkage rate has little effect on the bearing capacity of dry loose sand in both above mentioned cases.

2. Sand parameter $K_\alpha(K_\beta)$ decreases with the increase of the angle $\alpha(\beta)$, while the parameter $n_\alpha(n_\beta)$ has little to do with $\alpha(\beta)$.

3. The bearing capacity of dry loose sand under inclined load is lower than that under vertical load, and if the inclined load — sinkage relation is used in the prediction of a vehicle traction properties, a preciser result can be gained.

4. The beairng capacity of dry loose sand under inclined plate is higher than that under inclined load. Accordingly, camel foot is more efficient than conventional tires when walking in desert.

REFERENCES

1. M. G. Bekker, Introduction to the Terrain—Vehicle Systems, The Univercity of Michigan Press, 1966.

2. Zhuang Jide, Automobile Terramechanics, Publication of Engineering Industry of China, 1981.

3. Xu Peijun, Study on the Mechanism of Camels Walking in Desert and the Application to Legged Vehicle, Ph. D Dissertation of Jilin Univercity of Technology, 1992.

4. Ji Xuewu, Study on the Interaction of Tire—Sand and the Key Technique of Bionic Camel Foot Tire, Ph. D Dissertation of Jilin Univercity of Technology, Unpublished.

5. W. Y. Wong, Data Processing Methodology in the Characterization of the Mechanical Properties of Terrain, J. of Terramechanics, Vol. 17, No. 1, pp 13 to 41, 1980.

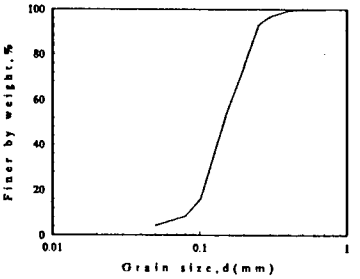

Fig.1 sand grain size distribution

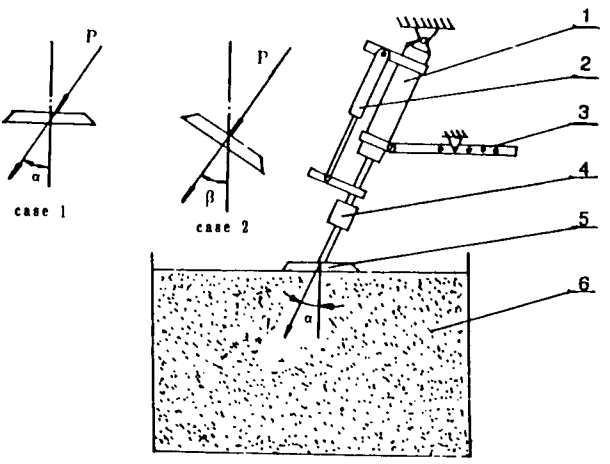

Fig.2 test rig
1. hydrolic acutator 2. displacement tansducer
3. holed bar 4. force tansducer 5. plate 6. siol bin

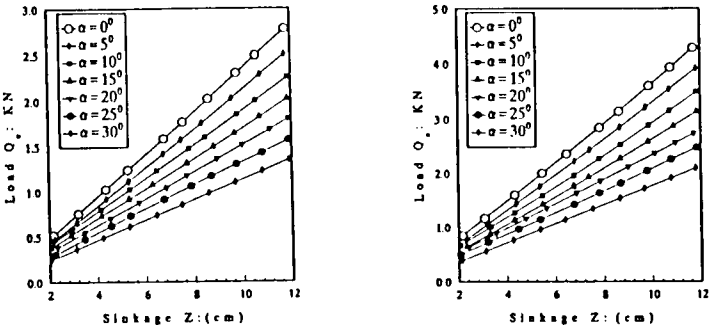

Fig. 3 load-sinkage curves in case 1
(a) circle plate, dia. =120mm
(b) circle plate, dia. =160mm

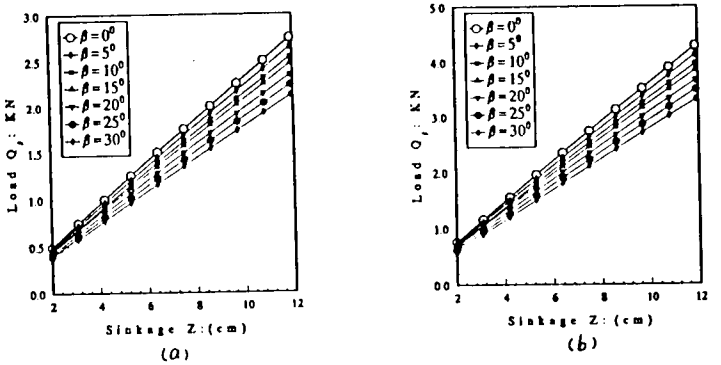

Fig. 4 load-sinkage curves in case 2
(a) circle plate, dia =120mm
(b) circle plate, dia =150mm

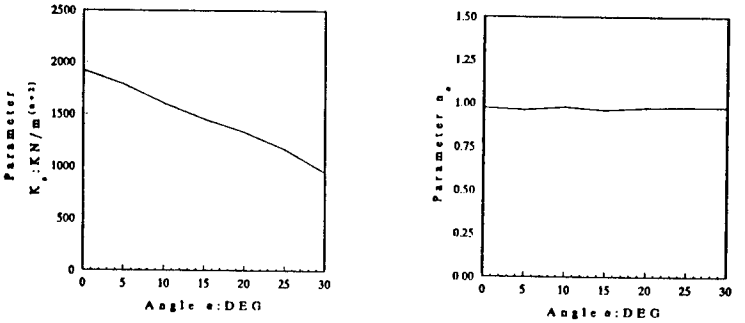

(a) (b)

Fig. 6 variation of K_α and n_α with α

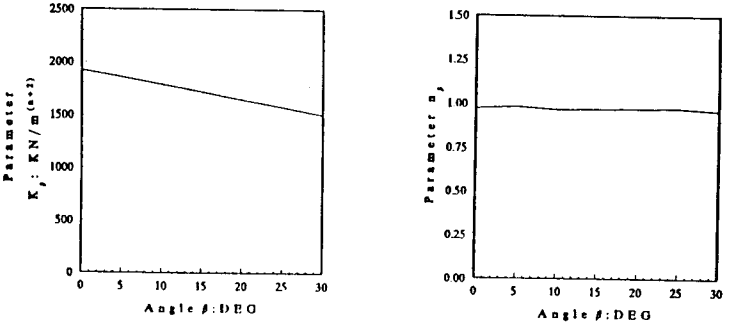

(a) (b)

Fig. 6 variation of K_β and n_β with β

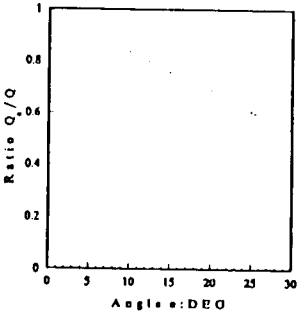

Fig. 7 variation of Q_c/Q with α

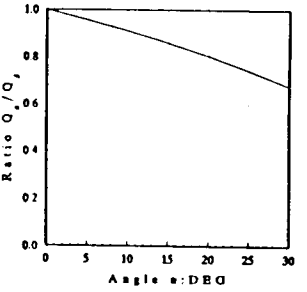

Fig 8 variation of Q_c/Q_p with α

ISSN 1022 - 0313

ISTVS thanks the European Research Office of the U.S. Army for the financial support to the conference.

ISSN 1022 - 0313